



**HAL**  
open science

# Analysis and implementation of second generation criteria in a stability computer code

François Grinnaert

► **To cite this version:**

François Grinnaert. Analysis and implementation of second generation criteria in a stability computer code. Fluid mechanics [physics.class-ph]. Université de Bretagne occidentale - Brest, 2017. English. NNT : 2017BRES0003 . tel-01578973

**HAL Id: tel-01578973**

**<https://theses.hal.science/tel-01578973>**

Submitted on 30 Aug 2017

**HAL** is a multi-disciplinary open access archive for the deposit and dissemination of scientific research documents, whether they are published or not. The documents may come from teaching and research institutions in France or abroad, or from public or private research centers.

L'archive ouverte pluridisciplinaire **HAL**, est destinée au dépôt et à la diffusion de documents scientifiques de niveau recherche, publiés ou non, émanant des établissements d'enseignement et de recherche français ou étrangers, des laboratoires publics ou privés.



université de bretagne  
occidentale

UNIVERSITE  
BRETAGNE  
LOIRE

**THÈSE / UNIVERSITÉ DE BRETAGNE OCCIDENTALE**

*sous le sceau de l'Université Bretagne Loire*

pour obtenir le titre de

**DOCTEUR DE L'UNIVERSITÉ DE BRETAGNE OCCIDENTALE**

*Mention : Génie mécanique, mécanique des fluides et énergétique*

**École Doctorale des Sciences de la Mer**

présentée par

**François Grinnaert**

Préparée à l'Ecole navale

# Etude et Implémentation des Critères de Seconde Génération dans un Code de Stabilité

**Thèse soutenue le 19 janvier 2017**

devant le jury composé de :

**Paola GUALENI**, Professeur, rapporteur  
Université de Gènes (Italie)

**Volker BERTRAM**, Professeur, rapporteur  
DNV GL, Hambourg (Allemagne)

**Pierre FERRANT**, Professeur, Président de Jury  
Ecole Centrale de Nantes

**Claude BALANANT**, Maître de Conférences  
Université de Bretagne Occidentale

**Jean-Marc LAURENS**, Enseignant Chercheur HDR, Co  
directeur  
ENSTA Bretagne

**Jean Yves BILLARD**, Professeur, Co directeur  
École navale

**Jérôme CAPUT**, invité  
Etat-major de la Marine

**Jean-François LEGUEN**, invité  
DGA Techniques Hydrodynamiques



# **Analysis and Implementation of Second Generation Criteria in a Stability Computer Code**

François Grinnaert

PhD Thesis

Supervised by Jean-Yves Billard and Jean-Marc Laurens

19 January 2017

Ecole navale

BCRM Brest – CC 600

F-29240 BREST Cedex 09



## ABSTRACT

The second generation intact stability criteria are currently under finalization by the International Maritime Organization. They are intended to improve the current intact stability rules by adding safety in waves. They are structured in five failure modes and three levels of assessment in each failure mode. The first level is based on a simplified deterministic approach of the phenomena and ensures high safety margins. The second level requires more complex computations based on hydrostatic considerations with regard to static waves and is expected to provide reduced safety margins. The third level, currently under development, would consist of numerical simulations of the ship's behavior in real sea states performed by specialized institutes. Level-one and level-two criteria of both pure loss of stability and parametric roll failure modes have been implemented in a stability code. The  $KG_{max}$  curves associated with these future criteria are computed for a selection of different ships of different types, both civilian and military, expected or known to have different behaviors with regard to the considered failure modes. The requirement and the relevance of the criteria are analyzed. The second check of parametric roll level-two criterion is thoroughly analyzed. A simplified method providing the maximum parametric roll angle assuming a linear GZ is developed and implemented in the corresponding criterion.

## RESUME

Les critères de stabilité à l'état intact de seconde génération sont en cours de finalisation par l'Organisation Maritime Internationale. Ils doivent compléter les critères actuels en apportant une sécurité accrue dans les vagues. Ils sont organisés en cinq modes de défaillance et trois niveaux d'évaluation dans chaque mode de défaillance. Le premier niveau est basé sur une approche déterministe simplifiée des phénomènes et assure des marges de sécurité importantes. Le second niveau requiert des calculs plus complexes basés sur des considérations hydrostatiques dans les vagues. Il est supposé assurer des marges de sécurité réduites. Le troisième niveau, actuellement en cours de développement, devrait consister en des simulations numériques du comportement du navire sur des états de mer réels réalisés par des instituts spécialisés. Les deux premiers niveaux des modes de défaillance perte pure de stabilité et roulis paramétrique ont été implémentés dans un code de stabilité. Les courbes de  $KG_{max}$  associées à ces critères sont calculées pour une sélection de navires civils et militaires de différents types ayant des comportements connus ou supposés différents vis-à-vis de ces modes de défaillance. Les exigences et la pertinence des critères sont analysées. La seconde vérification du critère de niveau deux en roulis paramétrique est étudiée en détail. Une méthode simplifiée de calcul de l'angle maximum de roulis paramétrique supposant un GZ linéaire est proposée et implémentée dans le critère correspondant.

## ACKNOWLEDGMENTS

This work is dedicated to my Father André Grinnaert and Xavier Castellani.

I am deeply grateful to Jean-Yves Billard, Jean-Marc Laurens and Alcino Ferreira.

I thank all people who helped, supported, encouraged me and everyone who made this project possible: Arman Ariffin, Jacques-André Astolfi, Anthony Auger-Ottavi, Benoit Augier, Jean-Luc Autret, Stéphane Baert, Claude Balanant, Thierry Barbu, Grégoire Bert, Volker Bertram, Romuald Bomont, Elisabeth Bondu, Luc Boucharé, Abdel Boudraa, Alain Boulch, Patricia Boutin, Jérôme Caput, Gilbert Caruana, Christophe Claramunt, David Colleau, Philippe Corrignan, Marie Coz, Jean-Louis d'Arbaumont, Marc de Briançon, Geoffroy de Kersauson, Maïté de La Broïse, François Deniset, Yannick Descorde, Rodrigue Devoye, Sébastien Drouelle, Vianney Droulle, Anne-Cécile Fauchaux, Pierre Ferrant, Alberto Francescutto, Lancelot Frédéric, Jean-Michel Gahéry, Gédéon Gnimavo, Paola Gualeni, Dominique Hannart, Philippe Hello, Jean-Luc Herviou, Reinhard Jahn, Fred Jean, Olivier Jodon, Isabelle Knab-Delumeau, Stefan Krüger, Magalie Lamandé, Anne-Charlotte Lecat, Pascal Leclaire, Jean-François Leguen, Laurent Le Guen, David Lemestre, Yves-Marie Le Roy, Gwénaél Le Vaillant, Charles Lorieux, Benoît Lugan, Jean-Claude Marchadour, Philippe Martel, Carlo Martinelli, Sébastien Mayan, Patricia Merrien, Emmanuel Mogenicato, Pierre Mouneyrou, Marie-France Mulard, Tri-an Nguyen, Christophe Olmi, Eric Pagès, Nicola Petacco, Xavier Pitollat, Anne Pitois, Philip Pons, Patrice Pourchau, Jean-Yves Pradillon, Yves Préaux, Stéphane Priou, Hannes van Rijn, Christine Rohou, Kostia Roncin, Stéphanie Rouge, Patrick Soufflot, Jacques Stéphan, Ludovic Thisselin, Bastien Tribout, Naoya Umeda, Rémi Urchulotégui, Pierre Vonier, Clève Wandji, Sylvie Yeomans, Anneke, the crew of the Schooner *Etoile* and the CRNAV Members.

And of course Fernanda and Charlotte.

## OUTLINE

Abstract .....	5
Résumé.....	5
Acknowledgments.....	6
Outline.....	7
Introduction.....	10
Chapter 1. Second Generation Intact Stability Criteria.....	17
1.1. Pure Loss of Stability Failure Mode .....	17
1.1.1. Physical Background and General Information .....	17
1.1.2. Level One .....	19
1.1.3. Level Two .....	20
1.2. Parametric Roll Failure Mode .....	24
1.2.1. Historical and Physical Background .....	24
1.2.2. Level One .....	26
1.2.3. Level Two .....	27
1.2.4. Maximum Roll Angle and $KG_{max}$ computation.....	31
Chapter 2. Hydrostatic Computation .....	36
2.1. Generation of Volume Mesh .....	36
2.1.1. First Step .....	37
2.1.2. Second Step .....	38
2.2. Cutting a Volume Mesh by a Plane.....	41
2.2.1. Decomposition of Elementary Volumes.....	41
2.2.2. Cutting a Tetrahedron by a Plane.....	41
2.3. Finding the Balance Position.....	44
2.3.1. Definition of the Balance Position .....	44
2.3.2. Inclined-Ship Planes.....	44
2.3.3. Hydrostatic Computation in Calm Water .....	45
2.3.4. Hydrostatic Computation in Waves.....	46
2.3.5. Balance.....	47

2.3.6.	Calculation of Transverse Metacentric Height .....	49
Chapter 3.	Results .....	50
3.1.	Preliminary Information.....	50
3.1.1.	General Information .....	50
3.1.2.	Application to Military Vessels .....	50
3.1.3.	Graphic Design.....	51
3.2.	Pure Loss of Stability .....	52
3.2.1.	General Results.....	52
3.2.2.	Influence of the Watertight Deck Height .....	56
3.2.3.	Influence of Speed .....	59
3.3.	Parametric Roll.....	60
3.3.1.	General Results.....	60
3.3.2.	Focus on Second Check .....	66
3.3.3.	Influence of Speed .....	70
3.3.4.	Influence of Computation Parameters .....	72
3.3.5.	Comparison with 6-Degrees-of-Freedom Simulation.....	83
Chapter 4.	Energy Analysis of Parametric Roll .....	85
4.1.	Introduction .....	85
4.2.	Parametric Roll in Resonance Condition .....	85
4.2.1.	Equation of Parametric Roll.....	85
4.2.2.	Assumptions .....	86
4.2.3.	Distribution of Energy.....	87
4.2.4.	Direct Calculation of the Maximum Roll Angle in Resonance Condition .....	88
4.3.	Parametric Roll in Other Conditions .....	91
4.3.1.	Non-Synchronized Parametric Roll.....	91
4.3.2.	Lock-in Field .....	92
4.3.3.	Second and Third Modes of Parametric Roll .....	93
4.3.4.	Shift Angle in the Lock-in Field .....	95
4.3.5.	Width of the Lock-in Field.....	95
4.4.	Method Providing Steady-State Parametric Roll Amplitude at Any Speed.....	97
4.4.1.	Energy Method .....	97
4.4.2.	Improvement of the Energy Method .....	98

4.4.3. Application to Second Generation Intact Stability Criteria .....	98
Conclusion .....	102
Annex 1. Calcoque Software .....	108
Annex 2. Presentation of Ships .....	117
Annex 3. Mathematical Proofs.....	126
Annex 4. Ship-Fixed Coordinate System .....	136
Résumé étendu .....	137
Glossary .....	151
References.....	157

## INTRODUCTION

### *Context*

Since the first SOLAS Conference (Safety Of Life At Sea) in 1914 [10] resulting from the highly mediated sinking of the *Titanic*, the safety of people and goods on ships has been the subject of many discussions that have led to the establishment of rules that are applied to new ships and then verified by classification societies throughout the life of the ship. The main causes of major ship accidents are multiple:

- Insufficient stability, leading to capsize and then sinking or grounding;
- Flooding through a breach in the hull, due to a collision with the ground (*Salem Express* 1991 [55], *Sea Diamond* 2007, *Costa Concordia* 2012), another ship (*Andrea Doria* 1956 Figure 1) or a floating object (*Titanic* 1912, *Explorer* 2007 [61] Figure 2) or due to a military aggression (*Lusitania* 1915, *Wilhelm Gustloff* 1945);
- Fire on board leading to flooding and sinking or capsize (*Normandie/La Fayette* 1942, *Achille Lauro* 1994 [55]) or leading to high damages (*Hyundai Fortune* 2006, *MSC Flaminia* 2012 [63]);
- Structural damage breaking the ship's hull (*Erika* 1999 [56], *Prestige* 2002 [57], *MSC Napoli* 2007 [58], *MOL Comfort* 2013 [62]) or leading to flooding and capsize or sinking (*Estonia* 1994 [55]);

All these causes are the object of specific rules (intact stability, damage stability, structure, fire safety ...) with the aim to eliminate accidents and reduce their consequences.



Figure 1 – Passenger vessel *Andrea Doria* during sinking (photo from US Coast Guard).



Figure 2 – Passenger vessel *Explorer* during sinking (photo by Reinhard Jahn).

### *First Generation Intact Stability Criteria*

The first intact stability rules were defined in 1968 by the Inter-Governmental Maritime Consultative Organization (IMCO, which was renamed as International Maritime Organization, IMO, in 1982). These rules were given as recommendations in Resolution A.167 [14]. They are based on the work of Rahola [11] which consists of a statistical analysis of a large amount of ships recognized as safe or unsafe with regard to the stability in intact condition. The rules are presented as criteria regarding the righting lever curve (GZ curve) in calm water and cited hereunder:

- “(a) The area under the righting lever curve (GZ curve) should not be less than 0.055 meter-radians up to  $\theta=30^\circ$  angle of heel and not less than 0.09 meter-radians up to  $\theta=40^\circ$  or the angle of flooding  $\theta_f$  if this angle is less than  $40^\circ$ . Additionally, the area under the righting lever curve (GZ curve) between the angles of heel of  $30^\circ$  and  $40^\circ$  or between  $30^\circ$  and  $\theta_f$  if this angle is less than  $40^\circ$ , should not be less than 0.03 meter-radians.*
- (b) The righting lever GZ should be at least 0.20 m at an angle of heel equal to or greater than  $30^\circ$ .*
- (c) The maximum righting arm should occur at an angle of heel preferably exceeding  $30^\circ$  but not less than  $25^\circ$ .*
- (d) The initial metacentric height  $GM_0$  should not be less than 0.15 m.”*

These six criteria (the first is triple) are completed by two concerning passenger ships, regarding the crowding of passengers to one side and the angle of heel while turning.

In 1985, these criteria were completed by the weather criterion provided in Resolution A.562 [16]. This more-physical-based criterion considers the combined actions of beam wind (established and gust) and waves.

Today, these well-known criteria are mandatory and embedded in part A of the Intact Stability Code of the IMO [18].

### *A Long Series of Unexpected Accidents in Waves in Intact Stability Condition*

The entry into force of intact stability rules did not eliminate accidents of ships in such a configuration. Some accidents are due to the non-compliance with the rules after ship's conversion (*Al Salam Boccaccio 98* 2006, Figure 3), overloading (*Neptune* 1993 [55], *Joola* 2002) or insufficient cargo securing (*Ice Prince* 2008 [59]). Unfortunately, some other accidents occurred in intact configuration despite full compliance with the rules. It is not possible to list all of them here. Only few, having sufficiently robust report or analysis, are listed hereunder. In all cases, the ship was considered as safe with regard to the intact stability criteria (computed within the scope of a post-analysis for the oldest cases, since these criteria did not exist at that time) and was in heavy weather, often in following seas. Other similarities are the fateful consequences in terms of human lives or high financial damages.

- The 2000-ton cargo *Lohengrin* capsized in the Baltic Sea in January 1950, possibly due to a negative stability on a wave crest, combined to poor initial stability after conversion. The accident is reported by Krüger and Kluwe in [40].

- A 55-meter LPG tanker sank in the Mediterranean Sea in March 1969, killing her 17 crewmembers. Taylan provides a thorough analysis of this accident in [36]. As possible causes, he mentions a loss of stability in longitudinal waves or broaching.
- In October 1998, the 4832-TEU container vessel *APL China* suffered an unexpected extreme roll accident in the Northern Pacific (Figure 112 page 119). Almost 400 containers were lost overboard and 400 others were damaged, making this accident one of the most expensive (over \$50 million). The accident is reported in [41] and analyzed as due to parametric resonance in roll motion.
- Few years later, in January 2003, a similar accident occurred on the 4324-TEU container vessel *Maersk Carolina* (Figure 4) in the Northern Atlantic. 133 containers were lost overboard and 50 others were damaged. The accident is reported and analyzed in [45].
- A 12-meter fishing vessel suddenly capsized and sank off the Northern coast of Spain in June 2004, killing all ten members of her crew. A detailed analysis of the accident, including tests in a towing tank, is provided by Maron *et al.* in [37]. As possible cause, the authors mention a loss of stability on the wave crest combined with water shifting on the working deck.
- The pure car carrier *Cougar Ace* attained a severe heel angle in the Northern Pacific in July 2006 (Figure 5). This accident was not fatal in itself but one member of the salvage team died during rescue operations. The ship was recovered. However, the damages were high since all 5,000 cars were scrapped after being extracted from the inclined garage decks. The accident was due to an insufficient stability on the wave crest in following seas combined to a ballast movement. It is reported by Krüger and Kluwe in [40].
- The Ro-Ro Vessel *Finnbirch* capsized and sank in the Baltic Sea in November 2006, killing two of her seamen (Figure 6). The accident is reported by Kluwe and Krüger in [38] and thoroughly analyzed by the Swedish Accident Investigation Board (SHK) in its report [39]. As main causes of the accident, SHK wrote “Finnbirch was on an unfavourable course at an unfavourable speed in a sea with high and long waves which resulted in a loss of stability with considerable but not exceptional heelings and a subsequent shifting of the cargo. The securing of the cargo on board was unsatisfactory.”

Moreover, several recommendations are formulated, as usual in such an official report. The first one is “SHK recommend that the Swedish Maritime Administration propose that stability requirements for ships with a following sea should be entered into the relevant international rules and regulations”.

- In September 2008, the 8749-TEU container vessel *Chicago Express* (Figure 114 page 120) suffered a violent roll accident during a typhoon off the coast of Hong Kong, killing one seaman and seriously injuring her master. The accident is reported and analyzed in [60]. One of the causes given by the experts is the insufficient roll damping. Moreover, the metacentric height was equal to 7.72 m, which is an unusually high value for this type of ship.



Figure 3 – Passenger vessel *Al Salam Boccacio 98* (photo by Carlo Martinelli from [www.shipspotting.com](http://www.shipspotting.com)).



Figure 4 – Container Vessel *Maersk Carolina* (photo by Hannes van Rijn from [www.shipspotting.com](http://www.shipspotting.com)).



Figure 5 – Pure Car Carrier *Cougar Ace* with severe heel on port side (photo from National Digital Library of the United States Fish and Wildlife Service).



Figure 6 – Ro-Ro vessel *Finnbirch* during sinking (photo by Swedish Maritime Administration).

### *Genesis of the Second Generation Criteria*

This type of accidents highlights the insufficiency of the intact stability criteria in some configurations of sailing in waves and has led the IMO to start developing new criteria focusing on these conditions. The work started in 2007 with the aim to define new intact stability criteria, also named “second generation intact stability criteria”. The work is performed by the Working Group on Intact Stability (WGIS) during the sessions of the Sub-Committee on Stability and Load Lines and on Fishing Vessels Safety (SLF, nowadays the Sub-Committee on Ship Design and Construction, SDC) of the IMO. In 2008, a correspondence group (ISCG) was created to continue working between sessions. The author of this thesis is a member of the Delegation of France in the correspondence group. The development of the second generation intact stability criteria is the topic of a large amount of scientific papers, most of which are presented in conferences and workshops dedicated to ship stability [25, 26, 27, 28, 29, 30, 31, 32, 33, 34, 35 and many others]. As related by Francescutto [34], it was decided to focus on the five following possible stability failures:

- Pure loss of stability due to reduced righting lever on a wave crest in following or stern quartering seas, leading to excessive heel angle or capsize;

- Parametric resonance in roll motion, due to variation of righting lever in waves;
- Broaching, i.e. excessive heel angle or capsize due to loss of course-keeping ability in surf-riding condition;
- Dead ship condition, i.e. ship without propulsion in beam waves and wind;
- Excessive accelerations in roll motion.

Moreover, it was decided to structure these new rules in a three-level approach with:

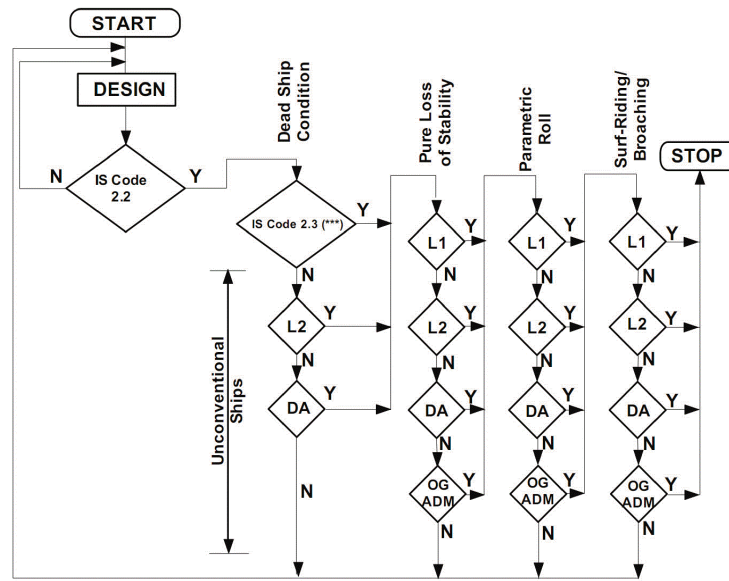
- A first level of assessment, based on a simplified physical and deterministic approach of the phenomena, eventually requiring basic hydrostatic computations and consequently ensuring large safety margins.
- A second level of assessment, based on a more-accurate physical analysis of the phenomena and considering hydrostatics in waves through a probabilistic approach. Hence, safety margins are expected to be reduced.
- A direct assessment, consisting in numerical simulations of the ship's behavior in waves and presumably allowing more awareness about safety margins.

Although this is not clearly written in the future regulation, the first level should be implemented by any shipyard or naval architect since it requires no specific tool. The second level should be implemented by shipyards or naval architects equipped with adequate stability software (presumably currently under development) since only specialized institutes would be able to perform direct assessment because of both the highly-specialized personnel and the specific computing tools it requires.

A ship that would not pass the first level criteria is designated as “unconventional” by the future regulation (Figure 7). In order to comply with future rules, a ship must comply with the current rules [18] and with at least one level of each failure mode (Figure 7). Like the current criteria, the future ones are intended for ships longer than 24 meters and not intended for naval ships, for which the corresponding regulation is imposed by the state, also ship-owner.

Nowadays, the first-and-second-level criteria of all five failure modes are fully defined in SDC 2/WP.4 and SDC 3/WP.5 [respectively 22 and 23]. Because of their relatively high complexity compared to the current intact stability criteria [18], the definition of level-one and level-two criteria is enriched by explanatory notes in SDC 3/WP.5 [23] providing explanations, comments, guidelines and calculation methods. Table 1 lists where to find the definition of level-one and level-two criteria of the five failure modes and their associated explanatory notes.

The direct assessment is currently under development and expected to be reported as draft guidelines at the 4<sup>th</sup> session of the Sub-Committee on Ship Design and Construction (SDC4) in the beginning of 2017 and finalized at the 5<sup>th</sup> session (2018). The second generation intact stability criteria are expected to enter into force firstly on part B as recommendations at the earliest in 2019. Umeda and Francescutto provide the current status of the development of the second generation intact stability criteria in [35].



\*\*\* = WeC possibly amended with steepness table from MSC.1/Circ.1200

Figure 7 – Future intact stability regulation (from Bulian and Francescutto [28]).

	Pure loss of stability	Parametric roll	Broaching	Dead ship condition	Excessive acceleration
Definition of criteria (level one and level two)	SDC 2/WP.4 Annex 1	SDC 2/WP.4 Annex 2	SDC 2/WP.4 Annex 3	SDC 3/WP.5 Annex 1	SDC 3/WP.5 Annex 2
Explanatory notes	SDC 3/WP.5 Annex 3	SDC 3/WP.5 Annex 4	SDC 3/WP.5 Annex 5	SDC 3/WP.5 Annex 6	SDC 3/WP.5 Annex 7

Table 1 – References of new intact stability criteria and the associated explanatory notes.

### Objective

Both pure loss of stability and parametric roll failure modes are consequences of the variation of the restoring moment in longitudinal waves. The former is a single-wave effect since the latter is due to the repetition of the encounter of the waves. However, both require the same tool to compute the restoring moment in waves.

The aim of the work performed within the scope of this to analyze the requirement and the relevance of the first- and second-level criteria of both failure modes. This requires to implement these criteria in a computer code able to perform computation in longitudinal waves. Calcoque software is used for this. This hydrostatic tool is developed and used at the French Naval Academy for academic and research activities. Hence, the first part of the work consists in rendering it able to perform hydrostatic computations in longitudinal waves and then implement the level-one and level-two criteria of pure loss of stability and parametric roll failure modes.

The criteria are computed for several ships of different types, both civilian and military, selected for their different expected behaviors with regard to both failure modes. Since the aim of the work is to evaluate criteria rather than ships, considering the loading conditions of ships does not matter as long as criteria are computed in the usual range of ships' displacement or draft. Consequently, results are provided as  $KG_{max}$  curves, giving the

maximum height of the center of gravity with regard to a specific criterion (or a set of criteria) as a function of the displacement or the draft.

Usually,  $KG_{\max}$  curves are included in the stability booklet. They allow the crew to assess the stability with regard to the regulation applied to the ship without any complex computation rather than KG. Here, considering  $KG_{\max}$  curves allows the comparison of the requirement of the criterion of each level and the comparison of different computation methods proposed for a specific criterion in order to determine the efficiency and the relevance of the new criteria. It also allows comparing the requirement of the new criteria with that of the current intact stability rules applied on the considered vessel. Although this is not the aim here, the comparison of the requirement of both current and new criteria allows assessing the vulnerability of the ship with regard to the considered failure mode.

### ***Outline***

The first chapter provides a presentation of the second generation criteria of level one and level two of both pure loss of stability and parametric roll failure modes. In particular, the method used in this thesis to compute the second check of level-two parametric roll criterion is thoroughly detailed.

The second chapter describes the main algorithms used in the Calcoque software to compute the equilibrium, the metacentric height and the righting arm in both calm water and longitudinal static waves. A general presentation of the software and its uses at the French Naval Academy and onboard several French Navy ships is provided in Annex 1. All geometric considerations are made in a unique ship-fixed coordinate system presented in Annex 4.

The third chapter provides results of future criteria of both pure loss of stability and parametric roll failure modes applied to six civilian vessels and three military vessels. It also proposes a focus on the second check of the parametric roll level-two criterion, which has an unusual behavior compared to other current and future criteria. The influence of the ship's speed is analyzed. The application of second generation intact stability criteria to naval vessels is argued in this chapter. The nine selected vessels are presented in Annex 2.

The second check of level-two criterion of parametric roll requires the computation of the maximum roll angle in resonance condition. Since both methods proposed by the future regulation are relatively complex to implement, the fourth and last chapter proposes an alternative method based on an energy analysis of the phenomenon and assuming a linear righting lever. This method is close to the analysis of parametric roll proposed by Kerwin in 1955 [12]. The associated mathematical proofs are deported in Annex 3.

The symbols used in this thesis are defined twice, inline when appearing for the first time and gathered in a glossary proposed in page 151. They are in accordance with the recommendations of the International Towing Tank Conference (ITTC, [71]) except the draft, denoted by  $d$  instead of  $T$ , for consistency with the text of both the current and future regulations [18, 22 and 23].

## CHAPTER 1. SECOND GENERATION INTACT STABILITY CRITERIA

### 1.1. PURE LOSS OF STABILITY FAILURE MODE

#### 1.1.1. Physical Background and General Information

##### *Physical Background*

When a ship is sailing in waves, the geometry of the submerged part of her watertight volume significantly changes. In longitudinal waves, i.e. in pure head seas or following seas, there is no transverse excitation. Hence, any transverse stability problem other than that in still water could be overlooked. However, the geometry of the waterplane, which is no longer flat, also significantly changes. Hence, its inertia and the associated metacentric heights vary with the wave encounter. Consequently, a risk of insufficient transverse stability exists possibly leading to large heel angle or even to capsizing.

Figure 8 shows the GZ curves in waves and in calm water computed for the C11 container vessel (presented in Annex 2) at a draft equal to 12 m and a KG equal to 18 m. The wave is sinusoidal and longitudinal. Its length is equal to the ship's length (262 m) and its height is equal to 8.75 m, corresponding to a wave steepness (i.e. ratio height over length) equal to 0.0334 (this value is proposed in the future regulation and is presented in this chapter). Ten positions of the ship relative to the wave are considered. Both curves corresponding to the maximum and minimum metacentric height (GM) in waves are colored in red (the dashed one corresponds to the minimum GM). Maximum and minimum values of the GM are respectively equal to 5.07 m and 0.31 m. The average value of the GM in waves is equal to 2.62 m since the GM in calm water (solid blue curve) is equal to 2.22 m.

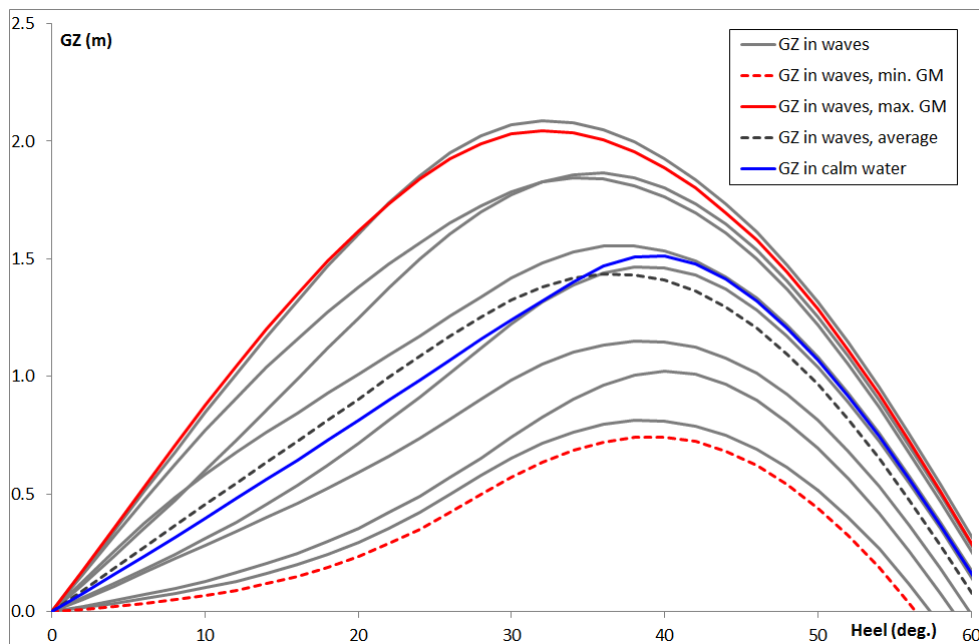


Figure 8 – GZ in waves and in calm water.

### *Influence of the Hull Form*

The displacement volumes corresponding to the maximum and minimum GM are respectively shown in Figure 9 and Figure 10. The hull is wall-sided amidships and flare-sided at the bow and at the stern (see Figure 110 in Annex 2 page 119). In Figure 9, the wave crests are centered at the bow and the stern. The waterplane area is larger than that in still water and so is its inertia. The associated GM is thus increased. In Figure 10, the wave crest is centered amidships. The waterplane area and its inertia are lower than in still water. Thus, the corresponding GM is also lowered.

Consequently, the hull form has a direct effect on the GM variation in longitudinal waves. The more the hull is flared at the bow and at the stern, the larger the GM variation is. A ship having a wall-sided hull over a major part of its length, such as the tanker presented in Annex 2, would have a low GM variation in waves and would thus be expected not to be vulnerable to the pure loss of stability.

Moreover, it is expected that the most critical wave has a length almost equal to the ship's length. In other configurations, the wave steepness seen along the hull is reduced (causing low GM variation) and the ship only pitches in long waves or surges in short waves.

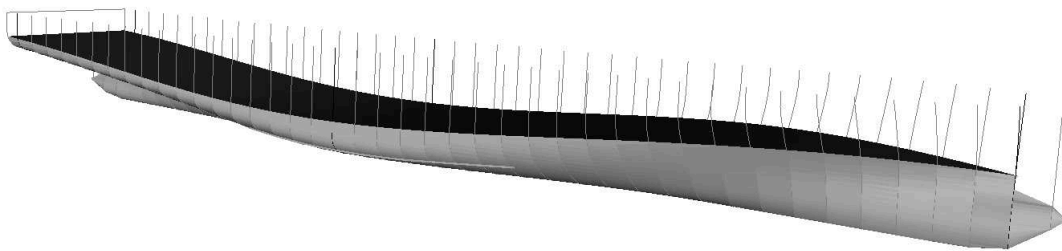


Figure 9 – Displacement volume corresponding to the maximum GM in waves.

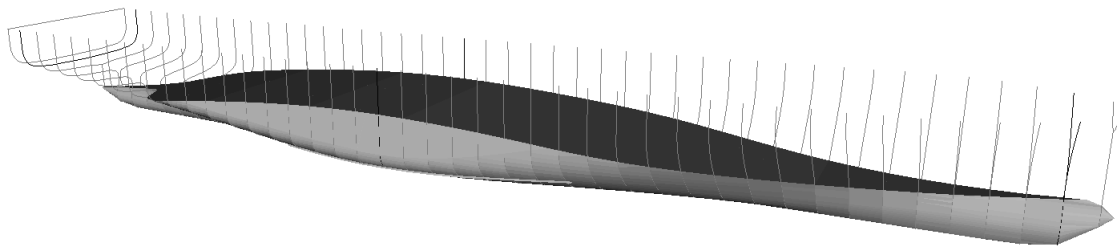


Figure 10 – Displacement volume corresponding to the minimum GM in waves.

### *Influence of the Speed*

Even if the GM reduction occurring when the wave crest is centered amidships is large, the ship should not capsize or even attain a large heel angle if the time in this critical configuration is too short. This time is function of the wave encounter frequency. Consequently, the ship's speed also has a great importance in the phenomenon. To maximize the time in the critical configuration, the ship must be in following seas at a speed equal to that of the wave crests. Hence, the corresponding Froude number is 0.4. The phenomenon cannot occur in head waves and should be reduced if the ship is clearly unable to attain a speed corresponding to such a Froude number. That is why these new criteria are intended for ships having a service speed Froude number larger than 0.24.

### 1.1.2. Level One

#### *General Principles*

The first level criterion of pure loss of stability failure mode considers waves having a steepness  $S_w$  equal to 0.0334. This value is calculated from the wave scatter diagram taken from recommendation 34 of the International Association of Classification Societies (IACS, [69]). The calculation method is described in the explanatory notes of the future regulation (SDC 3/WP.5, Annex 4, Appendix 1, [23]).

The minimum transverse metacentric height in waves (denoted by  $GM_{min}$ ) must be higher than 5 centimeters. Two methods are proposed to calculate its value.

#### *First Method*

The first method considers that the moment of inertia of the waterplane area in waves is equal to that of the parallel waterplane area in calm water at a lowest draft (denoted by  $d_L$ ) as shown in Figure 11 (the waterplane at lowest draft is the grey area). The lowest draft  $d_L$  is calculated as follows:

$$d_L = d - \left( d - 0.25d_{full}; \frac{LS_w}{2} \right) \quad (1)$$

With:

- d (m) draft corresponding to the considered loading condition in calm water (black line in Figure 11);
- $d_{full}$  (m) draft, full load;
- L (m) ship's length;
- $S_w$  0.0334 wave steepness.

In most cases, the lowest draft can be simplified as follows:

$$d_L = d - \frac{LS_w}{2} \quad (2)$$

Then, the minimum metacentric height in waves is calculated as follows:

$$GM_{min} = KB + \frac{I_L}{\nabla} - KG \quad (3)$$

With:

- KB (m) height of the vertical center of buoyancy in calm water;
- $I_L$  ( $m^4$ ) moment of inertia of the water-plane area at lowest draft  $d_L$  (grey area in Figure 11);
- $\nabla$  ( $m^3$ ) volume of displacement;
- KG (m) height of the vertical center of gravity.

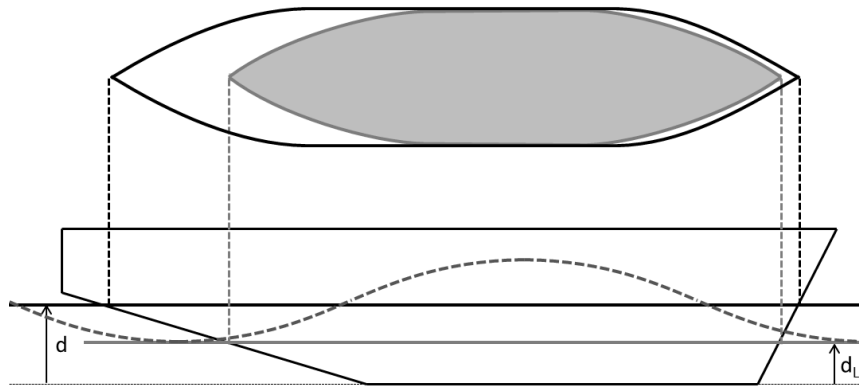


Figure 11 – Parallel waterplane at lowest draft  $d_L$ .

### Second Method

The second method consists of computing the minimum metacentric height of the ship balanced in trim and sinkage on sinusoidal waves. The wave length is equal to the ship's length  $L$  and the height is  $h=S_W L$ . The wave crest is centered at the longitudinal center of gravity and at each  $L/10$  forward and aft thereof.

#### 1.1.3. Level Two

##### General Principle

The second level consists of a probabilistic approach of the phenomenon associated with a wave scattering table. For an unrestricted sailing area, the new regulation imposes that included in the IACS Recommendation 34 corresponding to the Northern Atlantic (Table 2, from [69]). In this table, which lists 16 wave periods and 17 wave heights, 197 waves have a non-zero number of occurrence. The new regulation allows using another wave scattering table if the ship is sailing in a restricted area.

$H_s$ (m)	Zero-crossing period, $T_z$ (s)															
	3.5	4.5	5.5	6.5	7.5	8.5	9.5	10.5	11.5	12.5	13.5	14.5	15.5	16.5	17.5	18.5
0.5	1.3	133.7	865.6	1186	634.2	186.3	36.9	5.6	0.7	0.1	0	0	0	0	0	0
1.5	0	29.3	986	4976	7738	5569.7	2375.7	703.5	160.7	30.5	5.1	0.8	0.1	0	0	0
2.5	0	2.2	197.5	2158.8	6230	7449.5	4860.4	2066	644.5	160.2	33.7	6.3	1.1	0.2	0	0
3.5	0	0.2	34.9	695.5	3226.5	5675	5099.1	2838	1114.1	337.7	84.3	18.2	3.5	0.6	0.1	0
4.5	0	0	6	196.1	1354.3	3288.5	3857.5	2685.5	1275.2	455.1	130.9	31.9	6.9	1.3	0.2	0
5.5	0	0	1	51	498.4	1602.9	2372.7	2008.3	1126	463.6	150.9	41	9.7	2.1	0.4	0.1
6.5	0	0	0.2	12.6	167	690.3	1257.9	1268.6	825.9	386.8	140.8	42.2	10.9	2.5	0.5	0.1
7.5	0	0	0	3	52.1	270.1	594.4	703.2	524.9	276.7	111.7	36.7	10.2	2.5	0.6	0.1
8.5	0	0	0	0.7	15.4	97.9	255.9	350.6	296.9	174.6	77.6	27.7	8.4	2.2	0.5	0.1
9.5	0	0	0	0.2	4.3	33.2	101.9	159.9	152.2	99.2	48.3	18.7	6.1	1.7	0.4	0.1
10.5	0	0	0	0	1.2	10.7	37.9	67.5	71.7	51.5	27.3	11.4	4	1.2	0.3	0.1
11.5	0	0	0	0	0.3	3.3	13.3	26.6	31.4	24.7	14.2	6.4	2.4	0.7	0.2	0.1
12.5	0	0	0	0	0.1	1	4.4	9.9	12.8	11	6.8	3.3	1.3	0.4	0.1	0
13.5	0	0	0	0	0	0.3	1.4	3.5	5	4.6	3.1	1.6	0.7	0.2	0.1	0
14.5	0	0	0	0	0	0.1	0.4	1.2	1.8	1.8	1.3	0.7	0.3	0.1	0	0
15.5	0	0	0	0	0	0	0.1	0.4	0.6	0.7	0.5	0.3	0.1	0.1	0	0
16.5	0	0	0	0	0	0	0	0.1	0.2	0.2	0.2	0.1	0.1	0	0	0

Table 2 – IACS wave scatter diagram (from [69]).

The ship is found to be non-vulnerable to the pure loss of stability if both values of CR1 and CR2 are lower than  $R_{PL0}=0.06$ . CR1 and CR2 are computed as follows:

$$CR1 = \sum_{i=1}^{197} W_i C1_i \qquad CR2 = \sum_{i=1}^{197} W_i C2_i \qquad (4)$$

With:

- $W_i$  weighting factor of the wave number  $i$  taken from Table 2 (number of occurrences divided by 100,000);
- $C1_i$  coefficient for the wave number  $i$  regarding the minimum angle of vanishing stability  $\Phi_{V,\min}$  (Figure 12);
- $C2_i$  coefficient for the wave number  $i$  regarding the maximum angle of stable equilibrium  $\Phi_{S,\max}$  under action of a heeling lever  $R_{PL3}$  (Figure 12).

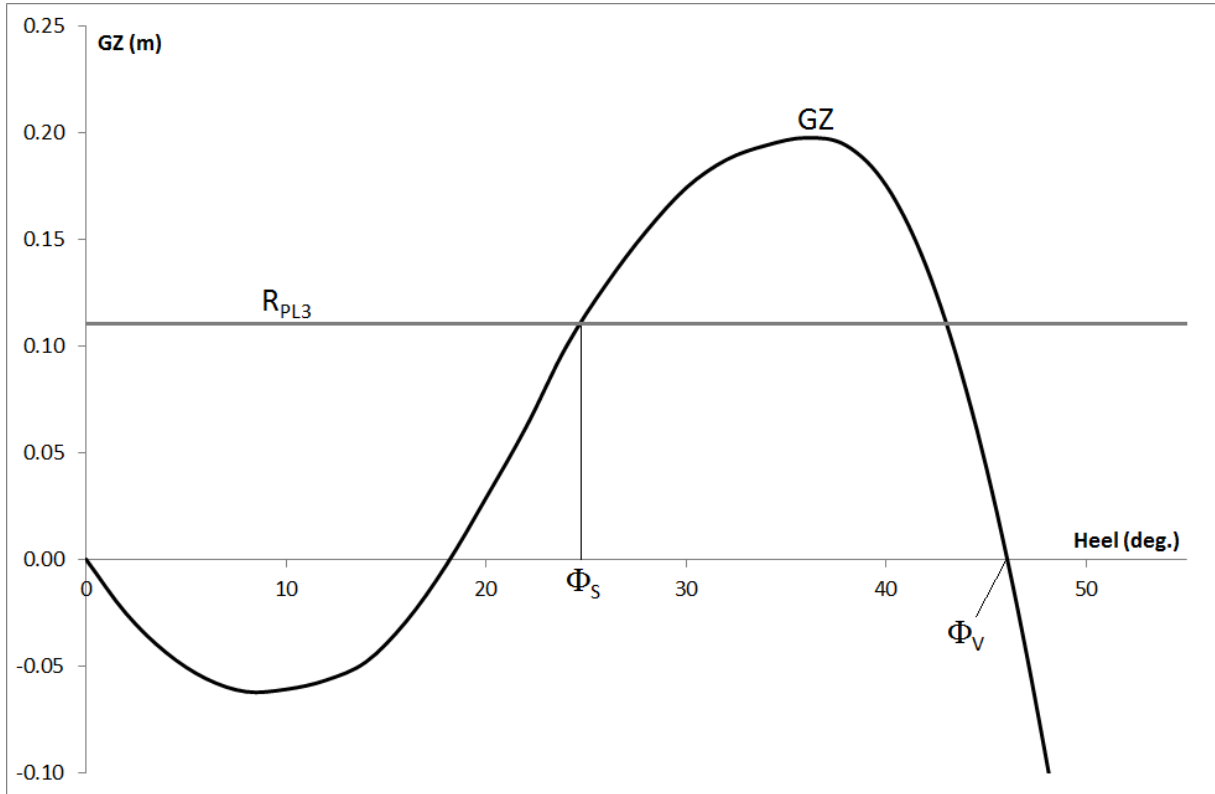


Figure 12 – Righting arm curve on static wave with angle of stable equilibrium under heeling lever  $R_{PL3}$  ( $\Phi_S$ ) and angle of vanishing stability ( $\Phi_V$ ).

Waves are supposed to be sinusoidal. Their height is from Table 2 ( $H_s$  is twice the wave amplitude). Their length  $\lambda$  is linked to their zero-crossing period  $T_z$  (Table 2) by the infinite-depth relation:

$$\lambda = \frac{gT_z^2}{2\pi} \qquad (5)$$

For each wave, the heeling lever  $R_{PL3}$  is defined as follows:

$$R_{PL3} = 8 \frac{H_s}{\lambda} d F_n^2 \qquad (6)$$

The minimum angle of vanishing stability ( $\Phi_{V,\min}$ ) and the maximum angle of stable equilibrium ( $\Phi_{S,\max}$ ) are computed for the 197 non-zero-weighted waves of the wave scatter diagram and used to calculate  $C1_i$  and  $C2_i$  as follows:

$$C1_i = \begin{cases} 1 & \text{if } \Phi_{V.min} < R_{PL1} \\ 0 & \text{otherwise} \end{cases} \quad C2_i = \begin{cases} 1 & \text{if } \Phi_{S.min} > R_{PL2} \\ 0 & \text{otherwise} \end{cases} \quad (7)$$

With:

$R_{PL1}$  30 degrees;

$R_{PL2}$  25 degrees (15 degrees for passenger vessels).

### ***Effective Wave Height Concept***

Since the number of non-zero-weighted waves is large, the new regulation proposes a method to make the computation faster. This method is based on the effective wave height concept proposed by Grim [65]. For each wave of the scattering diagram (Table 2) defined by its zero-crossing period ( $T_z$ ) and significant height ( $H_s$ ), this method consists in computing an effective height of the 3% highest waves  $H_{3\%eff}$  corresponding to an equivalent wave whose length  $\lambda$  is equal to the ship's length  $L$ . This effective wave provides the ship with the same energy than the original wave.

The effective wave height is calculated according to the following formulae:

$$H_{3\%}^{eff} = 5.9725\sqrt{m_0} \quad (8)$$

$$m_0 = \int_{0.01\omega_L}^{3\omega_L} \left\{ \frac{\frac{\omega^2 L}{g} \sin\left(\frac{\omega^2 L}{2g}\right)}{\pi^2 - \left(\frac{\omega^2 L}{2g}\right)^2} \right\}^2 A \omega^5 \exp(-B\omega^{-4}) d\omega \quad (9)$$

$$A = 173H_s^2 T_{01}^{-4} \quad (10)$$

$$B = 691T_{01}^{-4} \quad (11)$$

$$T_{01} = 1.086T_z \quad (12)$$

$$\omega_L = \sqrt{\frac{2g\pi}{L}} \quad (13)$$

Table 3 gives the effective wave heights computed according to this method for some vessels described in Annex 2 and associated to the waves of Table 2 having a zero-crossing period ( $T_z$ ) equal to 10.5 seconds.

For a given ship, all effective waves have the same length. We consider 11 effective waves having a height from zero to the maximum effective height corresponding to the length and all wave cases of the considered scatter diagram (Table 2). The minimum angle of vanishing stability ( $\Phi_{V.min}$ ) and the maximum angle of stable equilibrium ( $\Phi_{S.max}$ ) are pre-calculated for these 11 waves. This requires the computation of one GZ curve in calm water for the first effective wave whose height is equal to zero. For each of the 10 other effective wave heights, this requires the computation of 10 GZ curves considering the ship balanced in trim and sinkage and for the wave crest centered at the longitudinal center of gravity and at each  $\lambda/10$  forward and aft thereof.

Then, the values of  $\Phi_{V.min}$  and  $\Phi_{S.max}$ , required to calculate coefficients  $C1_i$  and  $C2_i$  associated to all wave cases of the scatter diagram, are simply calculated by linear interpolation in the interval formed by 2 successive values of the 11 previously considered effective heights.

H <sub>s</sub> (m)	DTMB-5415 L=142m	Container L=262m	Container L=319m	Ro-Ro L=135m	Tanker L=227.5m
0.5	0.430	0.539	0.538	0.417	0.526
1.5	1.289	1.618	1.614	1.251	1.579
2.5	2.149	2.697	2.691	2.085	2.631
3.5	3.008	3.776	3.767	2.919	3.683
4.5	3.868	4.855	4.843	3.753	4.736
5.5	4.727	5.934	5.919	4.587	5.788
6.5	5.587	7.013	6.996	5.421	6.841
7.5	6.446	8.092	8.072	6.255	7.893
8.5	7.306	9.171	9.148	7.089	8.945
9.5	8.165	10.250	10.225	7.923	9.998
10.5	9.025	11.329	11.301	8.757	11.050
11.5	9.884	12.408	12.377	9.591	12.103
12.5	10.744	13.487	13.453	10.425	13.155
13.5	11.603	14.566	14.530	11.258	14.207
14.5	12.463	15.645	15.606	12.092	15.260
15.5	13.322	16.724	16.682	12.926	16.312
16.5	14.182	17.803	17.758	13.760	17.365

Table 3 – Effective height of the 3% highest waves (m) for a zero-crossing period equal to 10.5 seconds.

## 1.2. PARAMETRIC ROLL FAILURE MODE

### 1.2.1. Historical and Physical Background

#### *Simplified Approach*

As previously shown in pure loss of stability failure mode, the restoring moment and the transverse metacentric height of a ship change while sailing in longitudinal waves. This phenomenon may occur to a lesser extent in quartering seas. Although longitudinal waves provide no transverse excitation, an amplification of the roll motion is possible if the wave encounter repeats the variation of restoring moment during a sufficiently long time in some particular conditions.

This phenomenon can appear if the GM variation frequency (equal to the roll encounter frequency) is twice the ship's natural roll frequency. If a ship rolls while the wave trough is centered amidships, the resulting increased GM provides a strong restoring moment and greatly accelerates the ship to the opposite side. As the ship approaches the upright position, her position in wave has changed and the wave crest is now centered amidships, reducing the restoring moment. Due to her inertia and roll speed, the ship rolls further to the opposite side, assuming the damping has a moderate effect. Then, the ship attains her maximum roll angle on this side when the next wave trough arrives amidships, repeating the cycle.

This simplified approach shows the conditions of appearance of parametric roll:

- The ship sails in head or following seas, possibly in bow or stern-quartering seas.
- The wave encounter frequency is twice the ship's natural roll frequency.
- The hull geometry provides sufficient restoring moment variation in longitudinal waves.
- The roll damping has a moderate effect.

#### *Historical background*

Parametric roll is a sort of parametric resonance, also called parametric pumping. This phenomenon is characteristic of oscillating systems having variations in their stiffness constant. It has long been known in several scientific domains. Since Galeazzi recently provided a detailed historical review in his thesis [47], we quote here only few important references.

Parametric pumping was already known and used in the Middle Ages. Known under the name of "O Botafumeiro", a 170-kg censer hangs in the transept of the cathedral of Santiago de Compostela (Spain). Its pendulum motion is excited by eight men using a cylinder varying the length of the rope. Sanmarin provides a detailed mechanical and mathematical analysis of this ingenious system [15].

In the 19<sup>th</sup> Century, parametric resonance was studied by mathematicians and naval architects [8 and 9]. In [9], Mathieu laid the basis of the mathematical analysis of this phenomenon. His name was given to the differential equation that governs it:

$$\frac{d^2x}{dt^2} + \omega_0^2(1 + \varepsilon_0 \cos t) = 0 \quad (14)$$

Parametric resonance is also used in optical oscillators as demonstrated by Giordmaine and Miller [13].

In 1955, Kerwin provided a detailed analysis of the parametric resonance applied to the roll motion of ships [12]. As he recognized, his mathematical work had no practical application on ships at that time.

However, Kerwin was visionary and parametric roll was highlighted a few decades later by several accidents on large container vessels. In particular, the *APL China* suffered from a severe parametric roll accident in the Northern Pacific Ocean in October 1998 [41]. This unexpected accident has been extensively studied and is part of the bases of the new generation criteria. Figure 112 page 119 shows some damage resulting from this accident.

Several similar accidents have occurred since that date, such as that of the *Maersk Carolina* in the Northern Atlantic in January 2003 [45] (Figure 4 page 13).

Although this phenomenon has become well-known by ship-masters, ship-owners and naval architects nowadays, it generates high safety and financial risk (respectively over \$50 million and \$4 million for the accidents that occurred on *APL China* and *Maersk Carolina*). Hence, it is one of the five failure modes considered in the new intact stability criteria developed by the IMO.

### ***Modes of Parametric Resonance***

Parametric resonance exists when the constant stiffness of the considered system varies according to a frequency that is twice a sub-multiple of the natural oscillating period of the system:

$$\omega_e = \frac{2}{n} \omega_0 \quad (15)$$

With:

$n$  - mode of parametric resonance: 1, 2, 3, 4, ...;

$\omega_e$  (rad/s) frequency of variation of the stiffness constant of the considered system;

$\omega_0$  (rad/s) natural frequency of the considered system.

Applied to the roll motion of a ship in longitudinal waves, the stiffness constant is the metacentric height (GM) and varies with the wave encounter frequency ( $\omega_e$ ) while  $\omega_0$  is the ship's natural roll frequency.

Hence, the first mode of parametric resonance occurs when the encounter frequency is twice the ship's natural roll frequency. The second mode occurs when both frequencies are equal and the third mode when the encounter frequency is 2/3 of the roll frequency.

Parametric resonance is stronger at first mode and decreases as the mode increases. Consequently, the first mode of parametric roll, occurring when the encounter frequency is twice the natural roll frequency, provides the largest risk for the ship and is considered prior.

## 1.2.2. Level One

### *General Principles*

While the pure loss of stability failure mode is a single-wave incident, the parametric roll results from the encounter of similar waves (having almost the same period) during a sufficiently long time to allow a significant amplification of the roll motion. Consequently, the considered wave height is reduced to that of the 1/3 highest waves instead of 3%. The associated wave steepness ( $S_W$ ) is equal to 0.0167 (instead of 0.0334 in pure loss of stability). This value is also calculated from the wave scatter diagram taken from the IACS recommendation number 34 with the same method than that of pure loss of stability (see SDC 3/WP.5, Annex 4, Appendix 1, [23]).

The first level of parametric roll requires that the non-dimensional amplitude of the variation of the metacentric height in waves ( $\Delta GM/GM$ ) is less than a coefficient  $R_{PR}$ . This coefficient depends largely on bilge keel area and to a lesser extent on the midship section coefficient (denoted by  $C_m$ ). The calculation method is described in SDC 2/WP.4 (Annex 2, [22]). The value of  $R_{PR}$  is comprised between 0.17 (ship with no bilge keels) and 1.87 (ships with large bilge keels).

The new regulation proposes two methods to calculate the variation of metacentric height in waves (denoted by  $\Delta GM$ ). They are described hereunder.

### *First Method*

The first method of level-one criterion of parametric roll failure mode is similar to that of pure loss of stability. Here, the first method considers that the minimum and maximum moments of inertia of the waterplane area in waves are respectively equal to that of parallel waterplanes at a lowest draft  $d_L$  (Figure 11 page 20, grey area) and at a highest draft  $d_H$  (Figure 13 page 27, dashed line). Both drafts are calculated as follows:

$$d_L = d - \min\left(d - 0.25d_{full}; \frac{LS_W}{2}\right) \quad d_H = d + \min\left(D - d; \frac{LS_W}{2}\right) \quad (16)$$

$d$  (m) draft corresponding to the loading condition;

$d_{full}$  (m) draft, full load;

$D$  (m) ship's depth;

$L$  (m) ship's length;

$S_W$  0.0167 wave steepness.

In most of cases, both drafts can be simplified:

$$d_L = d - \frac{LS_W}{2} \quad d_H = d + \frac{LS_W}{2} \quad (17)$$

Then, the amplitude of the variation of the metacentric height in waves is calculated as follows:

$$\Delta GM = \frac{I_H - I_L}{2V} \quad (18)$$

With:

- $I_H$  ( $m^4$ ) moment of inertia of the parallel waterplane associated with the highest draft  $d_H$ ;
- $I_L$  ( $m^4$ ) moment of inertia of the parallel waterplane associated with the lowest draft  $d_L$ ;

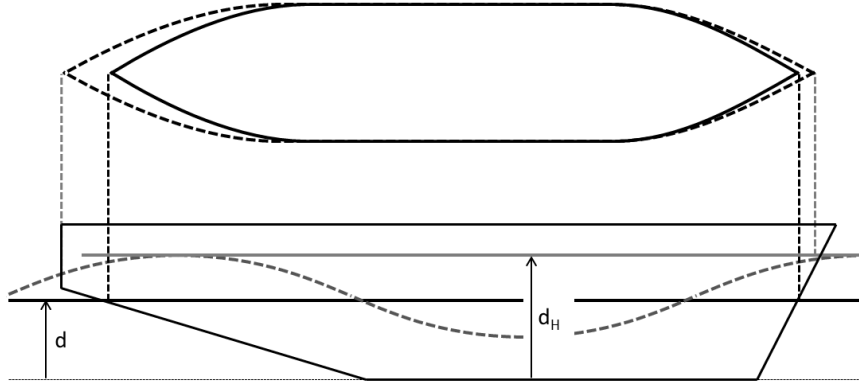


Figure 13 – Parallel waterplane at highest draft  $d_H$ .

### **Second Method**

The second method consists in computing 10 metacentric heights of the ship balanced in trim and sinkage in sinusoidal waves. The wave length is equal to the ship's length  $L$  and the height is  $h=S_wL$ . The wave crest is centered at the longitudinal center of gravity and at each  $L/10$  forward and aft thereof. The minimum and maximum values of  $GM$  are used to calculate  $\Delta GM$  as follows:

$$\Delta GM = \frac{GM_{max} - GM_{min}}{2} \quad (19)$$

### **1.2.3. Level Two**

The parametric roll level-two is divided in two checks marked C1 and C2, consisting of two independent probabilistic approaches of the phenomenon. The ship is found to be non-vulnerable to parametric roll if any of the values of C1 and C2 are lower than  $R_{PRO}=0.06$ .

#### **First Check**

The first check considers a shortlist of weighted waves calculated from the chosen wave scatter diagram according to the method described in the explanatory notes of the future regulation (SDC 3/WP.5 [23]). Table 4 shows this wave list calculated from the IACS wave scatter diagram [69] shown in Table 2.

The value of the C1 coefficient, associated with the first check, is computed as follows:

$$C1 = \sum_{i=1}^{16} W_i \cdot C_i \quad (20)$$

$W_i$  is the wave weighting factor from the shortlist (Table 4).  $C_i$  is equal to 0 if any of the conditions A or B is satisfied, 1 otherwise.

Condition A is:

$$GM_i > 0 \quad \text{And} \quad \frac{\Delta GM_i}{GM_i} < R_{PR} \quad (21)$$

With:

$GM_i$  (m) average value of the 10 metacentric heights computed for wave number  $i$ , with the wave crest centered at the longitudinal center of gravity and at each  $\lambda_i/10$  forward and aft thereof;

$\Delta GM_i$  (m) half of the difference between the maximum and the minimum values of the 10 metacentric heights.

Condition B is:

$$V_{PR.i} > V_S \quad \text{With} \quad V_{PR.i} = \left| \frac{2\lambda_i}{T_0} \sqrt{\frac{GM_i}{GM_0}} - \sqrt{\frac{g\lambda_i}{2\pi}} \right| \quad (22)$$

And:

$V_S$  (m/s) ship's speed;

$V_{PR.i}$  (m/s) reference speed corresponding to the first mode of parametric roll (encounter frequency is twice the ship's natural roll frequency); the relationship which gives its value is demonstrated in Annex 3 (page 126);

$\lambda_i$  (m) wave length (from the shortlist, Table 4);

$T_0$  (s) natural roll period of the ship in calm water;

$GM_i$  (m) as defined above;

$GM_0$  (m) metacentric height in calm water.

This criterion considers that, for each wave in the shortlist, the ship cannot attain the speed corresponding to the parametric resonance condition, otherwise the metacentric height in wave must remain positive and its variation must be acceptable.

Wave number $i$	Weight $W_i$	Wave length $\lambda_i$ (m)	Wave height $H_i$ (m)
1	0.000013	22.574	0.350
2	0.001654	37.316	0.495
3	0.020912	55.743	0.857
4	0.092799	77.857	1.295
5	0.199218	103.655	1.732
6	0.248788	133.139	2.205
7	0.208699	166.309	2.697
8	0.128984	203.164	3.176
9	0.062446	243.705	3.625
10	0.024790	287.931	4.040
11	0.008367	335.843	4.421
12	0.002473	387.440	4.769
13	0.000658	442.723	5.097
14	0.000158	501.691	5.370
15	0.000034	564.345	5.621
16	0.000007	630.684	5.950

Table 4 – Wave cases for the first check of parametric roll level-two criterion.

## Second Check

### General Principle

The second check of level-two parametric roll condition, which can be assessed only if the first check is not fulfilled, considers the maximum roll angle in each wave of a specified scattering diagram. As for the pure loss of stability failure mode, the new regulation imposes the scattering diagram proposed by IACS corresponding to the Northern Atlantic (Table 2, from [69]) for sailing in unrestricted areas, and allows the use of another diagram for sailing in restricted areas.

The C2 coefficient is associated with the second check. Its value, which must be lower than  $R_{PRO}=0.06$  to fulfill the criterion, is calculated from the maximum roll angle of the ship on each of the non-zero-weighted waves of the wave scatter diagram considering 7 speeds. For a given wave and a given speed, the maximum roll angle is the maximum absolute value of the solution  $\varphi(t)$  of the differential equation of parametric roll, which can be established as follows:

$$J_{44}\ddot{\varphi} + B_{44}\dot{\varphi} + WGZ(\varphi, t) = 0 \quad (23)$$

With:

$\varphi$	(rad)	roll angle;
$J_{44}$	(kg.m <sup>2</sup> )	roll moment of inertia, including added mass;
$B_{44}$	(N.m.s/rad)	damping coefficient;
$W$	(N)	ship's weight;
$GZ(\varphi, t)$	(m)	righting arm, function of both the roll angle $\varphi$ and time $t$ , varying with the wave encounter frequency;

The C2 coefficient is calculated as follows:

$$C2 = \frac{1}{7} \sum_{i=1}^{197} \sum_{j=1}^7 W_i C2_{i,j} \quad (24)$$

The weighting factor  $W_i$  is extracted from the wave scattering table (Table 2, number of occurrences divided by 100,000). The coefficient  $C2_{i,j}$  is equal to 1 if the maximum roll angle of the  $\varphi(t)$  function solution of the differential equation (23) for wave number  $i$  and the speed  $K_j V_S$  is higher than 25 degrees, 0 otherwise. The speed factors  $K_j$  are given in Table 5.

### Effective Wave Concept

Since the number of non-zero-weighted waves in the scattering table may be large, the new regulation imposes the use of the Grim effective wave height concept [65] to make the computation faster. The methodology is similar to that used in pure loss of stability. However, the considered effective height is that of the 1/3 highest waves. It is calculated as follows:

$$H_{\frac{1}{3}}^{eff} = 4.0043 \sqrt{m_0} \quad (25)$$

The maximum roll angle  $\Phi_{max}$  is pre-computed by solving the differential equation (23) for 10 effective waves whose heights are a fraction (from 0.1 to 1) of the maximum effective wave

height corresponding to the ship's length and the wave scatter diagram. The maximum roll angle associated with any effective wave height is calculated by linear interpolation. Table 6 gives the effective wave heights (in meters) computed according to the Grim method for some vessels and associated to the waves of Table 2 having a zero-crossing period ( $T_z$ ) equal to 10.5 seconds.

Number j	Speed factor $K_j$
1	-1
2	-0.866
3	-0.5
4	0
5	0.5
6	0.866
7	1

Table 5 – Speed factors  $K_j$ .

$H_s$ (m)	DTMB-5415 L=142m	Container L=262m	Container L=319m	Ro-Ro L=135m	Tanker L=227.5m
0.5	0.288	0.362	0.361	0.280	0.353
1.5	0.865	1.085	1.082	0.839	1.059
2.5	1.442	1.809	1.804	1.399	1.764
3.5	2.018	2.532	2.525	1.958	2.470
4.5	2.595	3.256	3.247	2.518	3.176
5.5	3.171	3.979	3.968	3.077	3.882
6.5	3.748	4.703	4.690	3.637	4.587
7.5	4.325	5.426	5.411	4.196	5.293
8.5	4.901	6.149	6.133	4.756	5.999
9.5	5.478	6.873	6.854	5.315	6.705
10.5	6.054	7.596	7.576	5.875	7.410
11.5	6.631	8.320	8.297	6.434	8.116
12.5	7.208	9.043	9.019	6.993	8.822
13.5	7.784	9.767	9.740	7.553	9.528
14.5	8.361	10.490	10.462	8.112	10.234
15.5	8.937	11.214	11.183	8.672	10.939
16.5	9.514	11.937	11.905	9.231	11.645

Table 6 – Effective height of the 1/3 highest waves (m) for a zero-crossing period equal to 10.5 seconds.

The future regulation proposes two different methods to compute the maximum roll angle. They are briefly described hereunder. Both methods consider a non-linear GZ, which renders their implementation relatively complex, especially for naval architects accustomed to the simplicity of the current intact stability regulation [18]. However, the linear-GZ option was considered as shown in a paper presented by Umeda at the International Ship Stability Workshop held in Brest in 2013 [30]. In Chapter 4, we propose a simplified method providing the maximum parametric roll angle assuming a linear GZ (Section 4.4 in page 97).

#### *First Method: Analytical Solution of the Differential Equation*

The first method is described in SDC 3/WP.5, Annex 4, Appendix 5 [23]. It is based on an averaging method, which provides an analytical solution for non-linear oscillators such as parametric ones. The method assumes non-linearity as small disturbances which make a slow evolution of the system response. Thus, the inertia and linear component of the restoring moment (GM) are assumed as leading characteristics since the non-linearity in the restoring moment and its variations have small magnitude. The averaging method is thoroughly described in [66].

This method requires a polynomial fit of the GZ curve in calm water at odd-degree (5<sup>th</sup> degree or higher). It provides directly the maximum roll angle, calculated as the solution of a scalar equation.

#### *Second Method: One-Degree-of-Freedom Numerical Simulation*

The second method consists in solving the differential equation (23) with a time-domain numerical simulation in one degree of freedom (1-DoF). During the 12<sup>th</sup> International Conference on the Stability of Ships and Ocean Vehicles, held in Glasgow (UK) in June 2015, Peters *et al.* formulated some recommendations for this numerical solving [32]. Their propositions are included as guidelines in the new regulation (SDC 3/WP.5, Annex 4, Appendix 3, [23]).

This second method is used in this thesis. It is described in more detail in Section 1.2.4.

#### *Comparison of Both Methods*

The first method (analytical solution) is not used in this thesis. However, a student project recently carried at the French Naval Academy showed very good accordance between results given by both methods for the C11 container vessel (described in Annex 2) in one condition of parametric roll [74].

### **1.2.4. Maximum Roll Angle and $KG_{\max}$ computation**

This section describes the method used in this thesis to solve the parametric roll differential equation (23) with a one-degree-of-freedom numerical situation in order to calculate the maximum roll angle.

#### ***Moment of Inertia***

The moment of inertia  $J_{44}$  is calculated as follows:

$$J_{44} = \Delta(1 + a)(kB)^2 \quad (26)$$

With:

$\Delta$	(kg)	ship's displacement;
$a$	-	added mass coefficient;
$k$	-	radius of inertia coefficient;
$B$	(m)	ship's breadth.

The ship's natural roll period in calm water ( $T_0$ ) is linked to her moment of inertia as follows:

$$T_0 = 2\pi \sqrt{\frac{J_{44}}{g\Delta GM}} = 2\pi kB \sqrt{\frac{1 + a}{gGM}} \quad (27)$$

With:

$g$	9.81 m/s <sup>2</sup>	gravitational acceleration;
$GM$	(m)	metacentric height in calm water.

When the ship's roll period is known, the coefficients  $a$  and  $k$  are chosen in consequence. Otherwise, the coefficient  $a$  is set to 0.1 and  $k$  to 0.4. Values of both coefficients are given in Table 15 and Table 16 (Annex 2 pages 118 and 123) respectively for civilian and naval ships.

### ***Roll Damping***

The roll damping coefficient  $B_{44}$  is calculated according to the method proposed by Kawahara, Maekawa and Ikeda [50]. The ship's speed is taken into account though the lift component according to the method proposed by Ikeda, Himeno and Tanaka [48]. The explanatory notes of parametric roll criteria give both methods (SDC 3/WP.5, Annex 4, Appendix 4, [23]). The roll damping coefficient  $B_{44}$  depends on the roll amplitude ( $\varphi_a$  in [50]). Here,  $B_{44}$  is pre-computed for 11 values of roll amplitude from 1 to 50 degrees and calculated by linear interpolation during the solving of the differential equation, using the value of the current roll amplitude. The roll damping coefficient  $B_{44}$  also depends on the distance between the center of gravity and the calm water surface (OG in [50]) and on the ship's roll period ( $T_0$ ). Both are linked to the KG. Thus, the pre-computation of  $B_{44}$  for all roll amplitudes is required in all iterations of the search of  $KG_{max}$ .

### ***Righting Arm***

The righting arm is calculated according to a simplified method proposed by Peters, Belenky, Chouliaras and Spyrou [32] and the new regulation (SDC 3/WP.5 [23]). This method consists in modulating the GZ in calm water by the GM in waves as follows:

$$GZ(\varphi) = GZ_0(\varphi) - (GM_0 - GM_{moy} - \Delta GM \cdot \sin(\omega_e t)) \sin \varphi \quad (28)$$

With:

- $GZ_0(\varphi)$  (m) righting arm in calm water associated to a user-defined height of the center of gravity ( $KG_0$ );
- $GM_0$  (m) metacentric height in calm water associated with  $KG_0$ .
- $GM_{moy}$  (m) average value of the metacentric height in waves, associated with the considered KG, which may differ from  $KG_0$ ;
- $\Delta GM$  (m) amplitude of the variation of the metacentric height in waves;
- $\omega_e$  (rad/s) wave encounter frequency.

Belenky, Bassler and Spyrou showed that this simplified method gives acceptable values of GZ up to an angle of 30 degrees [27]. Figure 14 shows the GZ curves resulting from this method applied to the C11 container vessel in the conditions of Figure 8 (page 17). The real GZ in waves in three configurations (maximum GM, minimum GM, average value of GZ in waves) is drawn as solid lines (respectively blue, red and grey). The GZ in calm water modulated by the GM in waves as dashed lines in the same configurations (same colors). We also observe that the differences are negligible under 15 degrees and acceptable under 25 degrees.

Note: the first method proposed by the future regulation to compute the maximum roll angle (analytical solution of the differential equation, page 30) also uses this approximation of the GZ in waves.

Since the C2 coefficient is increased if the maximum roll angle exceeds 25 degrees, this approximation method can be used here. It makes the computation of maximum roll angle and  $KG_{max}$  faster. The righting arm in calm water ( $GZ_0$ ) is pre-computed for heel angles from 0 to 50 degrees with a step equal to 5 degrees. During the simulation, its value for any roll angle  $\varphi$  is calculated by linear interpolation between two adjacent values.  $GM_{moy}$  and  $\Delta GM$  are computed before the simulation by computation of GM on the considered sinusoidal wave with 10 positions of the ship on the wave.  $GM_{moy}$  is the average value of the 10 metacentric heights.  $\Delta GM$  is half the difference between the maximum and the minimum values. During the finding of  $KG_{max}$ , the value of  $GM_{moy}$  is updated with the considered value of KG since the value of  $\Delta GM$  remains unchanged.

$GM_{moy}$  is used to calculate the ship's natural roll period  $T_0$ , which is required to calculate the damping coefficient  $B_{44}$ . Thus, if  $GM_{moy}$  is negative, the simulation is not possible and the C2 coefficient is forced to 1.

The wave encounter frequency  $\omega_e$  is calculated as follows:

$$\omega_e = \omega_w \left( 1 + \omega_w \frac{K_j V_s}{g} \right) \quad (29)$$

With:

$\omega_w$  (rad/s) wave frequency.

The speed factors  $K_j$  are given in Table 5. The positive values correspond to head seas. The negative values correspond to following seas.

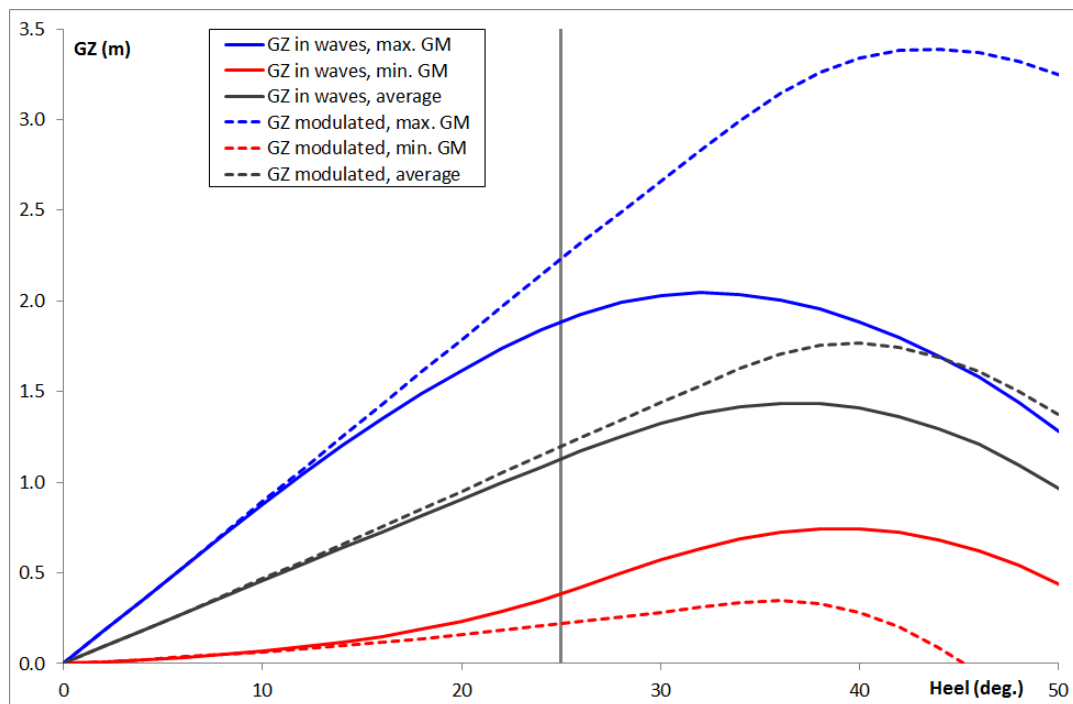


Figure 14 – Comparison of real GZ in waves and GZ in calm water modulated by the GM in waves for the C11 container vessel.

### ***Solving Method***

The solving of the differential equation is performed with the Runge-Kutta 4<sup>th</sup> order method. The implementation of this method is detailed in Annex 3 page 128.

### ***Initial Conditions***

As proposed by Peters *et al.* [32] and the new regulation (SDC 3/WP.5 [23]), the initial roll angle is equal to 5 degrees. The initial roll speed is null. The influence of an initial roll angle equal to 10 degrees is tested in Section 3.3.4 page 75.

### ***Simulation Duration***

The time duration of the simulation is equal to 15 times the ship's natural roll period. This value is proposed by Peters *et al.* [32] and the new regulation (SDC 3/WP.5 [23]). Moreover, it is validated by a series of computations performed with different durations, from 3 to 20 roll periods, which give the same  $KG_{max}$  from 10 roll periods.

The simulation is interrupted if the roll angle exceeds 50 degrees.

### ***Time Step***

The time step is set to one 40<sup>th</sup> of the ship's natural roll period. This value has been validated by removing the damping and GM variation from the differential equation, to simulate an undamped roll on calm water: The roll amplitude remains equal to the initial roll angle. This test fails if the Euler method is used to solve the differential equation instead of the Runge-Kutta method: the roll amplitude increases. Peters *et al.* [32] and SDC 3/WP.5 [23] propose a time step equal to one 30<sup>th</sup> of the ship's natural roll period.

### ***Simulation Implementation***

The hydrostatic computations are performed with Calcoque software as described in Chapter 2. The water density is equal to 1.025 t/m<sup>3</sup>. The solving of the differential equation and the damping coefficient calculation are also implemented in this software, in order to permit a user-friendly computation of the C2 coefficient and the associated  $KG_{max}$  curves.

### ***$KG_{max}$ computation***

The  $KG_{max}$  associated with the second check of level-two parametric roll criterion, i.e. the maximum value of KG ensuring the compliance with the criterion, is the highest value of KG which gives a value of C2 lower than  $R_{PR0}=0.06$ .

Since C2 is a discrete sum of weighting factors, the function C2 versus KG is not continuous. Moreover, this function may have many local peaks when the ship is vulnerable to parametric roll (see Section 3.3.2). These characteristics make inefficient a lot of root-finding algorithms. Hence, we propose the following basic algorithm to find the value of  $KG_{max}$  associated with C2. It is performed in two steps.

#### ***First Step***

The first step consists in finding a first value of KG for which the C2 coefficient is lower than  $R_{PR0}$  and a second value of KG for which C2 is larger than  $R_{PR0}$ . Finding this interval begins at a low value of KG for which C2 is lower than  $R_{PR0}$ , near zero. This value of KG is named

“Starting value of KG” and denoted by  $KG_{start}$ . The value of KG is increased by 10 centimeters at each iteration until C2 is higher than  $R_{PRO}$ .

### Second Step

The second step consists of a classical dichotomy to find the highest value of KG for which C2 is lower than  $R_{PRO}$ . The required precision is 0.1 mm. Since C2 is the sum of weighting coefficients drawn from the wave scatter diagram (number of occurrences of each wave in Table 2 divided by 100,000), it is not possible for C2 to be equal to  $R_{PRO}$ .

Table 7 shows the values of KG and C2 while finding the  $KG_{max}$  for the naval ship DTMB-5415 described in Annex 2 page 124 at a draft equal to 6.125 m. The associated  $KG_{max}$  is 9.2236 m (in bold in Table 7).

First step: finding the interval			
Iteration	KG (m)	C2	C2< $R_{PRO}$
1	$KG_{start} = 7$	0	Y
2	7.1	0	Y
3	7.2	0	Y
4	7.3	0	Y
5	7.4	0	Y
6	7.5	0	Y
7	7.6	0	Y
8	7.7	0	Y
9	7.8	2.86E-07	Y
10	7.9	1.57E-06	Y
11	8	4.29E-07	Y
12	8.1	0	Y
13	8.2	0	Y
14	8.3	0	Y
15	8.4	0	Y
16	8.5	0	Y
17	8.6	2.49E-05	Y
18	8.7	0.0293483	Y
19	8.8	0.017636	Y
20	8.9	0.00266057	Y
21	9	0.000234857	Y
22	9.1	3.13E-05	Y
23	9.2	0.0219234	Y
24	9.3	0.154703	N
Second step: dichotomy			
Iteration	KG (m)	C2	C2< $R_{PRO}$
25	9.25	0.0760626	N
26	9.225	0.0749527	N
27	9.2125	0.0371166	Y
28	9.21875	0.0449244	Y
29	9.22188	0.0462103	Y
30	9.22344	0.0464114	Y
31	9.22422	0.0740300	N
32	9.22383	0.0740291	N
33	<b>9.22363</b>	0.0502479	Y
34	9.22373	0.0740291	N

Table 7 – Finding the value of  $KG_{max}$ .

## CHAPTER 2. HYDROSTATIC COMPUTATION

The new generation criteria of both pure loss of stability and parametric failure mode, presented in Chapter 1, require a hydrostatic solver which performs computations in static longitudinal waves.

Calcoque is a three-dimension hydrostatic computer code developed at the French Naval Academy for academic and research use. It computes equilibrium, intact and damage stability and bending moment. The software can handle the current intact stability rules for civilian ships [18] and the regulation applied in the French Navy for naval vessels [17]. A detailed presentation of the software is proposed in Annex 1.

After improvements added within the scope of this thesis, the software is now able to perform hydrostatic computations in longitudinal waves. Level-one and level-two criteria of both pure loss of stability and parametric roll failure modes have been fully implemented.

This chapter describes the three main algorithms used to perform hydrostatic computations in still water and in longitudinal waves. The first algorithm transforms the classical representation of the ship's hull by stations into a volume mesh made of tetrahedrons, prisms and hexahedrons, which can have large dimensions without degradation of the numerical result. The second algorithm cuts this volume mesh with a plane, generating one volume sub-mesh on each side of the plane. This second algorithm is used by the third, which finds the balance position of the ship in three degrees of freedom (sinkage, heel, trim, two degrees if the heel is fixed while computing the GZ curve), in calm water and in static waves with a real three-dimension approach.

The content of this chapter has been presented at the 12<sup>th</sup> International Conference on the Stability of Ships and Ocean Vehicles, held in Glasgow (UK) in June 2015 [3]. Part of it is proposed in a handbook [1].

### 2.1. GENERATION OF VOLUME MESH

The ship is classically designed with stations, which are a list of (Y, Z) points with the same longitudinal coordinate X (see the ship-fixed coordinate system in Annex 4). Figure 15 shows the stations of the Offshore Patrol Vessel (OPV) *Adroit* in service in the French Navy (see her main particulars in Annex 2). The algorithm imposes the following constraints:

- Stations are ordered from aft to forward;
- Stations are symmetrical, defined on port side only;
- The first point of each station is on the ship's centerline (Y=0);
- Vertical coordinates of the points are increasing ( $Z_{i+1} > Z_i$ ).

This last constraint prevents the design of a multi-hull ship by sections. However, designing such a ship or floating structure remains possible by considering the hulls as appendages providing buoyancy.

In addition to the stations, some lines are defined by the user. They connect some points of stations in order to represent the main edges of the hull. A line starts at any station and ends at any other one located forward. It has a unique point on each station it intersects and cannot miss out any station. Two lines can intersect only at a station point.

Stations and lines (Figure 16) are used to generate a volume mesh of the ship through a matrix algorithm which builds the N-1 strips defined by the N stations. For each strip between stations indexed  $i$  and  $i+1$ , the process is divided in two steps.

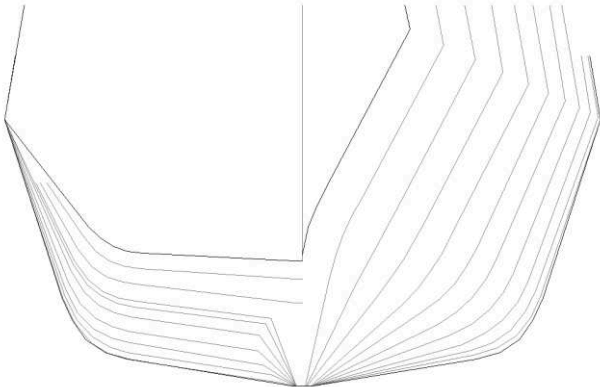


Figure 15 – Stations of the OPV *Adroit*.

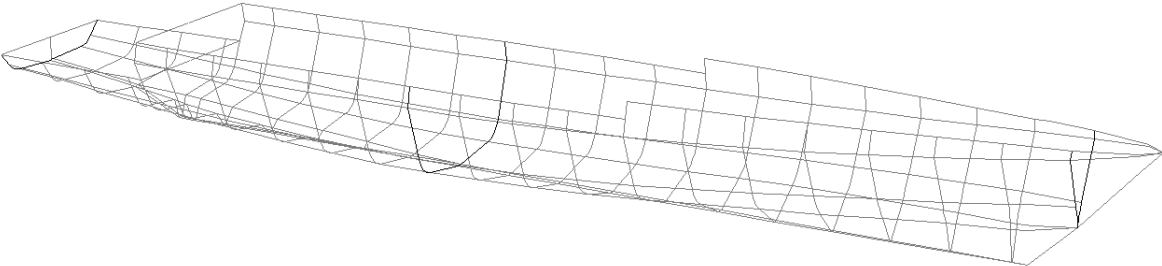


Figure 16 – Station and lines of the OPV *Adroit*.

**2.1.1. First Step**

The first step consists of the generation of a matrix defining the links between all the points of the station  $i$  and all the points of station  $i+1$ . Let us consider a strip defined by an aft station with 5 points (port side only) and a forward station with 4 points. Let us consider 3 user lines. The first one links point 1 of the aft station to point 1 of the forward station (keel line). The second one links point 2 (aft) to point 3 (forward). The third links point 5 (aft) to point 4 (forward). The strip and its links are represented in Figure 17 (stations in black, lines in grey).

Thus, a link matrix is defined with 5 rows associated with the 5 points of the aft station, and 4 columns associated with the 4 points of the forward station. The three user lines are represented in this matrix by three black dots in the appropriate cells (Figure 18).

Each link in the matrix defines two restricted zones which are the upper right cells and the lower left cells. This avoids considering a line which crosses another. In the current sample,

the restricted zones defined by the second link (2→3) appear in grey in Figure 18. The other links (1→1 and 5→4) define no restricted zone.

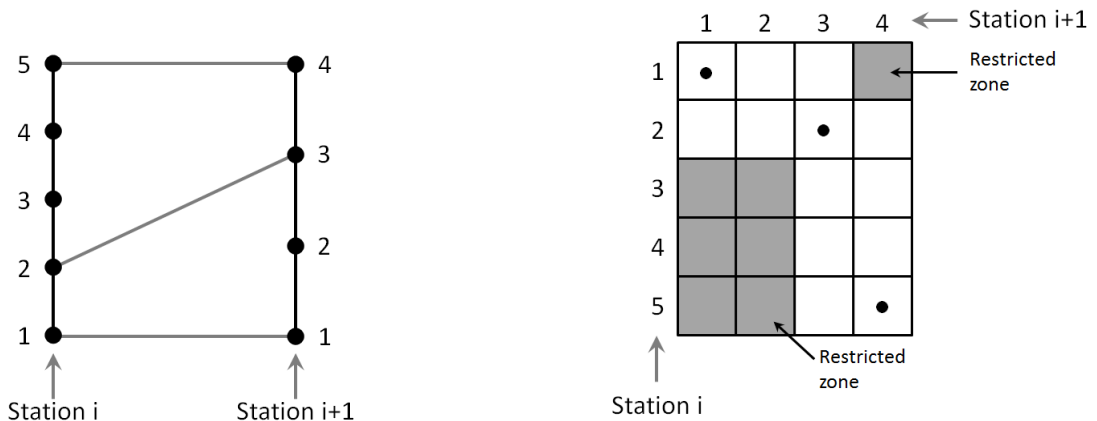


Figure 17 – Strip defined by two stations and three lines. Figure 18 – Link matrix associated with the strip.

Then, the matrix is automatically completed with other links by going from the upper left corner to the lower right corner without missing out any cells while passing by all cells associated with user links. A diagonal path is favored (link 1→1 to link 2→2). If not possible, the path is horizontal (2→2 to 2→3) or vertical (3→4 to 4→4). These added links are shown as grey dots in Figure 19. They are materialized by dotted lines on the strip diagram (Figure 20).

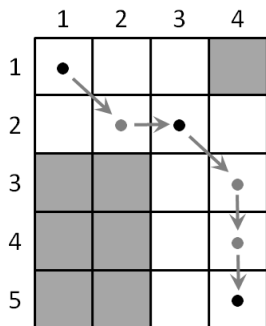


Figure 19 – Completed link matrix.

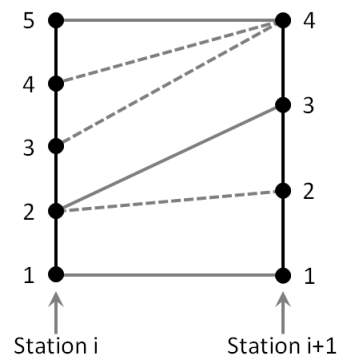


Figure 20 – Strip diagram associated with the completed link matrix.

### 2.1.2. Second Step

The second step consists of the generation of the volume and surface meshes defined by the completed link matrix. A diagonal path (1→1 to 2→2 and 2→3 to 3→4) generates a tetragon on each side of the hull and a hexahedron which connects both together. A horizontal path (2→2 to 2→3) generates a triangle on each side of the hull and a prism, whose bases are on the forward station. A vertical path (3→4 to 4→4 and 4→4 to 4→5) also generates two triangles and one prism, but their bases are on the aft station. All triangles and tetragons form the surface mesh of the strip while all prisms and hexahedrons form the volume mesh. Figure 21 shows the surface mesh associated with the current sample.

Flat volumes should be eliminated (same Z coordinate of the points). Some volumes may be simplified: in the sample, the first hexahedron is a prism because the Y coordinate of the first point of each station is null.

Both surface and volume meshes of the entire ship are created by concatenating respectively surface and volume meshes of all strips. Figure 22 and Figure 23 show respectively the surface and the volume meshes of the OPV *Adroit*.

The volume mesh may be corrected to represent the real hull. If necessary, it may be cut at the watertight deck and the void spaces (bow thruster tunnel, water inlets and possibly flooded rooms for damage stability ...) may be extracted. Both operations require a routine to cut the mesh by a plane, described in the next section. Moreover, volume meshes of appendages and propellers may be added. Figure 25 shows the watertight volume of the OPV *Adroit*. Its appendages (rudders, bilge keels, shafts) and propellers, shown in Figure 24, have been added. The struts are defined by surface meshes: they increase the ship's resistance but provide no buoyancy. Thus, they are not included in the watertight volume. Water inlets on each side of the engine room and both housings of fast rafts on the aft lower deck have been extracted from the mesh of the watertight volume.

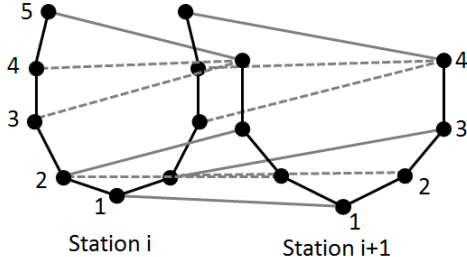


Figure 21 – 3D wireframe view of the strip and its surface mesh.

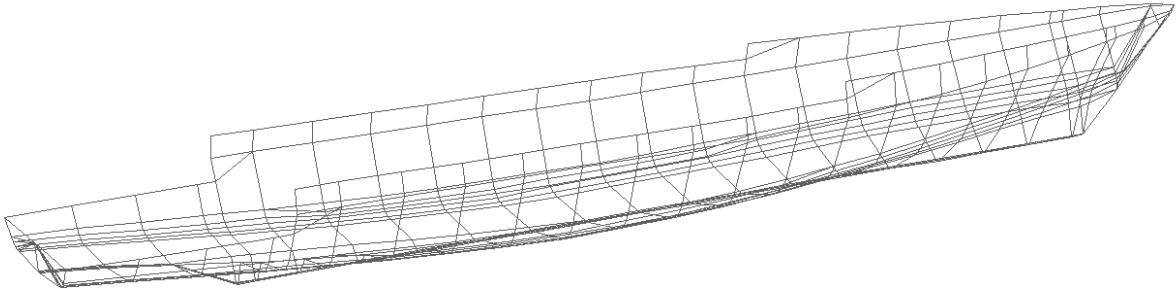


Figure 22 – Wireframe view of the surface mesh of the OPV *Adroit*.

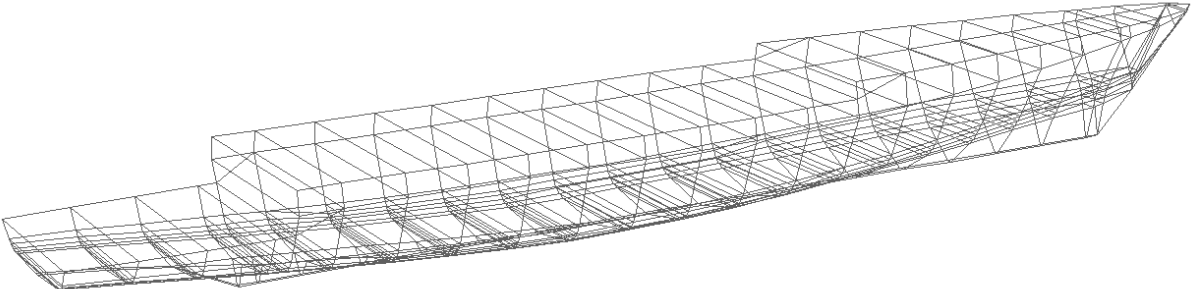


Figure 23 – Wireframe view of the volume mesh of the OPV *Adroit*.

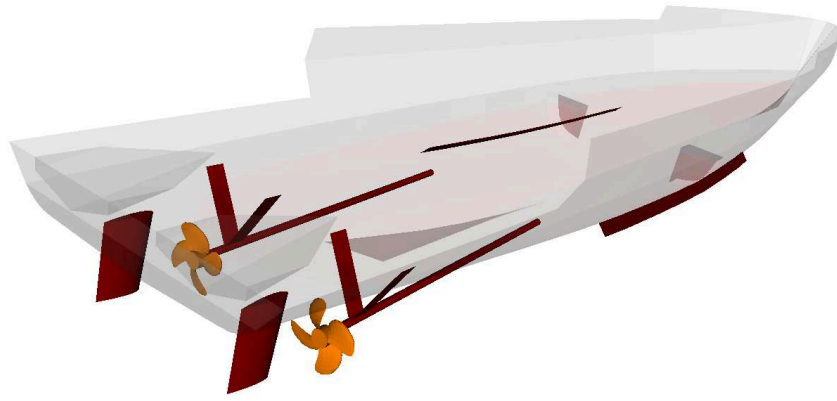


Figure 24 – Appendages and propellers of the OPV *Adroit*.

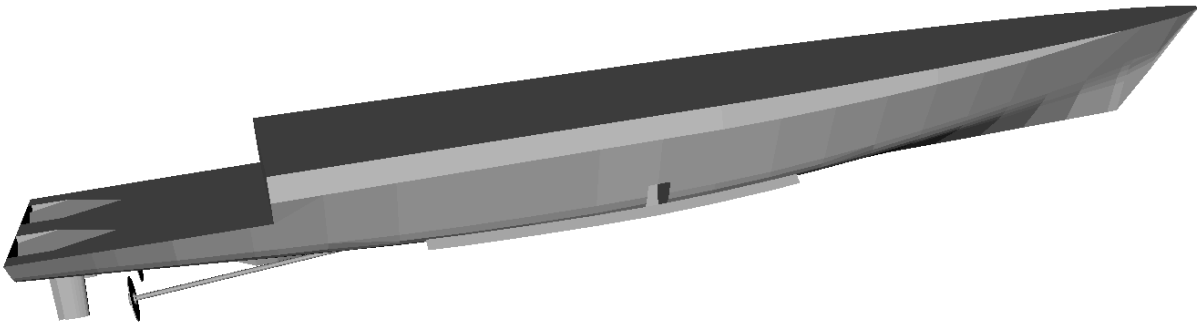


Figure 25 – Watertight volume of the OPV *Adroit*.

## 2.2. CUTTING A VOLUME MESH BY A PLANE

To define the watertight volume, the waterplane, the displacement volume and other elements, it is necessary to cut a volume mesh by a plane. The waterplane is the intersection of the mesh of the watertight volume and the still water surface as cutting plane. The displacement volume is the volume sub-mesh located under the cutting plane. This routine also permits to extract some volumes from the hull (void spaces or flooded rooms) and to define volume meshes of the compartments and surface meshes of the decks.

### 2.2.1. Decomposition of Elementary Volumes

As seen in the previous section, the volume mesh is made of prisms and hexahedrons. The former can be divided in three tetrahedrons (Figure 26) and the latter in two prisms or six tetrahedrons (Figure 27). The cutting routine of prisms and hexahedrons only handles simple cases: volume entirely on one side or the other of the plane, a face contained in the plane or face “parallel” to the plane. In other cases, the volume being cut is first decomposed into three or six tetrahedrons.

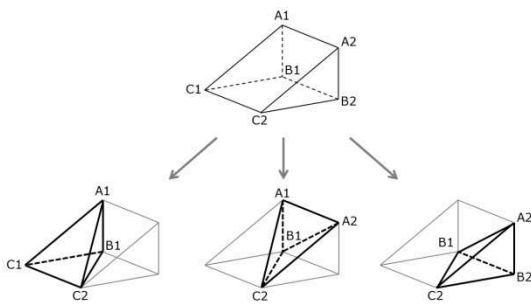


Figure 26 – Cutting a prism into 3 tetrahedrons.

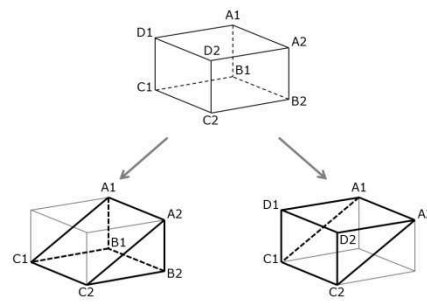


Figure 27 – Cutting a hexahedron into 2 prisms.

### 2.2.2. Cutting a Tetrahedron by a Plane

The cutting plane is modelled with a point P and a normal vector  $\vec{n}$ . We consider a point M to be located from the plane. Three cases are possible, function of the sign of the scalar product  $\overrightarrow{PM} \cdot \vec{n}$ . They are shown in Table 8.

$\overrightarrow{PM} \cdot \vec{n} > 0$	$\overrightarrow{PM} \cdot \vec{n} = 0$	$\overrightarrow{PM} \cdot \vec{n} < 0$
M is located above the plane	M is located in the plane	M is located under the plane

Table 8 – Location of a point from a plane.

Each of the four points of the tetrahedron is in one of those three cases. Thus, we have  $3^4=81$  possibilities. However, the order of points having no importance (unlike the necessary orientation of the vertices of a surface mesh), we build three lists containing points respectively above, in the plane and under, disregarding their original order. Thus, the number of cases is reduced to 15 as shown in Table 9. Moreover, gathering different cases which have the same result finally defines 8 different configurations (designated A to H), shown in Table 10.

Configurations C, (D and E), (F and G) and H are shown in Figure 28. The original tetrahedron is drawn in black and the intersection with the cutting plane is drawn in grey.

Note:

- In case 9 (configuration B), the intersection triangle is not to be considered since it is already considered in configuration A. If the cutting plane is located at the frontier between two adjacent elementary volumes (one on each side of the plane), the intersection surface must be considered only once.
- Since the order of the points of the original tetrahedron has been lost, it is possible to orientate the intersection vertices by assigning the normal vector of the cutting plane.

Case	Configuration	Number of points above the plane	Number of points in the plane	Number of points under the plane
1	A	0	0	4
2			1	3
3			2	2
4			3	1
5			4	0
6	D	1	0	3
7	F		1	2
8	H		2	1
9	B	2	3	0
10	C		0	2
11	G		1	1
12	B		2	0
13	E	3	0	1
14	B		1	0
15		4	0	0

Table 9 – 15 cases of cutting a tetrahedron with a plane.

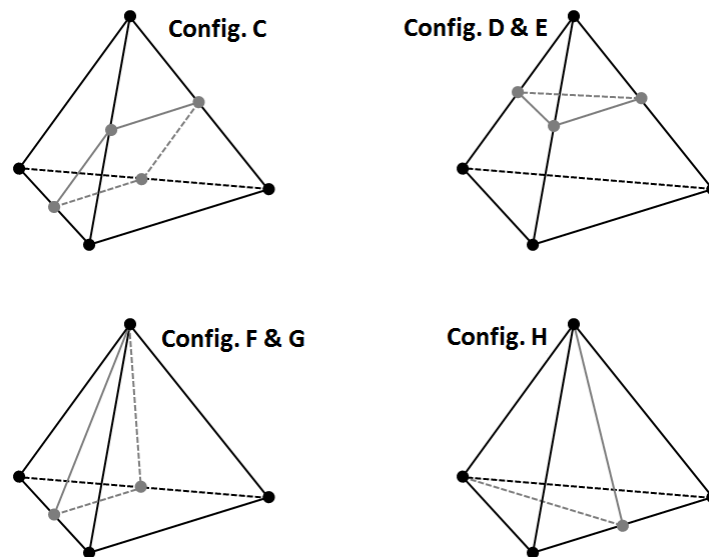


Figure 28 – Different configurations of cutting a tetrahedron with a plane.

Config.	Topology
<b>A</b>	No point above the plane 1 tetrahedron under the plane 1 intersecting triangle if 3 points in the plane
<b>B</b>	No point under the plane 1 tetrahedron above the plane
<b>C</b>	2 points above the plane 2 points under the plane 1 prism above the plane 1 prism under the plane 1 intersecting tetragon
<b>D</b>	1 point above the plane 3 points under the plane 1 tetrahedron above the plane 1 prism under the plane 1 intersecting triangle
<b>E</b>	3 points above the plane 1 point under the plane 1 prism above the plane 1 tetrahedron under the plane 1 intersecting triangle
<b>F</b>	1 point above the plane 1 point in the plane 2 points under the plane 1 tetrahedron above the plane 1 tetrahedron under the plane 1 intersecting triangle
<b>G</b>	2 points above the plane 1 point in the plane 1 point under the plane 1 tetrahedron above the plane 1 tetrahedron under the plane 1 intersecting triangle
<b>H</b>	1 point above the plane 2 points in the plane 1 point under the plane 1 tetrahedron above the plane 1 tetrahedron under the plane 1 intersecting triangle

Table 10 – 8 configurations of cutting a tetrahedron with a plane.

## 2.3. FINDING THE BALANCE POSITION

### 2.3.1. Definition of the Balance Position

The three considered degrees of freedom are the sinkage (denoted by  $e$ ), the heel ( $\varphi$ ) and trim ( $\theta$ ). The sinkage replaces the draft which has no sense while the heel approaches 90 degrees. The sinkage is defined as the algebraic distance between a ship-fixed point Q (coordinates  $L_{pp}/2, 0, Z$  of the reference waterline  $10H$ ) and its projected point P on the calm water waterplane (even for computation in static waves). See Figure 29.

Balance is achieved if the three following conditions are met together:

$$\varepsilon_{\nabla} = \nabla_0 - \nabla = 0 \qquad \varepsilon_x = 0 \qquad \varepsilon_y = 0 \qquad (30)$$

With:

- $\nabla$  ( $m^3$ ) computed displacement volume;
- $\nabla_0$  ( $m^3$ ) ship displacement volume;
- $\varepsilon_{\nabla}$  ( $m^3$ ) volume gap;
- $\varepsilon_x$  (m) longitudinal gap, defined hereunder in Equation (34);
- $\varepsilon_y$  (m) transverse gap, defined hereunder in Equation (34).

The heel can be free (when finding the balance position) or fixed (GZ curve computation). In that case, the third condition in (30) is ignored and the transverse gap  $\varepsilon_y$  is the righting arm lever GZ, to be calculated.

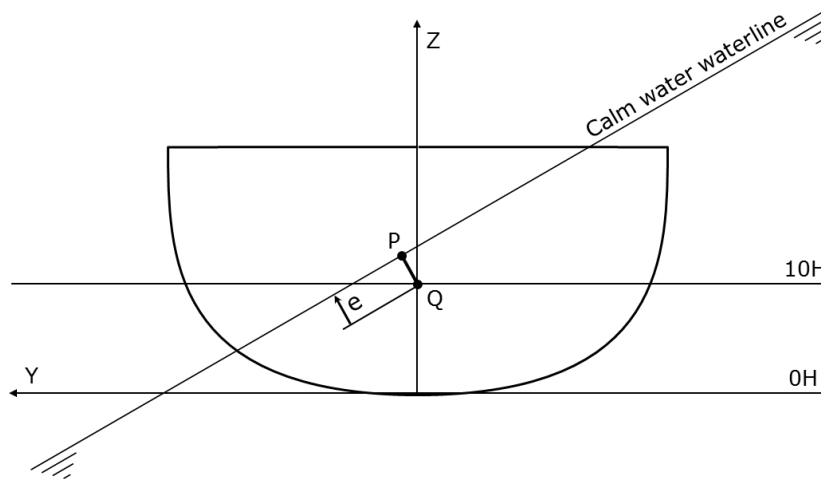


Figure 29 – Sinkage.

### 2.3.2. Inclined-Ship Planes

The gaps  $\varepsilon_x$  and  $\varepsilon_y$  are respectively the algebraic longitudinal and transverse distances between the center of gravity (G) and the Earth vertical through the center of buoyancy (B). Two inclined-ship planes are defined to compute these gaps. Their line of intersection is the Earth vertical whose director vector is  $\vec{n}_1$ .

The transverse plane of inclined ship also contains vector  $\vec{n}_2$  defined as:

$$\vec{n}_2 = \frac{\vec{n}_1 \wedge \vec{X}}{\|\vec{n}_1 \wedge \vec{X}\|} \quad (31)$$

$\vec{X}$  is the unit vector of the longitudinal axis of the ship-fixed coordinate system (Annex 4).

The longitudinal plane of inclined ship contains  $\vec{n}_1$  and  $\vec{n}_3$  vectors with:

$$\vec{n}_3 = \vec{n}_2 \wedge \vec{n}_1 \quad (32)$$

In the ship-fixed coordinate system, the three vectors are:

$$\begin{aligned} n_{1,x} &= -\sin \theta & n_{2,x} &= 0 & n_{3,x} &= \cos \theta \\ n_{1,y} &= -\sin \varphi \cos \theta & n_{2,y} &= \cos \varphi & n_{3,y} &= -\sin \varphi \sin \theta \\ n_{1,z} &= \cos \varphi \cos \theta & n_{2,z} &= \sin \varphi & n_{3,z} &= \cos \varphi \sin \theta \end{aligned} \quad (33)$$

Thus, the gaps  $\varepsilon_x$  and  $\varepsilon_y$  are respectively the algebraic distances between G and the transverse and longitudinal planes of the inclined ship. They are calculated as follows:

$$e_x = \vec{BG} \cdot \vec{n}_3 \quad e_y = GZ = \vec{BG} \cdot \vec{n}_2 \quad (34)$$

The gaps and the inclined-ship planes are shown in Figure 30.

This expression of the longitudinal gap is more accurate than that of the simplified strip method proposed by the SLF 52/INF.2 (see [19], Annex 6) which is:

$$e_x = LCB - LCG \quad (35)$$

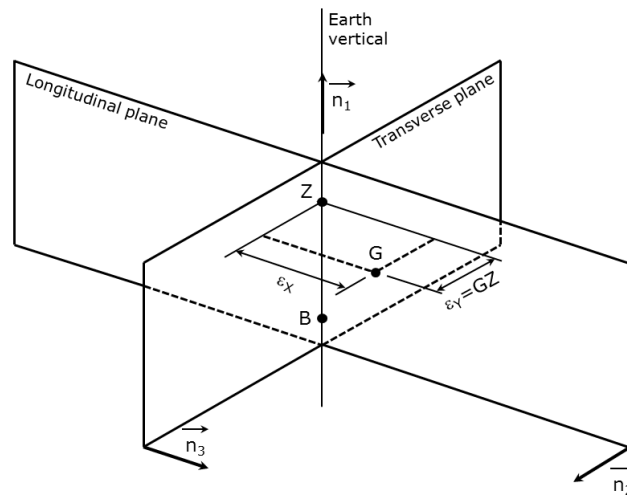


Figure 30 – Inclined-ship planes and gaps.

### 2.3.3. Hydrostatic Computation in Calm Water

The waterplane, depending on sinkage ( $e$ ), heel ( $\varphi$ ) and trim ( $\theta$ ), is defined with a point P (see Figure 29) and the vector  $\vec{n}_1$  (function of  $\varphi$  and  $\theta$ ) with:

$$\vec{QP} = e\vec{n}_1 \quad (36)$$

When finding the balance position, the displacement volume ( $\nabla$ ) and its center (B) are computed by cutting the mesh of the watertight volume by the considered waterplane.

### 2.3.4. Hydrostatic Computation in Waves

The watertight volume is previously divided in strips by cutting with transverse planes. SLF 52/INF.2 ([19], Annex 6) recommends at least 20 strips. In each strip, the following are defined (see Figure 31):

- Plane  $P_1$ : strip's aft plane.
- Plane  $P_2$ : strip's forward plane.
- Line  $D_3$ : through point P with director vector  $\vec{n}_3$  (longitudinal line located in the calm-water waterplane).
- Point  $I_1$ : intersection of  $P_1$  and  $D_3$ .
- Point  $I_2$ : intersection of  $P_2$  and  $D_3$ .

Three points (A, B and C) define the strip's local waterplane. They are defined as follows (Figure 31):

$$\vec{OA} = \vec{OI_1} + \vec{n}_2 + z_1 \vec{n}_1 \quad \vec{OB} = \vec{OI_1} - \vec{n}_2 + z_1 \vec{n}_1 \quad \vec{OC} = \vec{OI_2} + z_2 \vec{n}_1 \quad (37)$$

With:

$$z_1 = \frac{h}{2} \cos(k \cdot x_1 + \alpha) \quad z_2 = \frac{h}{2} \cos(k \cdot x_2 + \alpha) \quad \alpha \in [0, 2\pi[ \quad (38)$$

- h (m) Wave height;  
k ( $m^{-1}$ ) Wave number;  
 $x_1$  (m) Longitudinal position of the aft plane of the strip;  
 $x_2$  (m) Longitudinal position of the forward plane of the strip.

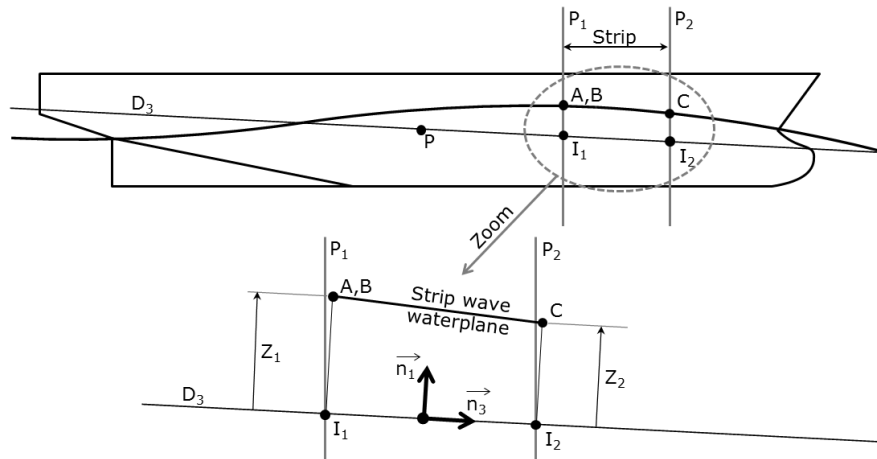


Figure 31 – Strip wave waterplane

The normal vector which defines the local strip's waterplane is calculated as follows:

$$\vec{n} = \frac{\vec{AB} \wedge \vec{AC}}{\|\vec{AB} \wedge \vec{AC}\|} \quad (39)$$

In each strip, the local waterplane cuts the strip's watertight volume to compute the submerged volume of the strip and its center. Then, the displacement volume  $\nabla$  of the entire ship in waves and its center B are calculated.

### 2.3.5. Balance

The balance position is found through an iterative process. Two methods are proposed.

#### *First Method*

At each step of the iterative process, three gaps ( $\varepsilon_{\nabla}$ ,  $\varepsilon_x$  and  $\varepsilon_y$ , two if fixed heel) are computed as explained above. The sinkage, heel and trim are corrected as follows before being used in the next step:

$$e_{i+1} = e_i + \frac{\varepsilon_{\nabla}}{A_{WP}} \quad \varphi_{i+1} = \varphi_i + \frac{\varepsilon_y}{|GM_T|} \quad \theta_{i+1} = \theta_i + \frac{\varepsilon_x}{|GM_L|} \quad (40)$$

With:

- $e_i$  sinkage at step i (m);
- $e_{i+1}$  sinkage at step i+1 (m);
- $\varphi_i$  heel at step i (rad);
- $\varphi_{i+1}$  heel at step i+1 (rad);
- $\theta_i$  trim at step i (rad);
- $\theta_{i+1}$  trim at step i+1 (rad).

Absolute values of the metacentric heights ( $GM_T$  and  $GM_L$ ) let the process diverge in case of transverse or longitudinal instability. Without this, the process should converge to an unstable balance position. At first iteration, the waterplane area ( $A_{WP}$ ) and local metacentric heights ( $GM_T$ ,  $GM_L$ ) are calculated with the hydrostatic table or by direct computation of area and inertia on the waterplane surface mesh, which must be projected on an Earth-horizontal plane in case of computation in waves. At next iterations, they are computed as follows:

$$A_{WP} = \frac{\nabla_{i+1} - \nabla_i}{e_{i+1} - e_i} \quad GM_T = \frac{\varepsilon_{y,i+1} - \varepsilon_{y,i}}{\varphi_{i+1} - \varphi_i} \quad GM_L = \frac{\varepsilon_{x,i+1} - \varepsilon_{x,i}}{\theta_{i+1} - \theta_i} \quad (41)$$

When the three gaps ( $\varepsilon_{\nabla}$ ,  $\varepsilon_x$  and  $\varepsilon_y$ ) are small enough, the balance position is considered reached. This method is compatible with a strong coupling between the heel and trim (unconventional floating structures). However, it is fragile if the coupling between the trim and sinkage is strong because the corrections of trim and sinkage may conflict.

## Second Method

The second method is also iterative and was developed after the publication of the handbook [1]. Before the iterative process, an initial hydrostatic computation gives the three gaps for initial values of  $e$ ,  $\varphi$  and  $\theta$ . At each step of the iterative process, three hydrostatic computations (two if the heel is fixed) are performed. They permit to evaluate separately the influence of a small increment of sinkage, heel and trim on the values of the three gaps. These computations are listed in Table 11.

	Input data			Output data		
1	$e+\varepsilon_e$	$\theta$	$\varphi$	$\varepsilon_{\nabla e}$	$\varepsilon_{xe}$	$\varepsilon_{ye}$
2	$e$	$\theta+\varepsilon_\theta$	$\varphi$	$\varepsilon_{\nabla\theta}$	$\varepsilon_{x\theta}$	$\varepsilon_{y\theta}$
3	$e$	$\theta$	$\varphi+\varepsilon_\varphi$	$\varepsilon_{\nabla\varphi}$	$\varepsilon_{x\varphi}$	$\varepsilon_{y\varphi}$

Table 11 – Hydrostatic computations performed to find balance position.

With:

- $\varepsilon_e$       $d_{full}/100$      small sinkage increment;
- $\varepsilon_\theta$      0.1 degree     small trim increment;
- $\varepsilon_\varphi$      1.0 degree     small heel increment;
- $d_{full}$      (m)     full loaded draft.

Then, still in the same iteration, the following system of three equations with three unknowns (2x2 if the heel is fixed) is solved:

$$\begin{pmatrix} \frac{\varepsilon_{\nabla e} - \varepsilon_{\nabla}}{\varepsilon_e} & \frac{\varepsilon_{\nabla\theta} - \varepsilon_{\nabla}}{\varepsilon_\theta} & \frac{\varepsilon_{\nabla\varphi} - \varepsilon_{\nabla}}{\varepsilon_\varphi} \\ \frac{\varepsilon_{xe} - \varepsilon_x}{\varepsilon_e} & \frac{\varepsilon_{x\theta} - \varepsilon_x}{\varepsilon_\theta} & \frac{\varepsilon_{x\varphi} - \varepsilon_x}{\varepsilon_\varphi} \\ \frac{\varepsilon_{ye} - \varepsilon_y}{\varepsilon_e} & \frac{\varepsilon_{y\theta} - \varepsilon_y}{\varepsilon_\theta} & \frac{\varepsilon_{y\varphi} - \varepsilon_y}{\varepsilon_\varphi} \end{pmatrix} \times \begin{pmatrix} de \\ d\theta \\ d\varphi \end{pmatrix} = \begin{pmatrix} -\varepsilon_{\nabla} \\ -\varepsilon_x \\ -\varepsilon_y \end{pmatrix} \quad (42)$$

The unknowns of this system are  $de$ ,  $d\theta$  and  $d\varphi$ , which are respectively increments of sinkage, trim and heel to be added to the current values to cancel the gaps. The second and third terms of the diagonal are respectively the local longitudinal and transverse metacentric heights. Thus, their sign may be used to detect instability and invert the sign of the trim and heel increments, in order to diverge from an unstable balance position.

At the end of the iteration, a final hydrostatic computation is done using corrected values of the sinkage, trim and heel. If the three gaps are small enough, the balance position is considered reached.

This second method is as suitable as the first for a strong coupling between the heel and trim. It is more robust in case of strong coupling between the trim and sinkage. The number of iterations is very small (1 or 2, see Table 12) but the number of hydrostatic computations is similar. If  $n$  is the number of iterations, the number of hydrostatic computations is  $3n + 1$  if the heel is fixed and  $4n + 1$  if it's free.

### Comparison of Both Methods

Table 12 shows the GZ computed for a 160 m passenger vessel (presented in Annex 2) using both methods. It also shows numbers of iterations (Nb. iter.) and hydrostatic computations (Nb. comp.) to find each balance position with fixed heel. The maximum allowed gaps are 1 m<sup>3</sup> in volume (to be compared to the 13,000-tons displacement) and 1 millimeter for  $\varepsilon_x$ . The maximum difference between both values of GZ is lower than 0.02 millimeters (not visible in Table 12).

Heel (deg.)	First method			Second method		
	GZ (m)	Nb. iter.	Nb. comp.	GZ (m)	Nb. iter.	Nb. comp.
0	0.000	8	8	0.000	2	7
1	0.042	6	6	0.042	1	4
2	0.085	7	7	0.085	1	4
3	0.130	11	11	0.130	1	4
4	0.176	7	7	0.176	1	4
5	0.224	7	7	0.224	1	4
10	0.484	8	8	0.484	2	7
15	0.774	8	8	0.774	2	7
20	1.103	8	8	1.103	2	7
25	1.441	7	7	1.441	2	7
30	1.737	8	8	1.737	2	7
35	1.984	5	5	1.984	2	7
40	2.179	5	5	2.179	2	7
45	2.252	6	6	2.252	2	7
50	2.189	6	6	2.189	2	7
	Sum		107	Sum		90

Table 12 – Comparison of both balance methods.

### 2.3.6. Calculation of Transverse Metacentric Height

The transverse metacentric height is computed using two first points of the GZ curve (0 and 1 degree).

$$GM_T = \left( \frac{dGZ}{d\varphi} \right)_{\varphi=0} \quad (43)$$

In the case of the hydrostatic computation on waves, the inertia of the projected waterplane is not used as proposed in the simplified strip method proposed by the IMO (see SLF 52/INF.2 Annex 6, [19]).

## CHAPTER 3. RESULTS

### 3.1. PRELIMINARY INFORMATION

#### 3.1.1. General Information

This chapter presents the results of the computations of the second generation intact stability criteria, in both pure loss of stability and parametric roll failure modes and in both level one and level two, applied to a panel of civilian and military ships presented in Annex 2. Six civilian ships are chosen for their variety of type and size: two large container vessels, one roll-on roll-off vessel, one tanker and two passenger vessels (one large, one small). Different behaviors with regard to both failure modes are expected. Some container vessels are already known to be vulnerable to parametric roll [41, 45] while tankers, characterized by a wall-sided hull shape, are expected not to be vulnerable. Although the future IMO intact stability rules are not intended for naval ships, it seems interesting to the author to assess such different vessels with regard to these future criteria. This choice is argued hereunder.

The results are given as  $KG_{max}$  curves. These curves indicate the maximum height of the center of gravity above the baseline ensuring the compliance of a specific criterion or a set of criteria as a function of the displacement or the draft. Considering  $KG_{max}$  curves allows to avoid any assumption about the height of the center of gravity and provides richer information than the classical binary “pass/fail” associated with a specific loading condition [29]. Especially, this permits the comparison of the requirement of the criterion of each level and the comparison of different computation methods proposed for a specific criterion in order to determine the efficiency and the relevance of the new criteria.

Moreover,  $KG_{max}$  curves associated with the new generation intact stability criteria are compared to those associated with both current IMO and current French military rules (respectively [18] and [17]). This allows assessing the vulnerability of the selected ships with regard to both failure modes. A ship may be considered vulnerable to pure loss of stability or parametric roll if her  $KG_{max}$  curve associated with the current regulation (civilian or military) is located above the highest curve associated with the pure loss of stability criteria (we formulate this consideration in this thesis) because the current regulation would allow sailing with a KG assessed as dangerous by the new criteria.

Similar works have already been performed [31, 33] although they deal with former versions of the new criteria (respectively SLF 54/19, 2012 [20] and SDC 1/INF.8, 2013 [21]).

The hydrostatic computations in calm water and in static waves are performed by Calcoque software as presented in Chapter 2. All computations are performed with the water density equal to  $1.025 \text{ t/m}^3$  and with zero trim (the sinkage and trim remain free while the ship is balanced in waves).

#### 3.1.2. Application to Military Vessels

Accidents caused by the failure modes considered in the second generation intact stability criteria may be fatal (see the report of the accident occurred to the *Chicago Express* off

Hong-Kong in 2008, [60]) or may cause significant financial losses (*APL China* in October 1998 [41], *Maersk Carolina* in January 2003 [45]), but they are fortunately rare. Since the number of naval ships in service is significantly smaller than the number of merchant vessels and their time at sea is smaller too, it is not surprising that none of the serious accidents causing the development of the new criteria has occurred on a naval ship. However it cannot be excluded in principle that naval ships be vulnerable to such stability failures. Although the new regulations are not intended for naval ships, it seems interesting to assess the outcome of their applications. In fact the hull geometry and the high speed of naval ship typology are in principle a remarkable combination worthy of attention.

Hence, a set of three military vessels, chosen for their variety of typology and size, has been included in this study: a 12,000-ton helicopter carrier, a 9,000-ton destroyer and a 1,500-ton Offshore Patrol Vessel.

### 3.1.3. Graphic Design

All figures showing the  $KG_{max}$  curves in paragraphs 3.2.1 (pure loss of stability) and 3.3.1 (parametric roll) have the same graphic design:

- The  $KG_{max}$  curve associated with the current IMO regulation [18] is drawn as a grey dashed line.
- The  $KG_{max}$  curve associated with the French military regulation (IG 6018A DGA [17]), computed only for naval vessels, is drawn as a grey dotted line.
- The light blue plain line indicates the height of the transverse metacenter above the baseline (KMT) which allows to determine the minimum GM required by all criteria.
- The vertical grey lines indicate the full-load displacement and, when it is known, the light displacement. Otherwise, a black dot corresponds to the standard loading condition of the ship.
- The  $KG_{max}$  curve associated with the first method of level one (parallel waterplane) criteria of both pure loss of stability and parametric roll failure modes is drawn in blue with square markers.
- The  $KG_{max}$  curve associated with the second method of level-one criteria (ship balanced in trim and sinkage on a wave with the same length) is drawn in red with round markers.
- The  $KG_{max}$  curve associated with the level-two criteria (first check only for parametric roll) is drawn as a green solid line with diamond markers.
- The  $KG_{max}$  curve associated with the second check of level-two parametric roll criterion is drawn as a green dashed line with diamond markers.

## 3.2. PURE LOSS OF STABILITY

Since neither the 319 m container vessel nor the tanker fulfill the condition on Froude number ( $F_n > 0.24$ ), their  $KG_{max}$  curves associated to level 1 and 2 criteria are not presented. Both vessels are assessed as non-vulnerable to the pure loss of stability by the new regulation.

Parts of the content of this section have already been presented in [3] (influence of the watertight deck height), [5] (results on naval vessels) and [2, 6] (results on some civilian vessels and one naval vessel).

### 3.2.1. General Results

The  $KG_{max}$  curves associated with level-one and level-two criteria of pure loss of stability failure mode are shown in Figure 32 to Figure 38. We can observe the following facts:

- 1) In Figure 34 (160 m passenger vessel), the curve associated with the first method of level one has a hook at a displacement equal to 12,200 tons (draft equal to 5.67 m). This particularity results from a loss of inertia on the parallel waterplane due to the stabilizers' housings (see dark grey waterplane in Figure 39). Using the bare hull would mask this phenomenon.
- 2) Each level-one method yields significantly different results for all vessels with no exception.
- 3) The  $KG_{max}$  associated with the second level-one method is relatively close to that given by level two for the C11 container vessel, the Ro-Ro vessel and the *Jeanne d'Arc*.
- 4) Level two can be more conservative than the second level-one method: one point for the C11 container vessel and completely for the Ro-Ro vessel, both passenger vessels and all naval ships. This is contrary to what seems to be the philosophy of the future regulation.
- 5) Level two is more conservative than the first level-one method for the 30 m passenger vessel, but this occurs at a significantly higher displacement than the standard loading condition. However, this proves the possibility of this unexpected configuration.
- 6) The C11 container vessel is found to be vulnerable to pure loss of stability according to these criteria. The 160 m passenger vessel is found to be slightly vulnerable since the gap between the  $KG_{max}$  required by the second method of level one is slightly lower than that required by the current regulation. None of the three naval ships is assessed as vulnerable. No conclusions can be drawn with regard to the Ro-Ro vessel since her superstructures are not modelled and the weather criterion is not taken into account.

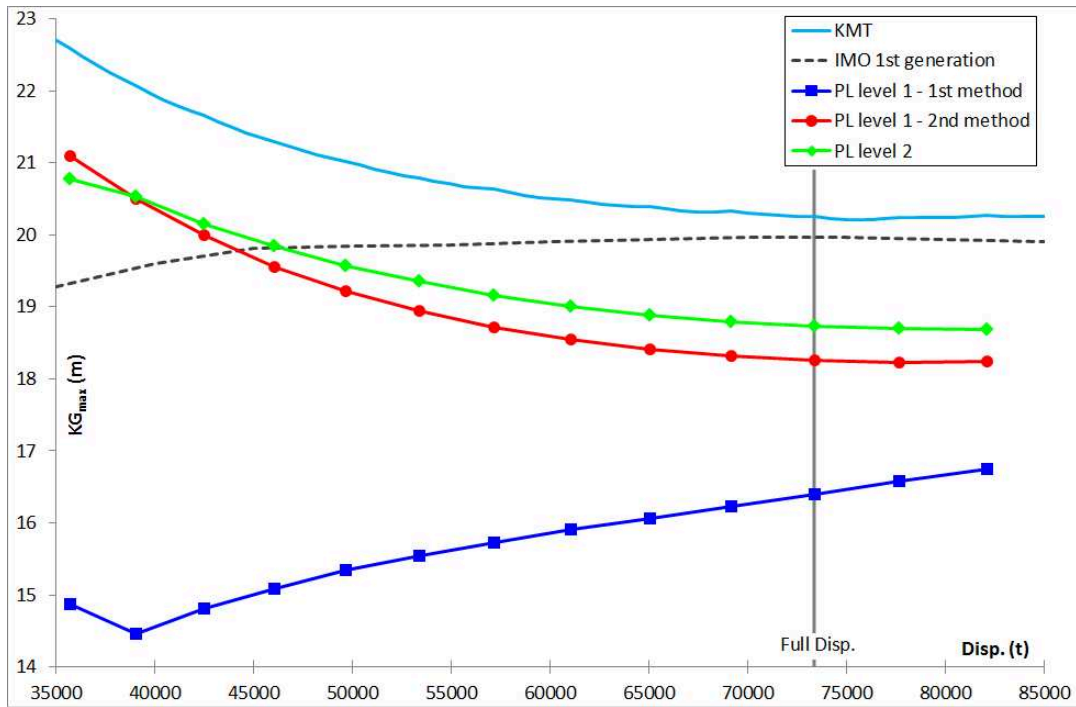


Figure 32 –  $KG_{max}$  curves associated with pure loss of stability criteria for the C11 container vessel.

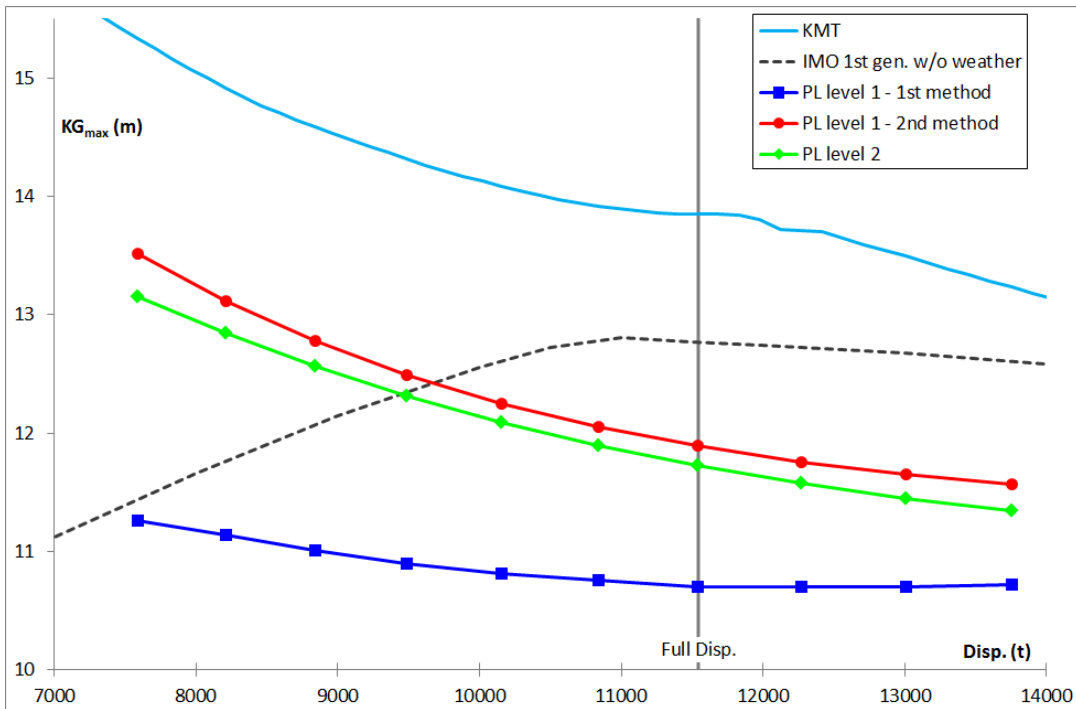


Figure 33 –  $KG_{max}$  curves associated with pure loss of stability criteria for the Ro-Ro vessel.

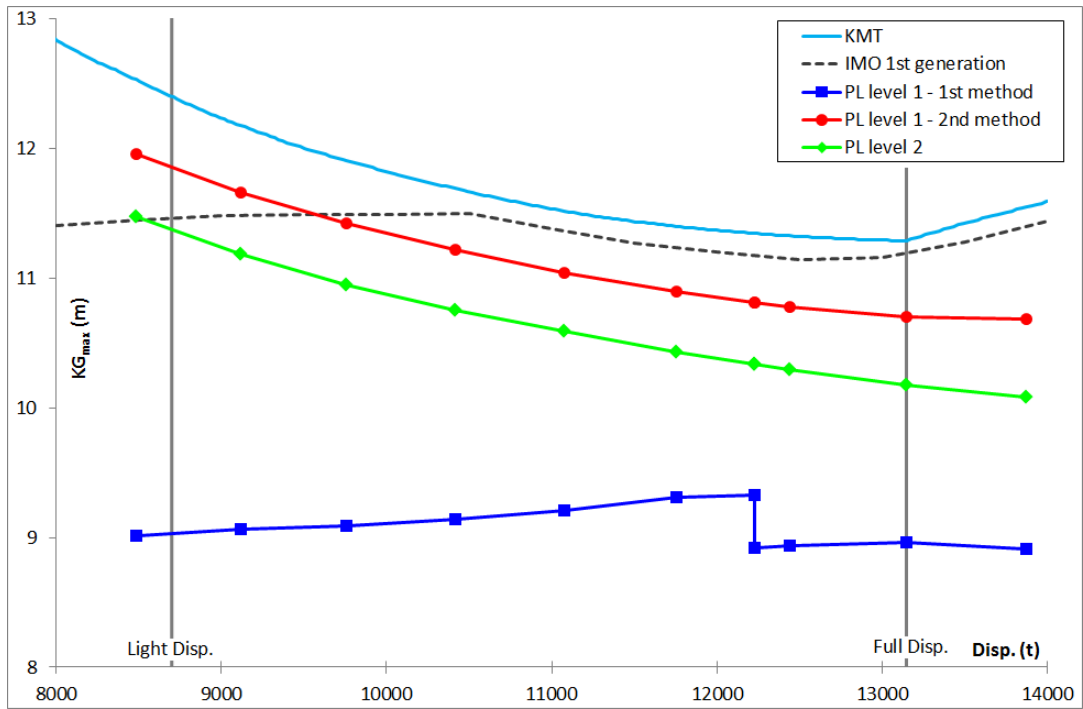


Figure 34 –  $KG_{max}$  curves associated with pure loss of stability criteria for the 160 m passenger vessel.

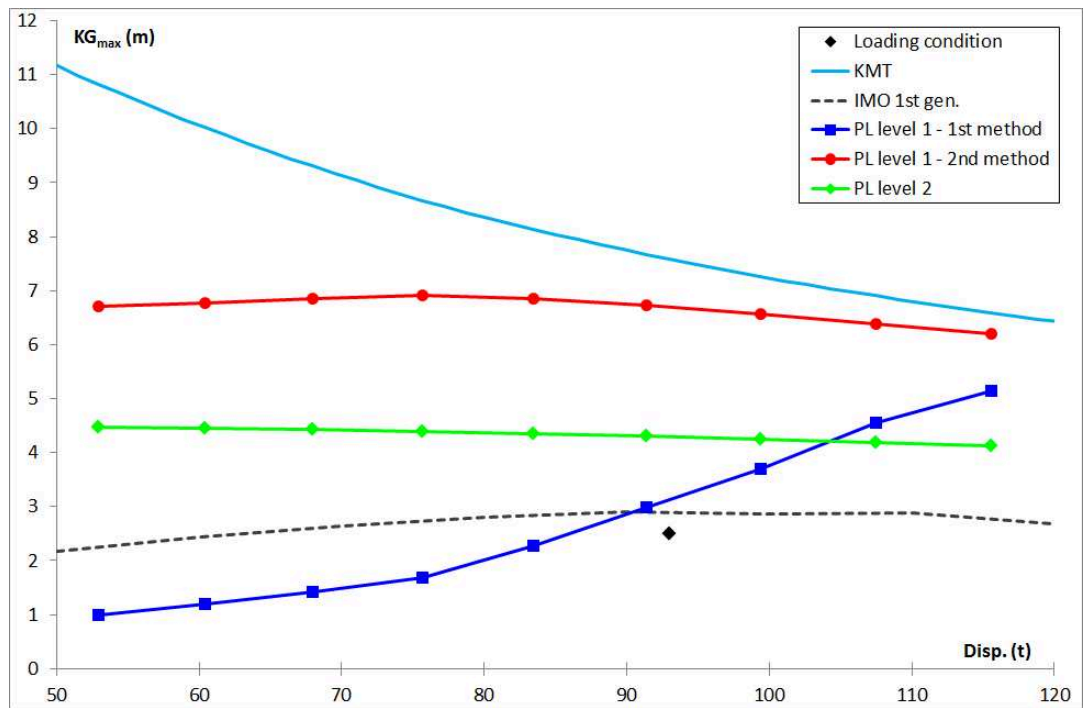


Figure 35 –  $KG_{max}$  curves associated with pure loss of stability criteria for the 30 m passenger vessel.

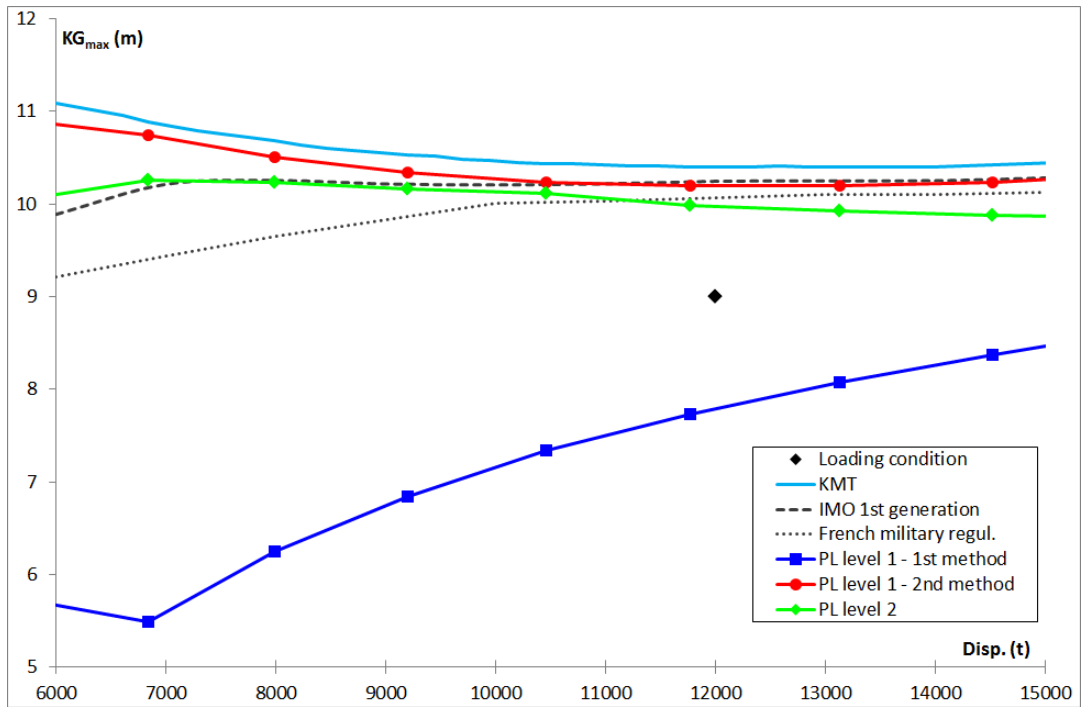


Figure 36 –  $KG_{max}$  curves associated with pure loss of stability criteria for the *Jeanne d'Arc*.

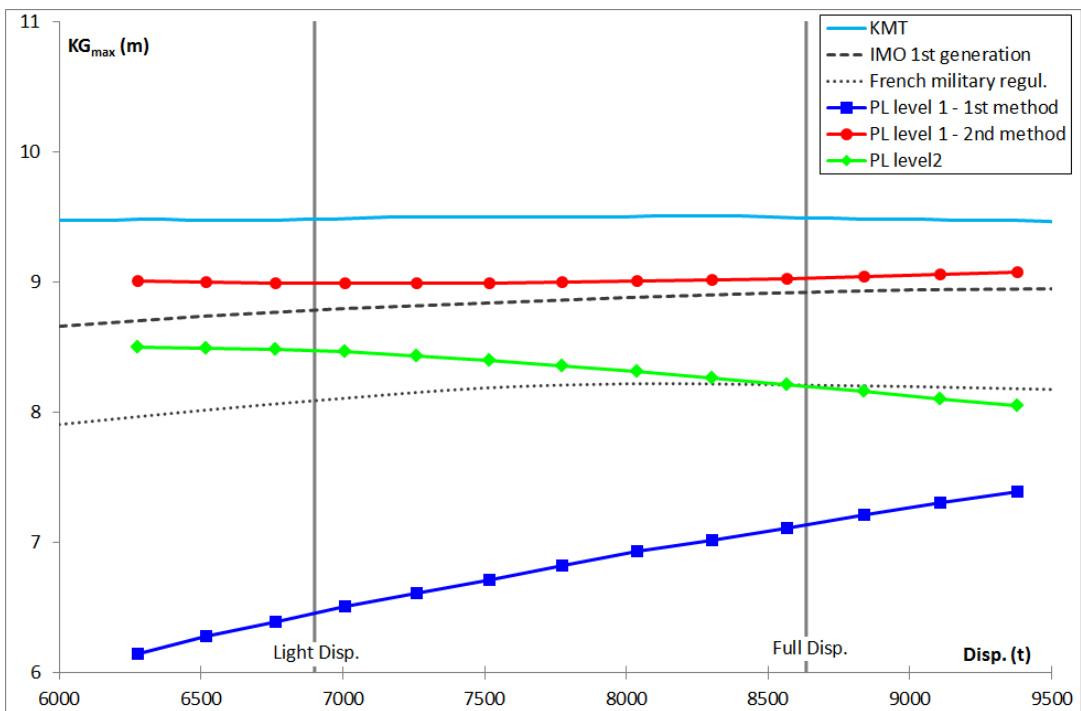


Figure 37 –  $KG_{max}$  curves associated with pure loss of stability criteria for the DTMB-5415.

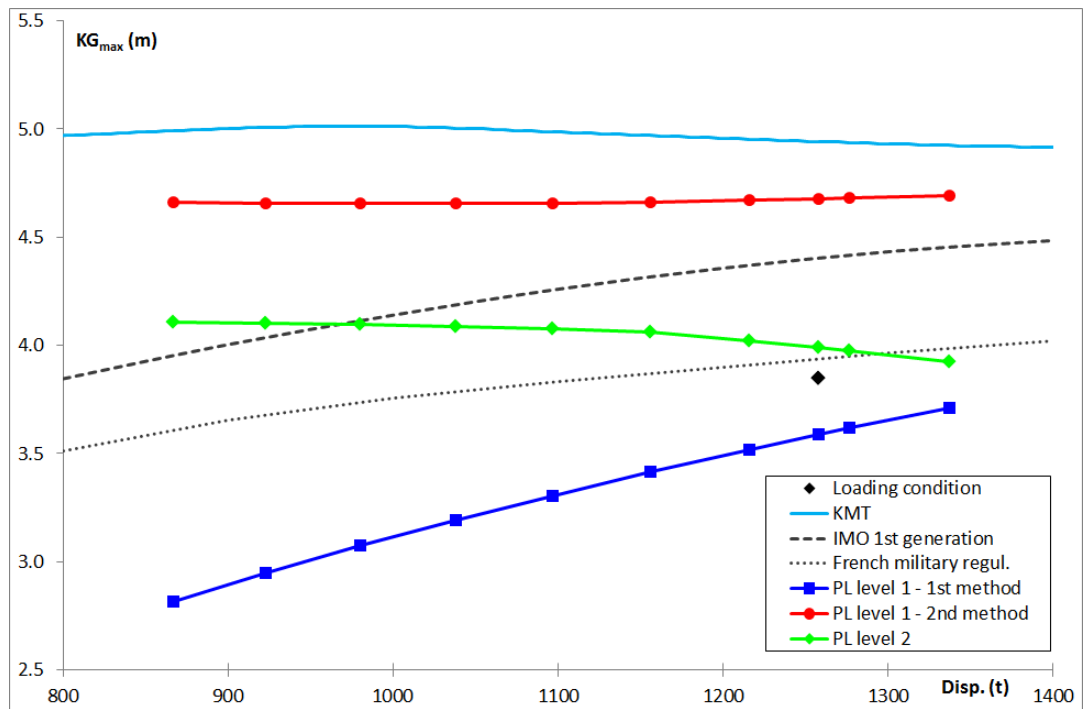


Figure 38 –  $KG_{max}$  curves associated with pure loss of stability criteria for the Offshore Patrol Vessel.



Figure 39 – Parallel waterplanes for  $d=6.00$  m (light grey) and  $d_L=3.33$  m (dark grey).

### 3.2.2. Influence of the Watertight Deck Height

In intact stability configuration, the watertight deck of the 160 m passenger vessel is the weather deck, located 14 m above the base line. The associated watertight volume includes the car garage as shown in Figure 119 (page 121).

We propose now to consider the bulkhead deck as new watertight deck. It is located 9 m above the baseline. The associated watertight volume excludes the car garage as shown in Figure 120.

#### *First Level*

Lowering the watertight deck has normally no influence on the level-one criterion which considers only metacentric height (hence small inclinations). For the first method (parallel waterplane at lowest draft), this is evident. For the second method (GM computation on wave), the wave crest should pass over the watertight deck, reducing the waterplane and its inertia. This situation does not occur with the watertight deck at 9 m (free-board at full load is 3 m, to be compared with wave half-height equal to 2.67 m). However, it appears at a draft over 6 m if the watertight deck is lowered at 8 m (in this case the ship does not fulfill the current regulation with any KG). See resulting  $KG_{max}$  curves in Figure 40.

The situation for the last point of the curve “Watertight deck @ 8 m” in Figure 40 ( $d=6.25$  m) is shown in Figure 41. The waterplane is truncated on a quarter of its length. This situation

should not occur in reality because the wave crest should not flood the garage deck even if its volume is considered as not watertight (Figure 42).

Note: The future regulation should clearly specify the watertight volume to consider. French military regulation (IG6018A, [17]) considers two different watertight volumes. The bulkhead deck is its upper limit which is tight to long-time immersion. This watertight volume is considered in damage stability. In this example, this deck is the garage deck at 9 m above baseline. The weather deck is the upper limit which is tight to short-time immersion. The weather deck of some naval ships coincides with the bulkhead deck (partially or totally). Otherwise the weather deck is located above. The increased watertight volume associated with this deck is considered in intact stability. In this example, this deck is the first passenger deck located 14 m above the baseline.

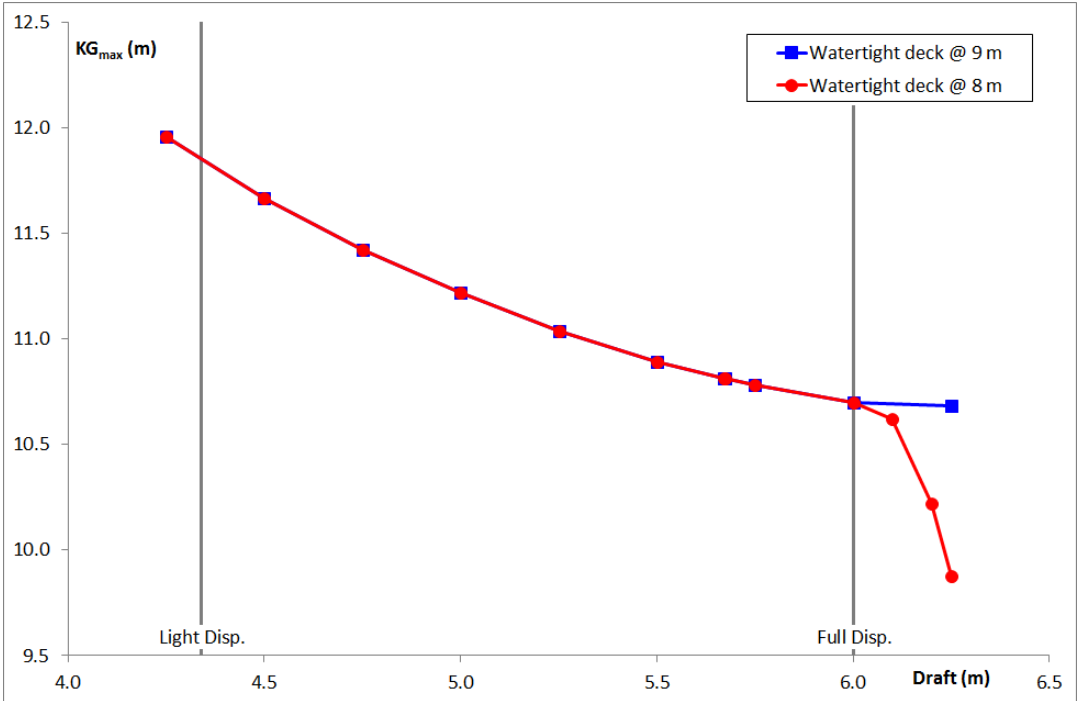


Figure 40 – KG<sub>max</sub> curves for 1<sup>st</sup> level criterion (2<sup>nd</sup> method) for watertight deck at 9 and 8 m.

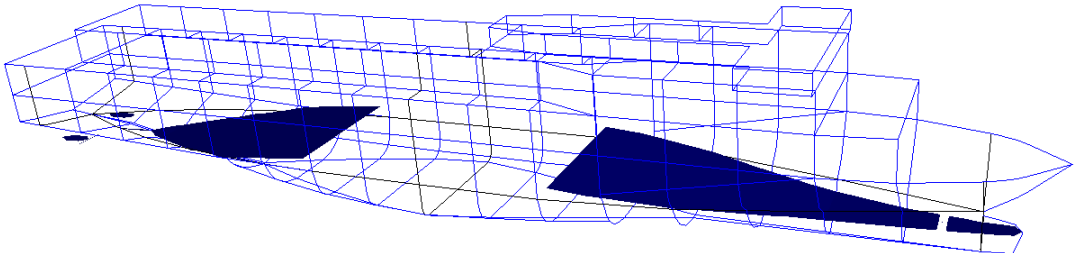


Figure 41 – Truncated waterplane.

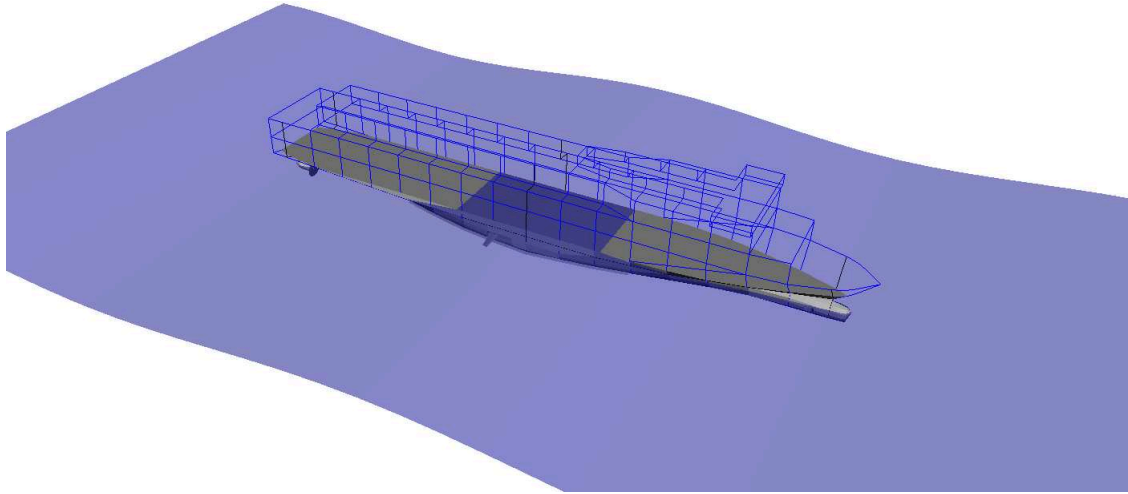


Figure 42 – Flooded garage deck in waves.

### Second Level

$KG_{max}$  curves associated with the second level criterion for both heights of the watertight deck are shown in Figure 43. We observe that lowering the watertight deck highly increases the requirement of the criterion by significantly lowering the associated  $KG_{max}$ . This is expected as a result of the strong reduction of the GZ from the heel angle corresponding to the immersion of the bulkhead deck edge. However, we note that first generation criteria also increase their requirement to such an extent that the ship is now assessed as non-vulnerable to the pure loss of stability failure mode.

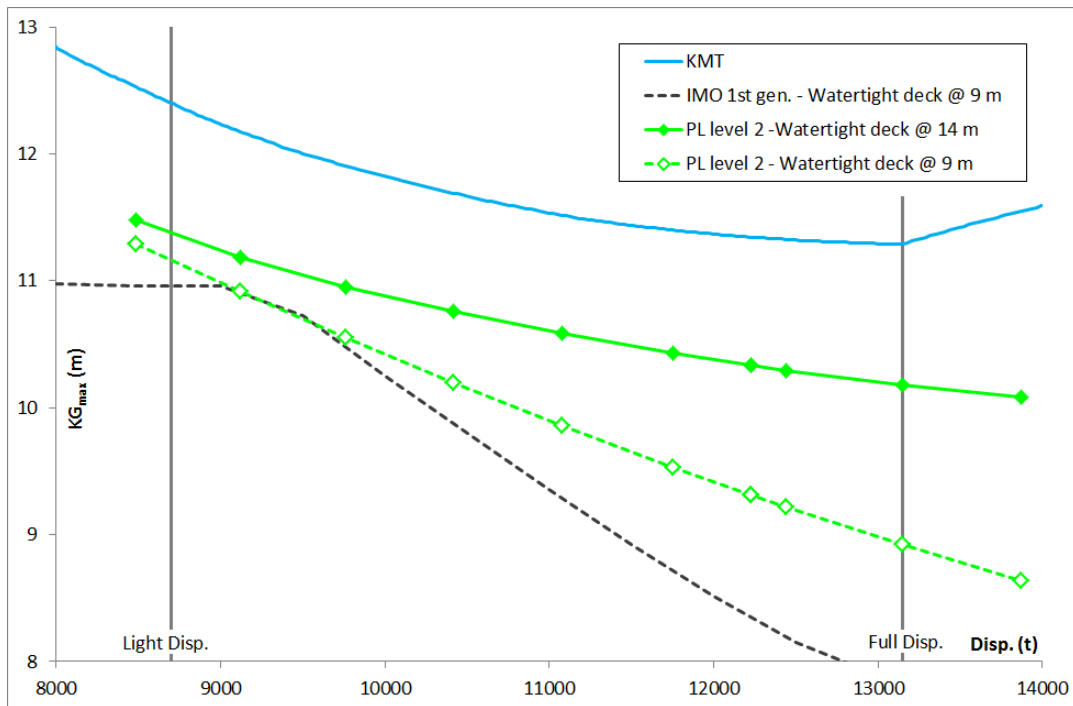


Figure 43 –  $KG_{max}$  curves associated with level-2 pure loss of stability criterion for the 160 m passenger vessel, watertight deck @ 14m and 9 m.

### 3.2.3. Influence of Speed

The pure loss of stability failure mode depends on the speed of the ship which must stay centered amidships on the wave crest during a sufficiently long time to attain a dangerous heel angle. Hence, the associated level-one and level-two criteria apply to ships having a service speed Froude number larger than 0.24.

The speed of the ship has no influence on the level-one criterion. However, it has an influence on the level-two criterion through the heeling lever  $R_{PL3}$  which depends on the Froude number (Equation (6) page 21).

The service speed of the Ro-Ro vessel is 20 knots. The associated Froude number is equal to 0.28. We consider two other service speeds equal to 17 and 25 knots, giving Froude numbers respectively equal to 0.24 (lowest value making the ship eligible to the pure loss of stability criteria) and 0.35. Figure 44 compares the  $KG_{max}$  curves associated with the three speeds. As expected, lowering the service speed increase  $KG_{max}$  since the vulnerability of the ship is reduced.

We perform the same test on the 30 m passenger vessel at speeds equal to 7.5 and 12.5 knots, corresponding to Froude numbers respectively equal to 0.24 and 0.4, since the original service speed is 22 knots and the associated Froude number is 0.7. We could expect a result similar to that of the Ro-Ro vessel. However, we observe that the speed has no influence on the  $KG_{max}$ . The shape of the hull, characterized by a large breadth-over-depth ratio (see Figure 122 page 122), causes the condition considering the angle of vanishing stability ( $C1_i$ , regarding  $\Phi_V$  vs  $R_{PL1}$ ) to be met before that considering the angle of stable equilibrium ( $C2_i$ , regarding  $\Phi_S$  vs  $R_{PL2}$ ) in all wave cases (Equation (7) page 22). The speed is not considered in the first condition while it is considered in the second through  $R_{PL3}$  (Equation (6) page 21).

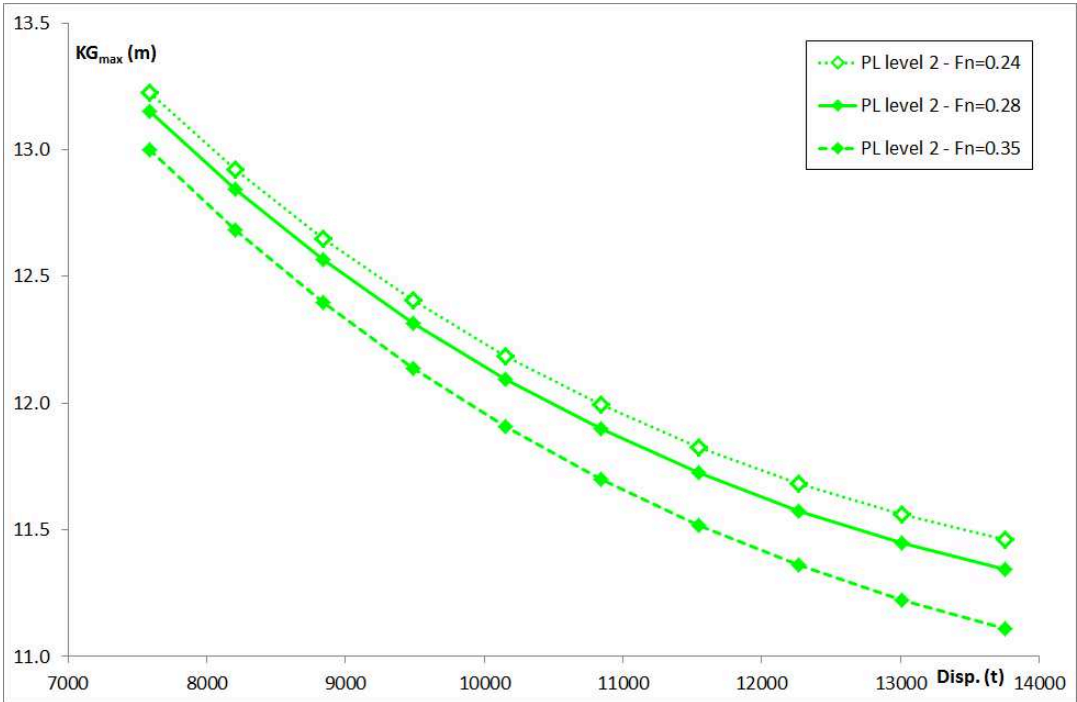


Figure 44 – Influence of speed on  $KG_{max}$  curves associated with pure loss of stability level-two criterion for the Ro-Ro vessel.

### 3.3. PARAMETRIC ROLL

#### 3.3.1. General Results

Parts of the content of this section have already been presented in [5] (results on naval vessels) and [6] (results on some civilian vessels and one naval vessel).

The  $KG_{max}$  curves associated with level-one and level-two criteria of parametric roll failure mode are shown in Figure 45 to Figure 53. Although both checks C1 and C2 are embedded to the same level-two criterion, they are considered separate criteria here. Hence, they are associated with two different  $KG_{max}$  curves. We can observe the following facts, some of which are similar to those observed for the pure loss of stability failure mode:

- 1) In Figure 49 (160 m passenger vessel), the curve associated with the first method of level one has two hooks at displacements equal to 8,700 tons and 11,300 tons, similar to that observed at 12,200 tons in pure loss of stability. The reason is the same (loss of inertia due to the stabilizers' housings) but the displacements are different because the considered wave heights are different too.
- 2) The results of both level-one methods significantly differ for the 160 m passenger vessel and all naval vessels.
- 3) The  $KG_{max}$  associated with the second level-one method is almost equal to that given by the first check of level two for the tanker, the 30 m passenger vessel and all naval vessels.
- 4) The first check of level two is partially more conservative than the second level-one method for the Ro-Ro vessel and the 160 m passenger vessel. However, this inconsistency is reduced with regard to that observed in pure loss of stability.
- 5) Both level-one methods give the same  $KG_{max}$  for the tanker at full-load displacement and beyond. This is expected as a result of the cylindrical shape of the hull.
- 6) The first check of level-two criterion is limited by zero-GM beyond the full-load displacement for the tanker (Equation (21) page 28).
- 7) Figure 48, Figure 49 and Figure 51 show that the  $KG_{max}$  associated with the second check of level-two criterion is coincident or almost coincident with KMT. This is due to the limit imposed by the negative average value of the metacentric height in waves ( $GM_{moy}$ , see Section 1.2.4 page 33) and shows that these vessels (tanker, 160 m passenger vessel and *Jeanne d'Arc*) are not vulnerable to parametric roll since the criterion is no longer fulfilled when the ship becomes statically unstable in waves.
- 8) The second check of level-two criterion is less conservative than the first check for all ships except the 30 m passenger vessel (Figure 50). This exception is probably due to the inadequacy of the Ikeda simplified roll damping method to ships having sharp bilge (see Figure 122 page 122). However, this method, taken from [48] for the lift component and [50] for other components, is explicitly described in the explanatory notes of parametric roll criteria (SDC 3/WP.5, Annex 4, Appendix 4, [23]). It would be wise to propose another simplified method for this type of ships in the future regulation.
- 9) The curve associated with the second check of level-two criterion for the 319 m container vessel has two strange jumps (at 75,000 and 105,000 tons, Figure 46). Lesser

jumps exist on the same curve for the C11 container vessel (at 45,000 and 50,000 tons, Figure 45). This point is developed in Section 3.3.2.

- 10) Both container vessels are considered to be vulnerable to parametric roll according to these criteria. This confirms what is already known for the C11 [41]. The Ro-Ro vessel may also be considered to be vulnerable at full-load displacement because the  $KG_{max}$  associated with C2 is lower than that associated with the 1<sup>st</sup> generation criteria. However, these criteria do not include the weather criterion and would probably be more conservative if the ship's superstructure were modelled. All other vessels are considered as non-vulnerable to parametric roll according to the new criteria.

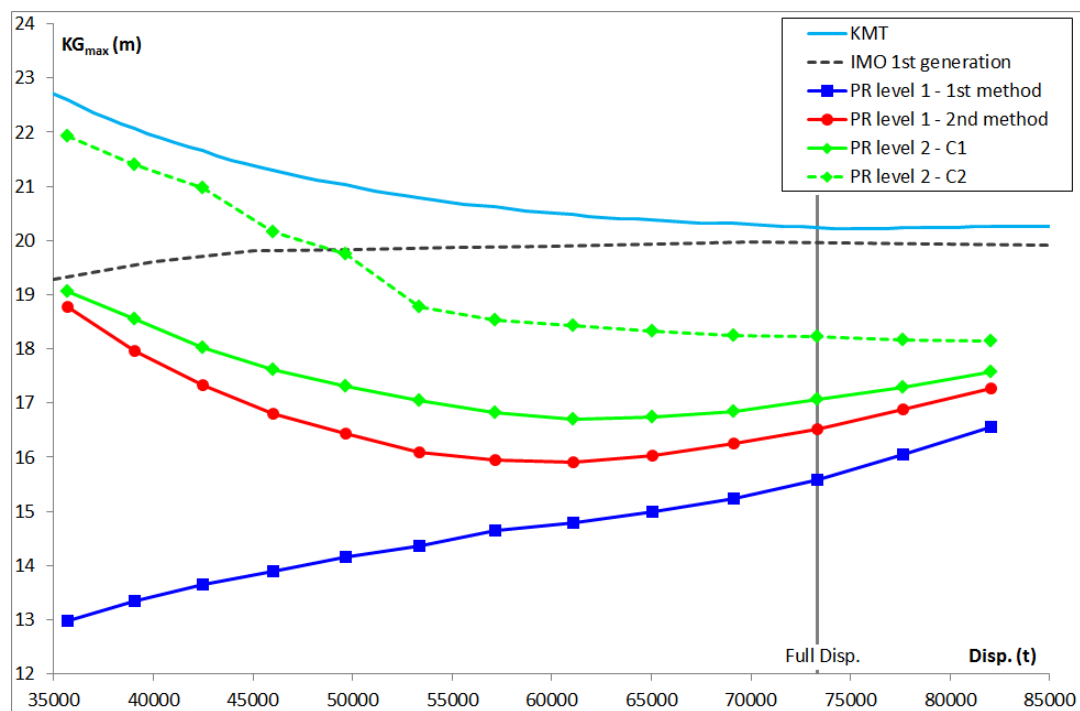


Figure 45 –  $KG_{max}$  curves associated with parametric roll criteria for the C11 container vessel.

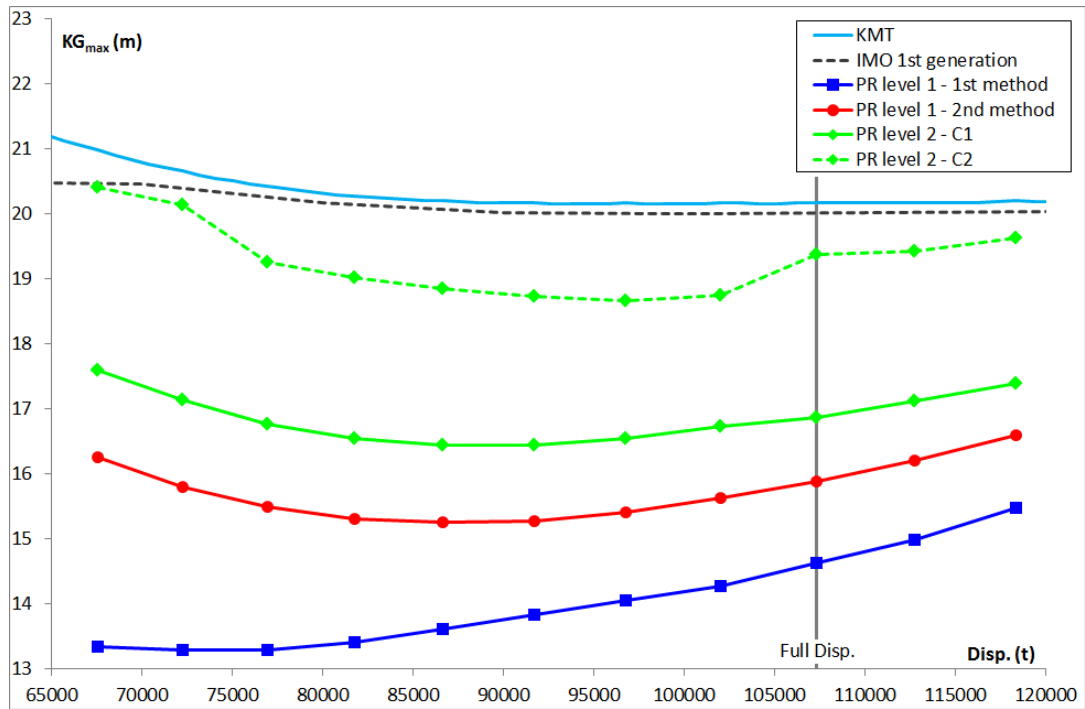


Figure 46 –  $KG_{max}$  curves associated with parametric roll criteria for the 319 m container vessel.

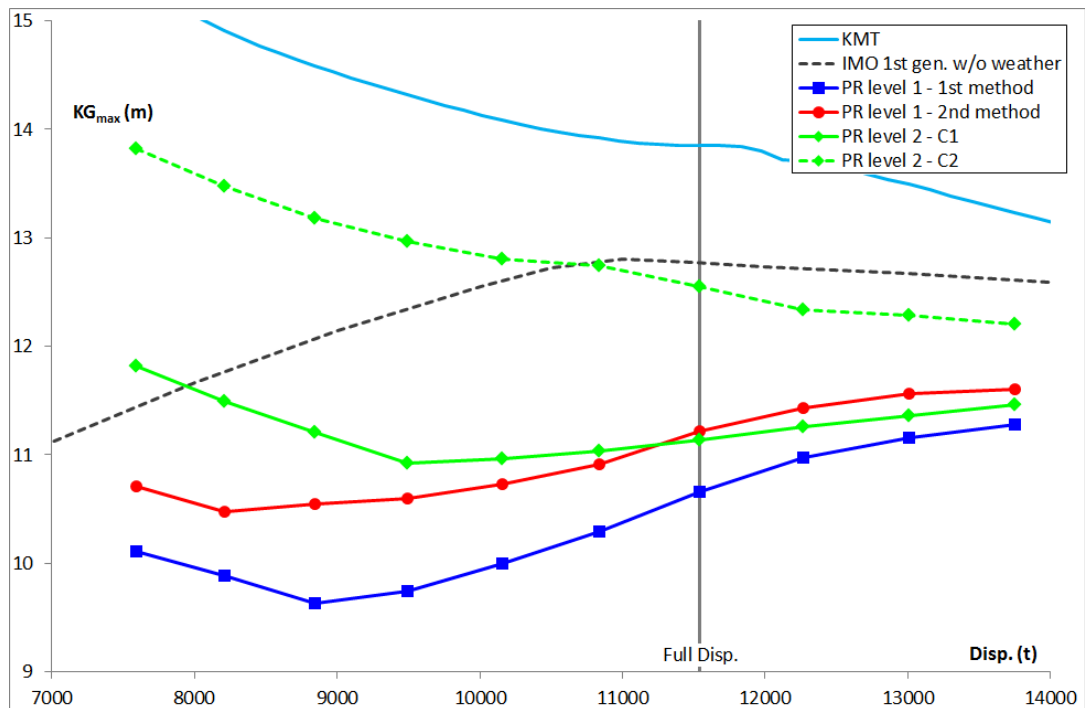


Figure 47 –  $KG_{max}$  curves associated with parametric roll criteria for the Ro-Ro vessel.

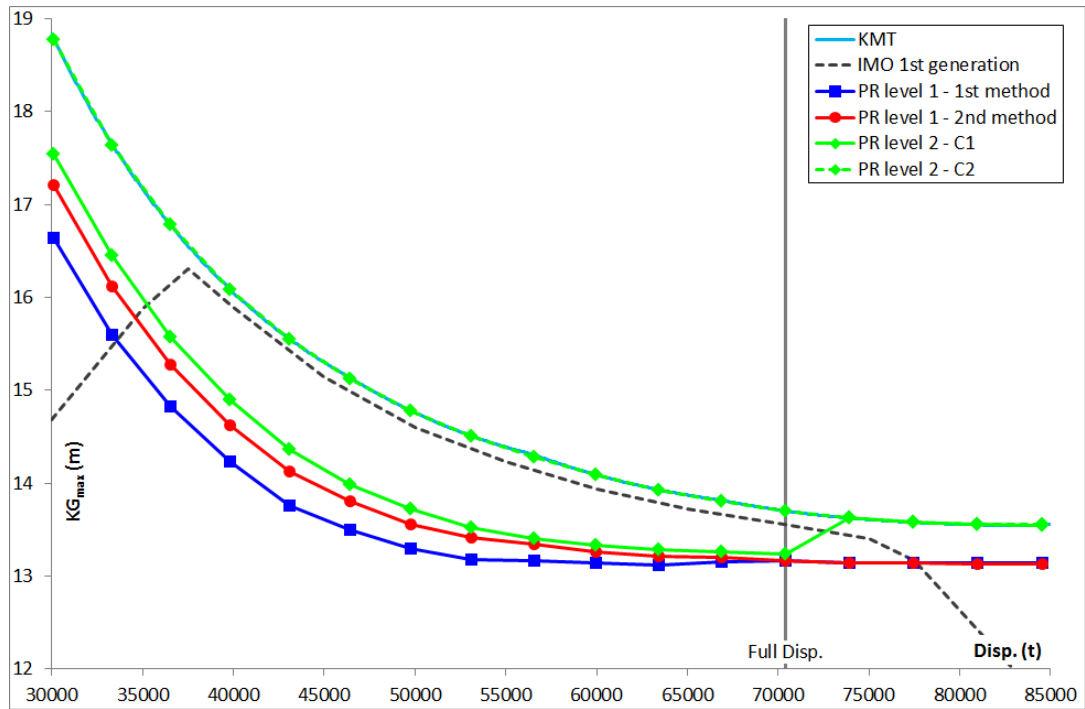


Figure 48 –  $KG_{max}$  curves associated with parametric roll criteria for the tanker.

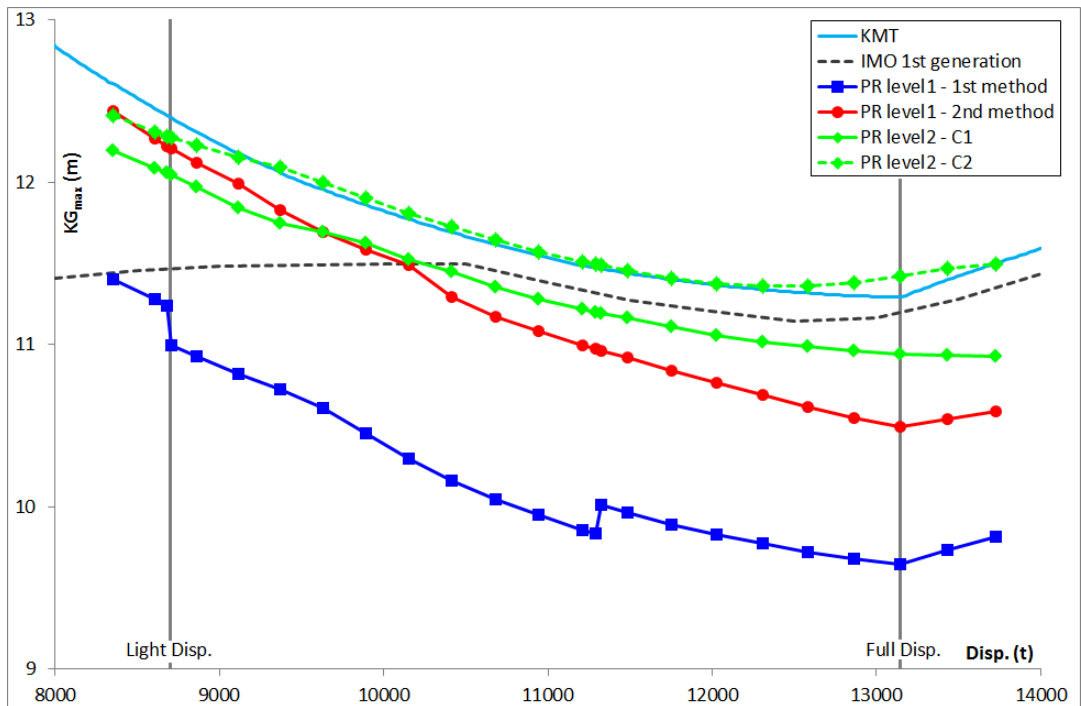


Figure 49 –  $KG_{max}$  curves associated with parametric roll criteria for the 160 m passenger vessel.

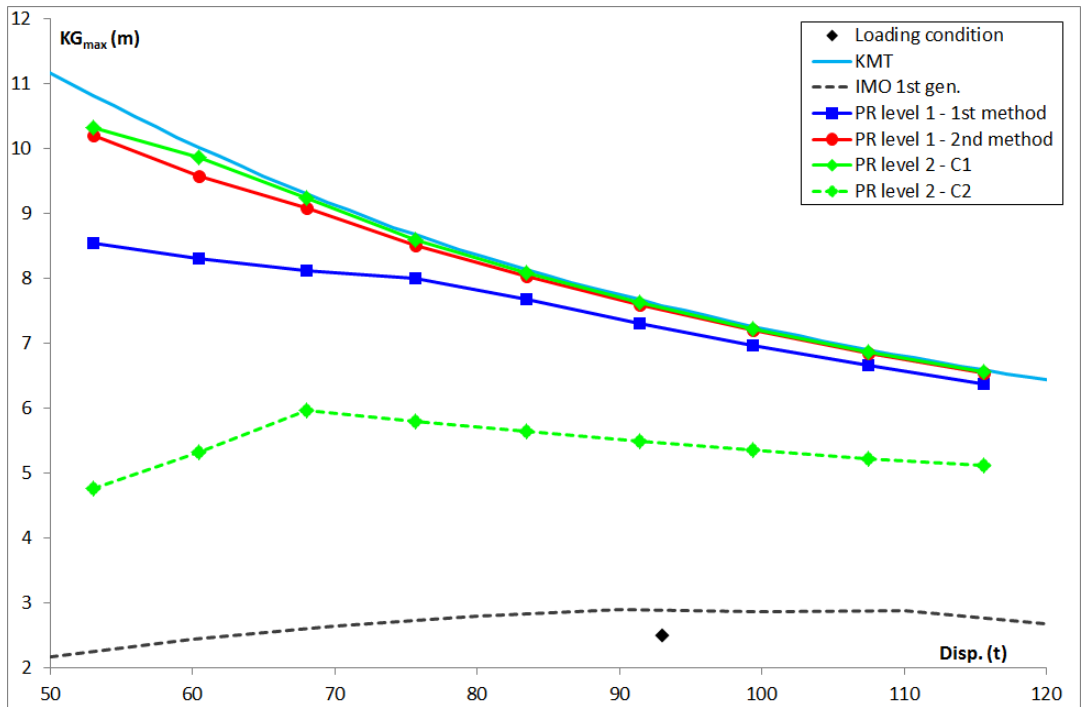


Figure 50 – KG<sub>max</sub> curves associated with parametric roll criteria for the 30 m passenger vessel.

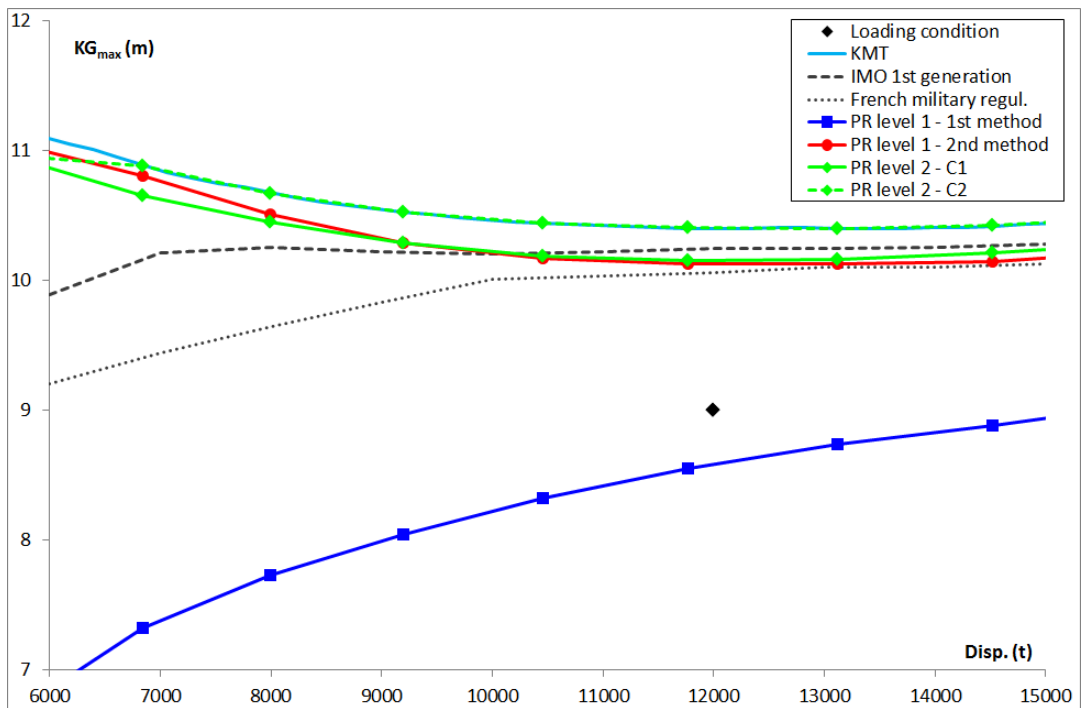


Figure 51 – KG<sub>max</sub> curves associated with parametric roll criteria for the *Jeanne d'Arc*.

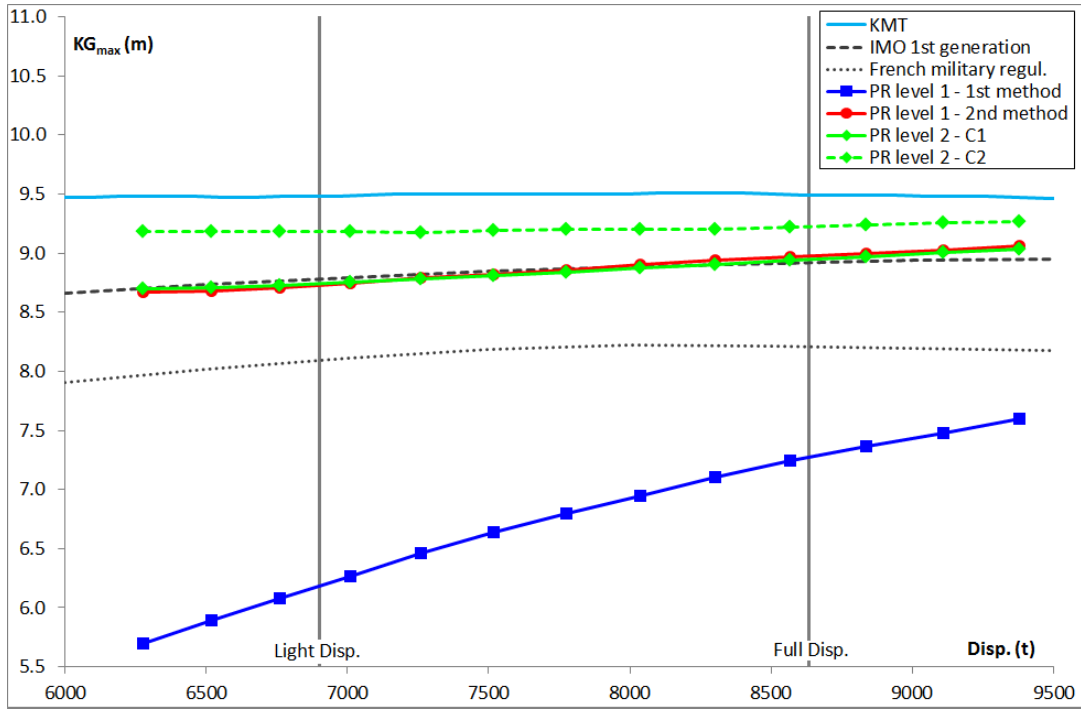


Figure 52 –  $KG_{max}$  curves associated with parametric roll criteria for the DTMB-5415.

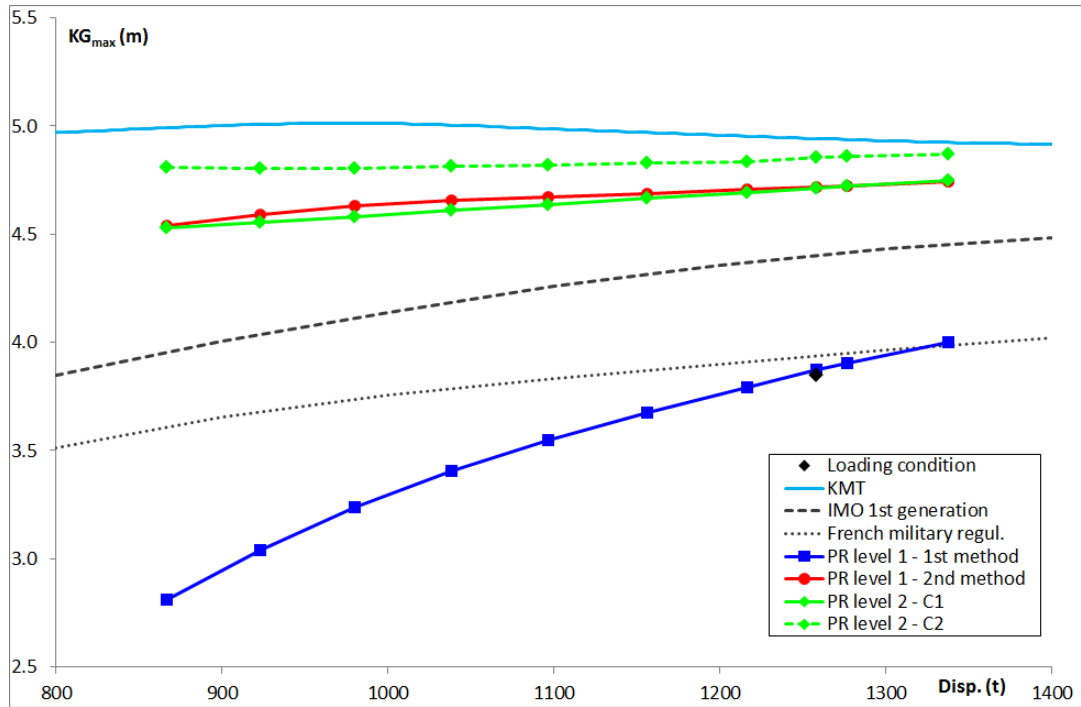


Figure 53 –  $KG_{max}$  curves associated with parametric roll criteria for the Offshore Patrol Vessel.

### 3.3.2. Focus on Second Check

The content of this section has already been presented in [6].

For any ship at any draft, the  $KG_{max}$  associated with the second check of level-two criterion (C2) is defined as the highest value of KG for which the value of C2 is lower than  $R_{PRO}=0.06$ . Thus, it is interesting to check the curve of C2 versus KG. These curves are shown in Figure 54 to Figure 58 for five of the vessels studied in this thesis. For the non-vulnerable ships (Ro-Ro, tanker, DTMB-5415), they are computed at full-load draft for an interval containing  $KG_{max}$  with a step of 2 centimeters. For both container vessels, assessed as vulnerable, they are computed for a larger interval of KG with a step of 1 centimeter, at a draft equal to 10 m (C11 container vessel, Figure 54) and 12 m (319 m container vessel, Figure 55).

Figure 57 shows the curve of the tanker. C2 is equal to 0 for all values of KG lower than  $KG_{max}$  (13.70 m) and to 1 for all higher values. This shows that the parametric roll never occurs on this ship. The value of C2 is forced to 1 when the average value of GM in waves becomes negative (see Section 1.2.4 page 33).

Figure 58 shows the curve for the DTMB-5415. We observe a small interval of KG (centered approximately at 8.70 m) in which C2 is non-zero. This shows that the parametric roll occurs for some lightly-weighted waves. For higher values of KG, C2 tends to zero and then rapidly increases to 1. Parametric roll occurs in these conditions of KG but the average value of GM is near zero: the ship becomes statically unstable on waves.

Figure 56 shows the curve C2 versus KG for the Ro-Ro vessel. We observe that the increasing part of the curve is longer than those of the tanker and the naval ship. We also observe that two values of KG larger than  $KG_{max}$  (12.57 m) give values of C2 lower than  $R_{PRO}$  (KG = 12.60 and 12.62 m, marked with \* in Figure 56).

Figure 54 and Figure 55 show the same curves respectively for the C11 and the 319 m container vessels. On both, we observe many peaks and relatively large intervals of KG larger than  $KG_{max}$  for which the value of C2 is lower than  $R_{PRO}$ , thus for which the associated criterion is fulfilled. These intervals are colored in grey in the corresponding figures. This non-monotonically-increasing configuration of the C2 curve makes the starting value of KG ( $KG_{start}$  in this thesis, 15 m for both container vessels) very important in the process of finding  $KG_{max}$ . The value of the increment used in this process is also very important. Both parameters must be chosen to avoid overlooking a small zone of KG for which C2 is larger than  $R_{PRO}$ .

We observe that the more the ship is vulnerable to parametric roll, the more the curve C2 versus KG has peaks and the longer the interval where C2 increase from 0 to 1 is.

The computation of C2 as a function of all possible values of both KG and draft defines authorized as well as restricted areas according to the C2 criterion. Figure 59 and Figure 60 show these zones for both container vessels (authorized areas in white, restricted areas in grey). The lower envelopes of the restricted areas give the  $KG_{max}$  curves associated with C2 shown in Figure 45 and Figure 46. The jumps observed on these curves correspond to the passage from the upper restricted area to the lower restricted area (at drafts equal to 10 m and 13 m for the 319 m container vessel).

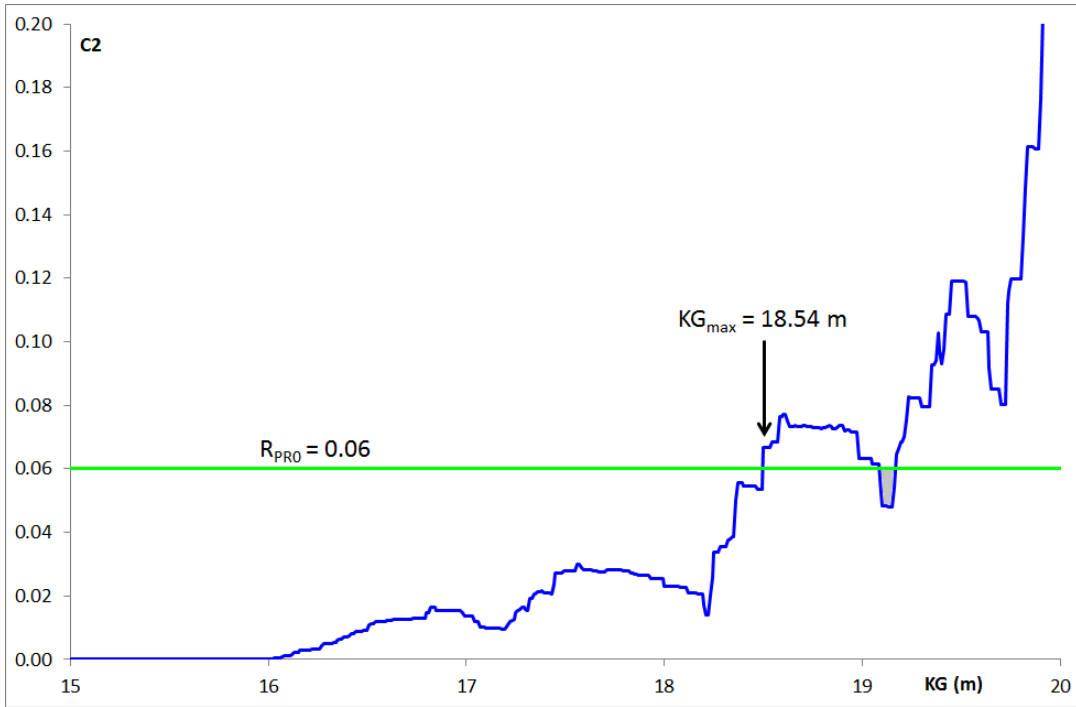


Figure 54 – Curve C2 versus KG for the C11 container vessel at a draft equal to 10 m.

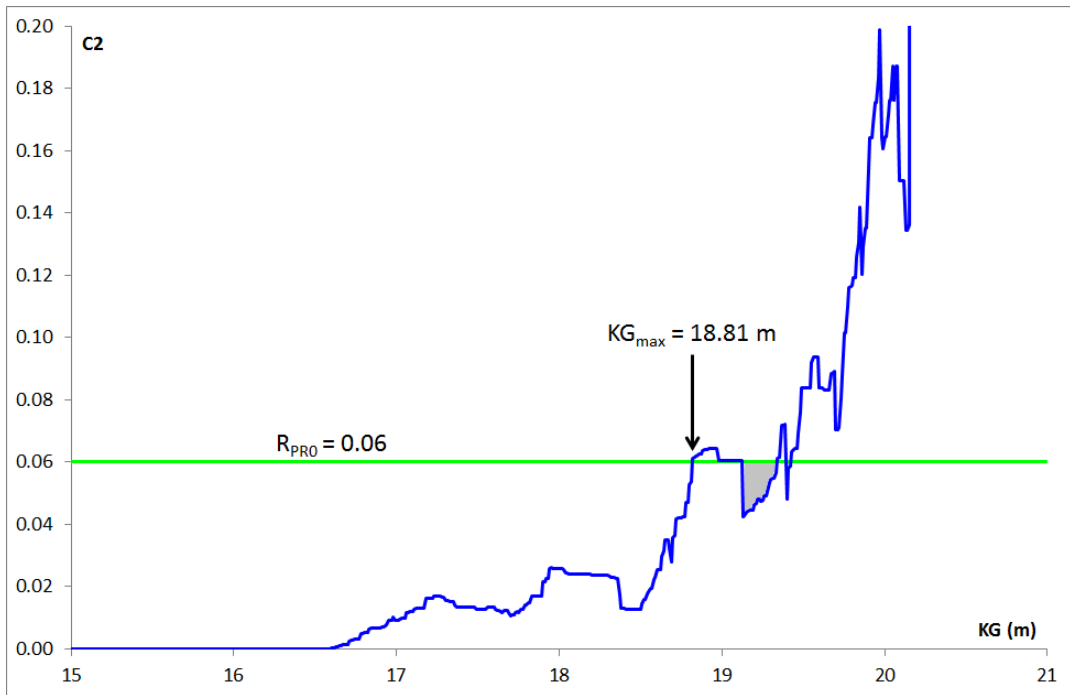


Figure 55 – Curve C2 versus KG for the 319 m container vessel at a draft equal to 12 m.

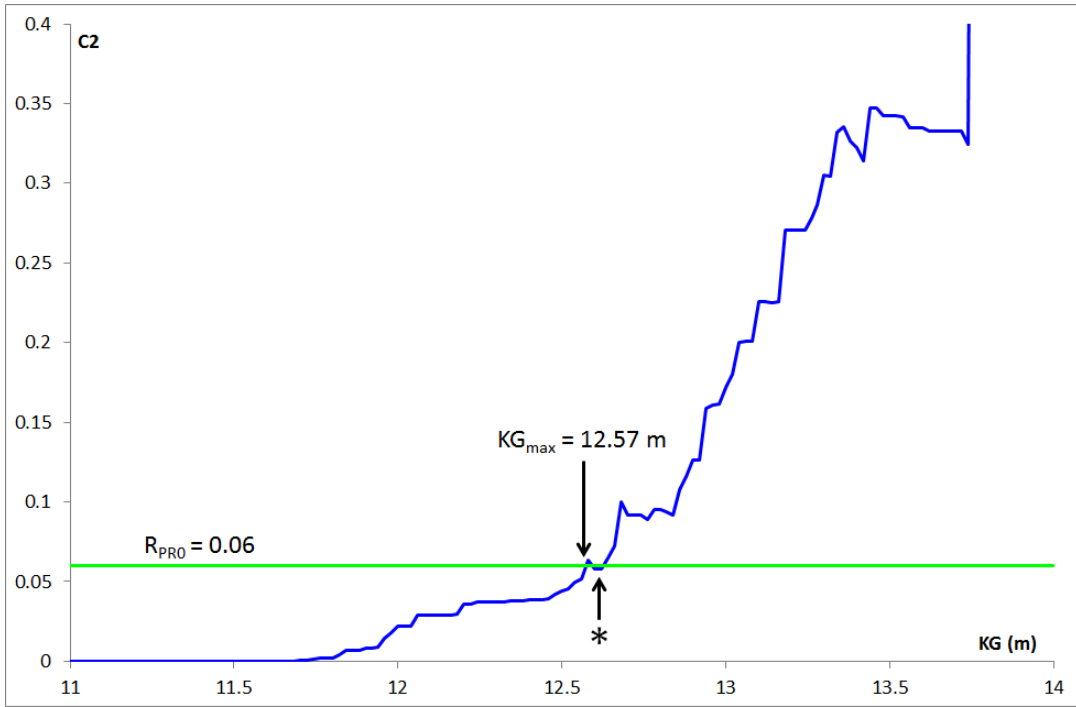


Figure 56 – Curve C2 versus KG for the Ro-Ro vessel at a draft equal to 5.5 m.

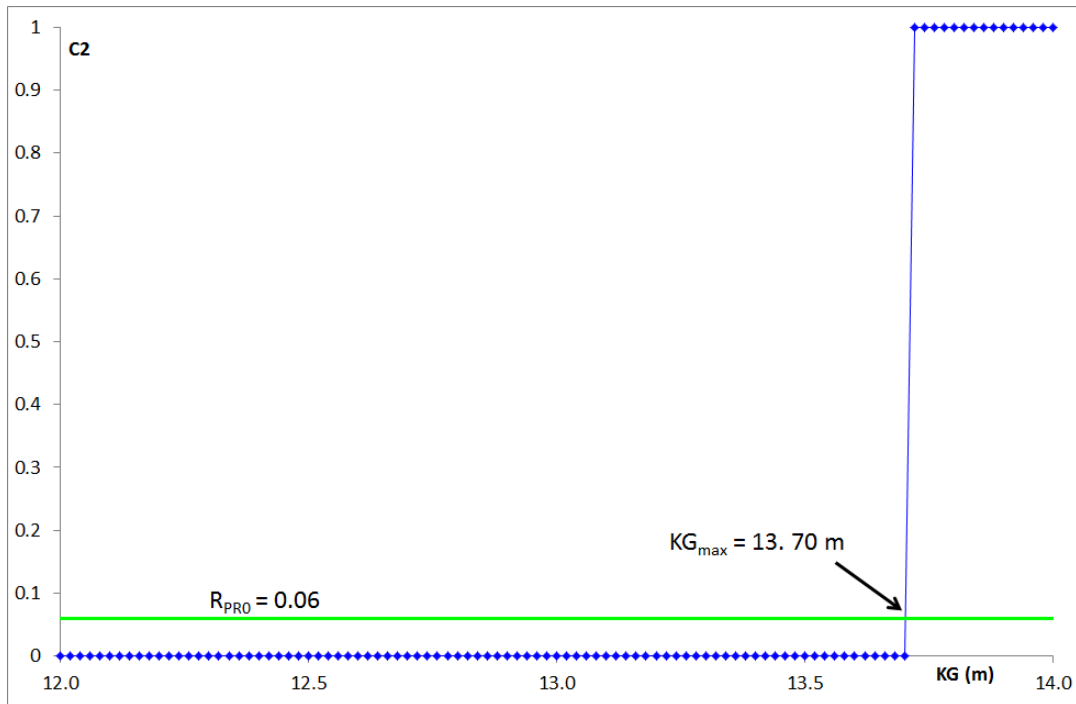


Figure 57 – Curve C2 versus KG for the tanker at a draft equal to 11 m.

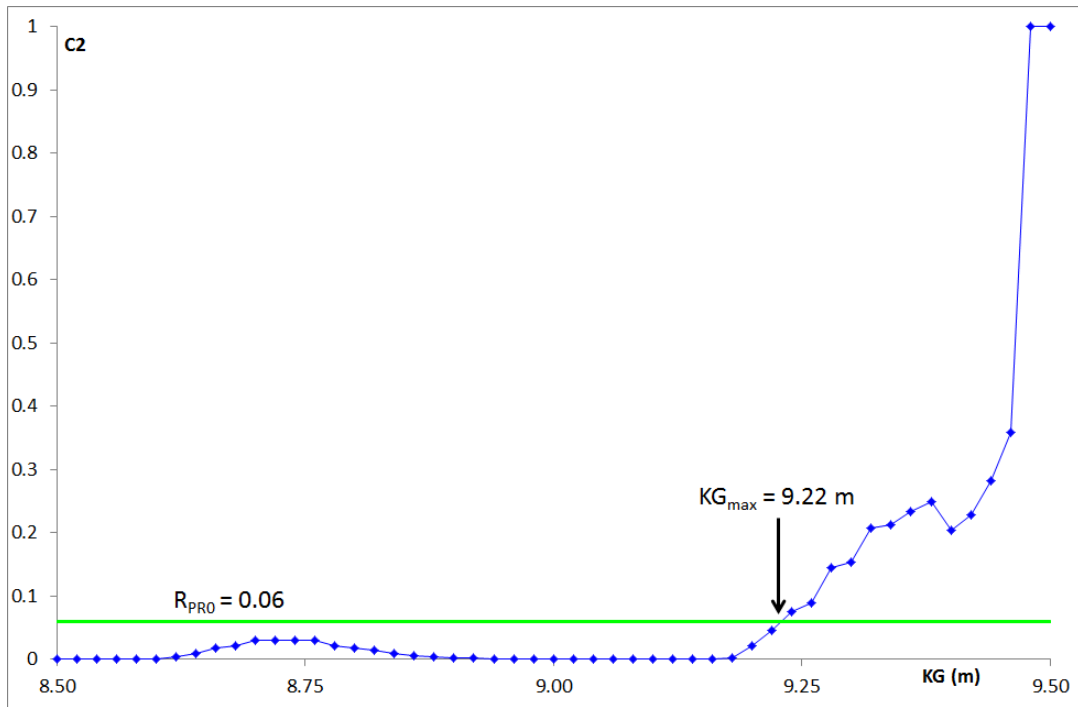


Figure 58 – Curve C2 versus KG for the DTMB-5415 at a draft equal to 6.125 m.

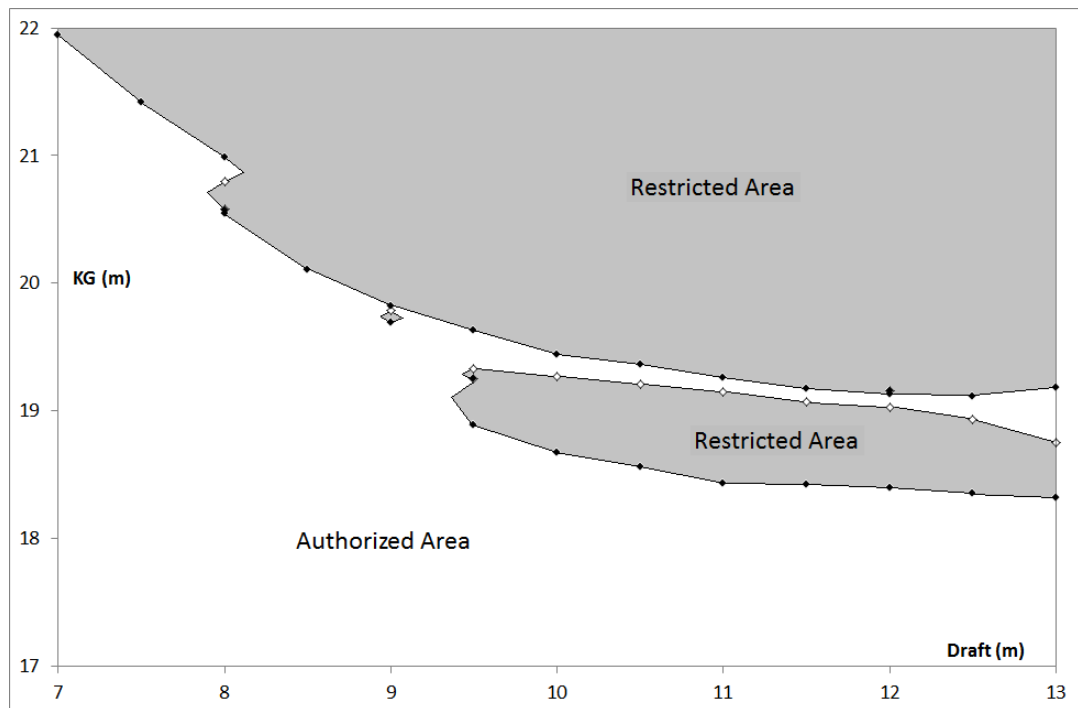


Figure 59 – Authorized and restricted areas according to the  $C_2$  criterion for the C11 container vessel.

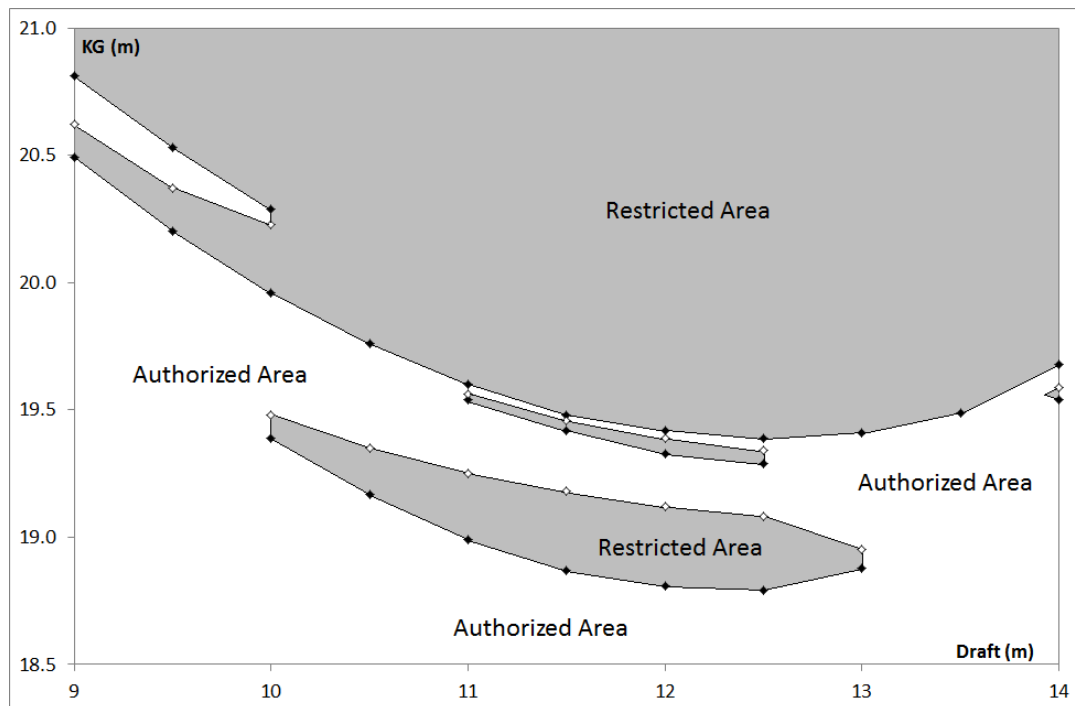


Figure 60 – Authorized and restricted areas according to the C2 criterion for the 319 m container vessel.

### 3.3.3. Influence of Speed

Since parametric roll results from the encounter of waves, the speed has a major influence in the behavior of the ship. The service speed of the C11 container vessel is 24.5 knots. However, a lot of papers in the literature consider this ship with a speed equal to 20 knots. Figure 61 shows the authorized and restricted areas of this vessel recomputed for this reduced service speed (since Figure 45 and Figure 59 are computed for 24.5 knots). We observe that the lower restricted area is partially merged with the upper one. However, the behavior of the ship with regard to the second check of level-two criterion remains unchanged.

Figure 62 compares the resulting  $KG_{max}$  curves. Except one point at 50,000 tons, both curves are close together. The gap observed at 50,000 tons results from the shift to the left of the lower restricted area when the service speed is reduced (the draft of its left boundary shifts from 9.5 to 9.0 m).

Note: although the speed is considered in one condition of the first check of level-two criterion (Equation (22) page 28), it has no influence on the associated  $KG_{max}$  curve for this vessel.

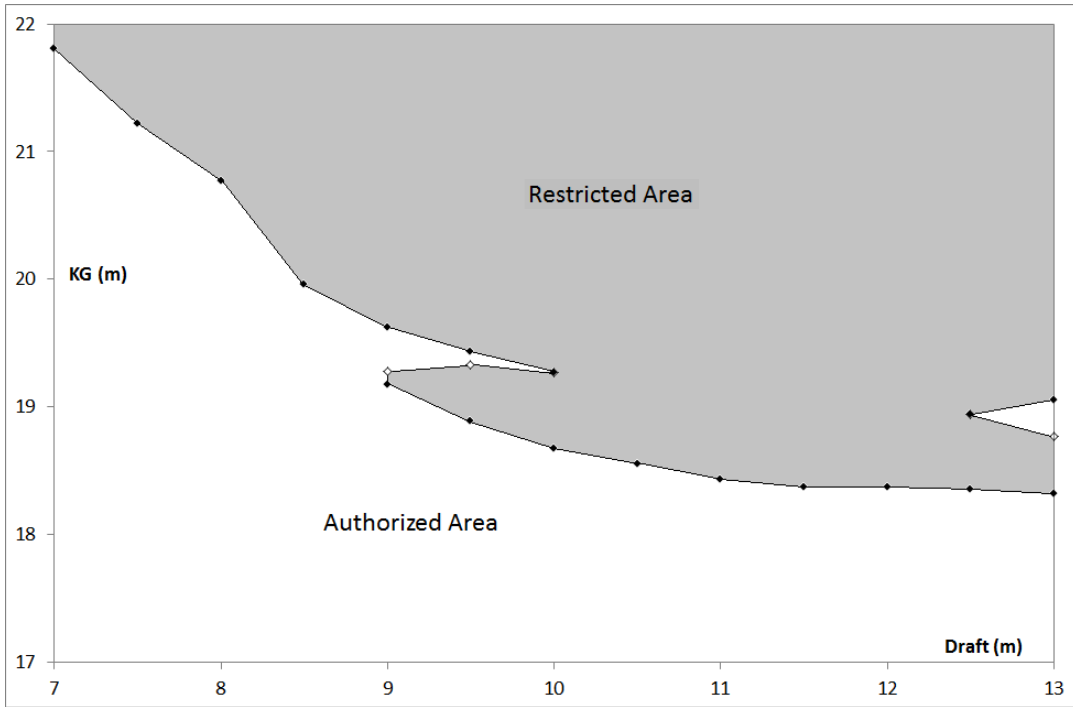


Figure 61 – Authorized and restricted areas according to the C2 criterion for the C11 container vessel with a service speed equal to 20 knots.

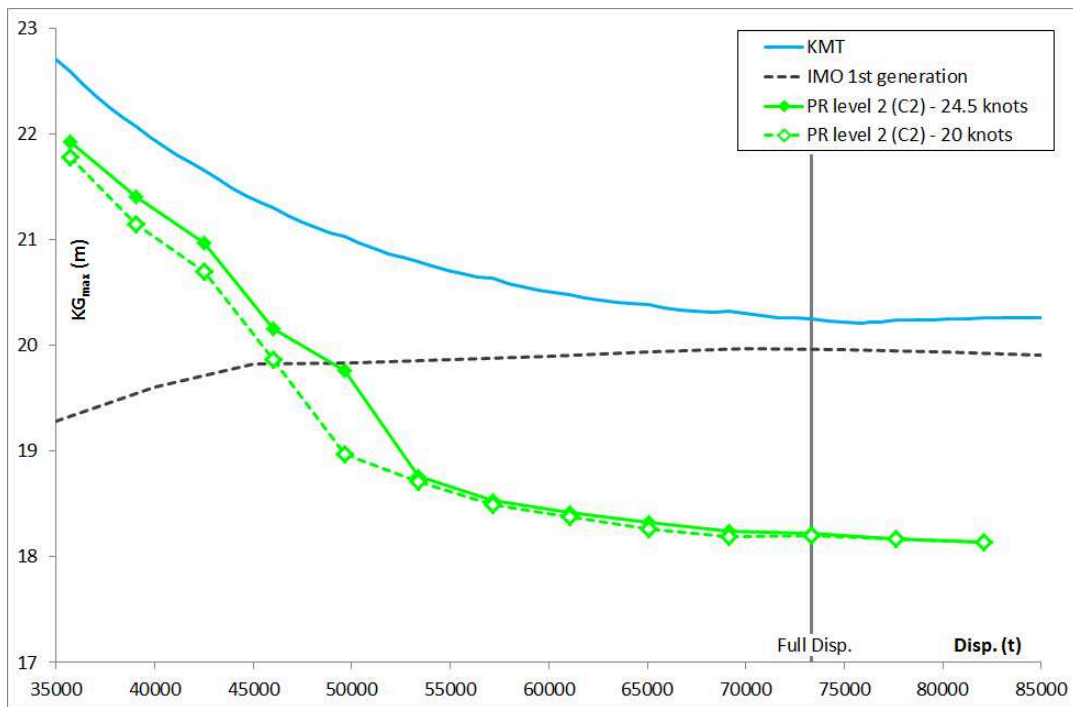


Figure 62 – Influence of speed on  $KG_{max}$  curves associated with the second check of parametric roll level-two criterion for the C11 container vessel.

### 3.3.4. Influence of Computation Parameters

During the 12<sup>th</sup> International Conference on the Stability of Ships and Ocean Vehicles, held in Glasgow (UK) in June 2015, Peters *et al.* [32] formulated some recommendations to solve the parametric roll differential equation (23) and calculate the associated maximum roll angle required in the second check of level-two criterion (coefficient C2, seen as a separate criterion here). Their proposals have been included in the explanatory notes of the new regulation (SDC 3/WP.5, Annex 4, Appendix 3 [23]).

Among other recommendations, Peters *et al.* propose to solve the differential equation with a simulation time equal to 15 natural roll periods of the ship and an initial roll angle equal to 5 degrees. They also recommended to consider a non-linear GZ.

In this section, we propose to study the influence of each of these proposals on the  $KG_{max}$  curves associated with the second check of level-two criterion for four selected ships: both container vessels (assessed as vulnerable to parametric roll by the new criteria) the Ro-Ro vessel (assessed as slightly vulnerable, although neither the test in the towing tank nor direct assessment computation have proven this yet) and the tanker (clearly non-vulnerable).

Note: in this section, the service speed of the C11 container vessel is set to 20 knots.

The content of this section has been presented at the 15<sup>th</sup> International Ship Stability Workshop held in Stockholm (Sweden) in June 2016 [4].

#### ***Simulation Duration***

Since parametric roll is a resonance phenomenon due to the repetition of the encounter of waves, attaining the steady state roll amplitude is essential to determine the vulnerability to this failure mode. Thus, the duration of the simulation is important. The  $KG_{max}$  curves associated with the second check of level-two criterion are computed for 6 different simulation durations, given as a number of the ship's natural roll period. The following durations are tested: 3, 4, 6, 10, 15 and 20 natural roll periods. Peters *et al.* [32] and SDC 3/WP.5 [23] recommend a simulation duration equal to 15 roll periods.

Figure 63 and Figure 64 show the results for both container ships. We observe that the  $KG_{max}$  significantly varies with the duration of the simulation, but the curves associated with 10, 15 and 20 roll periods are fully coincident for both ships. This proves that the steady state roll amplitude has been attained between 6 and 10 roll periods.

Figure 65 shows the results for the Ro-Ro vessel. We observe that all curves are close together. The  $KG_{max}$  is slightly affected by the simulation duration. As above, the curves associated with 10, 15 and 20 periods are fully coincident.

Figure 66 shows the results for the tanker. We observe that all curves are coincident and correspond to zero-GM. This proves again that the tanker is not vulnerable to parametric roll: parametric roll never occurs, regardless of the wave and speed (the C2 coefficient is set to 1 when the ship becomes statically unstable in waves, see Section 1.2.4 page 33). The simulation duration has no effect on  $KG_{max}$  curves.

This first test shows that:

- 1) The more the ship is vulnerable to parametric roll, the more the simulation duration has an influence on the  $KG_{max}$  curve associated with the second check of level-two criterion.

2) The relevance of the simulation duration equal to 15 natural roll periods of the ship proposed by Peters et al. [32] is confirmed.

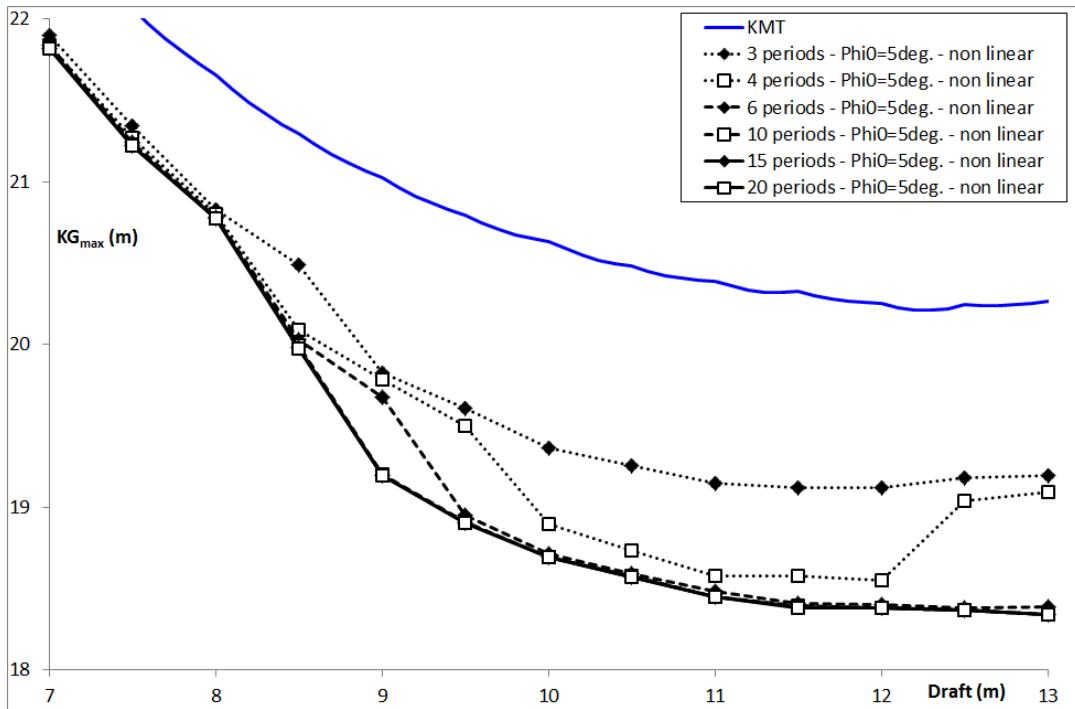


Figure 63 – Influence of the simulation duration on  $KG_{max}$  curves associated with the C2 criterion for the C11 container vessel.

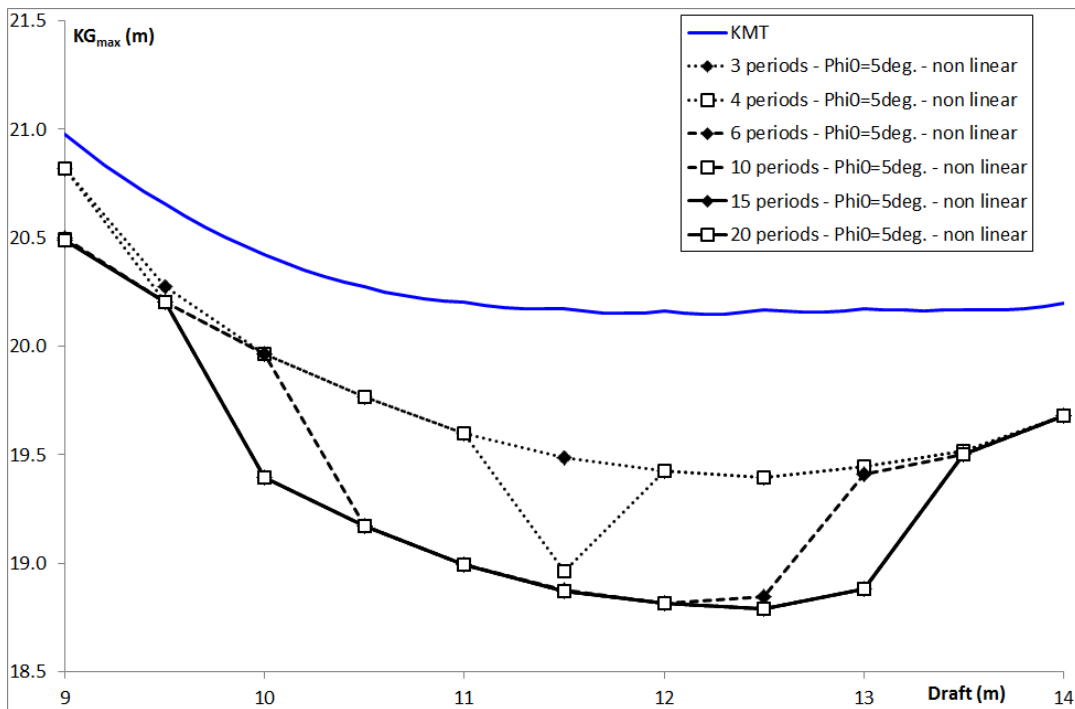


Figure 64 – Influence of the simulation duration on  $KG_{max}$  curves associated with the C2 criterion for the 319 m container vessel.

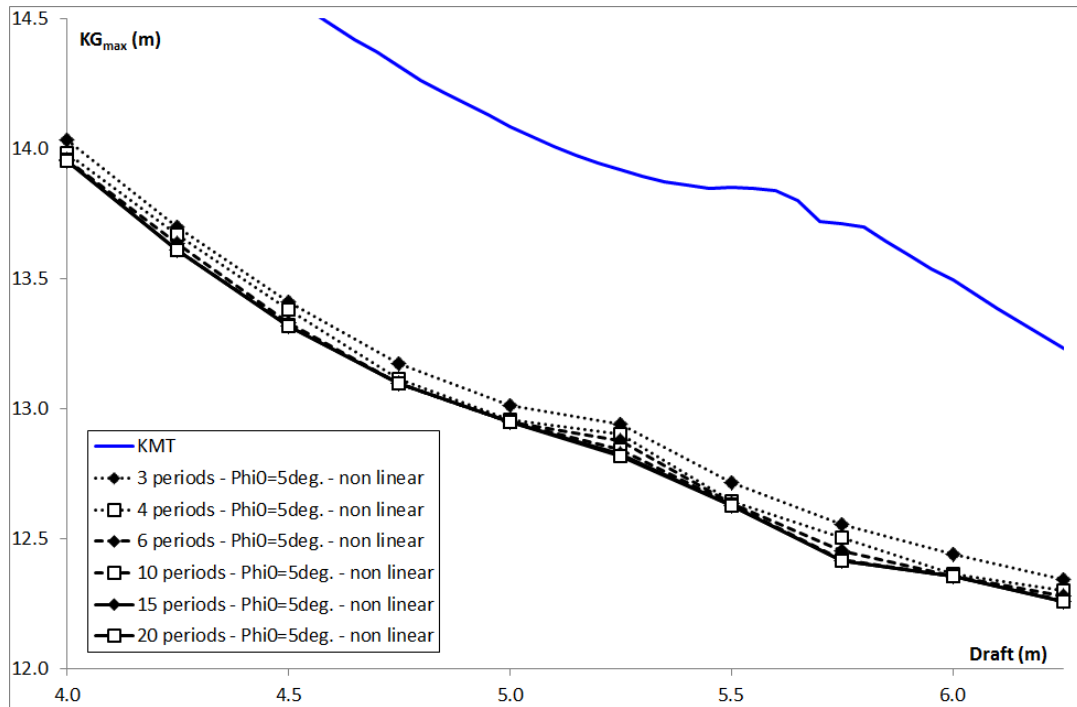


Figure 65 – Influence of the simulation duration on  $KG_{max}$  curves associated with the C2 criterion for the Ro-Ro vessel.

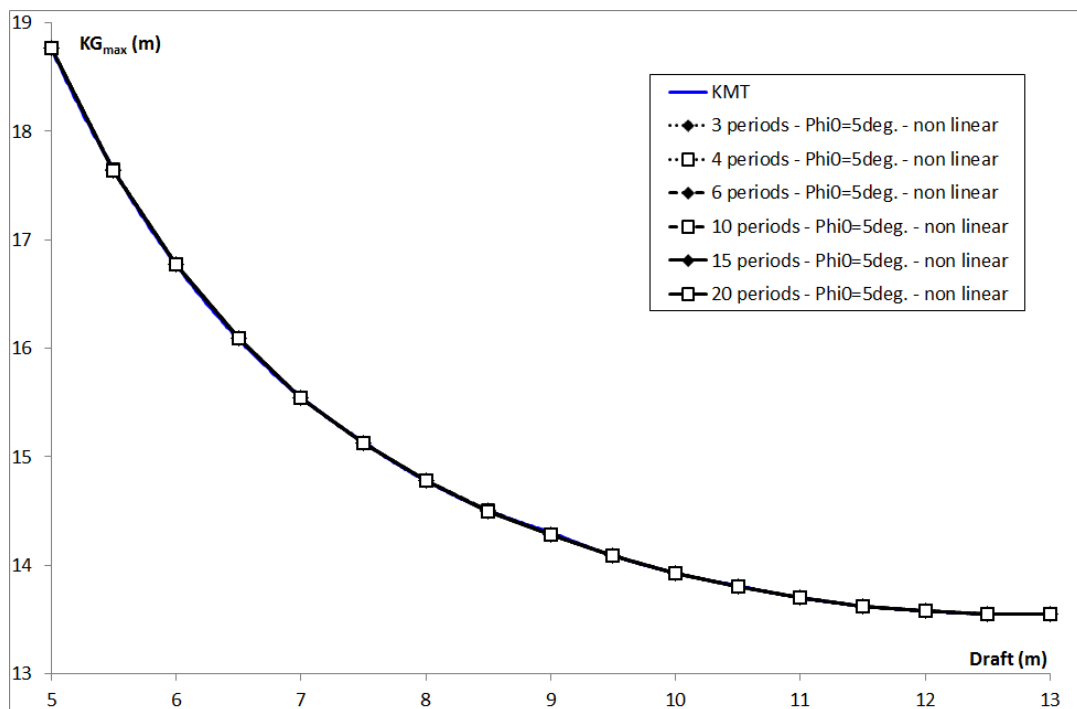


Figure 66 – Influence of the simulation duration on  $KG_{max}$  curves associated with the C2 criterion for the tanker (all curves coincide).

### ***Initial Roll Angle***

The right term of the differential equation (23) is equal to zero because there is no transverse excitation in parametric roll. The ship is assumed to sail in pure head or following seas. Thus, a non-zero initial roll angle (or a non-zero initial roll speed) must exist to initialize the numerical phenomenon during the simulation. Peters *et al.* [32] and SDC 3/WP.5 [23] recommend an initial roll angle equal to 5 degrees. Since the C2 coefficient increases if the maximum roll angle exceeds 25 degrees (see page 29), it may be interesting to start the simulation with an initial roll angle larger than 5 degrees, in order to reduce the number of natural roll periods of the ship which are required to attain the steady state roll amplitude. Computations performed with an initial roll angle equal to 10 degrees show that the steady state roll amplitude is attained between 6 and 10 roll periods, as if the initial roll angle were 5 degrees. Computations with other durations between 6 and 10 roll periods would probably prove that the initial roll angle has an influence on the duration needed to attain the steady state roll amplitude. However, the initial roll angle has no major influence on this duration.

Even if the influence of the initial roll angle on the duration needed to attain the steady state roll amplitude is limited, the initial roll angle may also have an influence on the  $KG_{max}$ . This should be limited, but not zero.  $KG_{max}$  curves are computed for the four selected ships with initial roll angles equal to 5 and 10 degrees. The results are shown in Figure 67 to Figure 70 respectively for the C11 container ship, the 319 m container ship, the Ro-Ro vessel and the tanker. As expected, the initial roll angle has no influence on the  $KG_{max}$  curves of the tanker since she is not vulnerable to parametric roll (Figure 70). On the three other ships, the initial roll angle has a minor influence on the  $KG_{max}$ . Only one point differs significantly for the 319 m container ship (Figure 68, draft equal to 9.5 m, difference of about 0.5 m between both  $KG_{max}$ ). This is due to the shift of the lower restricted area (see Section 3.3.2), also observed as influence of the service speed of the same vessel in Section 3.3.3.

To conclude, we can note the following:

- 1) The initial roll angle has no major influence on the duration needed to attain the steady state roll amplitude.
- 2) Since the initial roll angle has a limited influence on the  $KG_{max}$  associated with the second check of level-two criterion, it is wise to clearly specify its value in the future regulation.

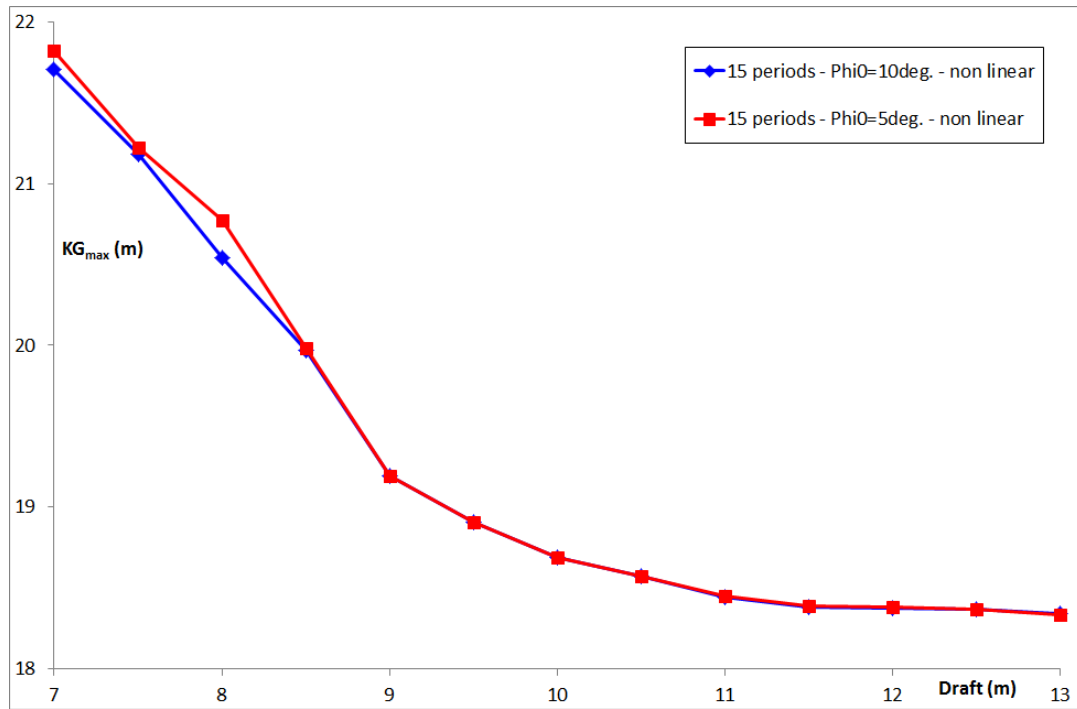


Figure 67 – Influence of the initial roll angle on KG<sub>max</sub> curves associated with the C2 criterion for the C11 container vessel.

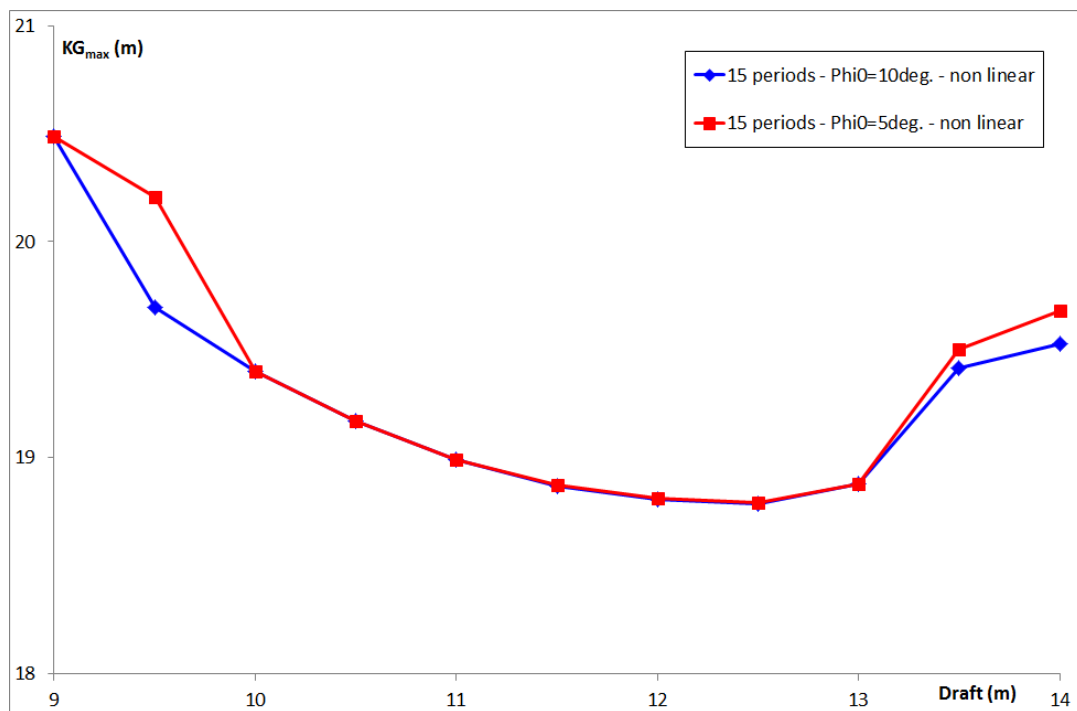


Figure 68 – Influence of the initial roll angle on KG<sub>max</sub> curves associated with the C2 criterion for the 319 m container vessel.

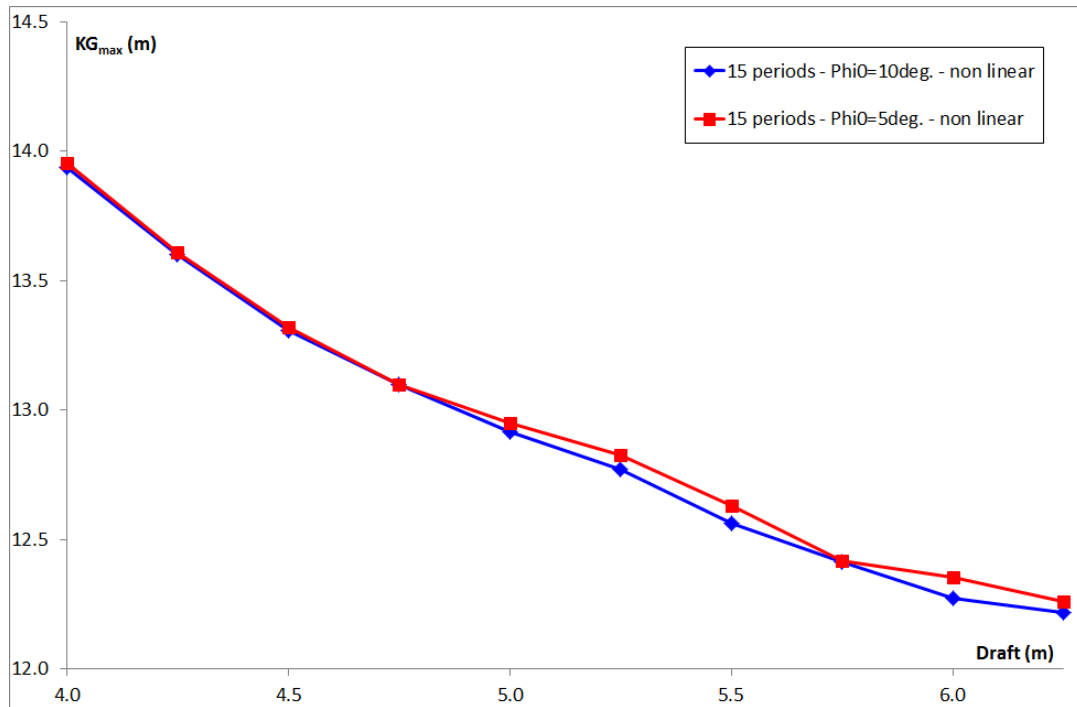


Figure 69 – Influence of the initial roll angle on  $KG_{max}$  curves associated with the C2 criterion for the Ro-Ro vessel.

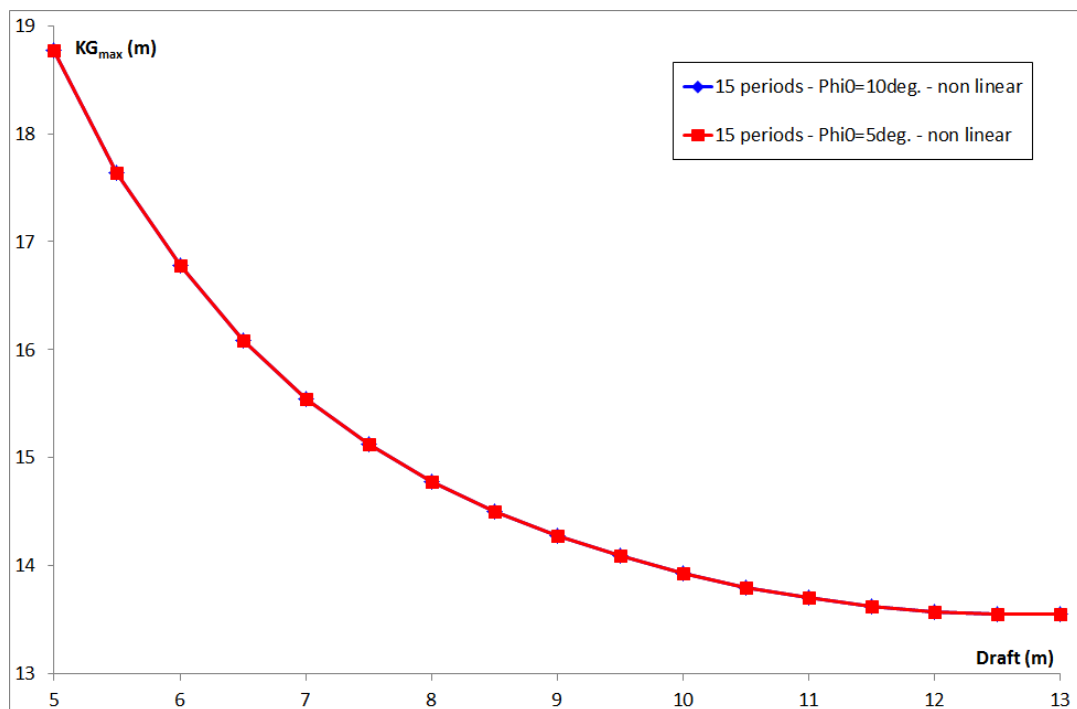


Figure 70 – Influence of the initial roll angle on  $KG_{max}$  curves associated with the C2 criterion for the tanker (both curves coincide).

## ***Linearizing GZ***

Parametric roll is a failure mode that could cause capsizing. Thus, it seems logical to study it at large roll angles with a non-linear GZ as recommended by Peters *et al.* [32] and SDC 3/WP.5 [23]. However, the C2 coefficient increases if the maximum roll angle exceeds 25 degrees (see page 29). Thus, an error on GZ at angles larger than 25 degrees has no influence on the result. Since many ships have a linear GZ up to an angle equal to 25 degrees, it is interesting to compare  $KG_{max}$  associated with the second check of level-two criterion computed with linear and non-linear GZ. GZ curves are computed in calm water for the four selected ships at full-load draft and KG equal to  $KG_{max}$  associated with C2 (except for the tanker where the KG has been chosen for GM equal to 0.175 m since her  $GM_{min}$  associated with C2 is zero). They are shown in Figure 75 to Figure 78. All possible configurations of GZ versus GM are presented: the non-linear GZ is significantly larger than the linearized GZ ( $GZ_{lin} = GM \times \varphi$ ) for both the 319 m container ship and tanker (Figure 76 and Figure 78). The non-linear GZ is lower than the linearized GZ for the Ro-Ro vessel (Figure 77) and the GZ of the C11 container ship is almost linear up to 30 degrees (Figure 75). The non-linear GZ and linearized GZ are used to compute the  $KG_{max}$  curves associated with C2. The results are shown in Figure 71 to Figure 74.

As expected, the linearized GZ reduces the  $KG_{max}$  of the 319 m container ship (Figure 72). In this case, linearizing the GZ provides an irrelevant safety margin (30 to 50 centimeters).

It would be logical to expect a similar result on the tanker (Figure 74) since her GZ curve has the same configuration, but the linearized GZ has no influence on  $KG_{max}$  at a full-load draft (11 m). However,  $KG_{max}$  is reduced at lower drafts: the tanker is assessed as vulnerable to parametric roll if her GM is lower than 50 centimeters. The jump of  $KG_{max}$  between drafts equal to 10 m and 10.5 m reveals the existence of a restricted area as defined in Section 3.3.2.

The result on the Ro-Ro vessel is unexpected (Figure 73): at full-load draft (5.5 m), the  $KG_{max}$  associated with the linearized GZ is more conservative than that given by the real GZ although the linearized GZ is larger than the real GZ. This is due to the highly non-linear behavior of the parametric roll differential equation.

The result on the C11 container ship is as expected (Figure 71): since the non-linear GZ and linearized GZ almost overlap up to an angle of 25 degrees, linearizing the GZ has a very limited influence on the  $KG_{max}$  associated with C2.

To conclude, we observe that, as expected, linearizing the GZ is not relevant, unless the real GZ is linear up to 25 degrees for all drafts scanned by the  $KG_{max}$  curve.

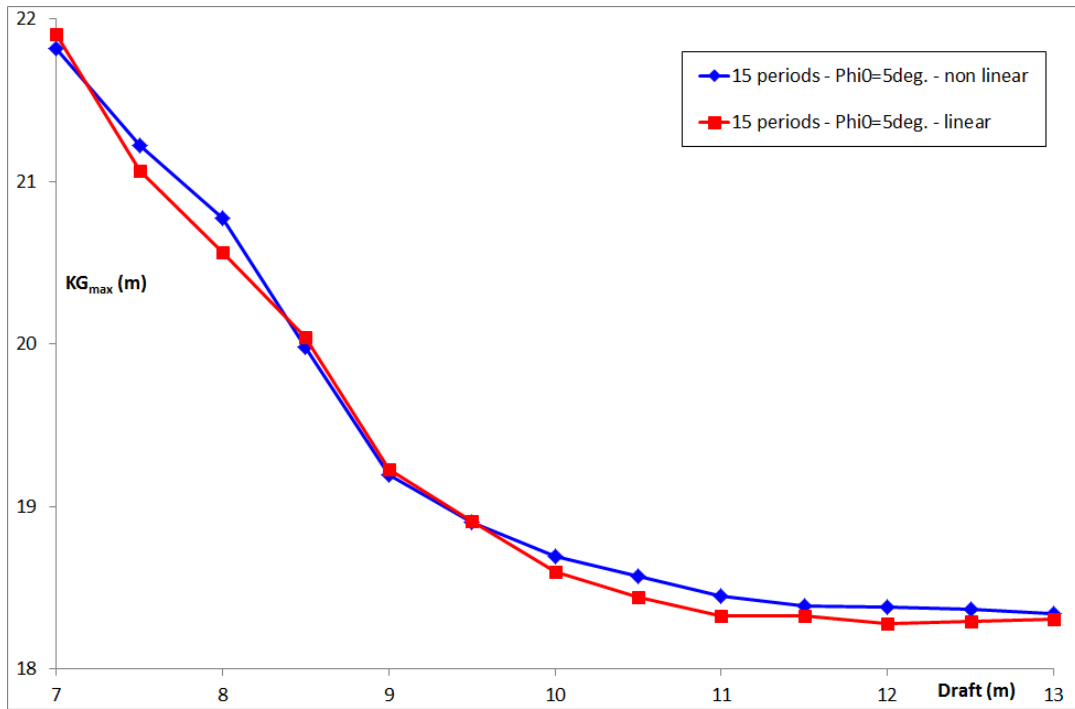


Figure 71 – Influence of GZ linearity on  $KG_{max}$  curves associated with the C2 criterion for the C11 container vessel.

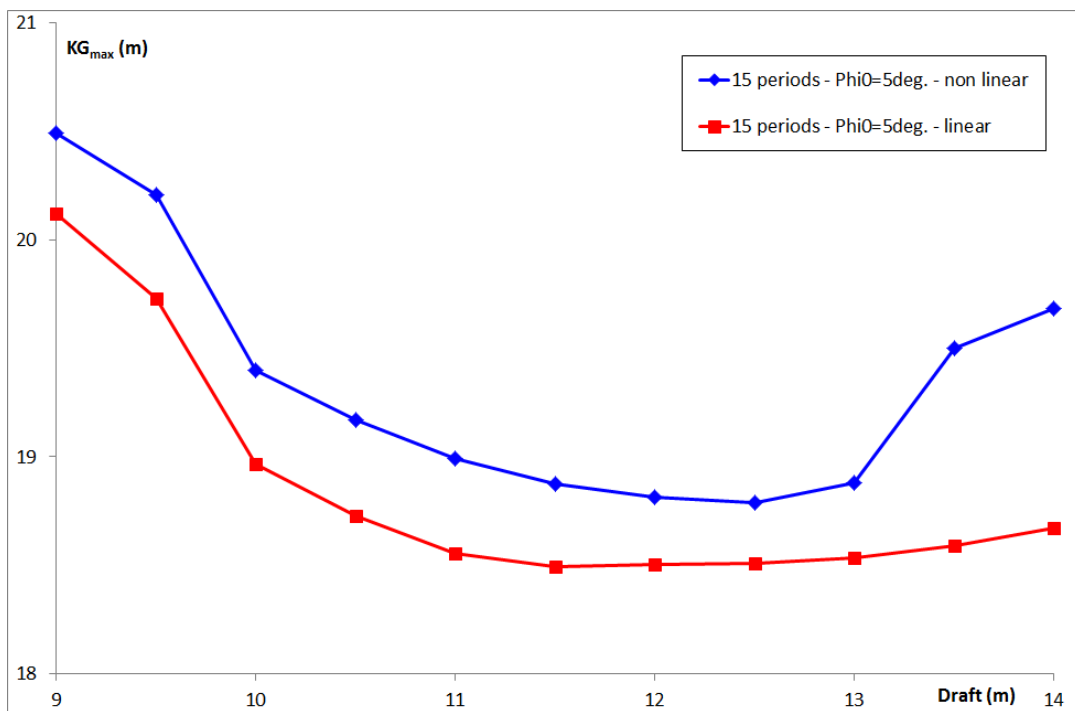


Figure 72 – Influence of GZ linearity on  $KG_{max}$  curves associated with the C2 criterion for the 319 m container vessel.

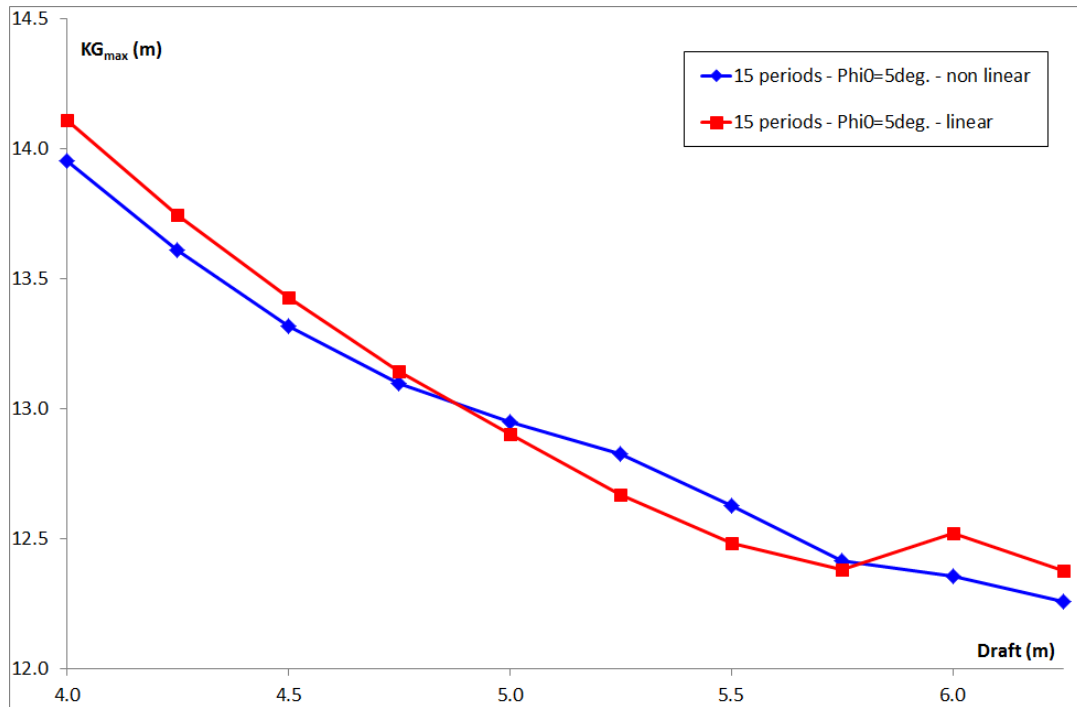


Figure 73 – Influence of GZ linearity on  $KG_{max}$  curves associated with the C2 criterion for the Ro-Ro vessel.

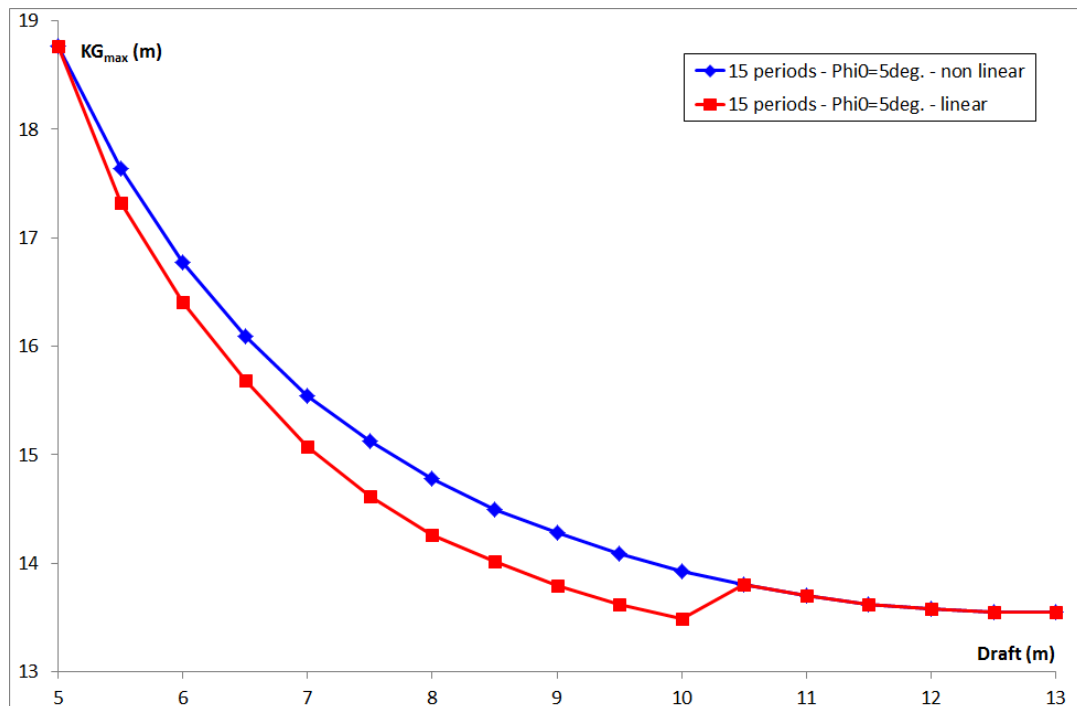


Figure 74 – Influence of GZ linearity on  $KG_{max}$  curves associated with the C2 criterion for the tanker.

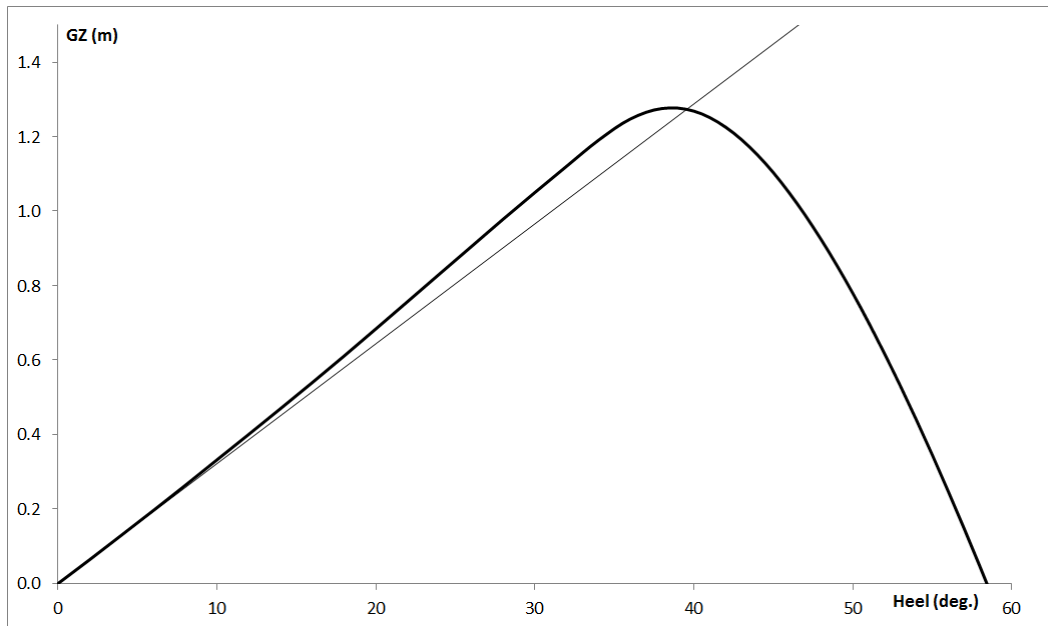


Figure 75 – GZ curve of the C11 container vessel at a draft equal to 12 m.

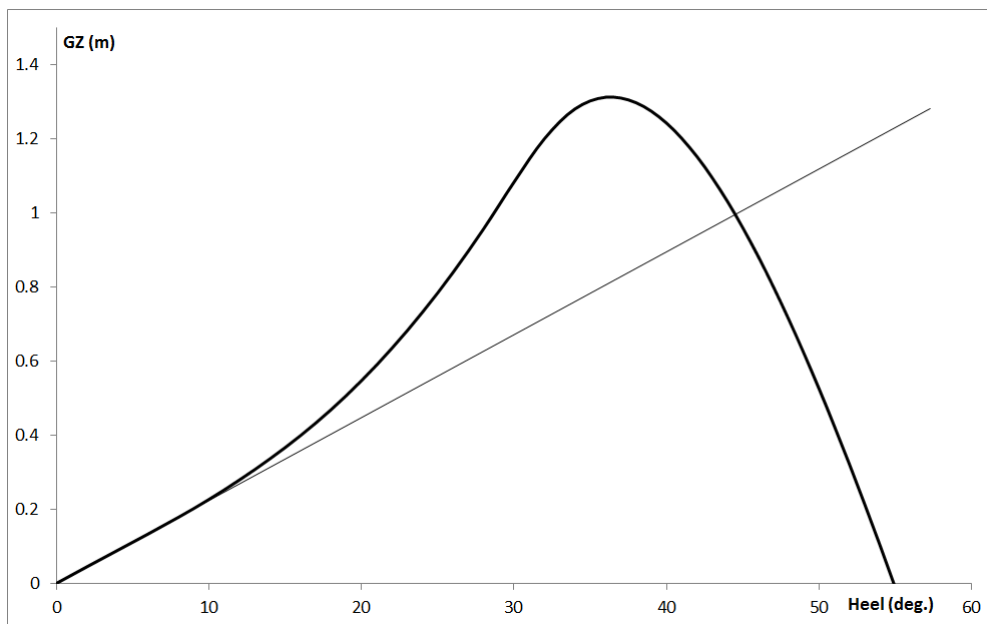


Figure 76 – GZ curve of the 319 m container vessel at a draft equal to 13 m.

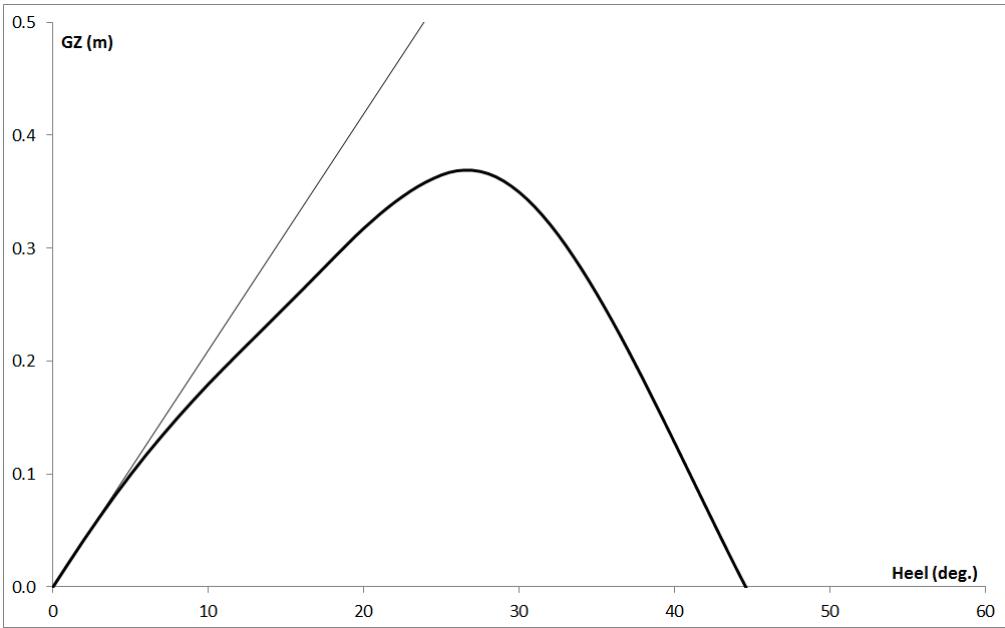


Figure 77 – GZ curve of the Ro-Ro vessel at a draft equal to 5.5 m.

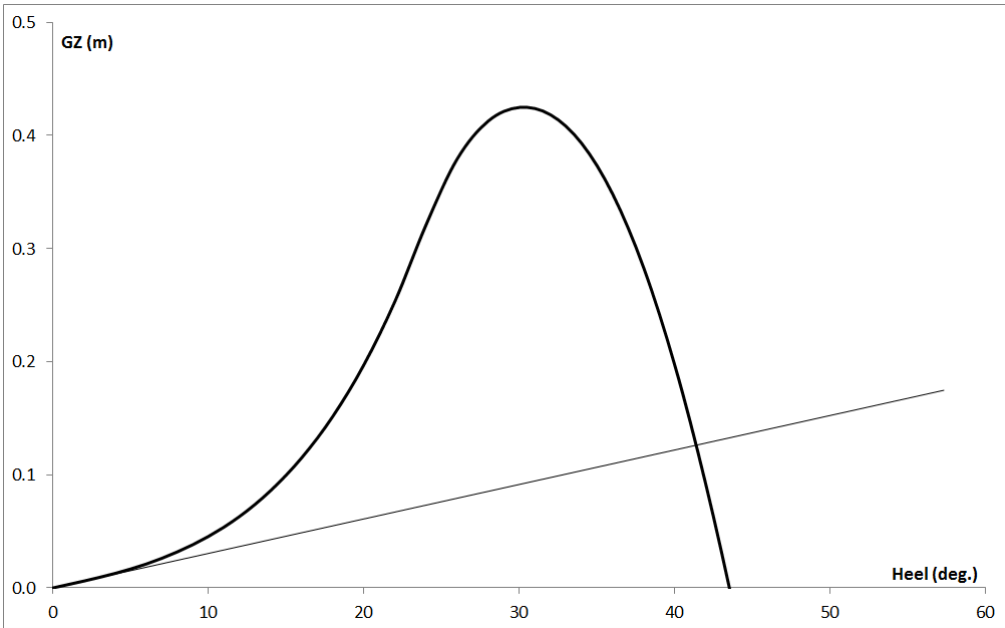


Figure 78 – GZ curve of the tanker at a draft equal to 11 m.

### 3.3.5. Comparison with 6-Degrees-of-Freedom Simulation

In this section, we propose to compare the  $KG_{\max}$  curves associated with both checks of level-two criterion with equivalent curves calculated from 6-degrees-of-freedom numerical simulations, in order to analyze the relevance of the proposed criterion. Fredyn software is used for this [70]. This software is developed by the members of Cooperative Research Navies (CRNAV, [www.crnnav.org](http://www.crnnav.org)) and performs non-linear 6-degrees-of-freedom simulations of steered ships in extreme seas and wind.

The simulations are performed on the C11 container vessel. Her numerical model is made of the hull, the propeller, the rudder and the bilge keels. Six different drafts are considered: 8, 9, 10, 11, 12 and 12.339 meters. Several parametric roll simulations are performed for each draft with increasing values of  $KG$ , in order to determine both values of  $KG$  providing a maximum roll angle equal to 25 degrees and causing the vessel to capsize.

As proposed by the level-one criterion, the waves are sinusoidal and their length is equal to the ship's length (262 m). This makes their period equal to 12.95 seconds. The wind is not considered.

For each simulation, the ship is placed in the conditions of the first mode of parametric roll: her speed is such that the encounter frequency is twice the natural roll frequency, which is previously measured from a roll-decay test in still water at almost same speed (expected speed calculated from the natural roll period obtained by ratio of  $GM$  and a reference situation). If the required speed is negative, the simulation is performed in following seas and the ship's speed remains positive. Otherwise, the simulation is performed in head seas.

Results are shown in Figure 79. The  $KG$  providing a maximum roll angle equal to 25 degrees is drawn as a black solid line with diamond markers. The  $KG$  causing the vessel to capsize is drawn as a black dotted line with white markers. We observe following facts:

- 1) At full-load displacement, the vessel may capsize with a value of  $KG$  allowed by the current IMO regulation. Moreover, the vessel may roll over 25 degrees with such a  $KG$  in any load configuration. Although the sinusoidal-wave assumption is subject to discussion, both observations prove the requirement for new intact stability regulation considering this failure mode.
- 2) Near full-load displacement, the  $KG_{\max}$  associated with the second check of level-two criterion is in relatively good accordance with that associated with 6-degrees-of-freedom simulation considering a maximum roll angle equal to 25 degrees. The latter is more conservative, due to the severe parametric roll conditions imposed at each simulation, since the second check of level-two criterion specifies 7 speeds which have no relation with the wave period (which remain the same for all wave cases of the scattering table because of the use of the Grim method). Moreover, the roll damping computation in Fredyn is based on [49] and differs from the method used in this thesis [48 and 50].

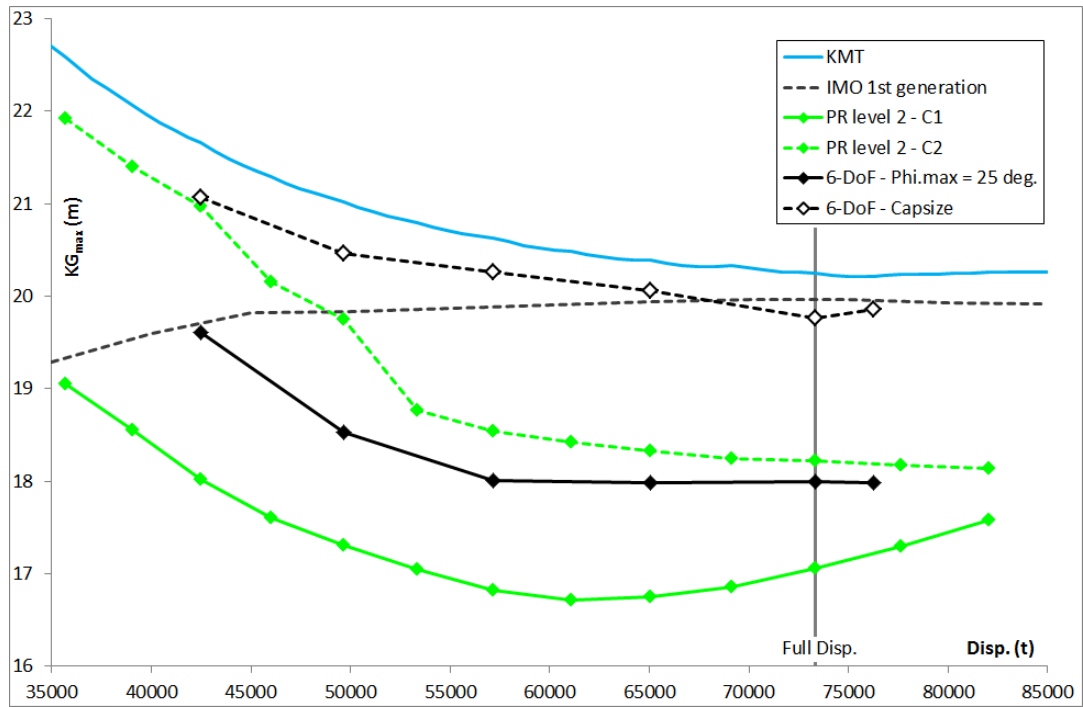


Figure 79 –  $KG_{max}$  curves associated with parametric roll 6-degrees-of-freedom simulations for the C11 container vessel.

## CHAPTER 4. ENERGY ANALYSIS OF PARAMETRIC ROLL

### 4.1. INTRODUCTION

As presented in Chapter 1, the second check of level-two criterion of parametric roll failure mode requires the computation of the maximum roll angle for several speeds in head and following seas for any considered loading condition defined by both the draft and KG. Future rules propose two methods: an analytical solution based on a polynomial fit of the GZ curve at the 5<sup>th</sup> order which directly yields the maximum roll angle (not studied in this thesis), and a numerical solving of the differential equation of parametric roll, equivalent to a one-degree-of-freedom simulation of the behavior of the ship during rolling. Both methods are relatively complex to implement and require tools that naval architects are not accustomed to.

Parametric roll has been extensively studied through analytical, numerical and experimental approaches [44, 46 and 42]. In some papers, authors explain that a steady-state roll amplitude occurs if the energy provided by the variation over time of the restoring moment is entirely dissipated by roll damping [27, 43]. However, to our knowledge, no paper explores the energy problem in a quantitative manner, except the contribution of Kerwin [12]. In this chapter, we propose to perform an energy analysis of parametric roll with the aim to provide a simplified method which yields the maximum roll amplitude assuming a linear GZ.

The first part of this chapter consists of an analytical approach of the energy transfer of parametric roll in the first-mode resonance condition, where the wave encounter frequency is twice the ship's natural roll frequency. Subsequently, the behavior of the ship in other conditions with and without parametric roll is observed and presented. Finally, a simplified method which provides the amplitude of steady-state parametric roll is proposed assuming a linear GZ.

In 1955, Kerwin provided a major contribution on parametric roll [12] based mainly on an analytical study of the motion. Our conclusions are strictly identical in resonance condition and equivalent outside this condition.

The content of this chapter has been submitted to a scientific journal [7].

### 4.2. PARAMETRIC ROLL IN RESONANCE CONDITION

#### 4.2.1. Equation of Parametric Roll

Parametric roll in pure head or following seas (i.e. with no transverse excitation) is represented in one degree of freedom by differential equation (23) previously presented in page 29 and rewritten hereunder:

$$J_{44}\ddot{\varphi} + B_{44}\dot{\varphi} + WGZ(\varphi, t) = 0 \quad (23)$$

With:

$J_{44}$  (kg.m<sup>2</sup>) roll moment of inertia, including added mass;

$B_{44}$	(N.m.s/rad)	damping coefficient;
$W$	(N)	ship's weight;
$GZ(\varphi,t)$	(m)	righting arm, function of both the instantaneous roll angle $\varphi$ and time $t$ with the wave encounter frequency.

We assume a linear GZ in this chapter. Hence, the differential equation is rewritten:

$$J_{44}\ddot{\varphi} + B_{44}\dot{\varphi} + W(GM + \Delta GM \cos \omega_e t)\varphi = 0 \quad (44)$$

With:

$GM$	m	average value of the metacentric height in waves;
$\Delta GM$	m	half-amplitude of the metacentric height variation in waves;
$\omega_e$	rad/s	wave encounter frequency.

Equation (44) is a linear differential equation with non-constant terms. The added mass in the first term depends on the roll frequency. The second term ( $B_{44}$ ) depends on the roll amplitude and frequency, especially if a simplified Ikeda method is used [48, 50]. The third term varies over time with the wave encounter frequency. We reformulate Equation (44) by moving the non-constant part of the restoring moment to the right as follows:

$$J_{44}\ddot{\varphi} + B_{44}\dot{\varphi} + WGM\varphi = -(W\Delta GM \cos \omega_e t)\varphi \quad (45)$$

The left-hand part of Equation (45) is identical to that of the well-known differential equation of a linear oscillating system. Although it is not properly correct because of the dependency on the roll angle  $\varphi$ , the right-hand part is considered as an exciting moment in this chapter.

#### 4.2.2. Assumptions

The first assumption, previously introduced, is the linearity of GZ. It is used throughout the chapter.

Other following assumptions are formulated in this section:

- The analysis is performed when the roll motion has reached steady-state amplitude (denoted by  $\Phi$ ), i.e. when the transient movement has finished;
- The ship rolls at its natural frequency  $\omega_0$  defined as:

$$\omega_0 = \sqrt{\frac{WGM}{J_{44}}} \quad (46)$$

- The wave encounter frequency  $\omega_e$  is twice the ship's natural roll frequency  $\omega_0$ . This corresponds to the resonance condition of the first mode of parametric roll as demonstrated by Mathieu [9].

Assumptions on both the roll amplitude and frequency render the first and second terms (respectively  $J_{44}$  and  $B_{44}$ ) constant in the differential equation. These assumptions provide expressions for the function of the roll angle over time and its first derivate:

$$\varphi(t) = \Phi \cos \omega_0 t \quad \text{And} \quad \dot{\varphi}(t) = -\omega_0 \Phi \sin \omega_0 t \quad (47)$$

### 4.2.3. Distribution of Energy

#### *Kinetic and Potential Energy*

Assuming the ship rolls at its natural frequency, the sum of kinetic energy ( $E_K$ ) and potential energy ( $E_P$ ), contained respectively in the first term (inertia) and third term (constant part of restoring moment) of Equation (45) is constant and equal to:

$$E_K + E_P = \frac{1}{2}WGM\Phi^2 \quad (48)$$

Consequently, the assumption of a constant roll amplitude  $\Phi$  causes the energy provided by the exciting moment ( $E_E$ ) to entirely dissipate by the damping moment as a “damping energy” ( $E_D$ ).

#### *Damping Energy*

The damping energy during one roll period is formulated as follows:

$$E_D = \int_{1 \text{ per}} B_{44}\dot{\varphi}d\varphi \quad \text{With} \quad d\varphi = \dot{\varphi}dt \quad (49)$$

Using Equation (47), the energy dissipated by the damping moment from 0 to a time t is:

$$E_D(t) = B_{44}\omega_0^2\Phi^2 \int_0^t \sin^2 \omega_0 t dt \quad (50)$$

The instantaneous power dissipated by damping is:

$$P_D(t) = \frac{dE_D}{dt} = B_{44}\omega_0^2\Phi^2 \sin^2 \omega_0 t \quad (51)$$

The average value of this power is:

$$P_D = \frac{1}{2}B_{44}\omega_0^2\Phi^2 \quad (52)$$

#### *Exciting Energy*

The exciting energy during one roll period is formulated as follows:

$$E_E = -W\Delta GM \int_{1 \text{ per}} \varphi \cos(\omega_e t + \alpha) d\varphi \quad (53)$$

The angle  $\alpha$  is required here because the variation of GM in waves may not be in phase with the roll motion. In this paper, this angle is called the shift angle. Using the expression of  $\varphi$  and  $d\varphi/dt$  in Equation (47) and the expression of  $d\varphi$  in Equation (49), we construct the following expression of the exciting energy between 0 and a time t:

$$E_E(t) = W\Delta GM\omega_0\Phi^2 \int_0^t \cos \omega_0 t \sin \omega_0 t \cos(\omega_e t + \alpha) dt \quad (54)$$

The instantaneous exciting power is:

$$P_E(t) = \frac{dE_E}{dt} = W\Delta GM\omega_0\Phi^2 \cos \omega_0 t \sin \omega_0 t \cos(\omega_e t + \alpha) \quad (55)$$

The assumption regarding the wave encounter frequency ( $\omega_e=2\omega_0$ ) and trigonometric identities allow a simplification of this equation (Annex 3 provides the mathematical proof in page 130):

$$P_E(t) = \frac{1}{4}W\Delta GM\omega_0\Phi^2[\sin(4\omega_0t + \alpha) - \sin \alpha] \quad (56)$$

Consequently, the average value of the exciting power is a function of the shift angle  $\alpha$ :

$$P_E = -\frac{1}{4}W\Delta GM\omega_0\Phi^2 \sin \alpha \quad (57)$$

The maximum value of the exciting power is obtained for  $\alpha=-\pi/2$ :

$$P_{E.max} = \frac{1}{4}W\Delta GM\omega_0\Phi^2 \quad (58)$$

#### 4.2.4. Direct Calculation of the Maximum Roll Angle in Resonance Condition

##### *Required Damping Coefficient*

Assuming the steady state of parametric roll amplitude and the worst case of shift angle ( $\alpha=-\pi/2$ ), the exciting energy is entirely dissipated if the damping coefficient can attain a required value  $B_{44.req}$  defined by the equality between  $P_D$  (Equation (52)) and  $P_{E.max}$  (Equation (58)):

$$B_{44.req} = \frac{W\Delta GM}{2\omega_0} \quad (59)$$

Surprisingly, the roll amplitude  $\Phi$  does not appear directly in this relationship. If the damping coefficient  $B_{44}$  is independent from the roll amplitude (i.e. linear damping), the parametric roll cannot appear when its value is larger than the required value ( $B_{44.req}$ ). When  $B_{44}$  is lower than  $B_{44.req}$ , parametric roll appears with very large roll amplitude or causes the vessel to capsize, subject to the linear-GZ assumption.

However, the damping coefficient is a function of the roll amplitude as proposed by Ikeda simplified methods [48, 50]. Consequently, this approach provides an easy direct calculation of the maximum parametric roll amplitude  $\Phi_{max}$  (corresponding to both the resonance condition and the worst case of shift angle) by solving the following equation:

$$B_{44}(\Phi_{max}) = \frac{W\Delta GM}{2\omega_0} \quad (60)$$

In 1955, Kerwin [12] arrived at the same conclusion using both analytical solving of the differential equation and energy consideration, assuming a non-linear damping. In the second method, the exciting energy is provided by a vertical movement of the center of gravity, causing an equivalent variation of GM while the metacenter is motionless.

##### *Comparison with Time-Domain Simulation*

The method described above is used to calculate the maximum roll angle in resonance condition for the C11 container vessel at a draft equal to 12 m. As required by the first-level criterion of the future regulation, hydrostatics are computed in waves which have a length equal to the length between perpendiculars (262 m) and a wave steepness equal to 0.0167

(see Section 1.2.2 or [22]). This causes the wave height to be equal to 4.375 m and the half-amplitude of the GM variation ( $\Delta GM$ ) equal to 1.511 m, independent of KG. The damping coefficients  $B_{44}$  are calculated according to Kawahara, Maekawa & Ikeda [50] and Ikeda, Himeno & Tanaka [48] for the lift component. The results are provided in Table 13 and Figure 80. For each value of KG, the speed is calculated for the parametric resonance condition. Positive speeds correspond to the head seas and negative speeds correspond to the following seas. The resulting maximum roll angle ( $\Phi_{\max}$  in Table 13) is compared to the value obtained by the numerical solving of the differential equation (Equation (44)) using the method of Runge-Kutta at the 4<sup>th</sup> order and a simulation duration equal to 20 times the ship's natural roll period ( $\Phi_{\max}$  sim in Table 13). We observe that both values of the maximum roll angle are almost equal (both calculations are limited to 50 degrees). In each case, the value obtained by the time-domain simulation is slightly lower than that obtained by the energy approach. This suggests that the duration of 20 natural roll periods of the ship is not long enough to precisely attain the steady-state roll amplitude.

Moreover, the direct calculation of the maximum roll angle is performed assuming the worst case of shift angle ( $\alpha = -\pi/2$ ). Equality between the values of the maximum roll angle calculated with both methods seems to show that this assumption is correct. Figure 81 shows the variation of roll angle over time during the numerical solving of the differential equation. This time-domain simulation in one degree of freedom starts with an initial angle equal to 10 degrees and a shift angle  $\alpha$  equal to zero, which reduces the exciting power to zero. During the first period, we observe a slight decrease of the roll amplitude (the roll angle is 8.9 degrees at the end of the period). After that, the amplitude increases up to the steady state. The frequency of the roll motion during the first period is 0.396 rad/s. Its value during the steady state is 0.369 rad/s. This shows that the roll motion automatically shifts in waves at the start of the simulation in order to attain the shift angle which provides maximum exciting energy ( $-\pi/2$ ). The assumption of the worst case of shift angle in parametric resonance condition is verified.

KG (m)	Average GM in waves (m)	$\omega_0$ (rad/s)	V (m/s)	$B_{44,req}$ (N.m.s/rad)	$\Phi_{\max}$ (deg.)	$\Phi_{\max}$ sim (deg.)
15.0	5.445	0.406	13.64	1.34E+09	17.96	17.83
15.5	4.945	0.387	12.05	1.40E+09	19.92	19.84
16.0	4.445	0.367	10.37	1.48E+09	22.26	22.20
16.5	3.945	0.346	8.60	1.57E+09	25.33	25.26
17.0	3.445	0.323	6.71	1.68E+09	29.75	29.66
17.5	2.945	0.299	4.68	1.82E+09	38.08	37.85
18.0	2.445	0.272	2.47	2.00E+09	50	50
18.5	1.945	0.243	0.01	2.24E+09	50	50
19.0	1.445	0.209	-2.78	2.60E+09	50	50
19.5	0.945	0.169	-6.12	3.21E+09	50	50
20.0	0.445	0.116	-10.55	4.68E+09	50	50

Table 13 – Maximum roll angle in parametric resonance condition for the C11 container vessel.

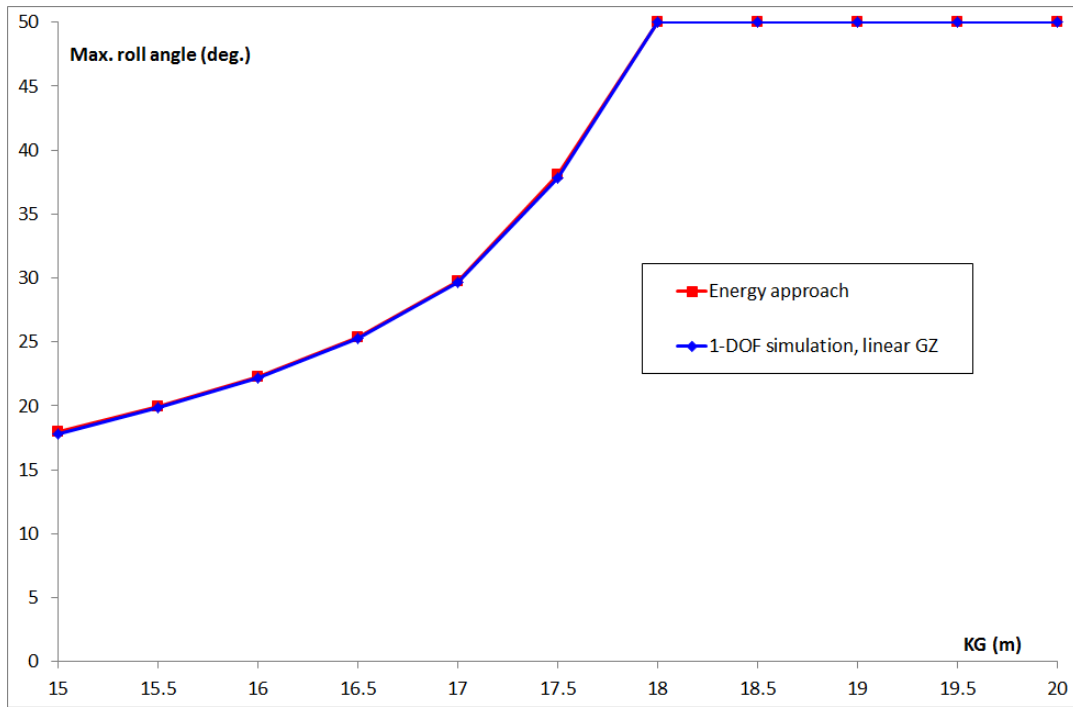


Figure 80 – Maximum roll angle in parametric resonance condition as a function of KG (both curve coincide).

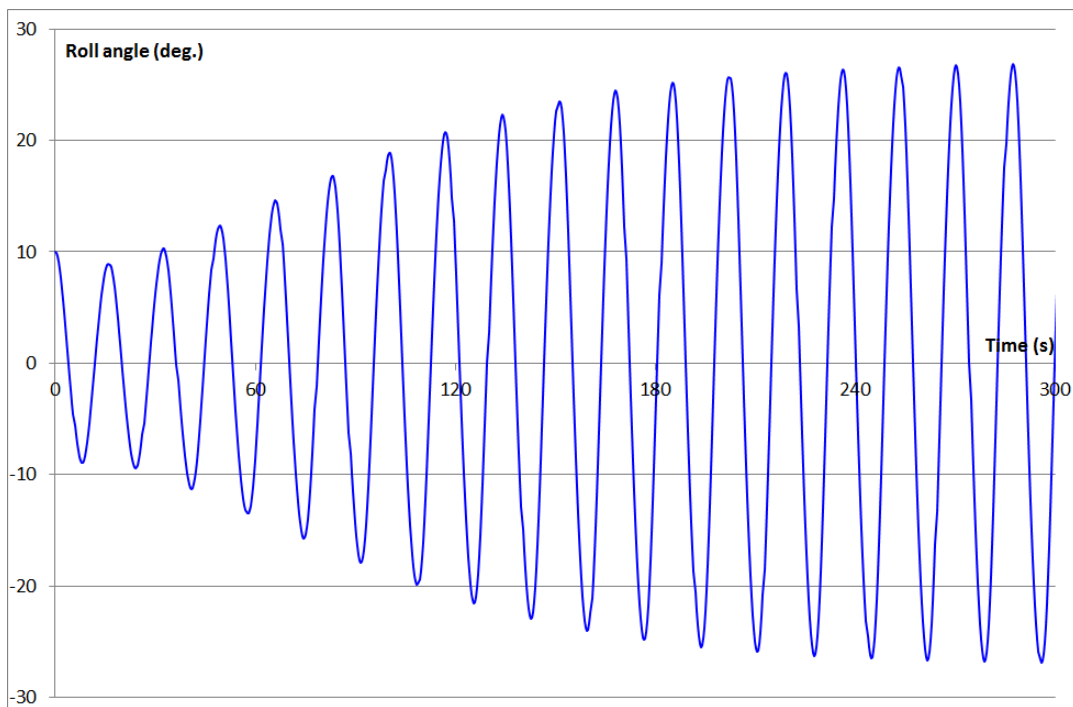


Figure 81 – Roll angle versus time in parametric resonance condition.

### 4.3. PARAMETRIC ROLL IN OTHER CONDITIONS

In this section and the next one, the roll frequency is denoted by  $\omega$  and may differ from the natural roll frequency  $\omega_0$ . The encounter frequency  $\omega_e$  may be non-synchronized with  $\omega$ . We introduce  $\gamma_0$  and  $\gamma$  as follows:

$$\gamma_0 = \frac{\omega_e}{\omega_0} \quad \text{And} \quad \gamma = \frac{\omega_e}{\omega} \quad (61)$$

#### 4.3.1. Non-Synchronized Parametric Roll

##### *Kinetic and Potential Energy*

If the roll frequency  $\omega$  differs from the natural roll frequency  $\omega_0$ , the sum of the kinetic and potential energies is not constant in time and Equation (48) (page 87) is no longer valid. However, the sum of these energies is a sinusoidal function. Hence, the average value of its derivate in time, equivalent to the average power required to maintain the roll motion, is zero. Annex 3 provides the mathematical proof in page 132.

Consequently, as for the synchronized parametric roll, the assumption of a constant roll amplitude  $\Phi$  causes the energy provided by the exciting moment ( $E_E$ ) to entirely dissipate by the damping moment as a damping energy ( $E_D$ ).

##### *Exciting Energy*

Modifying Equation (55) for the general case yields the following relationship for the exciting power:

$$P_E(t) = W\Delta GM\omega\Phi^2 \cos \omega t \sin \omega t \cos(\omega_e t + \alpha) \quad (62)$$

Trigonometric identities allow a modification of this relationship as follows (Annex 3 provides the mathematical proof in page 130):

$$P_E(t) = \frac{1}{4}W\Delta GM\omega\Phi^2 [\sin((2 - \gamma)\omega t - \alpha) + \sin((2 + \gamma)\omega t + \alpha)] \quad (63)$$

We observe that the average value of the exciting power is zero except if  $\gamma$  is equal to  $-2$  or  $+2$ . The case  $\gamma=-2$  corresponds to a non-realistically high speed in following seas. When the value of KG of the C11 container vessel is in the usual range from 15 to 20 m, the corresponding resonance speed is in the range from 54 m/s (KG=15 m) to 30 m/s (KG=20 m). This case is not considered here.

If  $\gamma$  is not equal to 2 but close to this value, the exciting power consists of two frequencies: a high frequency equal to  $(2+\gamma)\omega$  and a low one equal to  $(2-\gamma)\omega$ . Figure 82 shows the roll angle plotted as a function of time resulting from a time-domain simulation in this condition. The speed of parametric resonance is equal to 8.8 m/s and the ship's speed equal to 5.5 m/s. We observe long periods which could be seen as corresponding to the low frequency part of the exciting power. In these long periods, parametric roll successively appears and disappears passing through a maximum. The roll frequency during the two first long periods of this simulation (0 to 150 seconds and 150 to 300 seconds) remains almost unchanged (respectively 0.315 and 0.316 rad/s) but roll motions are not in phase. This shows again that the roll motion automatically shifts in waves in order to capture the maximum exciting

energy. The encounter frequency is equal to 0.617 rad/s, which renders  $\gamma$  equal to 1.95 during both first long periods of parametric roll. However, it is not possible to exactly find the low frequency of the exciting power  $((2-\gamma)\omega)$  in Figure 82 because of the shift of the roll motion.

Nevertheless, the roll amplitude rapidly tends to zero in this non-synchronized condition. Although parametric roll periodically exists during a short time, it may be ignored because the risk for the vessel is null.

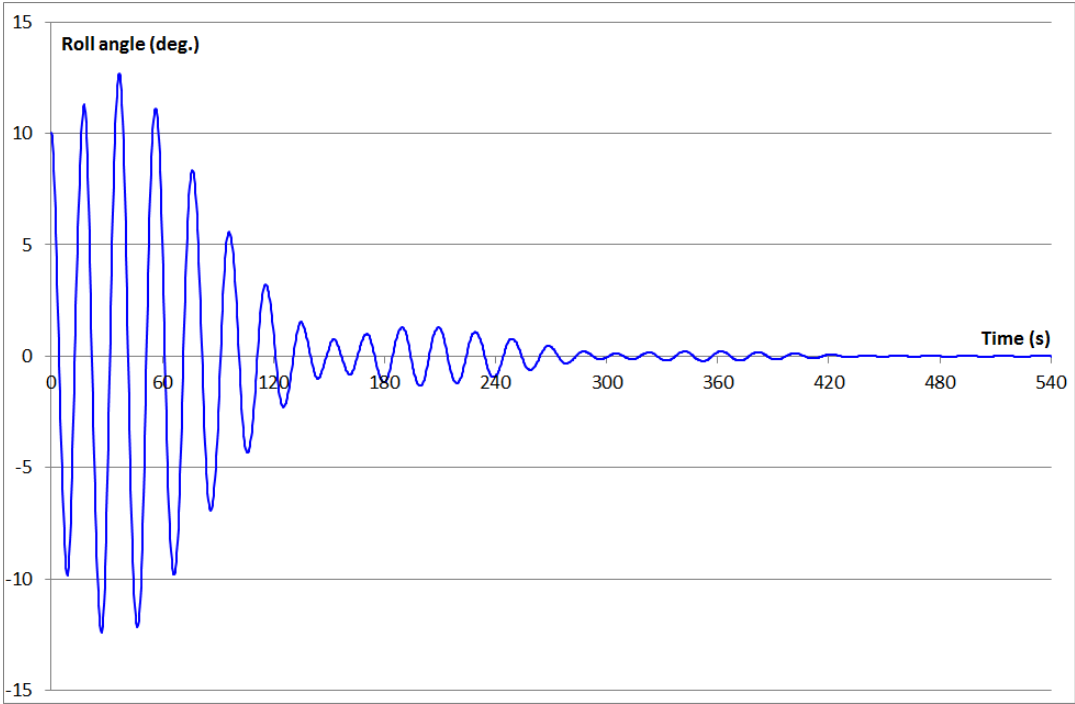


Figure 82 – Roll angle versus time in non-synchronized parametric roll condition.

**4.3.2. Lock-in Field**

We now propose to examine the behavior of parametric roll close to the resonance condition by performing numerical one-degree-of-freedom simulations for all possible speeds in head seas (positive speed) and following seas (negative speed) and to look at both the maximum roll angle and the ship’s roll period (called “observed roll period”, calculated at zero-crossing in the second half-time of the simulation). Results for the C11 container vessel with draft, KG and mean GM in waves respectively equal to 12, 17.5 and 2.95 meters and are shown in Figure 83. The vertical dashed line indicates the speed corresponding to the resonance condition. The horizontal dashed line indicates the natural roll period. The dashed hyperbole represents twice the encounter period and the black dot represents the maximum roll amplitude provided by the direct energy calculation. We observe the following facts:

- 1) The maximum roll angle occurs at a slightly lower speed than that of the resonance condition and is slightly higher than the speed calculated by the energy approach. We could believe that this is due to the reduction of roll damping at lower speeds but similar calculations performed with a roll damping coefficient independent of the speed yield similar results. This fact remains unexplained at this time. However, the analytical approach proposed by Kerwin [12] also observes this fact. The calculation of the frequency providing the actual maximum roll angle is proposed in Annex 3 page 133.

- 2) Parametric roll exists at a range of speeds from 1.5 to 7.7 m/s, in which the observed roll period is locked at twice the encounter period (i.e.  $\gamma_0=2$ ). We call this range lock-in field.
- 3) Outside this range, parametric roll does not occur (the maximum roll angle is roughly equal to the initial value used in the numerical solving, 1 degree) or is limited to the non-synchronized configuration previously presented. The observed roll period seems erratic; its calculation is disturbed by the shift of the roll motion. It tends to be close to the natural roll period.
- 4) As expected, the observed roll period in resonance condition is equal to the natural roll period and the maximum roll angle is equal to that calculated by the energy approach.

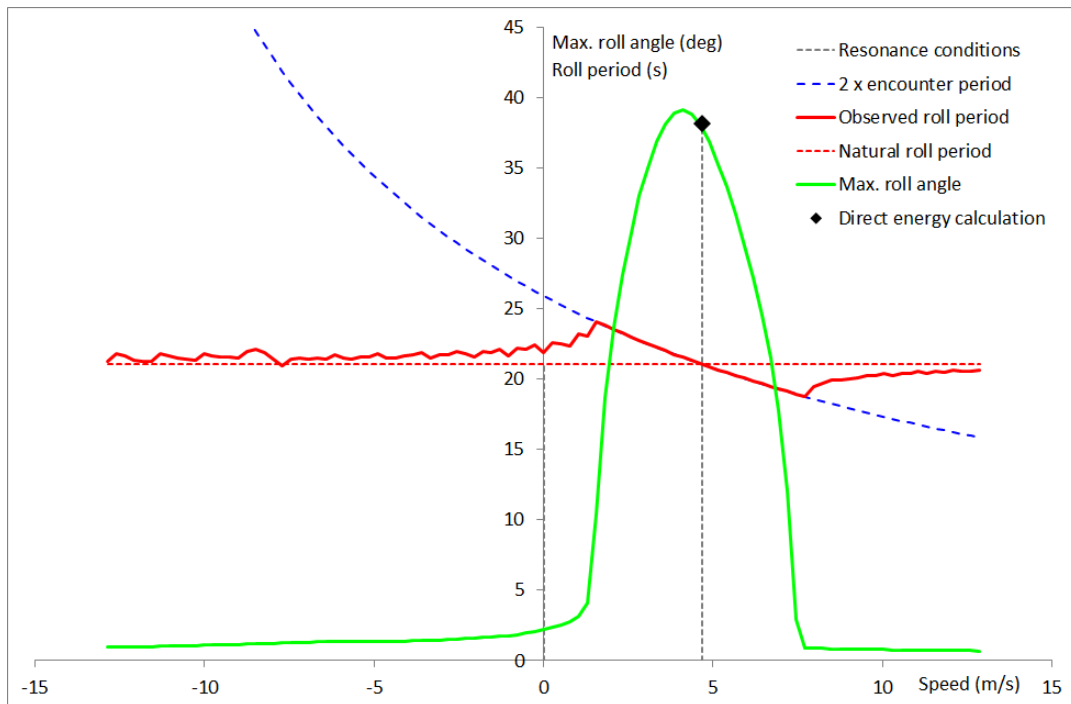


Figure 83 – Maximum roll angle and roll period versus speed.

### 4.3.3. Second and Third Modes of Parametric Roll

Figure 84 shows a similar calculation performed with a KG increased to 18.45 m and a mean GM in waves reduced to 2.00 m. The maximum roll angle in the lock-in field is larger than 50 degrees and the ship would possibly capsize in the vicinity of the resonance condition. We observe a second lock-in field corresponding to the second mode of parametric roll, characterized by equality between both the roll frequency and the encounter frequency ( $\gamma_0=1$ ). This lock-in field is not exactly centered on the second resonance speed (9.98 m/s, following seas) but passes through this value. The maximum roll angle occurs at a speed lower than the resonance speed, possibly for the same unexplained reasons than what is observed in the first mode of parametric roll. The value of the maximum roll angle is 2.2 degrees, negligible compared to what occurs in the first mode. The width of the second lock-in field is also reduced.

The third mode of parametric roll ( $\gamma_0=2/3$ ) is neither observable in the roll period nor in the roll amplitude for this vessel. In the conditions of Figure 84, the corresponding speed is 13.4 m/s in following seas. However, it can be observed in non-realistic conditions as shown

in Figure 85, where the speed range has been enlarged, the GM variation has been increased (i.e. the wave steepness does not correspond to the future regulation requirement any longer) and the damping coefficient has been customized. We observe that the third lock-in field is narrow and the corresponding maximum roll angle is negligible.

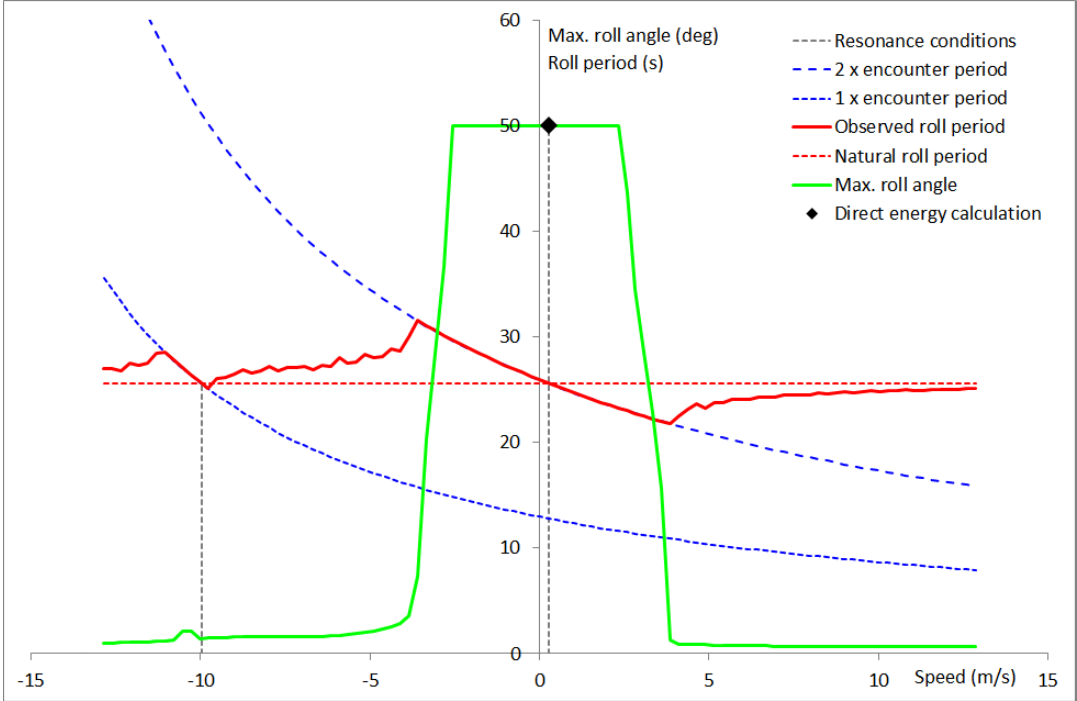


Figure 84 – Maximum roll angle and roll period versus speed with lower GM.

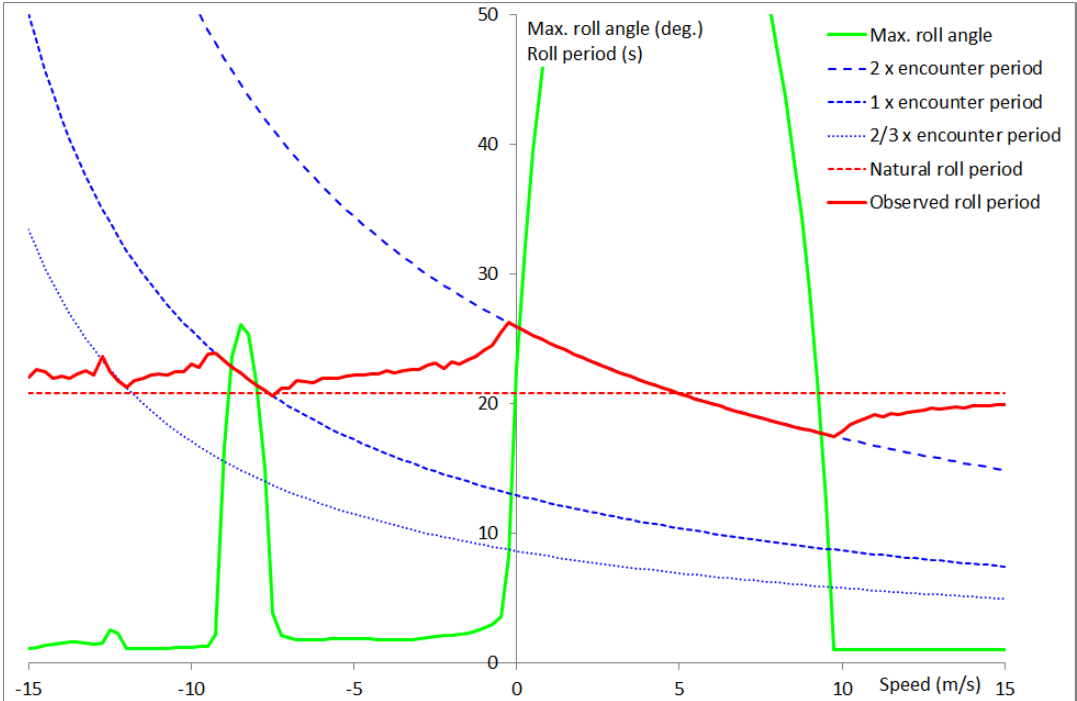


Figure 85 – Three modes of parametric roll.

### 4.3.4. Shift Angle in the Lock-in Field

The shift angle  $\alpha$  can be calculated by comparing the resulting variation of the roll angle and the variation of the metacentric height imposed during the time-domain simulation. Figure 86 shows the evolution of its absolute value as a function of  $\gamma_0$ . All data are dimensionless in this figure: the maximum roll angle is divided by the value obtained with the direct energy calculation, the periods are divided by the ship’s natural roll period and the shift angle is divided by  $-\pi/2$ . We observe that its value starts from near zero at the left (low-speed side of the lock-in field), is equal to  $-\pi/2$  near the resonance condition ( $\gamma_0=2$ ) and continues up to approximately  $-\pi$  at the right end of the lock-in field (high-speed side). Since the exciting power is reduced by  $\sin(\alpha)$ , this evolution is in accordance with the evolution of the maximum roll angle observed in the lock-in field. The shift angle is not drawn outside the lock-in field since it has no significance here.

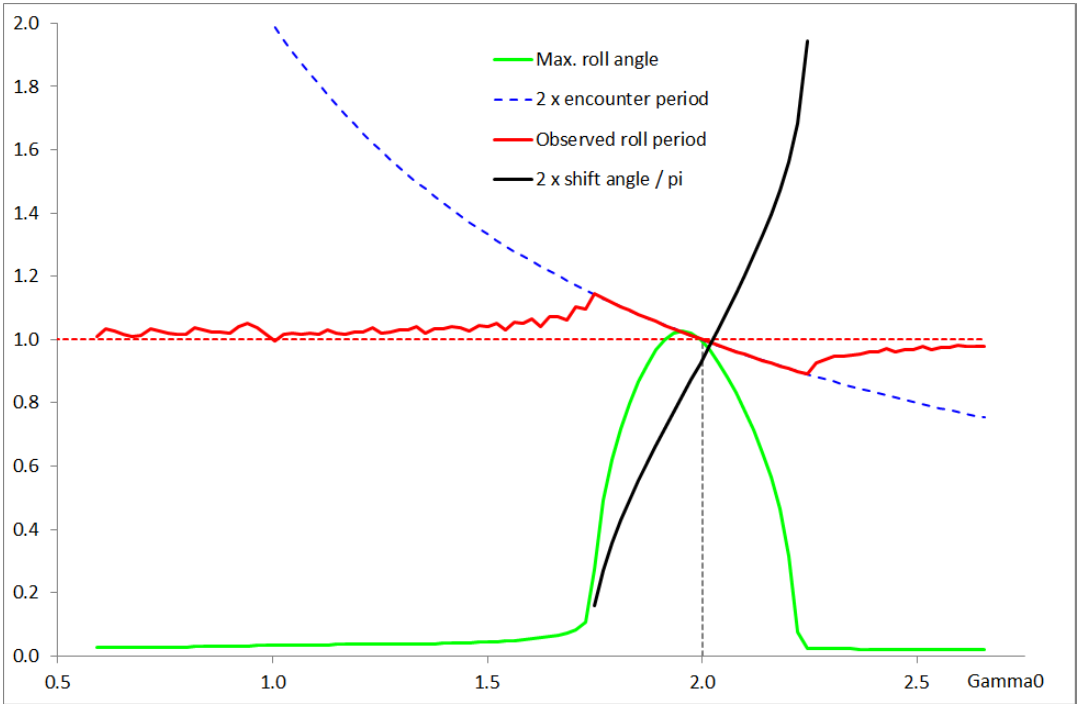


Figure 86 – Evolution of the shift angle in the lock-in field.

### 4.3.5. Width of the Lock-in Field

The width of the lock-in field is defined as the difference of  $\gamma_0$  at both ends of the field. Its value is almost equal to  $\Delta GM/GM$ . This observation has been made for all calculations performed on the C11 container vessel, for any values of the average metacentric height in waves and its variation (respectively  $GM$  and  $\Delta GM$ ). This observation has also been made for the other vessels examined within the scope of this chapter (the 319 m container vessel, the Ro-Ro vessel and the tanker). The second generation intact stability criteria of level one and level two assess these vessels as respectively vulnerable (similar to the C11 container vessel), slightly vulnerable and non-vulnerable to parametric roll (see Section 3.3.1).

In 1955, Kerwin [12] demonstrated an equivalent result both without and with damping from an approximate solution of Equation (44). The equivalence between his result and the observation made here is demonstrated in Annex 3 page 135.

Moreover, it seems interesting to validate the location and the width of the lock-in field with a computation of higher accuracy than that of the one-degree-of-freedom simulation with a linear GZ. Fredyn software [70], presented in Section 3.3.5, is used for this. It is used here to simulate the behavior of the C11 container vessel in one loading condition (draft 12 m, KG 18 m) in sinusoidal waves which have the required characteristics (length 262 m, steepness 0.0167), in head seas and following seas conditions. Figure 87 shows the maximum roll angle provided by both 1- and 6-degrees-of-freedom simulations. We observe the following facts:

- 1) Both fields of parametric roll coincide perfectly. The location and the width of the lock-in field obtained with 1-DoF simulations are validated.
- 2) The maximum roll angle provided by 6-DoF simulations occurs exactly at the resonance condition, contrarily to what has been observed with 1-DoF simulations and by Kerwin.
- 3) The maximum roll angle provided by 6-DoF simulations is significantly smaller than the amplitude obtained by 1-DoF simulations. This is due to the dispersion of energy in the 5 other degrees of freedom and to non-linear effects. Moreover, the methods used for roll damping are not the same in 1-DoF and 6-DoF simulations (roll damping computation in Fredyn is based on [49]).
- 4) Keeping the ship's heading is impossible at zero speed in waves. This causes the trough observed at this speed in the 6-DoF curve.
- 5) The second mode of parametric roll is clearly visible in 6-DoF simulations but its peak does not occur at the expected speed.

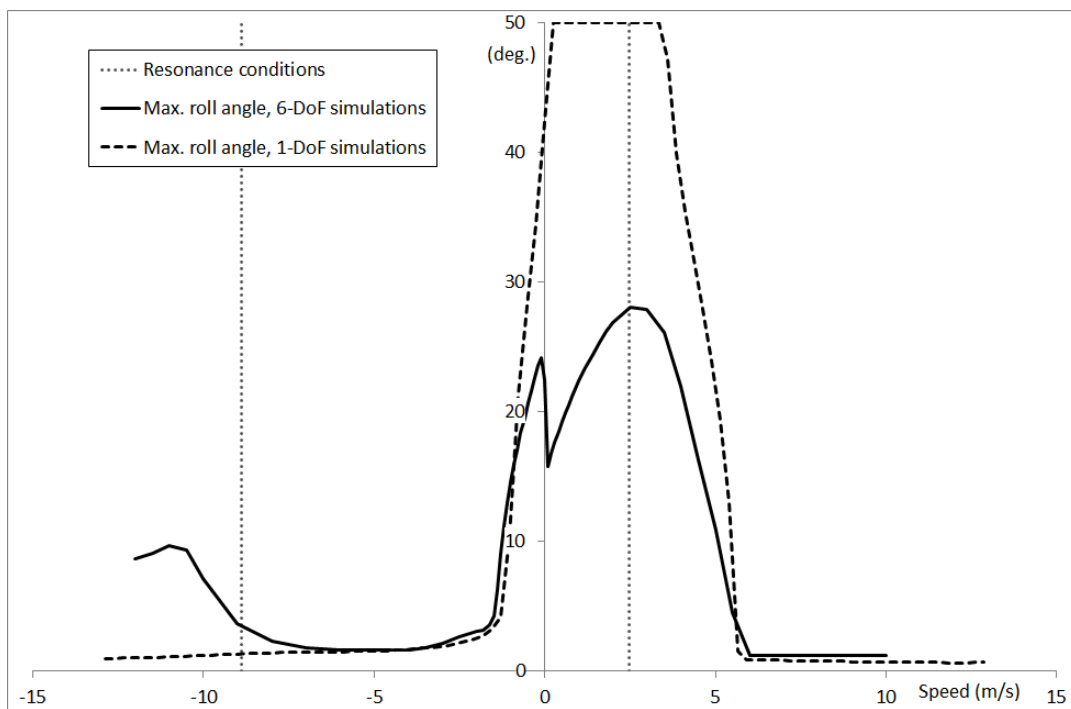


Figure 87 – Maximum roll angle versus speed provided by 1-DoF and 6-DoF simulations.

#### 4.4. METHOD PROVIDING STEADY-STATE PARAMETRIC ROLL AMPLITUDE AT ANY SPEED

We are able to easily calculate the maximum parametric roll amplitude which occurs in the first-mode resonance condition assuming a linear GZ. Moreover, we can predict the width of the lock-in field, in which parametric roll exists, and the evolution of the shift angle in this field. We assume a linear evolution from 0 to  $-\pi$ . These points allow the establishment of a simplified method providing the parametric roll amplitude in all speed conditions.

##### 4.4.1. Energy Method

We propose a practical method, called energy method, which provides the parametric roll amplitude in all speed conditions for a specific loading condition (draft and KG). Only the first mode is considered. This method consists of two steps.

###### *First Step*

The first step consists of computing the parametric roll amplitude at the speed corresponding to the resonance condition. This speed is obtained by the following relationship:

$$V_{1st\ mode} = (2\omega_0 - \omega_w) \frac{g}{\omega_w} \quad (64)$$

Where  $\omega_w$  is the wave frequency (rad/s) and  $g$  is the acceleration of gravity ( $m/s^2$ ).

The parametric roll amplitude at this speed, denoted by  $\Phi_{max}$ , is obtained by the solving of Equation (60), which can be easily done numerically on a spreadsheet.

The more difficult problems of this first step are:

- The handling of the Ikeda method: although the number of coefficients to be calculated is large, there is neither hard relationship nor integral to deal with.
- The computation of the GM variation in sinusoidal waves, which requires an adequate hydrostatic tool: several hydrostatic software packages, currently used by naval architects, can be used to perform such computations.

###### *Second Step*

For any speed  $V$  (m/s), we calculate  $\gamma_0$  as follows:

$$\gamma_0 = \frac{\omega_e}{\omega_0} = \frac{\omega_w}{\omega_0} \left( 1 + \frac{\omega_w V}{g} \right) \quad (65)$$

The parametric roll amplitude is zero outside the lock-in field (the second and third modes are not considered) and non-zero inside. The lock-in field is defined by  $\gamma_0$  in the range:

$$\text{From } 2 - \frac{\Delta GM}{2GM} \quad \text{To} \quad 2 + \frac{\Delta GM}{2GM} \quad (66)$$

Assuming a linear evolution of the shift angle  $\alpha$  in the lock-in field and a parametric roll amplitude proportional to  $\sin(\alpha)$ , this amplitude, denoted by  $\Phi$ , is obtained by:

$$\Phi = \Phi_{max} \cos\left(\pi(2 - \gamma_0) \frac{GM}{\Delta GM}\right) \quad (67)$$

#### 4.4.2. Improvement of the Energy Method

The evolution of the shift angle in the lock-in field is not exactly linear, as shown in Figure 86. The comparison of the roll amplitudes provided by the above method and those obtained with the 1-DoF simulation demonstrates that our method underestimates the amplitude. Consequently, we propose to introduce an exponent  $k$  in Equation (67) as follows:

$$\Phi = \Phi_{max} \cos^k\left(\pi(2 - \gamma_0) \frac{GM}{\Delta GM}\right) \quad (68)$$

Figure 88 shows the results provided by the proposed method with different values of the exponent for the C11 container vessel with the same loading condition as that in Figure 83. Setting  $k$  to zero renders the roll amplitude equal to the value obtained in the resonance condition inside the entire lock-in field and zero outside the field. We propose  $k=1/2$  (plain line in Figure 88). This value provides a good accuracy and a slight safety margin.

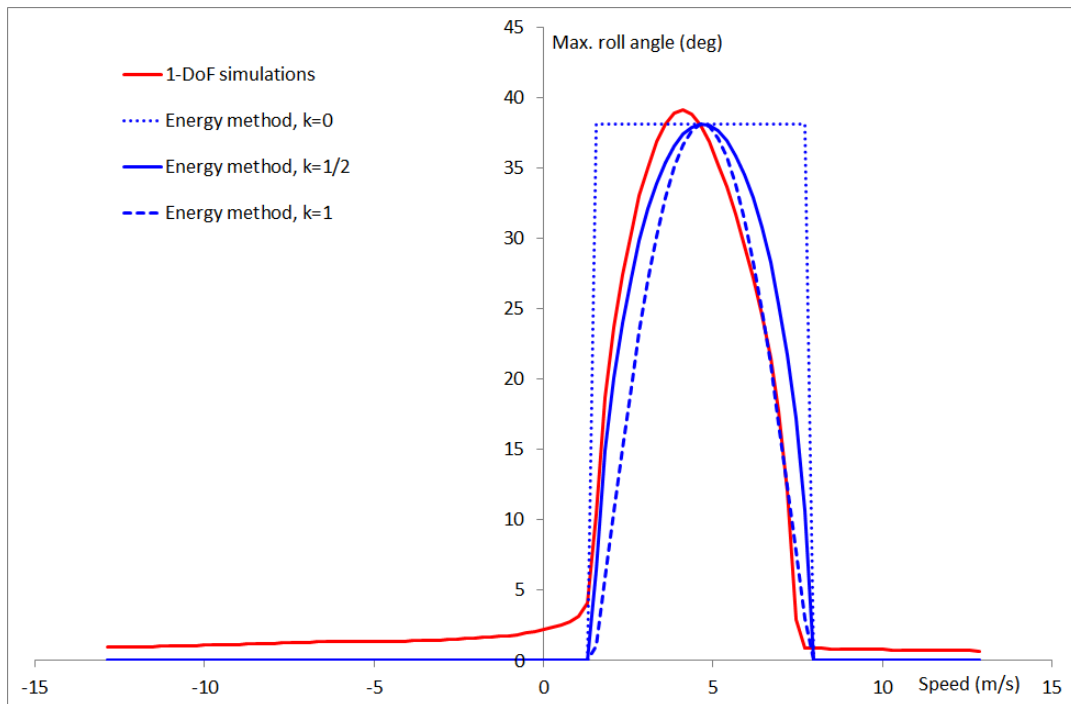


Figure 88 – Maximum roll angle versus speed, influence of exponent in energy method.

#### 4.4.3. Application to Second Generation Intact Stability Criteria

As mentioned in Section 1.2.3, the second check of the level-two criterion of the parametric roll failure mode requires computing the maximum roll angle for several wave cases and 7 speeds in head and following seas (independent from the resonance speed) for each wave and any considered loading condition. This criterion has been defined by the IMO in 2015 [22] and is enhanced by explanatory notes written in 2016 [23] providing explanations, comments and guidelines, such as the criteria of other failure modes because of their unusual complexity with regard to the current intact stability regulation [18].

We propose to implement the energy method in the computation of the second check of level-two criterion of parametric roll. Computations are performed on the C11 container vessel, the 319 m container vessel, the Ro-Ro vessel and the tanker. Results are provided in terms of  $KG_{max}$  curves and the second check (C2) is seen as a separate criterion. Results are given in Figure 89 to Figure 92.  $KG_{max}$  curves obtained with the energy method are compared to those obtained by numerical 1-DoF time-domain simulations assuming a linear and non-linear GZ in waves. The non-linear GZ in waves is calculated as the GZ in calm water modulated by the GM in waves, as proposed in the explanatory notes [23] and presented in Section 1.2.4 page 32. The comparison of  $KG_{max}$  curves obtained by 1-DoF time-domain simulations with a linear and non-linear GZ is previously presented in Section 3.3.4 page 78.

Figure 89 –  $KG_{max}$  curves associated with the 2<sup>nd</sup> check of the parametric roll level 2 criterion for the C11 container vessel. Figure 89 shows the results for the C11 container vessel. We observe a good accordance of the three methods.

Figure 90 shows the results for the 319 m container vessel. Both curves obtained with a linear GZ are in very good accordance.

Figure 91 shows the results for the Ro-Ro vessel. Both curves obtained with a linear GZ are in very good accordance except for one point located beyond the full-load draft. The extension of computations at larger non-realistic drafts shows that the curves meet again. This local jump is characteristic of the  $KG_{max}$  curves associated with the second check of level-two criterion as explained in Section 3.3.2.

Figure 92 shows the results for the tanker. The accordance between both curves associated with a linear GZ is very high again.

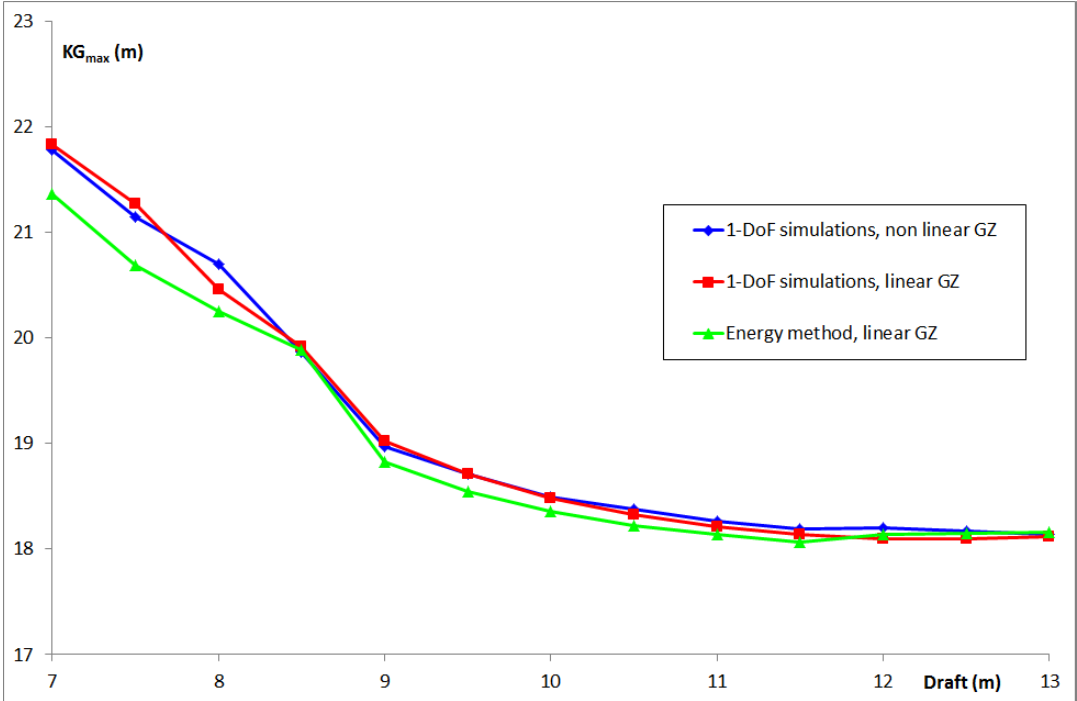


Figure 89 –  $KG_{max}$  curves associated with the 2<sup>nd</sup> check of the parametric roll level 2 criterion for the C11 container vessel.

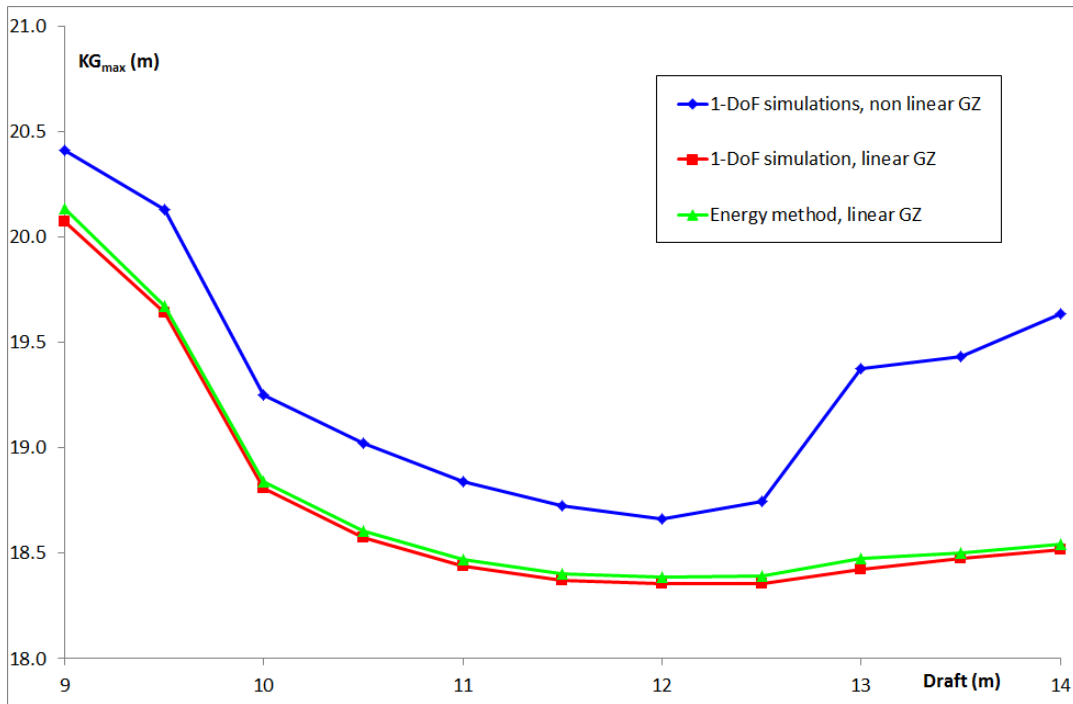


Figure 90 –  $KG_{max}$  curves associated with the 2<sup>nd</sup> check of the parametric roll level 2 criterion for the 319 m container vessel.

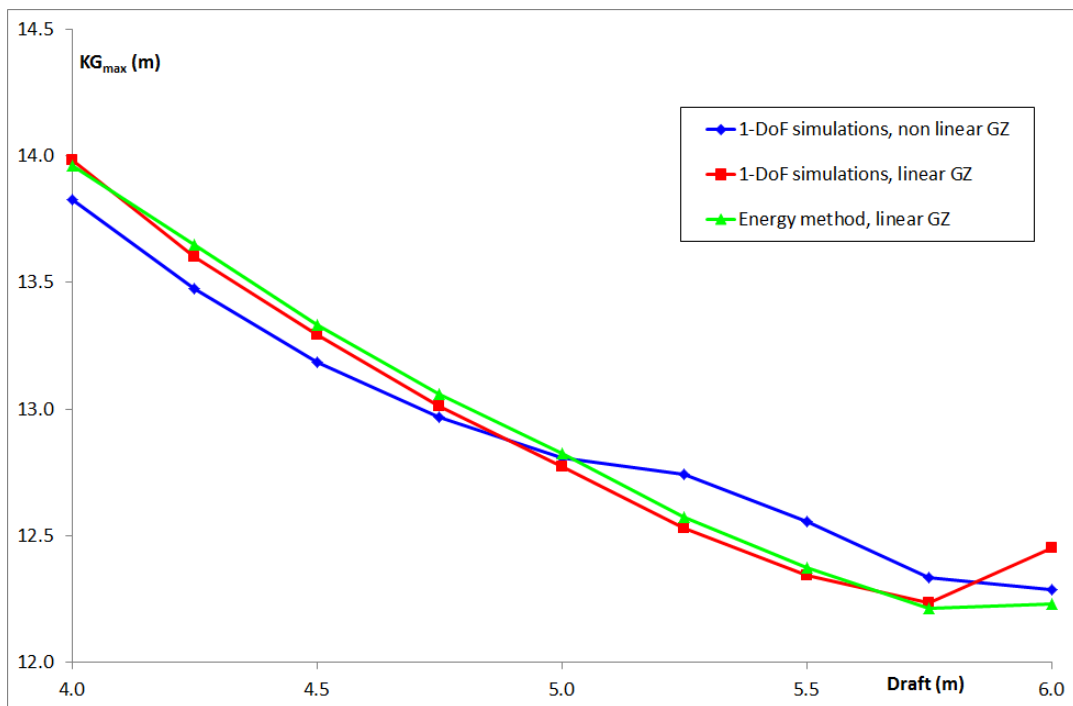


Figure 91 –  $KG_{max}$  curves associated with the 2<sup>nd</sup> check of the parametric roll level 2 criterion for the Ro-Ro vessel.

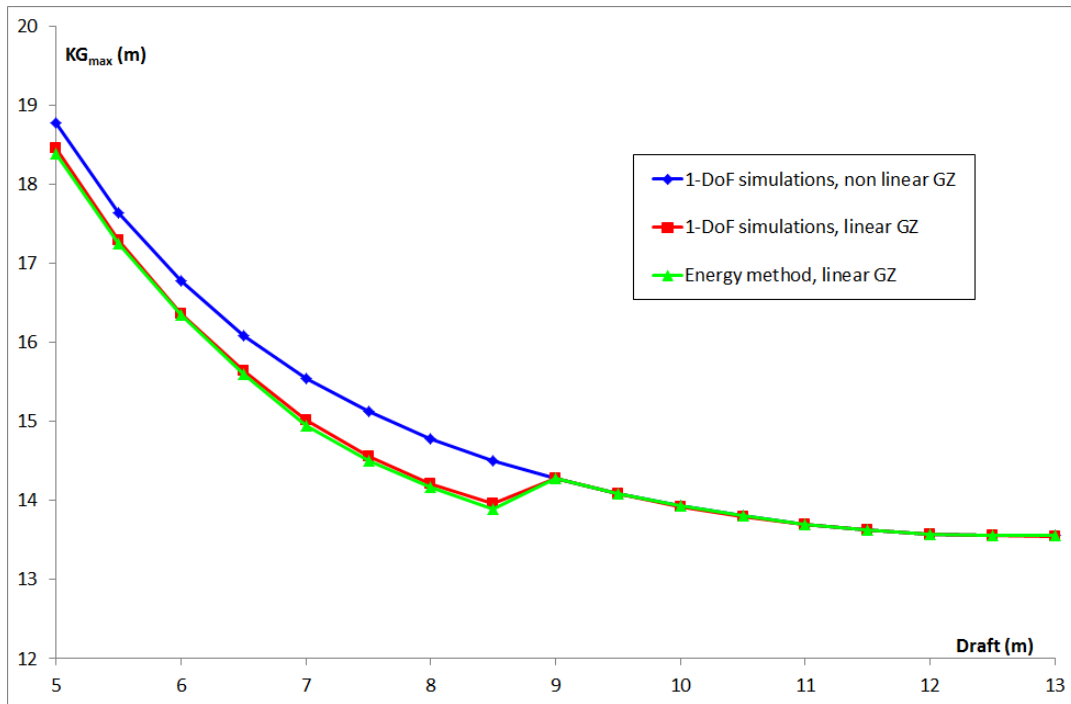


Figure 92 –  $KG_{max}$  curves associated with the 2<sup>nd</sup> check of the parametric roll level 2 criterion for the tanker.

## CONCLUSION

### *Objective*

The second generation intact stability criteria are currently under finalization and validation at the International Maritime Organization. These criteria are structured in five failure modes and three levels of assessment in each failure mode. Pure loss of stability and parametric roll failure modes are consequences of the variation of the restoring moment in longitudinal waves. The former is a single wave effect since the latter is due to the repetition of the encounter of waves. The aim of the work reported in this thesis was to implement the level-one and level-two criteria of these failure modes in order to analyze their relevance and their requirement.

The criteria are implemented in the Calcoque software. This real three-dimension hydrostatic code computes equilibrium, metacentric heights and righting arm curves in both calm water and longitudinal waves, using a matrix algorithm which generates a mesh of the watertight volume from the classical hull design by stations.

The criteria are computed for several ships of different types, both civilian and military, expected to have different behavior with regard to these failure modes. Although new criteria are not intended for naval ships, it cannot be excluded that naval ships be vulnerable to such stability failures. Moreover, if one is provided with an infra-red camera, although this is not mandatory, one will proceed to a thermal check of one's home in order to improve its efficiency in this domain at optimized cost. New criteria could be seen as this camera. They allow assessing any ship with regard to several failure modes at zero cost (a  $KG_{max}$  curve associated with a level-two criterion requires about 10 minutes of computation). Hence, it would be unfortunate to forego the analysis of naval ships while we consider civilian ones. The author recommends a change of military stability regulations in this direction after the new IMO regulation comes into force.

Results are provided as  $KG_{max}$  curves, giving the maximum height of the center of gravity ensuring the compliance of the considered criterion. This avoids any consideration of the vertical center of gravity and allows the evaluation of criteria rather than ships.

### *Results, Comments and Recommendations*

The computation of  $KG_{max}$  curves associated with the level-one and level-two criteria for different civilian and military vessels reveals that level two can be more conservative than the second level-one method for both failure modes. This configuration is not expected in the future regulation. This computation also shows that the gap between both level-one methods can be very large, especially for the pure loss of stability failure mode. The safety margins ensured by the first level-one method (parallel waterplane) seem to be excessive and may conflict with the excessive acceleration criteria. Thus, if they are equipped to compute hydrostatics in waves, naval architects and shipyards will probably not use the first level-one method. This first method could have a real added value if it ensures acceptable safety margins for small vessels, which are likely to be designed by architects with modest

means. This seems to be the case for the 30 m passenger vessel presented here since her standard loading condition complies with the first-method level-one criterion of both failure modes.

Although this is not the aim here, the  $KG_{max}$  curves associated with parametric roll criteria confirm the well-known vulnerability of the C11 container vessel to this failure mode. As expected, the other container vessel is also assessed as vulnerable to parametric roll. The tanker is assessed as non-vulnerable to both pure loss of stability and parametric roll, as expected due to her wall-sided hull.

$KG_{max}$  curves associated with the first method of level-one criteria of both failure modes have hooks due to void spaces in the hull form. Considering the bare hull masks this phenomenon. Moreover, the height of the watertight limit has an important influence on the level-two criterion of pure loss of stability. Both points show the importance of a rigorous definition of the watertight volume to be considered.

***Recommendation: The future regulation should clearly specify the watertight volume to be considered (bare or real hull, height of the watertight deck).***

The second check of parametric roll level-two criterion (C2) considers the maximum roll angle for 7 speeds in both head and following seas and all waves cases of a scattering table. The future regulation proposes two methods to compute its value. The method based on the numerical solving of the parametric roll differential equation is used and analysed here. The future regulation stipulates a simulation duration equal to 15 times the ship's natural roll period, based on a proposal of experts in the field [32]. This value is validated here by sensitivity tests.

The computation of the second check of parametric roll level-two criterion for all possible values of KG shows that the more the ship is vulnerable to this failure mode, the more her curve C2 versus KG has peaks and a long interval to let C2 go from 0 to 1. This creates jumps in the associated  $KG_{max}$  curves and makes the surface formed by both draft and KG foliated with authorized and restricted zones. Consequently, checking that C2 is lower than the specified threshold ( $R_{PRO}$ ) for a given ship's loading condition will not be sufficient. It will be necessary to check this condition for all lower values of KG.

***Recommendation: The future regulation should clearly specify the requirement of checking C2 for all values of KG lower than that of the considered loading condition.***

The future regulation imposes the use of the Grim method [65] in the second check of parametric roll level-two criterion. This causes all wave cases of the scattering table to be replaced by effective waves which have the same length and period. Hence, the 7 stipulated speeds may have a random effect with regard to this wave, depending on the ship's length, possibly overlooking the speed corresponding to the resonance condition. Increasing the number of speeds or focusing on the resonance speed should improve the criterion. This recommendation is also formulated by the Delegation of Sweden in the Intact Stability Correspondence Group (ISCG) [24].

***Recommendation: The number of speeds considered in the second check of level-two parametric roll criterion should be increased, or the criterion should focus on the speed corresponding to the first-mode resonance condition.***

The computation of the maximum parametric roll angle requires the roll damping coefficient. The future regulation provides the Ikeda simplified method in the explanatory

notes of parametric roll criteria (SDC 3/WP.5, Annex 4, Appendix 4, [23]). The proposed method is taken from [48] for the lift component and [50] for other components. However, this method underestimates the damping coefficient for hull having sharp bilges, such as that of the 30 m passenger vessel. This point is illustrated by the inconsistency between the very conservative  $KG_{\max}$  associated with C2 and the  $KG_{\max}$  associated with other parametric roll criteria.

***Recommendation: The future regulation should propose a method to provide the roll damping coefficient for hulls with sharp bilges.***

Since both methods proposed in the future regulation to compute the maximum roll angle required by the second check of parametric roll level-two criterion are relatively complex to implement, an alternative method is proposed. It consists firstly in calculating the steady state roll amplitude in resonance condition from energy considerations and assuming a linear GZ. A method providing the roll damping coefficient function of roll amplitude, such as a simplified Ikeda method, is required. The obtained value is the amplitude of parametric roll which may occur in the worst conditions, when the wave encounter frequency is twice the ship's natural roll frequency. Consequently, this easy calculation is compatible with the deterministic principle of the level-one criterion of the future intact stability regulation: a vessel having a roll amplitude lower than an adequate threshold in the worst condition of parametric roll should not be assessed as vulnerable to this failure mode.

The first mode of parametric roll occurs in a field where the ship's roll frequency, which may differ from her natural frequency, is locked to half the wave encounter frequency. Simulations on several ships exhibiting different behaviors with regard to parametric roll show that the non-dimensional width of this lock-in field is almost equal to the non-dimensional GM variation ( $\Delta GM/GM$ ). They also show that the shift angle, which corresponds to the phase between the GM variation and the roll motion and which reduces the exciting energy, is almost linear from 0 to  $-\pi$  in this field, passing  $-\pi/2$  near the resonance condition. Thus, the second part of the alternative method allows the estimation of the parametric roll amplitude in any condition, in particular for any speed.

The implementation of this alternative method in the second check of the level-two criterion is possible. It provides almost the same  $KG_{\max}$  than the one-degree-of-freedom numerical simulation with a linear GZ. The linear GZ assumption is doubtful for vessels having a highly-non-linear GZ such as the 319 m container vessel. However, the alternative method is so easy to implement that it would be unfortunate to go without in the case of vessels having an almost-linear GZ up to 25 degrees.

***Proposal: The future regulation should propose a simplified alternative method for vessels having a GZ almost linear up to 25 degrees.***

Although the mean value of the parametric exciting power is zero outside the first-mode lock-in field, parametric roll may occur with low amplitude in modes 2 and 3, where the ratios between the wave encounter frequency and ship's roll frequency are respectively equal to 1 and 2/3. An improvement of the alternative method in these conditions would be interesting, even if the financial and safety risk is almost null or significantly reduced.

## *Perspective*

### *Planned Improvements*

The work presented in this thesis could be completed by several planned developments and comparisons:

The six-degrees-of-freedom computations performed in parametric roll could be extended to pure loss of stability, in order to analyze the relevance of the  $KG_{\max}$  associated with the corresponding criteria. The computation of  $KG_{\max}$  curves associated with these criteria could be extended to vessels having suffered an accident due to this failure mode. In particular, the 55-meter LPG tanker reported by Taylan [36] sank presumably due to a stability failure on a wave crest as. This vessel had a Froude number equal to 0.23 and would consequently be assessed as non-vulnerable by the future rules. This unexpected case requires to be rigorously analyzed.

Although it is not proposed in the future regulation, a simplified method providing the roll damping coefficient for hulls with sharp bilges could be implemented in order to analyze the results for the 30 m passenger vessel, expecting the resulting  $KG_{\max}$  to be close to those associated with other parametric roll criteria.

Moreover, other computation methods providing the maximum parametric roll angle for the second check of level two could be implemented:

- considering the real GZ in waves instead of the GZ in calm water modulated by GM in waves;
- analytical method proposed by Kerwin [12], assuming a linear GZ, to be compared with both the energy method proposed in Chapter 4 and numerical time-domain simulation with a linear GZ;
- averaging method proposed in the future regulation, directly providing the maximum roll angle from a fit of the GZ curve at the 5<sup>th</sup> order, to be compared with the numerical time-domain simulation.

### *Entry into Force of the Second Generation Intact Stability Criteria*

The entry into force of the future rules, currently estimated at the earliest in 2019 as recommendations in part B of the IMO intact stability code, will shake up habits of shipyards and naval architects because of their unusual complexity with regard to the current intact stability rules. However, shipyards and naval architects nowadays handle the probabilistic rules of damage stability, which require a large amount of computations and represent a significant leap of complexity with regard to the former deterministic rules. The future intact stability rules require adapted computing tools which are presumably currently under development. Schools and universities specialized in naval architecture will teach these new rules to their students and will propose training courses updating the knowledge of senior naval architects. The author sees no major obstacle to the entry into force of pure loss of stability and parametric roll criteria, except for the second check of parametric roll level-two criterion because of its requirement of the roll damping coefficient.

Unfortunately, there is no universal simplified method providing the roll damping coefficient for any type of ship, as shown by the inadequacy of the method proposed in the future regulation to the sharp-bilge hull of the 30 m passenger ship. Hence, it would be desirable to

include several methods corresponding to all possible hull designs in the future regulation. However, it is not currently possible to predict the innovative hull designs that will exist in future decades. Consequently, including an exhaustive review of the simplified roll damping method in the future regulation is pointless. CFD (computational fluid dynamics, solving Navier-Stokes equations) is currently able to provide accurate (or at least acceptable) values of the roll damping coefficient for any hull design. Unfortunately, it is not compatible with the philosophy of the second level of assessment because of the highly specialized personnel and computing time it needs.

Consequently, in the author's personal opinion, the second check of parametric roll level-two criterion could be seen in its present form as a first step of third level of assessment, which will presumably be performed by specialized institutes. An alternative way could be to restrict the second check in its present form to the vessels compatible with the simplified roll damping method (or a panel of different methods) using objective simple criteria (Froude number, block-coefficient, bilge radius ...) to be clearly specified in the future regulation. For other vessels, the second level of assessment would be limited to its first check. In case of non-compliance with this check, the classification society should enjoin the implementation of the second check by a specialized institute, able to select and use an adequate method to provide the roll damping coefficient (including CFD if required), otherwise enjoin the direct assessment, also to be performed by a specialized institute.

#### *Direct Assessment*

Although some improvements are desirable and some points need to be clarified, the level-one and level-two criteria of pure loss of stability and parametric roll are now finalized, and so are those of the three other failure modes. This is not the case for the third level, which is yet in its earliest development.

The third level is planned to be a direct assessment, i.e. numerical simulations of the ship in waves, expected to evaluate the vulnerability regarding the five considered failure modes with good accuracy. These simulations are necessarily performed in six degrees of freedom. CFD does not seem to be adapted for this task because of the excessive computation time it currently needs. The Fredyn software, developed by the CRNAV members and used for some comparisons within the scope of this thesis, could be adapted for this task. In this software, hydrodynamics (radiation and diffraction forces) are computed first using potential theory. The simulation can consequently be accelerated up to 10 times the real time or more. Other similar existing 6-DoF hydrodynamic solvers may also be adapted.

The direct assessment in parametric roll failure mode could consist of an improved second check of level two, replacing both the numerical one-degree-of-freedom simulations and sinusoidal waves, respectively by six-degrees-of-freedom simulations and real sea-states with a wave spectrum to be determined. The author recommends increasing the number of considered speeds or focusing on resonance speed, as argued above.

A similar work could be performed for the pure loss of stability failure mode, considerably increasing the simulation time in order to capture a significant number of extreme waves.

It is also possible to merge direct assessments of all failure modes in a unique assessment made of a large amount of simulations in all wave cases of the scattering table, with all possible values of the ship's speed and all courses. Such a work has already been performed to calculate the capsizing probability of French frigates [72]. A preliminary analysis of a

significant number of vessels already known as safe or unsafe with regard to all failure modes would provide the threshold to be used as a global criterion of third level. This statistical analysis is similar to that performed by Rahola [11] but with modern computation tools and more realistic sailing conditions.

Such a process would provide a global criterion which would embed all failure modes. Although it is not possible to target a specific failure mode in simulations, it is possible to implement detectors in the 6-DoF solver indicating the failure mode which causes capsizing, excessive roll angle or excessive acceleration, such as both the surf-ride and broach detectors currently implemented in the Fredyn software.

## ANNEX 1. CALCOQUE SOFTWARE

Calcoque is a personal project started in 1993. It consists of naval architecture software dedicated to educational and research use at the French Naval Academy. Calcoque is also used onboard several French Navy ships as stability software.

### *Historical Review*

The project started in 1993 during a student project at the “Ecole Nationale Supérieure d’Arts et Métiers” (Lille, France) as a first version of the software which aim was to compute the hydrostatic table of fishing vessels for a shipyard. Then, the project is entering a phase of sleep during my boarding.

The current version of the software was recreated in 2003 as a Microsoft Windows application developed in C++ language. The initial goal was extended to the ship’s weights and successively to the other main steps of the ship design loop.

A first opportunity occurred in 2004 at the Saint-Mandrier Naval Training Center (France). I was responsible of a 70-hour exercise of naval architecture for officers which aim was to perform the preliminary design of a large civilian or military ship. This required a dedicated numerical tool. I decided to continue the development of the software for this. The exercise was conducted twice in 2005 and 2006.

A damage stability module using the lost-buoyancy method and 3D view, extensively used to illustrate this report, were developed during one-year training (2006-2007) at ENSTA Bretagne (Brest, France).

A second major opportunity occurred in 2008 at the French Naval Academy when the software was selected to equip some French Navy ships as stability software within the scope of an experiment. This required some deep modifications and improvements such as virtual mass (see [1], Chapter 3) or a lock to prevent modifications of the model by the crew. Calcoque was installed onboard the research ship *Beautemps Beaupré* in 2010.

Nowadays, the software is used onboard 12 French Navy ships. The onboard installation requires the prior creation of a numerical model. Some of them have been made by students and midships at the French Naval Academy.

The software is also used to teach ship stability and naval architecture to midships and civilian students of Master through practical exercises and scientific projects. In particular, historical and scientific study of the battleship Bouvet, which sank in the Dardanelles on 18 March 1915, was conducted jointly by students and teachers in 2012-2014 [73].

The experience acquired from the development of the software was capitalized in writing a ship stability handbook [1].

The software was awarded by the French Naval Academy alumni association in 2013.

## Ship Modeling

The ship modeling consists of the definition of a numerical model including the hull, weights, superstructures, decks and bulkheads, propellers and appendages. This requires from few days to few month working, depending on the required level of detail. The drawings of the ship and her stability booklet are required.

The hull form is created from stations and lines as described in Chapter 2. Both associated volume and surface meshes are the base of all hydrostatic computations, such as the watertight volume, obtained by cutting the volume mesh with the plane of watertight deck or the displacement volume by cutting the watertight volume with the waterplane.

Weights are added to the ship model. They are geometrical elements representing all weighting objects (engines, hull facilities ...), solid cargo (crew, passengers, ammunitions, containers, lifeboats ...) and superstructures, subject to wind effect. They are designed as basic geometric elements (box-shaped hexahedron, sphere, lines and cylinder) or as meshes. Figure 93 shows the superstructures of the Offshore Patrol Vessel *Adroit*, entirely defined as meshes by students.



Figure 93 – Superstructures of the Offshore Patrol Vessel *Adroit*.

Rooms and tanks are defined as the intersection of a hexahedron with the volume mesh of the ship. They may be truncated with other inclined plans and concatenated together to define rooms which have a complex geometry. Tanks contain all liquids (water, fuel, lube oil ...) and participate to the ship's weights with free surface effect. All rooms may be flooded occasionally for damage stability or permanently to create voids in the hull form such as bow thruster tunnels, water inlets or stabilizers' housings. Figure 94 shows all tanks of an A69-class frigate. Figure 95 shows all rooms defined in the numerical model of the same ship.

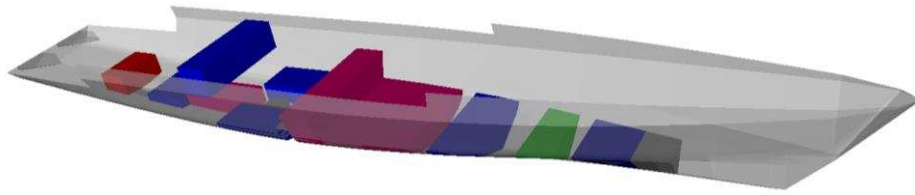


Figure 94 – Tanks of the Offshore Patrol Vessel *Adroit*.

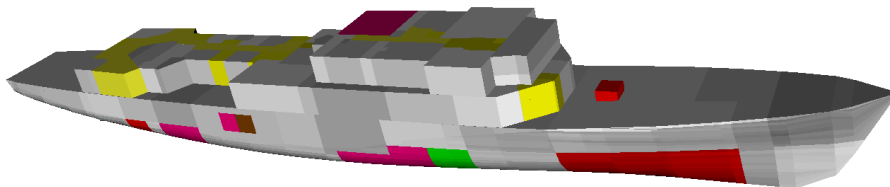


Figure 95 – All rooms of an A69-class Frigate.

Decks and bulkheads are defined as the intersection of the volume mesh with a plane. A weight may be assigned. Decks may be used as watertight or weather deck.

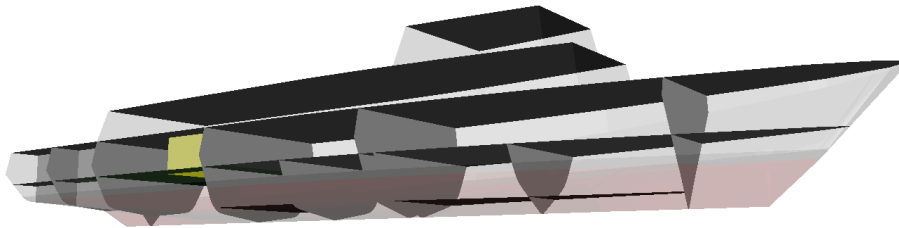


Figure 96 – Decks and bulkheads of a Patrol Vessel defined within the scope of a ship design exercise.

Appendages are volumes concatenated to the watertight volume. They participate to the buoyancy lift and may generate ship resistance. Classical appendages (rudders, stabilizers, shafts, POD ...) are automatically generated from their main characteristics (see Figure 24 page 40). Other appendages, such as sonar, may be defined as meshes created by the user (Figure 97).

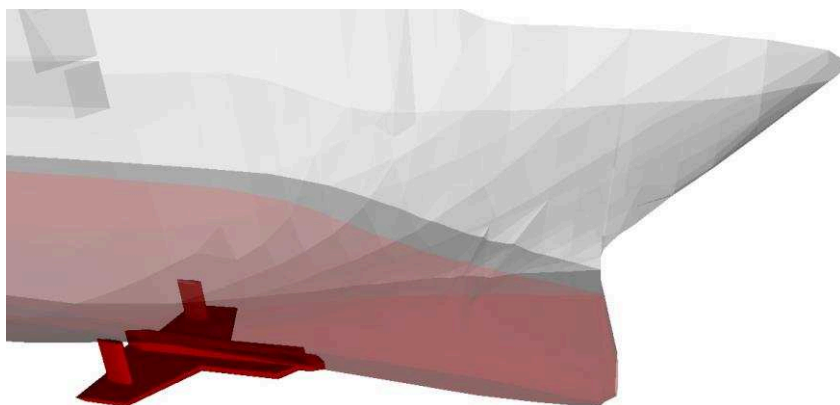


Figure 97 – Special appendage under the bow of the research ship *Beautemps Beaupré*.

Propellers are defined by volume meshes, created automatically from their main geometrical data. They are added to the watertight volume as appendages. Hydrodynamic computation of propellers is an intended improvement.

## Ship Computing

### Stability

Calcoque computes all buoyancy and stability particulars as well as the righting arm curve. These computations are performed in both intact and damage stability configurations, in still water or in longitudinal waves. If required, intact stability rules (IMO [18] and French military rules [17]) are checked. Results are saved and viewed in a HTML file which constitutes the daily stability report.

Damage stability can be treated with the lost buoyancy method in case of flooding, or with additional weight and free surface effect in case of water ingress or fire, extinguished with water, hence similar to water ingress with regard to the ship stability.

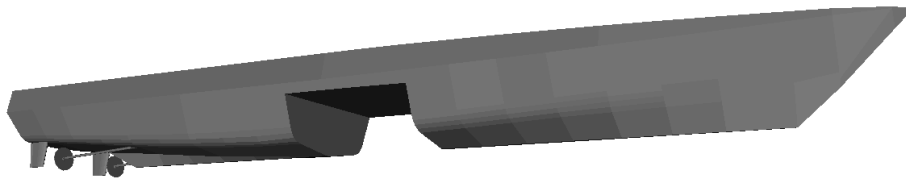


Figure 98 – Flooded room retired from the watertight volume in damage stability (lost buoyancy method).

### Shear Forces and Bending Moment

Calcoque computes the buoyancy, weight, shear forces and bending moment along the hull in still water or in longitudinal waves. Figure 99 and Figure 100 show the bending moment of an A69-class frigate in waves respectively in sagging and hogging conditions.

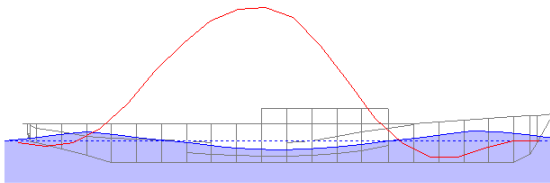


Figure 99 – Bending moment in sagging condition.

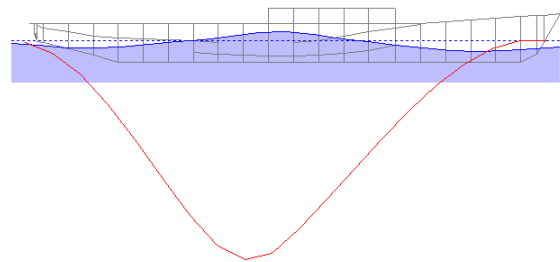


Figure 100 – Bending moment in hogging condition.

### Resistance and Motorization

Calcoque calculates the ship resistance according to empirical methods provided by the ITTC [51] for the viscous component and Holtrop and Fung [52, 53 and 54] for the wave component.

With a catalog of over 1,600 diesel engines and gas turbines, Calcoque finds automatically all possible solutions to form the propulsion device according to the previously determined resistance, the use of the ship specified by user and constraints in terms of architecture, mass and autonomy.

## Other Capabilities

Calcoque is also able to compute the followings:

- Windage area of the heeled ship. This allows the analysis of the relevance of the weather stability criteria (IMO criterion assumes a heeling lever independent from the heel since military equivalent criteria assume that the heeling lever of the wind reduces since the heel angle increases).
- Hydrostatic tables, cross curves, tank tables and  $KG_{\max}$  curves associated with IMO and French military intact stability rules. These computations allow the validation of the numerical models by comparison with tables included in the stability booklet. The computation of inertia required for the hydrostatic table is performed with the Green-Riemann method, which consists in replacing the two-dimension integral on a surface by a single-dimension integral on its closed border.

## Educational and Research Use

Calcoque is used for several teaching and research activities. The most important are briefly described hereunder.

### Stability Training

As conclusion of a 38-hours course dealing with mechanics and ship stability, students at French Naval Academy have a 3-hours exercise using Calcoque. They input the solid weights and liquid cargo of an A69-class frigate. Then, they compute the GZ curve and calculate intact stability criteria in a spreadsheet, in order to become accustomed to the military stability rules. In second part of this exercise, they calculate shear forces and bending moment of the ship in different longitudinal waves, in order to determine the wave length generating the most important moments amidships (Figure 101).

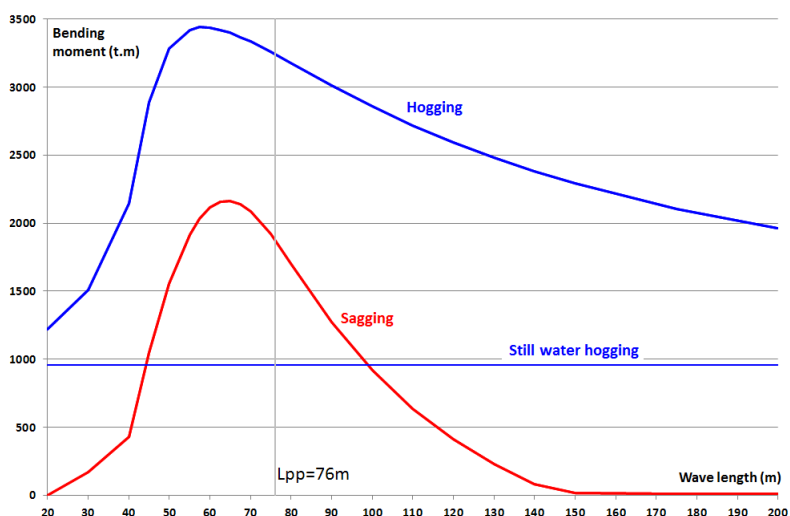


Figure 101 – Maximum bending moment as a function of the wave length in hogging and sagging conditions.

### *Naval Architecture Training*

Calcoque is used for several naval architecture practical exercises at the Saint-Mandrier Naval Training Center and at the French Naval Academy according to Table 14. During these exercises, the students are divided in pairs. They design a ship which specifications are provided by the teachers. They describe the classical design loop focusing on following steps:

- analysis of specifications and choice of main particulars;
- hull design: depending on the duration of the exercise, they totally design the hull or they modify a given one;
- definition of the general arrangement;
- definition of weights and liquid cargo;
- intact stability check according to the specified rules (IMO, military);
- estimation of ship's resistance;
- definition of the propulsion device.

Eventually, if the duration of exercise is sufficient:

- calculation of shear forces and bending moment, design of the midship section;
- check of seakeeping and maneuverability performances: Fredyn software is used for this.

Academy	Year	Duration of exercise	Students	Ships designed by students
Saint-Mandrier Naval Training Center	2004-2005	70 hours	~7-8 officers	amphibious vessel naval tanker fast passenger vessel container vessel
French Naval Academy	Since 2011	20 hours	~20 midships	400-ton trainee ship
	Since 2014	35 hours	~10 civilian students (Master)	Scientific vessel Supply vessel Patrol vessel
	Since 2016	35 hours	5 civilian students (Master)	Innovative supply vessel

Table 14 – Naval architecture practical exercises.

### *Bouvet Project*

The Battleship *Bouvet* sunk in the Dardanelles on 18 March 1915, killing 600 of her seamen. This drama is the topic of a major project carried out at the French Naval Academy in 2012-2014 in collaboration with DGA Techniques Hydrodynamiques (Val de Reuil, France) and foreign historians and naval architects. The aim of this historical and scientific project, which was conducted within the scope of the centennial of the Great War, is to investigate the causes of the wreck using modern tools. The first part of the work was the realization of a detailed numerical model of the vessel (Figure 102 and Figure 103). This work was done by both students and teachers. The campaigns of sonar surveys, conducted in situ by Turkish archaeologists, have validated the hypotheses locating the breach caused by the mine, previously made by French historians on the basis of testimonies. By issuing other hypotheses on the location of the bulkhead deck, it was possible to define a watertight volume in intact condition and after the mine impact (Figure 104). Righting arm curves in intact and flooded conditions (Figure 105) show that:

- The vessel had a good initial stability in intact condition. However, the area under GZ curves remains so insufficient that she would not have fulfilled the stability rules if they had existed at that time (blue curve).
- The vessel might have survived a symmetrical flooding since a stable equilibrium exists at zero-heel angle. However, a dynamic flooding simulation is required to confirm or refute this assumption (green curve).
- After asymmetrical flooding, as it is assumed to have occurred, the unique point of stable equilibrium is at a heel angle almost equal to 180 degrees. The capsizing of *Bouvet* was inevitable.

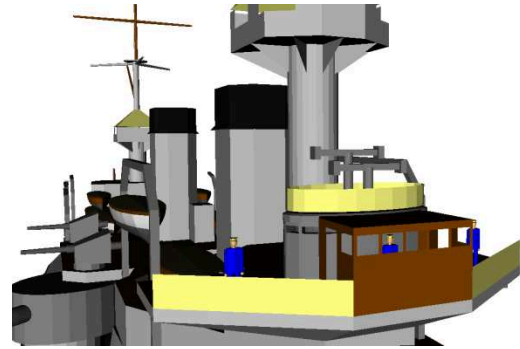


Figure 102 – Numerical model of the Battleship *Bouvet*. Figure 103 – Numerical model of the Battleship *Bouvet*, zoom on the bridge.

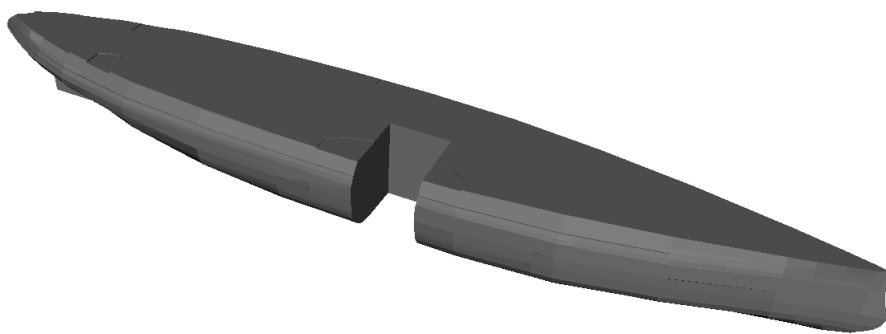


Figure 104 – Watertight volume after mine impact.

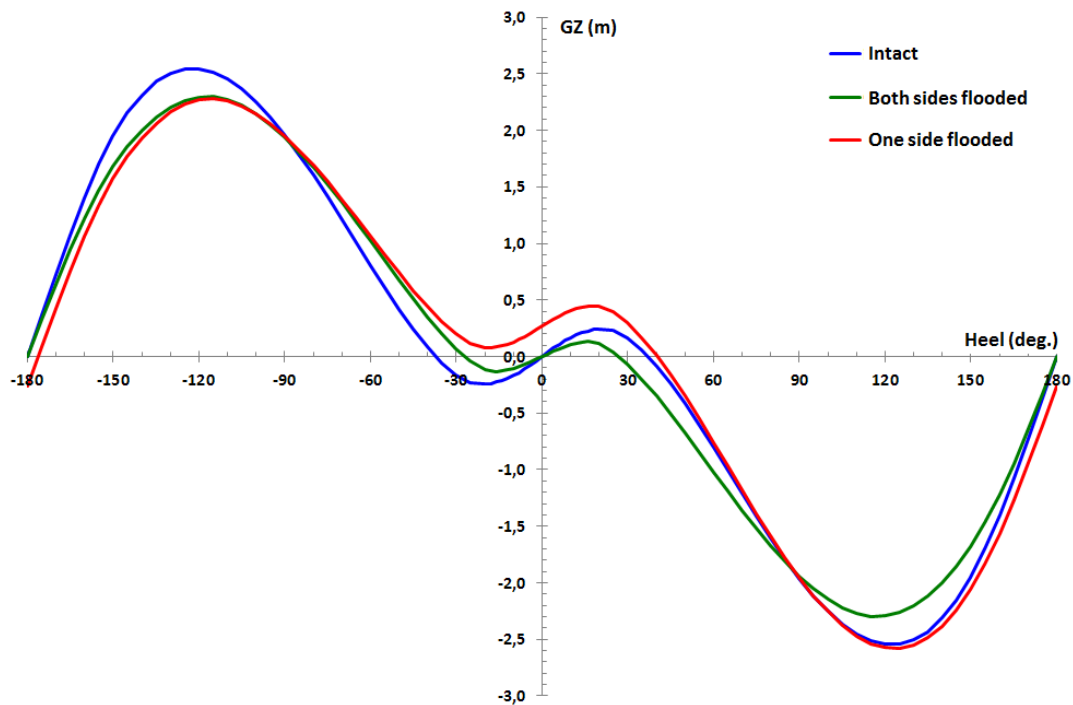


Figure 105 – GZ curves in intact and flooded conditions.

## ***Operational Use***

Calcoque is installed onboard 12 naval ships. Some corresponding numerical models are shown in Figure 106 to Figure 108.

While the ship is moored, a crew member inputs the weights (solid and liquid cargo) and drafts. Then, Calcoque computes a virtual mass fitting the weight situation to the observed hydrostatic situation, assuming the observed drafts are more accurate than the weight list (see [1], Chapter 3).

At sea, the software is used daily to compute stability data and to check the associated criteria [17 or 18] with an updated weight situation.

In case of damage situation such as flooding, water ingress or fire, the software is used to evaluate the stability in order to guide the ship's master to recover a safe situation.



Figure 106 – Numerical model of an Anti-Submarine Frigate.



Figure 107 – Numerical model of an A69-Frigate.



Figure 108 – Numerical model of the Research Ship *Beautemps Beaupré*.

## ANNEX 2. PRESENTATION OF SHIPS

Six civilian ships and three naval ships are considered in this thesis. Although second generation intact stability criteria are not intended for naval ships, it seems interesting to assess the outcome of their applications. This choice is argued in Section 3.1.2 page 50. These nine ships are briefly described hereunder. The Offshore Patrol Vessel *Adroit*, used to illustrate the generation of meshes in Chapter 2, is also presented. Since she is currently in service in the French Navy, her results with regard to the new criteria are not provided here.

### *Civilian Ships*

The main particulars of the six selected civilian ships are given in Table 15. The superstructures of some of them (except one) are modelled to permit the computation of the weather criterion (IMO IS Code 2.3, [18]) without taking into account their flooding points. The bilge keels of all ships are modelled.

The first ship is the C11 container vessel. Her numerical model is shown in Figure 109 and her stations are shown in Figure 110. This vessel is well-known by the scientific community since one ship of this class, *APL China* (Figure 111), suffered from a parametric roll accident in October 1998 in the Northern Pacific Ocean. This accident is described in [41] (Figure 112). The 49-MW MAN B&W diesel engine of this vessel is capable of powering her at speeds up to 24.5 knots. This value is considered as service speed in most parts of this thesis. However, her service speed is often set equal to 20 knots in the literature. Computations in Section 3.3.4 have been performed with this reduced value.

The second civilian ship is another container vessel, 319 m long. Her numerical model is shown in Figure 113. A fatal accident due to an extreme roll motion (not parametric roll) occurred on a vessel of this class in 2008 (*Chicago Express*, Figure 114). One of the causes given by the experts is the insufficient roll damping [60]. This accident is one of those behind the development of excessive acceleration criteria by the IMO [23].

The numerical models of both container vessels include the containers in full-load configuration as shown in Figure 109 and Figure 114. The associated windage area is considered in the  $KG_{max}$  curves associated with the current IMO regulation provided in Chapter 3 through the weather criterion.

The third civilian ship is a 135-meter-long Roll-on Roll-off vessel presented by Garne [67]. Her data have been provided by the KTH Royal Institute of Technology. Her superstructures are not modelled. Consequently, the  $KG_{max}$  curve associated with the first generation criteria does not take the weather criterion into account. Her watertight volume is shown in Figure 115.

The fourth ship is a 227-meter-long tanker. She is wall-sided on 80% of her length and has been chosen for her supposed non vulnerability to both pure loss of stability and parametric roll failure modes. She has been taken from DELFTship database ([www.delftship.net](http://www.delftship.net)). A simplified box-shaped superstructure has been added to her model but has no influence on

the  $KG_{max}$  curve associated with the current criteria. Her watertight volume is shown in Figure 116.

The fifth ship is a 160-meter-long passenger vessel. Her numerical model is shown in Figure 118. Her characteristics and her hull are inspired from those of the high-speed ferry *Mega Express* (Figure 117), sailing from Mainland France and Italy to Corsica and Sardinia. Two different watertight volumes are considered. The first is limited by the weather deck (14 m above baseline) and includes the volume of the garage car (Figure 119). The second is limited by the bulkhead deck (9 m above baseline) and excludes this volume (Figure 120).

The sixth and last civilian ship is a 30-meter-long passenger vessel named *Le Palais* (Figure 121). In summer, she sails from the Mainland South Brittany (France) to the Gulf of Morbihan Islands. Outside this period, she crosses the Bay of Brest (France) between the Naval Base and Lanvéoc, where the Naval Academy and Naval Air station are located. Her hull is classically designed with sharp bilge and no bilge keels. Her watertight volume is shown in Figure 122.

In Table 15 (civilian ships) and Table 16 (naval ships), the reference height of the center of gravity ( $KG_{ref}$ ) is used to calculate both the associated metacentric height in calm water ( $GM_{ref}$ ) and natural roll period ( $T_0$ ) of each ship. The latter depends on the added mass coefficient and radius of inertia coefficient (denoted by  $a$  and  $k$ , defined in Section 1.2.4 page 31). The roll period is given for the full-load displacement except for the C11 container vessel whose associated draft is 12.339 m (see [41]). The roll damping coefficient  $B_{44}$  is calculated as described in Section 1.2.4 (page 32). Its value is given for the reference height of the center of gravity ( $KG_{ref}$ ), the full-load draft (12.339 m for the C11 container vessel), the service speed ( $V_S$ ) and a roll amplitude of 10 degrees.

			Container C11	Container 319m	Ro-Ro	Tanker	Passenger 160 m	Passenger 30 m
Length overall	$L_{OA}$	m	275.8	335.5	147.9	236.5	175	29.6
Length between perpendiculars	$L_{PP}$	m	262	319	135	227.5	160	26.4
Breadth	$B$	m	40	42.8	24.2	32.2	24	7.8
Draft, full load	$d_{full}$	m	12	13	5.50	11	6	1.05
Freeboard, full load	$f$	m	12.45	11.60	12.50	7.00	8.00	1.53
Displacement, full load	$\Delta$	t	73,340	107,350	11,544	70,397	13,147	93
Speed	$V_S$	knots	24.5	25	20	15	25	22
Froude number	$F_n$	-	0.203	0.230	0.283	0.163	0.325	0.703
Block coefficient	$C_b$	-	0.569	0.590	0.625	0.852	0.554	0.433
Bilge keels length	$L_{bk}$	m	76.53	81	45	75	69	-
Bilge keels breadth	$B_{bk}$	m	0.40	0.50	0.30	0.30	0.70	-
Bilge keels projected area	$A_k$	$m^2$	58.02	57.28	19.09	31.82	91.85	-
Added mass coefficient	$a$	-	0.1	0.1	0.094	0.1	0.1	0.1
Radius of inertia coefficient	$k$	-	0.429	0.4	0.41	0.4	0.4	0.4
Reference height of G	$KG_{ref}$	m	18.24	18.00	12.22	12.00	9.00	2.50
Metacentric height @ $KG_{ref}$	$GM_{ref}$	m	1.97	2.17	1.64	1.70	2.29	5.00
Roll period @ $KG_{ref}$	$T_0$	s	25.7	24.43	16.27	20.78	13.35	2.95
Starting value of KG	$KG_{start}$	m	14	15	9	10	9	2.5
Pure loss limit angle	$R_{PL2}$	-	25	25	25	25	15	15
GM variation limit	$R_{PR}$	-	0.405	0.348	0.418	0.355	1.187	1.87
Roll damping coefficient	$B_{44}$	N.m.s/ rad	1.027e9	1.099e9	1.721e8	2.463e8	1.785e8	6.414e-5
Superstructures	-	-	Yes	Yes	No	Yes	Yes	Yes

Table 15 – Main particulars of civilian ships.

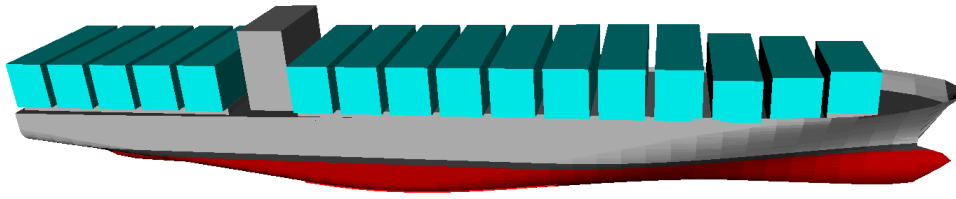


Figure 109 – Numerical model of the C11 container vessel.

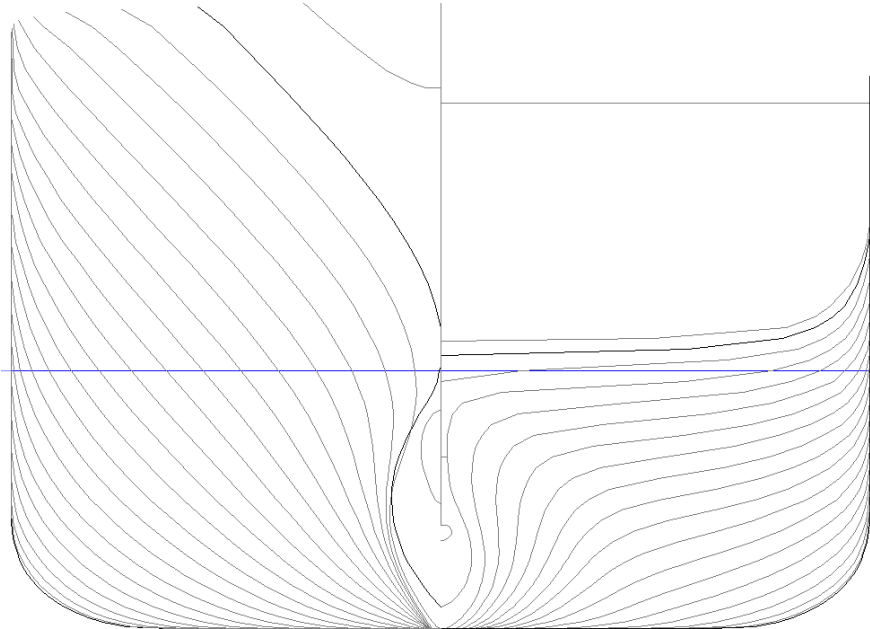


Figure 110 – Stations of the C11 container vessel.



Figure 111 – *APL China* container vessel (photo by Jan Svendsen from [www.containership-info.com](http://www.containership-info.com)).



Figure 112 – Damage occurred on the *APL China* after a parametric roll accident in October 1998 (from [afcan.org](http://afcan.org)).

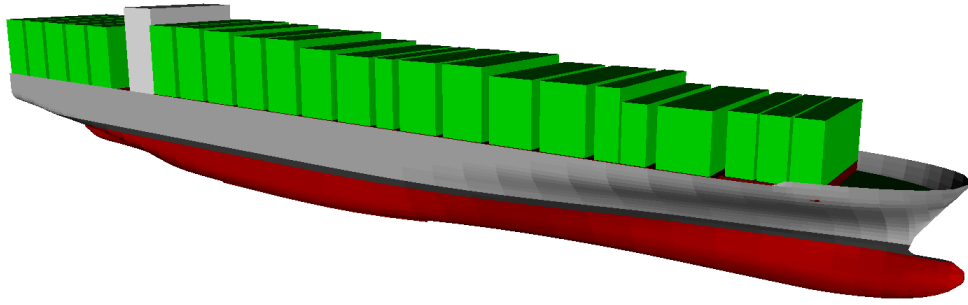


Figure 113 – Numerical model of the 319 m container vessel.



Figure 114 – *Chicago Express* container vessel (photo by Jan Svendsen from [www.containership-info.com](http://www.containership-info.com)).

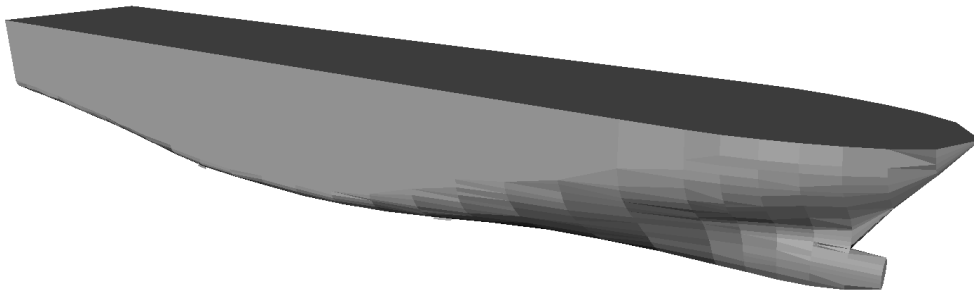


Figure 115 – Watertight volume of the Ro-Ro vessel.

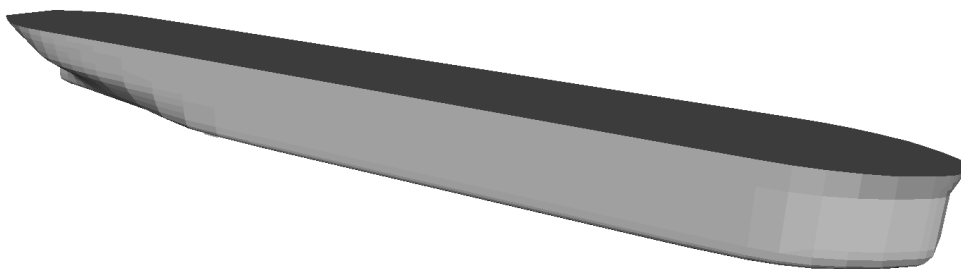


Figure 116 – Watertight volume of the tanker.



Figure 117 – High-speed passenger vessel *Mega Express*.

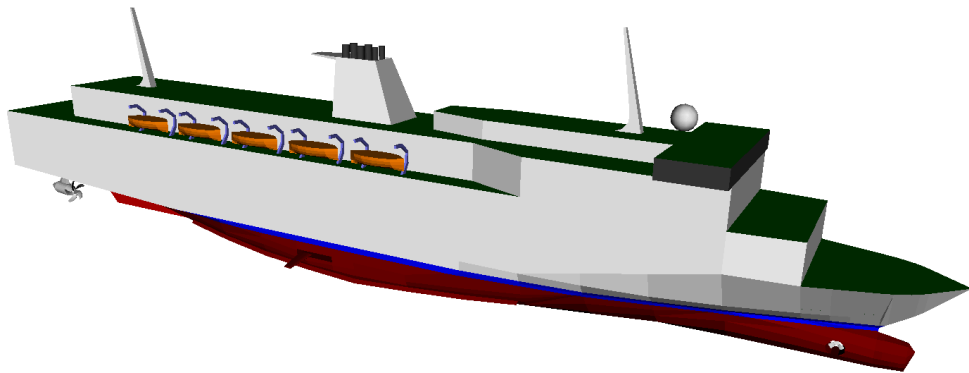


Figure 118 – Numerical model of the 160 m passenger vessel.

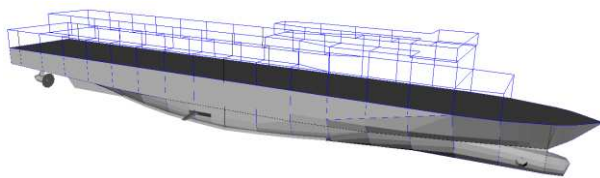


Figure 119 – Watertight volume of the 160 m passenger vessel, limited by the weather deck.

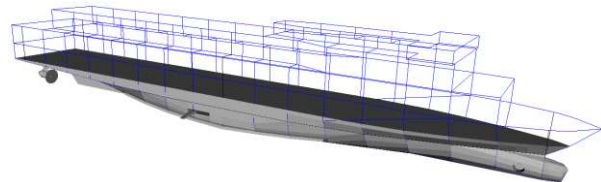


Figure 120 – Watertight volume of the 160 m passenger vessel, limited by the bulkhead deck.



Figure 121 – Passenger vessel *Le Palais*.

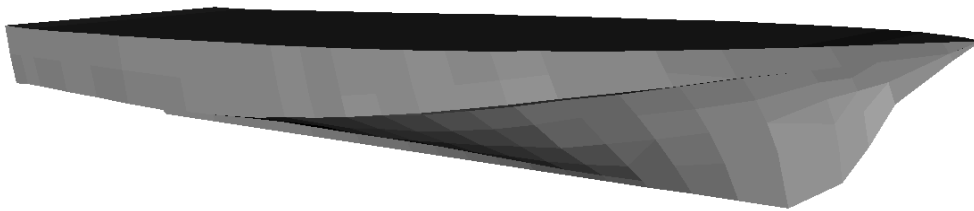


Figure 122 – Watertight volume of the 30 m passenger vessel.

## Naval Ships

The main particulars of the four selected naval ships are listed in Table 16.

The first naval ship is the well-known former French Helicopter Carrier *Jeanne d'Arc* (Figure 123). She is known as non-vulnerable to heavy seas after serving for over 45 years as trainee ship on all seas around the World. She has been retired in 2010. Her numerical model (Figure 124) has been created from the drawings provided by the French Historic Service of Defense [64]. Her watertight volume is shown in Figure 125.

The second naval ship is the David Taylor Model Basin hull number 5415, denoted in this thesis by the symbol DTMB-5415. She is presented in [68]. Her hull form is close to that of the well-known DDG-51 *Arleigh Burke* (Figure 126). Imaginary superstructures inspired by those of this vessel are added to the numerical model to allow the computation of weather criteria of current IMO and French military regulations. Her watertight volume is shown in Figure 127.

The third naval ship is representative of a 1,200-ton class Offshore Patrol Vessel. Her hull is shown in Figure 128. She is denoted in this thesis by the symbol OPV or Offshore Patrol Vessel. An imaginary box-shaped superstructure is added to the model to allow the computation of weather criteria.

The last naval ship presented here is the Offshore Patrol Vessel *Adroit* (Figure 129), currently in service in the French Navy and used in Chapter 2 to illustrate the generation of volume and surface meshes. Her full numerical model, used onboard by their crew, is shown in Figure 130.

			<i>Jeanne d'Arc</i>	DTMB-5415	OPV	<i>Adroit</i>
Length overall	$L_{OA}$	m	182	152.9	87.5	87
Length between perpendiculars	$L_{PP}$	m	172	142	80.6	81.5
Breadth	B	m	24	19.06	9.6	13
Draft, full load	$d_{full}$	m	6.50	6.15	3.37	3.30
Freeboard, full load	f	m	5.5	3.85	2.63	1.65
Displacement, full load	$\Delta$	t	11,768	8,634	1,250	1,450
Service speed	$V_S$	knots	27	30	25	21
Froude number	$F_n$	-	0.338	0.413	0.457	0.382
Block coefficient	$C_b$	-	0.465	0.507	0.471	0.405
Bilge keels length	$L_{bk}$	m	55.7	35.7	24.0	-
Bilge keels breadth	$B_{bk}$	m	1.20	0.55	0.30	-
Bilge keels projected area	$A_k$	$m^2$	94.53	34.01	10.18	-
Added mass coefficient(*)	a	-	0.1	0.1	0.1	-
Radius of inertia coefficient(*)	k	-	0.4	0.4	0.4	-
Reference height of G	$KG_{ref}$	m	8.90	8.00	3.85	-
Metacentric height @ $KG_{ref}$	$GM_{ref}$	m	1.50	1.50	1.09	-
Roll period @ $KG_{ref}$	$T_0$	s	16.48	14.12	8.00	-
Starting value of $KG$ (*)	$KG_{start}$	m	8	7	3	-
Pure loss limit angle(*)	$R_{PL2}$	-	25	25	25	-
GM variation limit(*)	$R_{PR}$	-	0.657	0.418	0.433	-
Roll damping coefficient	$B_{44}$	N.m.s/ rad	9.813e7	4.018e7	2.436e6	-
Superstructures	-	-	Yes	Yes	Yes	Yes

Table 16 – Main particulars of naval ships.



Figure 123 – Last arrival of the *Jeanne d'Arc* in Brest after 45 years sailing around the World, May 27, 2010 (photo by Lancelot Frederic).

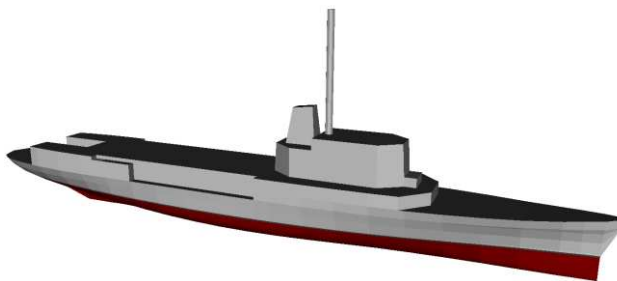


Figure 124 – Numerical model of the *Jeanne d'Arc*.



Figure 125 – Watertight volume of the *Jeanne d'Arc*.



Figure 126 - DDG-51 *Arleigh Burke* (US Navy).

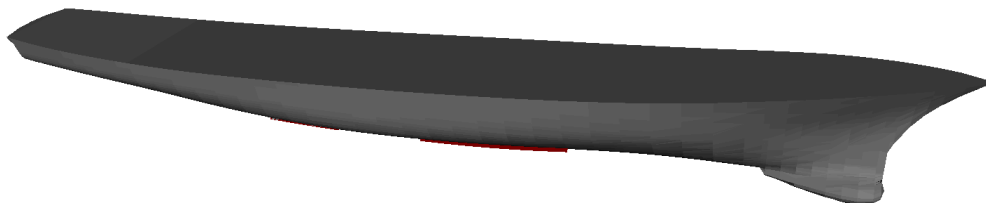


Figure 127 – Watertight volume of the DTMB-5415.

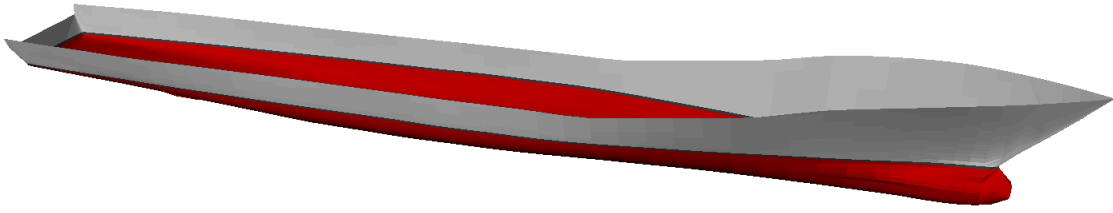


Figure 128 – Hull of the Offshore Patrol Vessel.



Figure 129 – Offshore patrol vessel *Adroit* (Marine Nationale).



Figure 130 – Numerical model of the OPV *Adroit*.

### ANNEX 3. MATHEMATICAL PROOFS

#### *Reference Speed Corresponding to the First Mode of Parametric Roll*

The objective is to demonstrate the relationship (22) (page 28) providing the value of the reference speed of the first mode of parametric roll (denoted here by  $V_{PR}$ ) and rewritten hereunder:

$$V_{PR} = \left| \frac{2\lambda}{T_0} \sqrt{\frac{GM}{GM_0}} - \sqrt{\frac{g\lambda}{2\pi}} \right| \quad (69)$$

With:

- $V_s$  (m/s) ship's speed;
- $\lambda$  (m) wave length;
- $T_0$  (s) natural roll period of the ship in calm water;
- $GM$  (m) average value of the metacentric height in waves;
- $GM_0$  (m) metacentric height in calm water.

As demonstrated by Mathieu [9], the first mode of parametric roll occurs when the wave encounter frequency (denoted by  $\omega_e$ ) is twice the ship's roll frequency (denoted by  $\omega$ ):

$$\omega_e = 2\omega \quad (70)$$

Since the average value of the metacentric height in waves ( $GM$ ) may differ from the metacentric height in calm water ( $GM_0$ ), the ship's roll frequency in longitudinal waves ( $\omega$ ) may differ from her natural roll frequency in calm water ( $\omega_0$ ) and is corrected as follows:

$$\omega = \omega_0 \sqrt{\frac{GM}{GM_0}} \quad (71)$$

The encounter frequency is given by the following relationship:

$$\omega_e = \omega_w - \frac{\omega_w^2 V}{g} \cos \beta \quad (72)$$

$\beta$  denotes the angle between the ship's heading and the wave direction. Its value is 180 degrees in head seas and 0 degrees in following seas. Hence, the relationship becomes:

$$\omega_e = \omega_w + \frac{\omega_w^2 V}{g} \quad \text{in head seas} \quad (73)$$

$$\omega_e = \omega_w - \frac{\omega_w^2 V}{g} \quad \text{in following seas} \quad (74)$$

$\omega_w$  denotes the wave frequency.

Mixing Equations (73) and (74) with the sign  $\pm$  and replacing  $\omega_e$  with the expression of  $\omega$  (Equations (70) and (71)) give:

$$2\omega_0 \sqrt{\frac{GM}{GM_0}} = \omega_w \pm \frac{\omega_w^2 V_{PR}}{g} \quad (75)$$

Since the condition of the first mode of parametric resonance is met (Equation (70)),  $V_{PR}$  replaces the ship's speed  $V$ .

Assuming an infinite depth, following relationship links the wave frequency to its length ( $\lambda$ ) and the acceleration of gravity ( $g$ ):

$$\omega_w = \sqrt{\frac{2\pi g}{\lambda}} \quad (76)$$

Introducing Equation (76) in Equation (75), we have:

$$2\omega_0 \sqrt{\frac{GM}{GM_0}} = \sqrt{\frac{2\pi g}{\lambda}} \pm \frac{2\pi V_{PR}}{\lambda} \quad (77)$$

The ship's natural roll frequency  $\omega_0$  is linked to her natural roll period ( $T_0$ ) as follows:

$$\omega_0 = \frac{2\pi}{T_0} \quad (78)$$

Hence, Equation (77) becomes:

$$\frac{4\pi}{T_0} \sqrt{\frac{GM}{GM_0}} = \sqrt{\frac{2\pi g}{\lambda}} \pm \frac{2\pi V_{PR}}{\lambda} \quad (79)$$

Or:

$$\frac{2\pi V_{PR}}{\lambda} = \pm \left( \frac{4\pi}{T_0} \sqrt{\frac{GM}{GM_0}} - \sqrt{\frac{2\pi g}{\lambda}} \right) \quad (80)$$

Hence:

$$V_{PR} = \pm \left( \frac{2\lambda}{T_0} \sqrt{\frac{GM}{GM_0}} - \sqrt{\frac{g\lambda}{2\pi}} \right) \quad (81)$$

We introduce an absolute value in order to define a unique positive speed of parametric roll resonance.

$$V_{PR} = \left| \frac{2\lambda}{T_0} \sqrt{\frac{GM}{GM_0}} - \sqrt{\frac{g\lambda}{2\pi}} \right| \quad (69)$$

QED

The first check of the level-two criterion of parametric roll considers that if her service speed is lower than this resonance speed, the ship cannot attain the resonance condition.

### ***Solving the Parametric Roll Differential Equation with the Method of Runge-Kutta at 4<sup>th</sup> Order***

The objective is to solve the parametric roll one-degree-of-freedom differential equation (23) with the Runge-Kutta method at 4<sup>th</sup> order. This equation is given in page 29 and rewritten hereunder in a slightly different form:

$$\ddot{\phi} + \frac{B_{44}}{J_{44}}\dot{\phi} + \frac{W}{J_{44}}GZ(\phi, t) = 0 \quad (82)$$

The Runge-Kutta method treats only 1<sup>st</sup> order equations, which are formatted as follows:

$$\dot{y} = f(y, t) \quad (83)$$

In order to solve the second-order parametric roll differential equation with this method, we rewrite it as a first-order vector differential equation where  $\vec{V}$  is the unknown vector and  $\vec{f}$  is a vector function of both  $\vec{V}$  and the time t:

$$\dot{\vec{V}} = \vec{f}(\vec{V}, t) \quad (84)$$

Vector  $\vec{V}$  and function  $\vec{f}$  are defined as follows:

$$\vec{V} = \begin{pmatrix} V_x = \phi \\ V_y = \dot{\phi} \end{pmatrix} \quad (85)$$

$$\vec{f}(\vec{V}, t) = \begin{pmatrix} f_x = V_y \\ f_y = -\frac{W}{J_{44}}GZ(V_x, t) - \frac{B_{44}}{J_{44}}V_y \end{pmatrix} \quad (86)$$

Expanding Equation (84) with the expressions of  $\vec{V}$  (85) and  $\vec{f}$  (86) gives:

$$\begin{pmatrix} \dot{\phi} \\ \ddot{\phi} \end{pmatrix} = \begin{pmatrix} \dot{\phi} \\ -\frac{W}{J_{44}}GZ(\phi, t) - \frac{B_{44}}{J_{44}}\dot{\phi} \end{pmatrix} \quad (87)$$

The second component of this vector equality is the second-order differential equation (82) since the first component is neutral.

The first-order vector differential equation (84) is solved numerically with an iterative process. The initial conditions are specified in the vector  $\vec{V}$  at the first iteration (indexed 0), with a chosen roll angle  $\phi_0$  and a roll speed equal to zero:

$$\vec{V}_0 = \begin{pmatrix} \phi_0 \\ \dot{\phi}_0 = 0 \end{pmatrix} \quad (88)$$

The time step is set to one 40<sup>th</sup> of the ship's natural roll angle. It is denoted by dt. At each iteration, we compute successively four values of the function vector  $\vec{f}$  as follows:

$$\begin{aligned}
\vec{f}_1 &= \vec{f}(\vec{V}, t) \\
\vec{f}_2 &= \vec{f}\left(\vec{V} + \frac{dt}{2}\vec{f}_1, t + \frac{dt}{2}\right) \\
\vec{f}_3 &= \vec{f}\left(\vec{V} + \frac{dt}{2}\vec{f}_2, t + \frac{dt}{2}\right) \\
\vec{f}_4 &= \vec{f}(\vec{V} + dt\vec{f}_3, t + dt)
\end{aligned} \tag{89}$$

Vector  $\vec{V}$  at the next iteration (denoted by  $\vec{V}_{n+1}$ ) is built from its value at the previous iteration (denoted by  $\vec{V}_n$ ) as follows:

$$\vec{V}_{n+1} = \vec{V}_n + \frac{dt}{6}(\vec{f}_1 + 2\vec{f}_2 + 2\vec{f}_3 + \vec{f}_4) \tag{90}$$

The roll angle and the roll speed at each iteration are given respectively by the first and the second component of vector  $\vec{V}$ .

The Runge-Kutta methods are well-known to provide very stable solutions. For example, if we remove both the damping and GM variation in differential equation (23), it becomes that of an undamped oscillating system. The response is characterized by a constant amplitude, equal to the initial angle if the initial speed is zero. The Runge-Kutta method accurately restores this behavior (even with large time step) while the Euler method diverges after few periods.

## Exciting Power of Parametric Roll

*Any Condition*

The objective is to demonstrate the following equality:

$$\cos \omega t \sin \omega t \cos(\omega_e t + \alpha) = \frac{1}{4} [\sin((2 - \gamma)\omega t - \alpha) + \sin((2 + \gamma)\omega t + \alpha)] \quad (91)$$

With:

$$\gamma = \frac{\omega_e}{\omega} \quad (92)$$

Following trigonometric identities are used for this:

$$\cos a \sin a = \frac{1}{2} \sin 2a \quad (93)$$

$$\sin a \sin b = \frac{1}{2} [\cos(a - b) - \cos(a + b)] \quad (94)$$

$$\sin a \cos b = \frac{1}{2} [\sin(a - b) + \sin(a + b)] \quad (95)$$

$$\sin(a + b) = \sin a \cos b + \cos a \sin b \quad (96)$$

$$\cos(a + b) = \cos a \cos b - \sin a \sin b \quad (97)$$

The function of time  $t$  to be transformed is denoted by  $f(t)$ :

$$f(t) = \cos \omega t \sin \omega t \cos(\omega_e t + \alpha) \quad (98)$$

Identity (93) gives:

$$f(t) = \frac{1}{2} \sin 2\omega t \cos(\omega_e t + \alpha) \quad (99)$$

Identity (97) and the definition of  $\gamma$  (92) give:

$$\cos(\omega_e t + \alpha) = \cos \gamma \omega t \cos \alpha - \sin \gamma \omega t \sin \alpha \quad (100)$$

Hence:

$$f(t) = \frac{1}{2} \sin 2\omega t \cos \gamma \omega t \cos \alpha - \frac{1}{2} \sin 2\omega t \sin \gamma \omega t \sin \alpha = \frac{1}{2} a \cos \alpha - \frac{1}{2} b \sin \alpha \quad (101)$$

With

$$a = \sin 2\omega t \cos \gamma \omega t \quad \text{And} \quad b = \sin 2\omega t \sin \gamma \omega t \quad (102)$$

Identities (94) and (95) give following relationships for  $a$  and  $b$ , respectively:

$$a = \frac{1}{2} [\sin((2 - \gamma)\omega t) + \sin((2 + \gamma)\omega t)] \quad (103)$$

$$b = \frac{1}{2} [\cos((2 - \gamma)\omega t) - \cos((2 + \gamma)\omega t)] \quad (104)$$

Hence:

$$f(t) = \frac{1}{4} [(\sin((2 - \gamma)\omega t) + \sin((2 + \gamma)\omega t)) \cos \alpha - (\cos((2 - \gamma)\omega t) - \cos((2 + \gamma)\omega t)) \sin \alpha] \quad (105)$$

We expanse this relationship:

$$f(t) = \frac{1}{4} [\sin((2 - \gamma)\omega t) \cos \alpha + \sin((2 + \gamma)\omega t) \cos \alpha - \cos((2 - \gamma)\omega t) \sin \alpha + \cos((2 + \gamma)\omega t) \sin \alpha] \quad (106)$$

We replace once  $\cos \alpha$  and  $\sin \alpha$  respectively by  $\cos(-\alpha)$  and  $-\sin(-\alpha)$ :

$$f(t) = \frac{1}{4} [\sin((2 - \gamma)\omega t) \cos(-\alpha) + \cos((2 - \gamma)\omega t) \sin(-\alpha) + \sin((2 + \gamma)\omega t) \cos \alpha + \cos((2 + \gamma)\omega t) \sin \alpha] \quad (107)$$

Using twice the identity (96), we have:

$$f(t) = \frac{1}{4} [\sin((2 - \gamma)\omega t - \alpha) + \sin((2 + \gamma)\omega t + \alpha)] \quad (91)$$

QED

### *Resonance Condition*

The resonance condition of the first mode of parametric roll is characterized by:

$$\omega = \omega_0 \quad \text{And} \quad \gamma = \gamma_0 = \frac{\omega_e}{\omega_0} = 2 \quad (108)$$

Hence, the equality (91) previously demonstrated becomes:

$$f(t) = \cos \omega_0 t \sin \omega_0 t \cos(2\omega_0 t + \alpha) = \frac{1}{4} [\sin(4\omega_0 t + \alpha) - \sin \alpha] \quad (109)$$

### ***Kinetic and Potential Energy of Roll Motion at any Frequency***

The function of roll angle over time and its first derivate are given by following relationships:

$$\varphi(t) = \Phi \cos \omega t \quad \text{And} \quad \dot{\varphi}(t) = -\omega_0 \Phi \sin \omega t \quad (110)$$

Consequently, the potential energy and kinetic energy are respectively:

$$E_P = \frac{1}{2} WGM \varphi^2 = \frac{1}{2} \Phi^2 WGM \cos^2 \omega t \quad (111)$$

$$E_K = \frac{1}{2} J_{44} \dot{\varphi}^2 = \frac{1}{2} \Phi^2 \omega^2 J_{44} \sin^2 \omega t \quad (112)$$

Their sum is:

$$E_P + E_K = \frac{1}{2} \Phi^2 (WGM \cos^2 \omega t + \omega^2 J_{44} \sin^2 \omega t) \quad (113)$$

This function is not constant in time. We introduce x as:

$$x = \frac{\omega}{\omega_0} \quad \text{With} \quad \omega_0^2 = \frac{WGM}{J_{44}} \quad (114)$$

Equation (113) becomes:

$$E_P + E_K = \frac{1}{2} \Phi^2 \left( WGM \cos^2 \omega t + \underbrace{J_{44} \omega_0^2}_{=WGM} x^2 \sin^2 \omega t \right) \quad (115)$$

Replacing  $x^2$  by  $1 + (x^2 - 1)$ , we have:

$$E_P + E_K = \frac{1}{2} WGM \Phi^2 (\cos^2 \omega t + \sin^2 \omega t + (x^2 - 1) \sin^2 \omega t) \quad (116)$$

Or:

$$E_P + E_K = \frac{1}{2} WGM \Phi^2 (1 + (x^2 - 1) \sin^2 \omega t) \quad (117)$$

Using identity (94) with a=b, we have:

$$E_P + E_K = \frac{1}{2} WGM \Phi^2 \left( 1 + \frac{1}{2} (x^2 - 1) (1 - \cos 2\omega t) \right) \quad (118)$$

Or:

$$E_P + E_K = \frac{1}{4} WGM \Phi^2 (1 + x^2 + (1 - x^2) \cos 2\omega t) \quad (119)$$

At the natural roll frequency, x=1 and the relationship becomes the Equation (48) previously introduced page 87:

$$E_P + E_K = \frac{1}{4} WGM \Phi^2 (1 + x^2 + (1 - x^2) \cos 2\omega t) \quad (48)$$

In general cases, this function is sinusoidal. The average power required to maintain the roll motion is zero. The average value of the energy is:

$$E_P + E_K = \frac{1}{4} WGM \Phi^2 (1 + x^2) \quad (120)$$

### ***Frequency of Maximum Parametric Roll Amplitude According to Kerwin***

In 1955, Kerwin [12] gave the maximum parametric roll angle  $\Phi$  as the result of the following relationship:

$$\Phi = \frac{\omega}{n} \sqrt{\frac{2}{x^2} + \frac{\frac{b^2}{4} - 1}{x^4} - 1} - \frac{m}{n} \quad (121)$$

Where:

$$x = \frac{\omega}{\omega_0} = \frac{\omega_e}{2\omega_0} \quad (122)$$

Coefficients  $m$  and  $n$  define the non-linear roll damping as a function of the roll amplitude:

$$B_{44} = m + n\Phi \quad (123)$$

Coefficient  $b$  denotes the non-dimensional half amplitude of GM variation:

$$b = \frac{\Delta GM}{GM} \quad (124)$$

Note: Kerwin defines  $\Delta GM$  as the full amplitude of GM variation since we define it (such as future rules do [22, 23]) as the half amplitude. Hence, relationship giving  $b$  used here differs from that given in Kerwin's paper.

The relationship (121) is rewritten using the expression of  $x$  in Equation (122).

$$\Phi = \frac{x\omega_0}{n} \sqrt{\frac{2}{x^2} + \frac{\frac{b^2}{4} - 1}{x^4} - 1} - \frac{m}{n} = \frac{\omega_0}{n} \sqrt{2 + \frac{\frac{b^2}{4} - 1}{x^2} - x^2} - \frac{m}{n} \quad (125)$$

The maximum value of  $\Phi$  is obtained (in the interval where the term in the square root is positive) for:

$$\frac{d\Phi}{dx} = 0 \quad (126)$$

Hence:

$$\frac{d\Phi}{dx} = \frac{\omega_0}{2n} \times \frac{-2 \frac{\frac{b^2}{4} - 1}{x^3} - 2x}{\sqrt{2 + \frac{\frac{b^2}{4} - 1}{x^2} - x^2}} = 0 \quad (127)$$

The value of  $x=\omega/\omega_0$  corresponding to the maximum value of  $\Phi$  is defined by:

$$-\frac{\frac{b^2}{4} - 1}{x^3} - x = 0 \quad \text{Or} \quad x^4 = 1 - \frac{b^2}{4} = 1 - \left(\frac{\Delta GM}{2GM}\right)^2 \quad (128)$$

Consequently, the frequency providing the maximum parametric roll amplitude is given by the following relationship:

$$\omega = \omega_0 \sqrt{1 - \left(\frac{\Delta GM}{2GM}\right)^2} \quad (129)$$

Figure 131 shows the evolution of  $\omega/\omega_0$  as a function of  $\Delta GM/GM$ . The ratio  $\Delta GM/GM$  must be lower than 2, i.e. the metacentric height must remain positive at any time. The maximum parametric roll amplitude always occurs at a frequency lower than the ship's natural roll frequency  $\omega_0$ . If  $\Delta GM/GM$  is small, it occurs almost at the natural roll frequency.

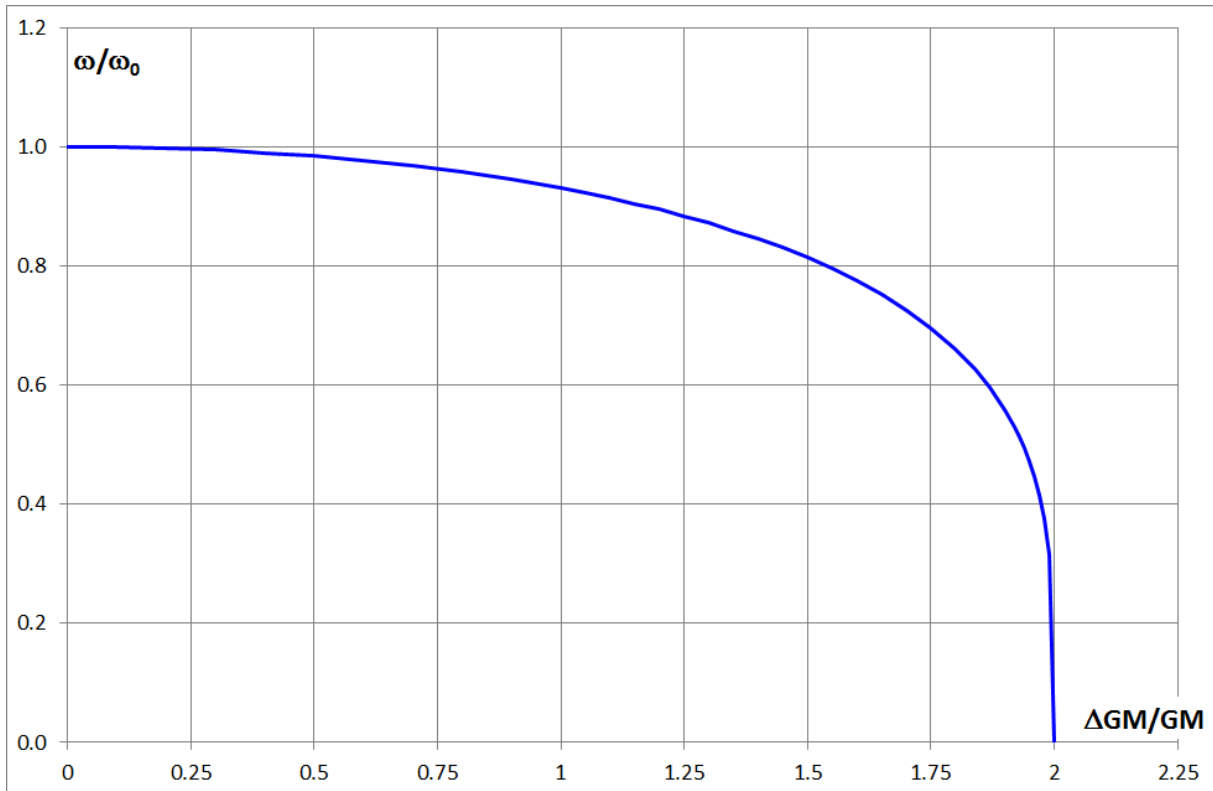


Figure 131 – Frequency of maximum parametric roll amplitude as a function of  $\Delta GM/GM$ .

### **Width of the Lock-in Field According to Kerwin**

The relationship providing the value of the maximum parametric roll amplitude proposed by Kerwin (Equation (121) page 133, taken from [12]) is rewritten hereunder:

$$\Phi = \frac{\omega}{n} \sqrt{\frac{2}{x^2} + \frac{\frac{b^2}{4} - 1}{x^4} - 1} - \frac{m}{n} \quad (121)$$

The lock-in field, in which parametric roll exists, is such as:

$$\frac{2}{x^2} + \frac{\frac{b^2}{4} - 1}{x^4} - 1 \geq 0 \quad (130)$$

Its frontiers are defined by both positive roots  $x_1$  and  $x_2$  of the following 4<sup>th</sup> order equation:

$$-x^4 + 2x^2 + \left(\frac{b^2}{4} - 1\right) = 0 \quad (131)$$

This equation is solved as a 2<sup>nd</sup> order equation. The discriminant  $\Delta$  is:

$$\Delta = \left(\frac{\Delta GM}{GM}\right)^2 \quad (132)$$

Both roots of the 2<sup>nd</sup> order equation are:

$$x_1^2 = 1 - \frac{\Delta GM}{2GM} \quad \text{And} \quad x_2^2 = 1 + \frac{\Delta GM}{2GM} \quad (133)$$

Thus, parametric roll exists if the roll frequency  $\omega = \omega_e/2$  is located in the following interval:

$$\text{From} \quad \omega_0 \sqrt{1 - \frac{\Delta GM}{2GM}} \quad \text{To} \quad \omega_0 \sqrt{1 + \frac{\Delta GM}{2GM}} \quad (134)$$

The Taylor expansion at 1<sup>st</sup> order allows simplifying the frontiers of the interval as following:

$$\text{From} \quad \omega_0 \left(1 - \frac{\Delta GM}{4GM}\right) \quad \text{To} \quad \omega_0 \left(1 + \frac{\Delta GM}{4GM}\right) \quad (135)$$

In the lock-in field, the encounter frequency  $\omega_e$  is twice the roll frequency  $\omega$ . Hence, the interval is defined with  $\gamma_0 = \omega_e/\omega_0$  (Equation (61) page 91) in the range defined in Equation (66) page 97 and reminded hereunder:

$$\text{From} \quad 2 - \frac{\Delta GM}{2GM} \quad \text{To} \quad 2 + \frac{\Delta GM}{2GM} \quad (66)$$

Note: The parametric roll amplitude given by Kerwin is negative in the close vicinity of the frontiers of the lock-in field as calculated above, since the following condition is met:

$$\omega \sqrt{\frac{2}{x^2} + \frac{\frac{b^2}{4} - 1}{x^4} - 1} < m \quad (136)$$

Hence, the lock-in field is slightly narrower than as calculated above.

#### ANNEX 4. SHIP-FIXED COORDINATE SYSTEM

The coordinates of all points are given in a unique coordinate system linked to the ship, illustrated in Figure 132 and defined as follows:

- The X axis is the baseline (also called OH), positive forward,  $X=0$  on the aft perpendicular.
- The Y axis is the transverse axis, positive portside,  $Y=0$  on the ship's centerline.
- The Z axis is the aft perpendicular, positive upward,  $Z=0$  on the baseline.

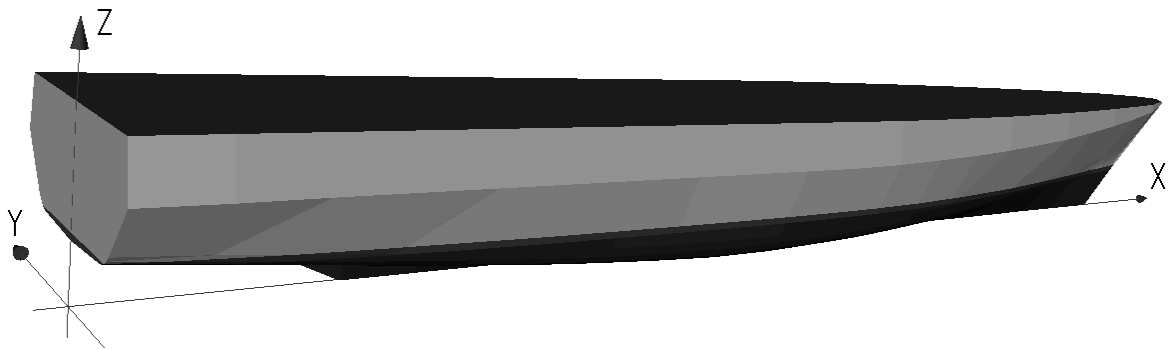


Figure 132 – Ship-fixed coordinate system.

## RESUME ETENDU

### INTRODUCTION

Depuis la première conférence SOLAS en 1914 [10], la sécurité des biens et des personnes en mer fait l'objet de nombreuses discussions internationales ayant abouti à l'établissement de règles appliquées à la construction du navire et vérifiées par la société de classification durant son exploitation. Les causes principales des grands accidents de navires sont multiples : stabilité insuffisante, envahissement (collision avec un autre navire, le fond ou un objet flottant, agression militaire), incendie, avarie structurelle. Toutes ces causes font l'objet de nombreux règlements.

Les premières règles de stabilité à l'état intact ont été définies par l'OMI en 1968, sous la forme de recommandations [14]. Elles ont été complétées par le critère météorologique en 1985 [16]. Aujourd'hui, ces règles bien connues sont obligatoires et font l'objet de la partie A du code de stabilité à l'état intact de l'OMI [18]. L'entrée en vigueur de ces règles n'a malheureusement pas éliminé les accidents des navires à l'état intact. Certains sont dus à la non-conformité avec les règles ou à un chargement excessif ou mal arrimé. D'autres accidents montrent que la stabilité peut être mise à défaut dans les vagues, majoritairement par mer de l'arrière, malgré le respect des règles de stabilité et de chargement. Quelques-uns, suffisamment documentés, sont listés ci-dessous :

- perte du cargo *Lohengrin* en mer Baltique en 1950, probablement due à une stabilité négative sur une crête de vague [40] ;
- perte d'un navire de transport de GPL en Méditerranée en 1969, due à une cause similaire [36] ;
- roulis excessif du porte-conteneurs *APL China* dans le Pacifique nord en 1998, consécutif à une résonance paramétrique dans les vagues longitudinales [41] ;
- roulis excessif du porte-conteneurs *Maersk Carolina* dans l'Atlantique nord en 2003 pour une raison identique [45] ;
- perte d'un navire de pêche au large de l'Espagne en 2004, probablement due à une stabilité négative sur une crête de vague combinée à un embarquement d'eau sur le pont de travail [37] ;
- chavirement du roulier *Cougar Ace* dans le Pacifique nord en 2006 consécutif à une stabilité insuffisante sur une crête de houle combinée à un mouvement de ballast [40] ;
- perte du roulier *Finnbirch* en mer Baltique en 2006 consécutif à une stabilité insuffisante sur houle ; dans son rapport [39], l'administration maritime suédoise préconise la mise en place de règles de stabilité sur mer de l'arrière ;
- roulis excessif du porte-conteneurs *Chicago Express* durant un typhon au large de Hong-Kong en 2008 dû à une hauteur métacentrique excessive [60].

Ces accidents, parmi d'autres, ont pointé l'insuffisance des règles de stabilité à l'état intact dans certaines configurations de navigation dans les vagues et ont amené l'OMI à développer des nouvelles règles à partir de 2007. Appelées « critères de stabilité à l'état intact de seconde génération », ces règles sont organisées en 5 modes de défaillance :

- perte pure de stabilité en mer de l'arrière ;
- roulis paramétrique ;
- perte de manœuvrabilité en mer de l'arrière ;
- navire dans propulsion en mer et vent traversiers ;
- accélération de roulis excessive.

Dans chaque mode de défaillance, 3 niveaux d'évaluation sont définis :

- le niveau 1 est basé sur une approche déterministe simplifiée du phénomène et suppose procurer des marges de sécurité élevées ;
- le niveau 2 est basé sur une approche physique plus poussée du phénomène couplée à une étude probabiliste ; les marges de sécurité correspondantes sont supposées réduites ;
- le niveau 3, actuellement en cours de définition, devrait consister en des simulations numériques du comportement du navire sur la houle et devrait procurer des marges de sécurité optimisées ; il devrait être mis en œuvre par des instituts spécialisés.

Cette nouvelle réglementation est définie par l'OMI dans deux documents [22 et 23] décrivant les règles proprement dites et proposant des notes explicatives dont la présence est motivée par la complexité inhabituelle des règles. La réglementation entrera en vigueur au plus tôt en 2019, sous la forme de recommandations dans un premier temps.

La perte pure de stabilité et le roulis paramétrique sont tous deux consécutifs à la variation du couple de redressement dans les vagues longitudinales. La première défaillance est un événement sur une vague extrême tandis que la seconde est consécutive à la répétition de la rencontre des vagues. Quoi qu'il en soit, l'évaluation de ces deux modes de défaillance nécessite le même outil informatique capable de calculer le couple de redressement dans les vagues longitudinales.

Le but du travail effectué dans le cadre de cette thèse est l'analyse de l'exigence et de la pertinence des critères des premiers et deuxièmes niveaux de ces deux modes de défaillance. Cela nécessite l'implémentation de ces critères dans un code informatique. Le logiciel hydrostatique Calcoque, utilisé à l'Ecole navale pour l'enseignement et la recherche, est modifié pour cela. Les critères sont calculés pour plusieurs navires de différents types, civils et militaires, choisis pour leurs comportements différents connus ou supposés vis-à-vis de ces modes de défaillance. Ces navires sont présentés en annexe 2. Le but étant d'évaluer les critères et non les navires, les résultats sont fournis sous la forme de courbes de  $KG_{max}$ , indiquant la hauteur maximale du centre de gravité garantissant le respect du (des) critère(s) considéré(s).

La première partie de ce résumé présente les critères de niveau 1 et niveau 2 de perte pure de stabilité et de roulis paramétrique. La seconde partie décrit les principaux algorithmes utilisés pour calculer le couple de redressement dans sur mer plate et dans les vagues. Les résultats sont fournis dans la troisième partie. La seconde vérification du critère de niveau 2 du roulis paramétrique nécessite le calcul de l'angle de roulis maximum en condition de résonance. Une méthode de calcul alternative aux deux méthodes décrites dans la réglementation est proposée dans la quatrième et dernière partie de ce résumé.

## **1. CRITERES DE STABILITE A L'ETAT INTACT DE SECONDE GENERATION**

### **Perte pure de stabilité**

#### *Description physique*

Lorsqu'un navire navigue dans les vagues, la géométrie de la partie immergée de son flotteur est modifiée en permanence. Dans les vagues longitudinales (c.-à-d. mer de l'avant ou mer de l'arrière), la géométrie de la surface de flottaison gauche change également, provoquant des variations de son inertie, donc de la hauteur métacentrique (GM) et du couple de redressement. Il existe en conséquence un risque de stabilité insuffisante ou même de chavirement si la configuration défavorable, caractérisée par la crête de la vague centrée sur le milieu du navire, dure suffisamment longtemps. Le risque de perte pure de stabilité est conditionné par :

- la géométrie des vagues, qui auront d'autant plus d'effet que leur longueur est proche de celle du navire et que leur hauteur est importante ;
- la géométrie de la carène, qui doit présenter un dévers important à l'avant et à l'arrière ainsi que des murailles verticales en section médiane pour que la variation de GM soit significative ;
- la vitesse du navire, qui doit être proche de celle de la crête des vagues en mer de l'arrière.

En conséquence, les nouveaux critères de perte pure de stabilité s'appliquent aux navires dont le nombre de Froude est supérieur à 0,24.

#### *Niveau 1*

Le critère de niveau 1 impose que la hauteur métacentrique minimale sur houle ( $GM_{\min}$ ) soit supérieure à 5 centimètres. Deux méthodes de calcul de sa valeur sont proposées. La première méthode considère une surface de flottaison isocline à tirant d'eau réduit supposée avoir une inertie similaire à celle de la surface de flottaison gauche lorsque le navire est centré sur la crête de vague. La seconde méthode consiste à retenir la plus petite valeur de 10 hauteurs métacentriques calculées pour 10 positions différentes sur une vague sinusoïdale ayant la même longueur que le navire.

#### *Niveau 2*

Le critère de niveau 2 consiste en une approche probabiliste du phénomène associée à un diagramme de dispersion de vagues. Le diagramme proposé dans la recommandation n° 34 de l'IACS [69] est imposé pour une navigation sans limitation géographique. Un autre diagramme peut être choisi pour une navigation en zone limitée. Pour que le navire soit jugé non vulnérable, deux coefficients CR1 et CR2 doivent être simultanément inférieurs à 0,06. Le premier coefficient considère l'angle de chavirement statique sur chaque vague du diagramme de dispersion. Cet angle doit être inférieur à 25 degrés ou 15 degrés pour les navires à passagers. Le second considère l'angle d'équilibre stable résultant d'un moment inclinant proportionnel au carré de la vitesse du navire sur chaque vague. Le nombre de vagues dans le diagramme de dispersion étant important, la future réglementation impose l'utilisation du concept de hauteur de vague effective de Grim [65] permettant de réduire le nombre de calculs hydrostatiques.

## Roulis paramétrique

### *Description physique et historique*

Le couple de redressement varie avec la rencontre des vagues en mer longitudinale. Bien qu'il n'y ait pas d'excitation transverse dans une telle configuration, une amplification du roulis est possible si la fréquence de rencontre est proche du double de la fréquence de roulis naturelle du navire et si l'amortissement, dû notamment aux quilles anti-roulis, est insuffisant. Ce phénomène, appelé résonance paramétrique, est connu depuis longtemps dans de nombreux domaines en mécanique [15], en mathématiques [9] ou en optique [13]. Il est utilisé par les enfants sur les balançoires. L'existence théorique du roulis paramétrique est mise en évidence par Froude [8] en 1861. En 1955, Kerwin en fait une étude analytique et pratique poussée [12], quelques décennies avant les premiers accidents survenus sur des porte-conteneurs [41 et 45].

### *Niveau 1*

Le critère de niveau 1 impose que la variation adimensionnelle de la hauteur métacentrique ( $\Delta GM/GM$ ) soit inférieure à un seuil dont la valeur dépend principalement de l'aire des quilles anti-roulis. Deux méthodes sont proposées pour déterminer  $\Delta GM$ . Elles sont similaires à celles proposées en perte pure de stabilité. La première méthode considère deux flottaisons isoclines, à tirant d'eau réduit et à tirant d'eau augmenté, supposées avoir une inertie similaire à celle de la surface de flottaison gauche lorsque le navire est centré respectivement sur la crête et le creux de la vague. La seconde méthode consiste à retenir la plus petite et la plus grande valeurs de 10 hauteurs métacentriques calculées pour 10 positions différentes sur une vague sinusoïdale ayant une longueur entre crêtes égale à celle du navire.

### *Niveau 2*

Le critère niveau 2 est constitué de deux conditions portant sur deux coefficients notés C1 et C2 et devant être l'un ou l'autre inférieur à 0,06. Chacune de ces deux vérifications consistent en une approche probabiliste du phénomène associé à un diagramme de vagues, choisi dans les mêmes conditions que celui du critère de niveau 2 de perte pure de stabilité.

La première vérification (C1) considère la variation de hauteur métacentrique et la vitesse de résonance paramétrique sur chacune des vagues d'une liste réduite déterminée à partir du diagramme de dispersion de vagues.

La seconde vérification (C2) considère l'angle de roulis maximum sur chaque vague du diagramme de dispersion et pour 7 vitesses différentes du navire en mer de l'avant ou mer de l'arrière. Deux méthodes sont proposées pour calculer sa valeur. La première méthode est basée sur la méthode des moyennes, qui donne une solution analytique pour les oscillateurs non linéaires en assimilant les non linéarités à des petites perturbations provoquant une évolution lente de la réponse du système. Cette méthode est décrite en détail par Nayfeh [66]. La seconde méthode consiste en la résolution numérique de l'équation différentielle à un degré de liberté régissant le roulis paramétrique. Des recommandations pour sa mise en œuvre sont données par Peters *et al.* [32] et reprises dans les notes explicatives de la future réglementation [23]. Seule cette seconde méthode est mise en œuvre dans la thèse. Les méthodes simplifiées d'Ikeda [48 et 50] sont utilisées pour estimer le coefficient d'amortissement en roulis pour les deux méthodes. Le concept de vague effective de Grim [65] est imposé pour réduire le nombre de calculs hydrostatiques,

en ramenant les vagues du diagramme de dispersion à des vagues équivalentes dont la longueur entre crêtes est égale à celle du navire.

## **2. CALCULS HYDROSTATIQUES**

Le logiciel hydrostatique Calcoque est utilisé pour l'enseignement et la recherche à l'Ecole navale. Il a été modifié dans le cadre de la thèse pour permettre le calcul de la hauteur métacentrique et de la courbe de GZ sur houle longitudinale et des critères de niveaux 1 et 2 de perte pure de stabilité et de roulis paramétrique. Les calculs hydrostatiques sont basés sur trois algorithmes principaux décrits ci-dessous.

### **Maillage volumique du navire**

Le premier algorithme transforme la représentation classique des formes d'un navire par couples en un maillage volumique à partir duquel sont réalisés les calculs hydrostatiques proprement dits. Ces couples sont une suite de points (Y,Z) situés à une même coordonnée longitudinale X (voir le repère lié au navire en annexe 4). En complément, des lignes reliant certains points des couples sont définies par l'utilisateur afin de matérialiser les arêtes principales du navire (livet de pont, bouchain, ...). Le maillage est réalisé tranche par tranche, celles-ci étant définies entre deux couples successifs. Une matrice représentant les liens entre les points d'un couple et ceux du couple suivant est renseignée par les lignes imposées par l'utilisateur, puis complétée automatiquement par d'autres liens de manière à définir des triangles et des quadrilatères sur chaque face latérale de la tranche. Deux triangles symétriques définissent un prisme et deux quadrilatères définissent un hexaèdre. La concaténation des volumes élémentaires de toutes les tranches définit le maillage volumique du navire. Ce maillage est coupé par le pont d'étanchéité et complété par les appendices afin de représenter le flotteur réel.

### **Coupure d'un maillage volumique par un plan**

Le deuxième algorithme coupe un maillage par un plan. Il constitue la base des calculs hydrostatiques proprement dits, en coupant le maillage volumique du flotteur par le plan de la mer afin de définir la surface de flottaison et le volume de carène. La coupure d'un maillage par un plan permet également la définition du volume des compartiments ou des ponts et des cloisons du navire. L'algorithme de coupure traite successivement tous les volumes élémentaires du maillage. Seul les cas simples sont considérés pour les prismes et les hexaèdres. Pour les autres cas, ceux-ci sont préalablement divisés respectivement en 3 et 6 tétraèdres. La coupure d'un tétraèdre quelconque par un plan est ramenée à 8 cas simples et génère 0 ou 1 tétraèdre ou prisme de chaque côté du plan et 0 ou 1 triangle ou quadrilatère d'intersection avec le plan.

### **Recherche de la position d'équilibre**

La recherche de la position d'équilibre se fait en 3 degrés de liberté (enfoncement, gîte, assiette) ou 2 degrés de liberté lors du calcul de la courbe de GZ (gîte imposée). L'équilibre est considéré atteint quand l'écart en volume, l'écart transversal et l'écart longitudinal sont suffisamment petits. L'écart en volume représente la différence entre le volume de carène visé et le volume calculé avec l'enfoncement, la gîte et l'assiette courants. Pour définir les deux autres écarts, on définit deux plans perpendiculaires, l'un transversal et l'autre longitudinal, dont la droite d'intersection est la verticale terrestre passant par le centre de carène. L'écart longitudinal est la distance entre le centre de gravité et le plan transversal.

L'écart transversal est la distance entre le centre de gravité et le plan longitudinal et correspond au bras de levier de redressement  $GZ$ , à annuler lors de la recherche de la position d'équilibre du navire sur mer plate ou sur houle figée, sinon à déterminer (courbe de  $GZ$ ).

Le plan de la mer est défini par l'enfoncement, la gîte et l'assiette dans le repère lié au navire. Il sert de plan de coupure du maillage du volume étanche lors de la recherche de l'équilibre sur mer plate. En cas de recherche de l'équilibre sur sur vagues longitudinales statiques, le volume étanche est préalablement découpé en tranches transversales. Dans chaque tranche, un plan de coupure local est défini en fonction des caractéristiques des vagues et de la position du navire (enfoncement, gîte assiette).

La recherche de la position d'équilibre sur mer plate ou sur houle figée consiste en la résolution d'un système non linéaire de 3 équations et 3 inconnues (ou  $2 \times 2$  si la gîte est figée). Elle suit un processus itératif. Deux méthodes coexistent.

Dans la première méthode, l'enfoncement, la gîte et l'assiette de l'itération suivante sont calculés à partir de ceux de l'itération précédente en utilisant respectivement l'écart en volume et l'aire de la surface de flottaison, l'écart transversal et la hauteur métacentrique transversale, l'écart longitudinal et la hauteur métacentrique longitudinale. L'évolution du volume de carène, et des écarts transversal et longitudinal d'une itération à l'autre permet de réévaluer l'aire de la surface de flottaison et les deux hauteurs métacentriques. Ces 3 grandeurs sont calculées classiquement avant la première itération.

Dans la seconde méthode, à chaque itération, 3 calculs hydrostatiques (2 si la gîte est figée) permettent de déterminer l'impact d'un incrément élémentaire d'enfoncement, de gîte puis d'assiette sur les 3 écarts (volume, transversal, longitudinal). S'en suit la résolution d'un système linéaire de dimension 3 (2 si la gîte est figée) pour déterminer les incréments d'enfoncement, de gîte et d'assiette permettant de faire converger les écarts vers zéro. Un quatrième calcul hydrostatique donne les écarts résiduels que l'on cherche à réduire à nouveau lors de l'itération suivante.

Dans les deux méthodes, le signe des hauteurs métacentriques est vérifié afin de diverger d'une éventuelle position d'équilibre instable. Les deux méthodes convergent vers la même position d'équilibre et nécessitent des nombres de calculs hydrostatiques similaires.

### **3. RESULTATS**

Les courbes de  $KG_{\max}$  associées aux critères de niveau 1 et niveau 2 de perte pure de stabilité et de roulis paramétrique sont calculées pour 6 navires civils (2 porte-conteneurs dont un connu pour être vulnérable au roulis paramétrique, 2 navires à passagers, 1 navire roulier et 1 pétrolier). Bien que l'application de ces nouveaux critères aux navires militaires ne soit pas envisagée aujourd'hui, rien ne garantit la non-vulnérabilité de ces navires. Par ailleurs, le faible nombre de navires militaires en service, comparé à celui des navires civils, rend quasi inexistant le retour d'expérience dans le domaine des modes de défaillance considérés. Ainsi, il paraît intéressant de tester l'application des nouveaux critères aux navires militaires. Trois d'entre eux ont été sélectionnés à cet effet (porte-hélicoptère *Jeanne d'Arc*, destroyer type DDG-51 et patrouilleur hauturier). Les navires testés sont présentés en annexe 2.

## Perte pure de stabilité

Les courbes de  $KG_{\max}$  associées aux critères de niveau 1 et 2 en perte pure de stabilité montrent les points suivants :

- La courbe associée à la première méthode du critère de niveau 1 présente un décrochement lorsque la flottaison isocline intercepte les évidements dans la coque (logements des ailerons stabilisateurs). L'utilisation de la coque nue (sans appendice ni évidement) masque ce phénomène.
- Les deux méthodes du critère de niveau 1 fournissent des résultats très différents pour tous les navires. La première méthode (flottaison isocline) est très conservative.
- Le critère de niveau 2 est plus conservatif que la seconde méthode du critère de niveau 1 pour certains navires, contrairement à l'esprit de la nouvelle réglementation.
- La hauteur du pont étanche peut avoir une très légère influence sur la seconde méthode du niveau 1. Elle a en revanche une influence considérable sur le critère de niveau 2. Il paraît sage en conséquence que la future réglementation spécifie clairement le pont étanche à prendre en compte.
- L'influence de la vitesse du navire n'est pas systématique. Lorsqu'elle existe, l'augmentation de la vitesse augmente la vulnérabilité du navire, comme attendu.

## Roulis paramétrique

Les courbes de  $KG_{\max}$  associées aux critères de niveau 1 et 2 en roulis paramétrique montrent les points suivants (dont certains sont similaires à ceux observés en perte pure de stabilité) :

- La courbe associée à la première méthode du critère de niveau 1 présente un décrochement lorsque la flottaison isocline intercepte les évidements dans la coque. Cependant, les décrochements interviennent à des tirants d'eau ou des déplacements différents de ceux observés en perte pure de stabilité car la cambrure de vague considérée est différente.
- Les deux méthodes du critère de niveau 1 fournissent des résultats très différents pour certains navires (dont tous les navires militaires). La première méthode (flottaison isocline) est toujours plus conservative.
- Le critère de niveau 2 est plus conservatif que la seconde méthode du critère de niveau 1 pour certains navires. Cependant, cette incohérence est moins marquée que celle observée en perte pure de stabilité.
- Pour certains navires, le  $KG_{\max}$  associé à la seconde vérification du critère de niveau 2 (C2) correspond à un GM nul (pétrolier, navire à passager, *Jeanne d'Arc*). Cela est dû au fait que l'angle de roulis maximal autorisé (25 degrés) n'est atteint que lorsque le navire devient statiquement instable. Ces navires ne sont pas vulnérables au roulis paramétrique.
- Le résultat de la seconde vérification du critère de niveau 2 est incohérent pour l'un des deux navires à passagers. La méthode de calcul du coefficient d'amortissement imposée dans la réglementation est inadaptée à sa coque à bouchain vif.

- Le porte-conteneurs C11, connu pour être vulnérable au roulis paramétrique à la suite de l'accident survenu en 1998 [41], est bien jugé comme tel par les nouveaux critères. Il en est de même pour l'autre porte-conteneurs.

La seconde vérification du critère de niveau 2 (C2), vue ici comme un critère indépendant, a un comportement sensiblement différent de celui des autres critères. Le calcul de C2 pour un tirant d'eau donné et toutes les valeurs possibles de  $KG_{max}$  génère une courbe présentant de nombreux pics lorsque le navire est vulnérable au roulis paramétrique. Il en résulte que le critère C2 peut être respecté au-delà de  $KG_{max}$ , configuration impossible pour les autres critères. Le calcul de C2 pour toutes les valeurs possibles de tirant d'eau et de  $KG$  génère des surfaces autorisées et interdites au regard du critère associé. Il résulte de cela que la vérification du respect du critère pour un cas de chargement donné (correspondant à un couple tirant d'eau et  $KG$ ) ne suffira pas. En effet, il est possible que le critère ne soit plus vérifié si le  $KG$  est légèrement inférieur à celui du cas de chargement. Cette particularité devrait être indiquée clairement dans la nouvelle réglementation.

Le calcul de l'angle de roulis maximum, requis dans le critère C2, est réalisé par résolution numérique de l'équation différentielle du roulis paramétrique. Des conditions de résolution ont été proposées par Peters *et al.* [32] et reprises dans les notes explicatives de la future réglementation [23]. Sont proposés entre autres :

- une durée de simulation égale à 15 périodes naturelles de roulis du navire ;
- un angle de gîte initial de 5 degrés et une vitesse initiale nulle ;
- de considérer le GZ non linéaire.

Une étude de sensibilité réalisée sur plusieurs navires présentant des vulnérabilités différentes montre que :

- quelle que soit la vulnérabilité du navire, les courbes de  $KG_{max}$  associées au critère C2 sont confondues pour une durée de simulation égale ou supérieure à 10 périodes naturelles de roulis ;
- l'influence de l'angle de gîte initiale sur les courbes de  $KG_{max}$  associées au critère C2 est faible ;
- la linéarisation du GZ n'est pas pertinente, excepté dans le cas particulier où le GZ réel est relativement linéaire jusqu'à 25 degrés ou au-delà.

Des simulations numériques du comportement du porte-conteneurs C11 réalisées en 6 degrés de liberté à l'aide du logiciel Fredyn [70] montrent que :

- à pleine charge, le navire peut chavirer en roulis paramétrique avec un  $KG$  autorisé par les critères de stabilité à l'état intact actuellement en vigueur [18] et dépasser 25 degrés de roulis quelle que soit son chargement ; cela montre bien la nécessité d'une nouvelle réglementation considérant ce mode de défaillance ;
- la courbe de  $KG_{max}$  associée au critère C2 est proche de la courbe équivalente considérant un angle de roulis paramétrique maximum de 25 degrés calculée à l'aide des simulations en 6 degrés de liberté.

#### **4. ANALYSE ENERGETIQUE DU ROULIS PARAMETRIQUE**

La seconde vérification du critère de niveau 2 du roulis paramétrique (C2) requiert le calcul de l'angle de roulis maximum pour différentes vitesses en mer de l'avant et en mer de l'arrière. Les deux méthodes de calcul proposées dans la future réglementation étant relativement complexes à implémenter, notamment pour les architectes navals habitués à la simplicité des critères actuels, nous proposons ici une méthode alternative simplifiée basée sur des considérations énergétiques et supposant un GZ linéaire.

##### **Roulis paramétrique en condition de résonance**

L'équation différentielle du roulis paramétrique est réécrite avec un GZ linéaire et en assimilant la composante non constante du moment de redressement à un moment d'excitation. On suppose que le navire roule à sa fréquence propre en condition de résonance paramétrique. La fréquence de rencontre des vagues est égale au double de la fréquence propre. On suppose également que le navire a atteint un régime permanent de roulis paramétrique à amplitude constante. Ces hypothèses rendent constants les termes d'inertie et d'amortissement de l'équation différentielle.

La somme de l'énergie cinétique et de l'énergie potentielle est constante à tout instant car le navire roule à sa fréquence propre. En conséquence, l'hypothèse d'une amplitude de roulis constante impose que la totalité de l'énergie apportée par l'excitation soit dissipée par l'amortissement. En supposant le cas le plus défavorable (c.-à-d. l'excitation la plus importante) concernant le décalage angulaire entre la rencontre des vagues et le roulis du navire, on détermine un coefficient d'amortissement dit « requis » permettant une amplitude de roulis constante. Si le coefficient d'amortissement réel est supérieur à cette valeur, le roulis paramétrique n'apparaît pas. Si, à l'opposé, le coefficient réel ne peut pas atteindre la valeur requise, l'amplitude du roulis paramétrique est théoriquement infinie, provoquant le chavirement du navire sous réserve de compatibilité avec l'hypothèse du GZ linéaire. Cela étant, le coefficient d'amortissement est fonction de l'amplitude du roulis. De fait, l'égalité entre le coefficient d'amortissement réel et la valeur requise permet, dans la plupart des cas, de poser une équation simple dont la racine est l'amplitude de roulis. Le résultat obtenu ici est identique celui obtenu par d'autres moyens par Kerwin en 1955 [12].

Des simulations numériques en condition de résonance paramétrique donnent une amplitude de roulis finale identique à la valeur précédemment calculée. Cela donne une première validation de l'hypothèse du cas le plus défavorable concernant le décalage angulaire (noté  $\alpha$ ) entre la rencontre des vagues et le roulis. Par ailleurs, ces simulations sont lancées avec un décalage angulaire différent et on montre que celui-ci évolue au début de la simulation vers la valeur la plus défavorable ( $\alpha = -\pi/2$ ). L'hypothèse concernant ce décalage en condition de résonance paramétrique est validée.

##### **Roulis paramétrique dans les autres conditions**

Lorsque le navire roule à une fréquence autre que sa fréquence propre, la somme de l'énergie cinétique et de l'énergie potentielle n'est pas constante. Cependant, sa valeur moyenne l'est. En conséquence, l'hypothèse d'amplitude de roulis constante fait que l'énergie apportée par l'excitation paramétrique est entièrement dissipée par l'amortissement, comme précédemment.

On note  $\gamma$  le rapport entre la fréquence de rencontre et la fréquence de roulis du navire. Il est égal à 2 en condition de résonance.

On montre que l'énergie d'excitation est portée par un signal sinusoïdal à deux fréquences : une basse fréquence égale à  $2-\gamma$  et une haute fréquence égale à  $2+\gamma$ . Le cas  $\gamma=2$  correspond à une vitesse du navire irréaliste et n'est pas considéré. La coexistence de ces deux fréquences peut être montrée par une simulation numérique avec une vitesse du navire sensiblement différente de la vitesse de résonance. Cependant, l'observation de la basse fréquence est impossible dans ces conditions car le mouvement de roulis se décale automatiquement sur la houle pour capter un maximum d'énergie (changement de l'angle  $\alpha$  au cours de la simulation). Dans ces conditions de vitesse, l'amplitude de roulis paramétrique est très faible et le risque pour le navire est inexistant ou très limité.

Les simulations numériques à un degré de liberté montrent que le roulis paramétrique apparaît lorsque la vitesse du navire est proche de la vitesse de résonance. Dans ce cas, la fréquence de roulis est exactement égale à la moitié de la fréquence de rencontre ( $\gamma=2$ ). L'amplitude maximale est observée à une fréquence légèrement inférieure à la fréquence de résonance. Le second mode de roulis paramétrique, caractérisé par l'égalité entre la fréquence de roulis et la fréquence de rencontre, est observable mais son amplitude n'est pas significative. Le troisième mode de roulis paramétrique (fréquence de rencontre égale aux deux tiers de la fréquence de roulis) n'est pas observable en conditions courantes.

Dans le domaine de roulis paramétrique centré sur la résonance du premier mode, les simulations montrent que l'angle de décalage  $\alpha$  évolue de 0 à  $-\pi$  en passant par  $-\pi/2$  au voisinage de la résonance. Ce décalage modère la puissance d'excitation. La valeur  $-\pi/2$  correspond à l'excitation maximale.

On observe que la largeur du domaine de roulis paramétrique, exprimée à l'aide du rapport entre la fréquence de rencontre et la fréquence de roulis naturelle du navire, est égale à la variation adimensionnelle de la hauteur métacentrique ( $\Delta GM/GM$ ). Kerwin a démontré un résultat similaire en 1955 [12]. Des simulations numériques à six degrés de liberté sur une houle sinusoïdale avec un GZ non linéaire positionnent le domaine de roulis paramétrique aux mêmes fréquences.

### **Méthode alternative**

Le calcul de l'angle de roulis maximum en condition de résonance au moyen de considérations énergétiques, la connaissance des fréquences limitant le domaine de roulis paramétrique et l'évolution de l'angle de décalage dans ce domaine permettent de bâtir une méthode alternative simple donnant l'angle de roulis maximal en fonction de la vitesse du navire et de la variation de la hauteur métacentrique. Cette méthode, basée sur l'hypothèse d'un GZ linéaire, est compatible avec une implémentation dans la seconde vérification du critère de niveau 2 (C2). Les courbes de  $KG_{\max}$  qui lui sont associées coïncident avec celles obtenues par résolution numérique de l'équation différentielle avec GZ linéaire, et ce pour plusieurs navires plus ou moins vulnérables au roulis paramétrique.

## **CONCLUSION**

Les critères de stabilité à l'état intact de seconde génération sont actuellement en cours de finalisation à l'OMI. Ces critères sont organisés en cinq modes de défaillance et trois niveaux d'évaluation dans chaque mode. La perte pure de stabilité et le roulis paramétrique sont deux défaillances consécutives à la variation du couple de redressement dans les vagues longitudinales. Le but du travail réalisé dans le cadre de cette thèse est l'analyse de l'exigence et de la pertinence des critères de premier et deuxième niveaux de ces deux modes de défaillance. Ces critères ont été implémentés dans un logiciel hydrostatique modifié pour l'occasion.

Les critères ont été calculés pour plusieurs navires de différents types, tant civils que militaires, supposés ou connus pour avoir des comportements différents vis-à-vis de ces modes de défaillance. Bien que l'application de cette nouvelle réglementation aux navires militaires ne soit pas prévue, rien ne garantit la non-vulnérabilité de ces navires. Par ailleurs, les nouveaux critères constituent un outil à coût négligeable (environ 10 minutes de calcul pour une courbe de  $KG_{max}$  associée à un critère de niveau 2) qu'il serait regrettable d'ignorer. L'auteur recommande la modification des règlements militaires de stabilité à l'état intact après l'entrée en vigueur de ces nouveaux critères dans le civil. Les résultats sont donnés sous la forme de courbes de  $KG_{max}$  indiquant la hauteur maximale du centre de gravité garantissant le respect du (des) critère(s) considéré(s). Cela permet d'ignorer les cas de chargement des navires étudiés et d'analyser les critères plutôt que les navires eux-mêmes.

Le calcul des  $KG_{max}$  associés aux nouveaux critères montre que les critères de niveau 1 peuvent être plus conservatifs que les critères de niveau 2 dans les deux modes de défaillance, contrairement à ce qui est attendu. Il montre également que les deux méthodes de calcul proposées dans le niveau 1 fournissent des  $KG_{max}$  sensiblement différents, notamment en perte pure de stabilité. Les marges de sécurité conférées par la première méthode de calcul (flottaison isocline) sont tellement élevées que les critères correspondant pourraient être incompatibles avec les critères d'accélération excessive. En conséquence, s'ils sont équipés d'un outil de calcul hydrodynamique sur houle, les chantiers navals et les architectes navals devraient être tentés d'ignorer cette méthode. Celle-ci aurait cependant une réelle valeur ajoutée si elle conférait des marges de sécurité acceptables pour les navires de faible déplacement, normalement conçus par des chantiers ou des cabinets d'architecture équipés plus modestement. Les résultats obtenus sur un navire à passagers de 30 mètres montrent que cela peut être le cas.

Bien que cela ne soit pas l'objectif premier ici, les résultats confirment la vulnérabilité au roulis paramétrique bien connue du porte-conteneurs C11. Ils confirment également la non-vulnérabilité d'un pétrolier vis-à-vis de la perte pure de stabilité et du roulis paramétrique, attendue en raison de la présence de murailles verticales sur une majeure partie de la coque du navire.

Les courbes de  $KG_{max}$  associées à la première méthode des critères de niveau 1 des deux modes de défaillance montrent des décrochés consécutifs aux évidements de la coque (logements des ailerons stabilisateurs). L'utilisation de la coque nue (sans appendice ni évidement) masque ce phénomène. Par ailleurs, la limite supérieure du volume étanche a une influence majeure sur le  $KG_{max}$  associé au critère de niveau 2 de la perte pure de stabilité.

**Recommandation : la future réglementation devrait clairement spécifier le volume étanche à considérer (coque nue ou avec appendices et évidements, hauteur du pont étanche).**

La seconde vérification du critère de niveau 2 du roulis paramétrique (C2) considère l'angle de roulis maximal pour 7 vitesses en mer de l'avant et en mer de l'arrière pour tous les cas d'un diagramme de dispersion de vagues. La future réglementation propose deux méthodes pour déterminer sa valeur. La méthode basée sur une résolution numérique de l'équation différentielle du roulis paramétrique est utilisée et analysée ici. La durée de simulation proposée dans la réglementation est validée par des tests de sensibilité.

Le calcul de C2 pour toutes les valeurs possibles du tirant d'eau et de KG permet de définir des zones autorisées et interdites par le critère associé. En particulier, le critère peut être respecté au-delà de  $KG_{max}$  et nécessite donc d'être évalué prudemment.

**Recommandation : la future réglementation devrait clairement spécifier l'obligation de vérifier C2 pour toutes les valeurs de KG inférieures à celle du cas de chargement considéré.**

La future réglementation impose la méthode de Grim [65] pour le calcul de C2, donnant la même longueur à toutes les vagues du diagramme de dispersion. En conséquence, les 7 vitesses considérées par le critère sont positionnées aléatoirement par rapport à la vitesse de résonance, en fonction de la longueur du navire. L'augmentation du nombre de vitesses ou la prise en compte de la vitesse de résonance devrait améliorer le critère.

**Recommandation : le nombre de vitesses considérées dans la seconde vérification du critère de niveau 2 de roulis paramétrique devrait être augmenté, ou le critère devrait considérer la vitesse correspondant à la résonance paramétrique.**

Le calcul de l'angle de roulis paramétrique maximum fait intervenir le coefficient d'amortissement. La future réglementation fournit une méthode simplifiée d'Ikeda [48, 50] à cet effet. Cependant, cette méthode n'est pas adaptée aux coques à bouchain vif.

**Recommandation : la future réglementation devrait proposer une méthode de calcul du coefficient d'amortissement en roulis adaptée aux coques à bouchain vif.**

Les deux méthodes de calcul de l'angle de roulis paramétrique maximum proposées dans la réglementation étant relativement complexe à implémenter, une méthode alternative simplifiée, basée sur une hypothèse de GZ linéaire, est proposée ici. Cette méthode peut être implémentée dans la nouvelle réglementation et donne une valeur de  $KG_{max}$  identique à celle fournie par la résolution numérique de l'équation différentielle utilisant la même hypothèse de GZ. Cette hypothèse est douteuse pour les navires ayant GZ fortement non linéaire, mais la méthode alternative est si simple qu'il serait regrettable de l'ignorer si le GZ est à peu près linéaire jusqu'à 25 degrés.

**Proposition : la future réglementation pourrait proposer une méthode alternative simplifiée de calcul de l'angle de roulis maximum pour les navires ayant un GZ linéaire jusqu'à 25 degrés.**

L'entrée en vigueur de la future réglementation, prévue au plus tôt en 2019 sous la forme de recommandations dans la partie B du code de stabilité à l'état intact, risque de bousculer les habitudes dans les chantiers navals et les cabinets d'architecture navale en raison de sa complexité notablement accrue par rapport à celle des critères actuels. Néanmoins, les chantiers et cabinets ont récemment intégré la nouvelle réglementation probabiliste de stabilité après avarie, qui requiert un nombre de calculs considérablement supérieur à celui

de l'ancienne réglementation déterministe. Les écoles et universités dispensant des formations en architecture navale vont enseigner la nouvelle réglementation de stabilité à l'état intact à leurs élèves et proposer des stages de mise à niveau pour les architectes navals en activité. L'entrée en vigueur de cette réglementation ne devrait en conséquence pas rencontrer d'obstacle majeur, si ce n'est concernant la seconde vérification du critère de niveau 2 du roulis paramétrique.

En effet, il n'existe malheureusement aucune méthode simplifiée fournissant le coefficient d'amortissement au roulis pour tous les types de navires. Il pourrait être tentant de proposer plusieurs méthodes correspondant à toutes les géométries existantes, mais il est impossible d'imaginer aujourd'hui les géométries que les architectes navals dessineront dans les prochaines décennies. L'utilisation de calculs CFD (résolution des équations de Navier-Stokes) n'est pas envisageable dans le cadre de cette réglementation en raison du temps de calcul trop important et de la haute qualification nécessaire à sa mise en œuvre.

En conséquence, de l'avis de l'auteur, la seconde vérification du critère de niveau 2 de roulis paramétrique dans sa forme actuelle pourrait être considérée comme une première étape de niveau 3, lequel devrait être mis en œuvre par des instituts spécialisés, à même de choisir la méthode de calcul de l'amortissement la mieux adaptée. Une alternative pourrait être de limiter cette vérification aux navires dont la géométrie est compatible avec la méthode proposée dans la réglementation (éventuellement plusieurs méthodes) en utilisant des critères simples et objectifs pour s'assurer de cette compatibilité (coefficient bloc, nombre de Froude, rayon du bouchain, ...). En cas d'incompatibilité et si la première vérification du critère de niveau 2 (ou le critère de niveau 1) ne suffisait pas, la société de classification prescrirait la mise en œuvre de cette vérification par un institut spécialisé, voire une évaluation de niveau 3.

Bien que quelques améliorations soient souhaitables, les critères de niveau 1 et 2 des cinq modes de défaillance sont parfaitement définis. Ce n'est pas le cas pour les critères de niveau 3, aujourd'hui encore à l'étape de la réflexion.

Il est établi que ce niveau consiste en une simulation numérique du navire dans les vagues, supposée indiquer sa vulnérabilité vis-à-vis des modes de défaillance avec une précision accrue par rapport aux critères des deux premiers niveaux. Ces simulations seront nécessairement réalisées avec six degrés de liberté. Les calculs CFD ne paraissent pas adaptés aujourd'hui en raison du temps de calcul élevé qu'ils nécessitent, incompatible avec le déroulement d'un projet de navire standard. En revanche, des codes informatiques à 6 degrés de liberté, basés sur des calculs hydrodynamiques potentiels réalisés avant la simulation, paraissent bien adaptés à cette tâche.

L'évaluation de niveau 3 en roulis paramétrique pourrait être une évaluation de niveau 2 améliorée dans laquelle la simulation à un degré de liberté serait remplacée par une simulation à six degrés de liberté, prenant en compte les effets non linéaires sur des états de mer réels. Une évaluation similaire pourrait être conduite en perte pure de stabilité, avec un temps de simulation augmenté afin de capter un nombre significatif de vagues extrêmes.

Il est également possible de fusionner les évaluations de niveau 3 des cinq modes de défaillance en une unique évaluation réalisée à l'aide d'un nombre important de simulations dans tous les états de mer du diagramme de dispersion, avec toutes les vitesses et toutes les routes possibles. Un tel travail a déjà été réalisé pour évaluer les probabilités de chavirement de frégates françaises [72]. Une analyse préliminaire d'un nombre significatif de

navires connus comme vulnérables et non vulnérables est nécessaire afin de définir le seuil qui doit être utilisé comme critère global, dans une démarche dont l'esprit est similaire à celui du travail réalisé par Rahola en 1939 [11], mais avec un outil de calcul plus moderne.

Une telle démarche fournirait un critère global encapsulant tous les modes de défaillance (y compris des modes de défaillance éventuellement non considérés par la future réglementation). Bien que les simulations ne soient pas orientées vers un mode de défaillance particulier, il est possible d'implémenter des détecteurs dans le simulateur afin de renseigner l'utilisateur sur les phénomènes ayant causé la perte du navire ou un angle de roulis indésirable.

## GLOSSARY

<i>Symbol</i>	<i>Unit</i>	<i>Definition</i>
<b>Numbers</b>		
0H	-	Baseline, X-axis of the ship-fixed coordinate system
10H	-	Reference waterplane, parallel to 0H
<b>A</b>		
A	-	Point defining the strip's local waterplane
a	-	Coefficient of added mass in roll
A <sub>WP</sub>	m <sup>2</sup>	Area of waterplane
<b>B</b>		
B	-	Center of buoyancy
B	-	Point defining the strip's local waterplane
B	m	Ship's breadth
B <sub>44</sub>	N.m.s/rad	Roll damping coefficient
B <sub>44.req</sub>	N.m.s/rad	Required roll damping coefficient
<b>C</b>		
C	-	Point defining the strip's local waterplane
C1	-	First check of parametric roll level-two criterion
C1 <sub>i</sub>	-	Coefficient of first check of parametric roll level-two criterion for the wave number i
C2	-	Second check of parametric roll level-two criterion
C2 <sub>i</sub>	-	Coefficient for the wave number i regarding the minimum angle of stable equilibrium under heeling lever (PL)
C2 <sub>i,j</sub>	-	Coefficient for the wave number i and the speed factor number j regarding the minimum parametric roll angle
CFD	-	Computational fluid dynamics
C <sub>m</sub>	-	Midship section coefficient of the fully loaded condition in calm water
CR1	-	Coefficient for all waves wave regarding the minimum angle of vanishing stability (PL)
CR2	-	Coefficient for all waves regarding the minimum angle of stable equilibrium under heeling lever (PL)
CRNAV	-	Cooperative Research Navies
<b>D</b>		
D	m	Ship's depth

<b>Symbol</b>	<b>Unit</b>	<b>Definition</b>
d	m	Ship's draft
D <sub>3</sub>	-	Longitudinal line located in the calm-water waterplane
d <sub>full</sub>	m	Full loaded draft
d <sub>H</sub>	m	Highest draft
d <sub>L</sub>	m	Lowest draft
DoF	-	Degree(s) of freedom
DTMB	-	David Taylor Model Basin

## E

e	m	Sinkage
E <sub>D</sub>	J	Damping energy
E <sub>E</sub>	J	Exciting energy
E <sub>K</sub>	J	Kinetic energy
E <sub>P</sub>	J	Potential energy

## F

F <sub>n</sub>	-	Froude number
----------------	---	---------------

## G

G	-	Center of gravity
g	m/s <sup>2</sup>	Acceleration of gravity
GM	m	Transverse metacentric height
GM <sub>0</sub>	m	Transverse metacentric height in calm water
GM <sub>L</sub>	m	Longitudinal metacentric height
GM <sub>max</sub>	m	Maximum value of transverse metacentric height in waves
GM <sub>min</sub>	m	Minimum value of transverse metacentric height in waves
GM <sub>moy</sub>	m	Average value of transverse metacentric height in waves
GM <sub>T</sub>	m	Transverse metacentric height
GZ	m	Righting arm

## H

h	m	Wave height
H <sub>1/3</sub> <sup>eff</sup>	m	Effective height of the 1/3 highest waves
H <sub>3%</sub> <sup>eff</sup>	m	Effective height of the 3% highest waves
H <sub>eff</sub>	m	Effective wave height
H <sub>S</sub>	m	Significant wave height

## I

I <sub>1</sub>	-	Intersection point of P <sub>1</sub> and D <sub>3</sub>
I <sub>2</sub>	-	Intersection point of P <sub>2</sub> and D <sub>3</sub>
IACS	-	International Association of Classification Societies
I <sub>H</sub>	m <sup>4</sup>	Inertia of parallel waterplane at highest draft
I <sub>L</sub>	m <sup>4</sup>	Inertia of parallel waterplane at lowest draft

<b>Symbol</b>	<b>Unit</b>	<b>Definition</b>
IMCO	-	Inter-Governmental Maritime Consultative Organization, former name of the IMO (until 1982)
IMO	-	International Maritime Organization
ISCG	-	Intact Stability Correspondence Group

## **J**

$J_{44}$	$\text{kg}\cdot\text{m}^2$	Ship's roll moment of inertia
----------	----------------------------	-------------------------------

## **K**

$k$	$\text{m}^{-1}$	Wave number
$k$	-	Coefficient of radius of inertia in roll
KB	m	Vertical coordinate of the center of buoyancy in the ship's fixed coordinate system
KG	m	Vertical coordinate of the center of gravity in the ship's fixed coordinate system
$KG_{\max}$	m	Maximum vertical coordinate of the center of gravity ensuring the compliance of a specific criterion or a panel of criteria
$K_j$	-	Speed factor number $j$
$KG_{\text{start}}$	m	Starting value of KG in the process of finding $KG_{\max}$
KMT	m	Vertical coordinate of the transverse metacenter in the ship's fixed coordinate system

## **L**

L	m	Ship's length
LCB	m	Longitudinal coordinate of the center of buoyancy in the ship's fixed coordinate system
LCG	m	Longitudinal coordinate of the center of gravity in the ship's fixed coordinate system
$L_{pp}$	m	Length between perpendiculars

## **M**

$m_0$	$\text{m}^2\text{s}$	Zero-order moment of the wave spectrum (Grim effective wave height concept)
-------	----------------------	---

## **N**

$\vec{n}$	-	Normal vector, defining any plane, the calm-water waterplane or the strip's local waterplane
$\vec{n}_1$	-	Vertical vector of the inclined-ship's planes, defining the Earth-vertical
$\vec{n}_2$	-	Transverse vector of the inclined-ship's planes
$\vec{n}_3$	-	Longitudinal vector of the inclined-ship's planes

<b>Symbol</b>	<b>Unit</b>	<b>Definition</b>
<b>O</b>		
O	-	Origin point of the ship-fixed coordinate system
<b>P</b>		
P	-	Point defining the waterplane
P <sub>1</sub>	-	Strip's aft plane
P <sub>2</sub>	-	Strip's forward plane
P <sub>D</sub>	W	Damping power
P <sub>E</sub>	W	Exciting power of parametric roll
PL	-	Pure Loss of Stability
PR	-	Parametric Roll
<b>Q</b>		
Q	-	Point located amidships on the reference waterplane, used to define any waterplane
<b>R</b>		
R <sub>PL</sub>	m	Minimum allowed value of GM in waves of pure loss of stability level-one criterion
R <sub>PL0</sub>	-	Required index of pure loss of stability level-two criterion
R <sub>PL1</sub>	deg	Minimum allowed value of angle of vanishing stability of pure loss of stability level-two criterion
R <sub>PL2</sub>	deg	Maximum allowed value of angle of stable equilibrium under heeling lever of pure loss of stability level-two criterion
R <sub>PL3</sub>	m	Heeling lever
R <sub>PR</sub>	-	Maximum allowed value of non-dimensional GM variation of parametric roll level-one and level-two criteria
R <sub>PRO</sub>	-	Required index of parametric roll level-two criterion
<b>S</b>		
SDC	-	Sub-Committee Ship Design and Construction of the IMO
SHK	-	Swedish Accident Investigation Board
SOLAS	-	Safety Of Life At Sea
S <sub>W</sub>	-	Wave steepness (ratio height over length)
<b>T</b>		
t	s	Time
T <sub>0</sub>	s	Ship's natural roll frequency
TEU	-	Twenty-foot equivalent unit, defining the cargo capacity of a container vessel in terms on number on 20-ft containers
T <sub>Z</sub>	s	Zero-crossing wave period

<i>Symbol</i>	<i>Unit</i>	<i>Definition</i>
---------------	-------------	-------------------

## V

V	m/s	Ship's speed
$V_{1st\ mode}$	m/s	Speed of first mode of parametric roll
$V_{PR,i}$	m/s	Speed of first mode of parametric roll corresponding to the wave number i
$V_S$	m/s	Ship's service speed

## W

W	N	Ship's weight
WGIS	-	Working Group on Intact Stability
$W_i$	-	Weighting factor of the wave number i

## X

$\vec{X}$	-	Unit vector defining the longitudinal axis of the ship-fixed coordinate system
-----------	---	--

## Z

Z	-	Projection of the center of gravity on the Earth-vertical through the center of buoyancy
$z_1$	m	Height defining the strip's local waterplane
$z_2$	m	Height defining the strip's local waterplane

## Greek symbols

$\alpha$	rad	Shift angle
$\beta$	rad, deg	Angle between the ship's heading and the wave direction
$\gamma$	-	Ratio $\omega_e/\omega_0$
$\gamma_0$	-	Ratio $\omega_e/\omega$ characterizing the parametric roll synchronization
$\Delta$	kg	Ship's displacement
$\Delta GM$	m	Amplitude of variation of transverse metacentric height in waves
$\varepsilon_e$	m	Sinkage increment
$\varepsilon_x$	m	Longitudinal gap
$\varepsilon_y$	m	Transverse gap
$\varepsilon_\theta$	rad	Trim increment
$\varepsilon_\varphi$	rad	Heel increment
$\varepsilon_V$	$m^3$	Volume gap
$\theta$	rad, deg	Trim angle
$\lambda$	m	Wave length
$\rho$	$kg/m^3$	Water density
$\Phi$	rad, deg	Roll amplitude
$\varphi$	rad, deg	Roll angle or heel angle
$\Phi_{max}$	rad, deg	Maximum roll angle
$\Phi_S$	deg	Angle of stable equilibrium under a heeling lever

<b>Symbol</b>	<b>Unit</b>	<b>Definition</b>
$\Phi_V$	deg	Angle of vanishing stability
$\omega$	rad/s	Ship's roll frequency
$\omega_0$	rad/s	Ship's natural roll frequency
$\omega_e$	rad/s	Wave encounter frequency
$\omega_w$	rad/s	Wave frequency

## Other symbols

$\nabla$	$m^3$	Ship's displacement volume, computed displacement volume during the finding of the equilibrium position
$\nabla_0$	$m^3$	Ship's displacement volume during the finding of the equilibrium position

## REFERENCES

### *Papers Published within the Scope of this Thesis*

1. Grinnaert F., Laurens J.-M. (2013). *Stabilité du navire – Théorie, réglementation, méthodes de calcul – Cours et exercices corrigés*. Ellipses, collection Technosup, ISBN 978-2-7298-80644.
2. Grinnaert F., Leguen J.-F., Billard J.-Y. (2015). *Application de différents règlements civils et militaires du domaine stabilité sur le cas de navires de la Marine Nationale*. 113<sup>ème</sup> session de l'ATMA, Paris, France.
3. Grinnaert F., Billard J.-Y., Laurens J.-M. (2015). *Calcoque: a fully 3D Ship Hydrostatic Solver*. Proceedings of the 12<sup>th</sup> International Conference on the Stability of Ships and Ocean Vehicles, Glasgow, UK.
4. Grinnaert F., Billard J.-Y., Laurens J.-M. (2016). *Different Computations of Parametric Roll Level 2 Criterion*. Proceedings of the 15<sup>th</sup> International Ship Stability Workshop, 13-15 June 2016, Stockholm, Sweden.
5. Grinnaert F., Gualeni P., Billard J.-Y., Laurens J.-M., Petacco N. (2016). *Application of 2<sup>nd</sup> Generation Intact Stability Criteria on Naval Ships*. Proceedings of the 15<sup>th</sup> International Ship Stability Workshop, 13-15 June 2016, Stockholm, Sweden.
6. Grinnaert F., Billard J.-Y., Laurens J.-M. (2016). *KG<sub>max</sub> curves associated with 2<sup>nd</sup> Generation Intact Stability Criteria for Different Types of Ships*. Journal of Marine Science and Application. DOI: 10.1007/s11804-016-1369-3.
7. Grinnaert F., Billard J.-Y., Laurens J.-M. (2016). *An Energy Analysis of Parametric Roll*. Submitted to the Journal of Marine Science and Technology.

### *Historical References*

8. Froude W. (1861). *On the rolling of ships*. Transaction of the Institution of Naval Architects, vol. 2, pp 180–227.
9. Mathieu E. (1868). *Mémoire sur le mouvement vibratoire d'une membrane de forme elliptique*. Journal de Mathématiques Pures et Appliquées, vol. 13, pp 137–203.
10. International Conference on Safety of Life at Sea (1914). *Text of the Convention for the Safety of Life at Sea*. London, January 20, 1914.
11. Rahola J. (1939). *The Judging of the Stability of Ships and the Determination of the Minimum Amount of Stability Especially Considering the Vessels Navigating Finnish Waters*. Ph.D. Thesis, Technical University of Finland, Helsinki.
12. Kerwin J. E. (1955). *Notes on rolling in longitudinal waves*. International Ship-Building Progress, vol. 2(16), pp 597–614.

13. Giordmaine J. A., Miller R. C. (1965). *Tunable Coherent Parametric Oscillation in LiNbO<sub>3</sub> at Optical Frequencies*. Physical Review Letters, 14(24), 973.
14. International Maritime Organization (1968). Res. A.167. *Recommendation on intact stability for passenger and cargo ships under 100 meters*. London.
15. Sanmartín Losada J. R. (1984). *O Botafumeiro: parametric pumping in the Middle Age*. American Journal of Physics, 52, pp 937-945.
16. International Maritime Organization (1985). Res. A.562. *Recommendation on a severe wind and rolling criterion (weather criterion) for the intact stability of passenger and cargo ships of 24 meters in length and over*. London.

### **Current Military and Civilian Intact Stability Regulation**

17. Direction Générale de l'Armement (1999). *Stabilité des bâtiments de surface de la marine nationale*. Instruction générale n° 6018 A.
18. International Maritime Organization (2009). *International Code of Intact Stability, 2008*. London.

### **Development of Second Generation Intact Stability Criteria**

19. International Maritime Organization (2009). SLF 52/INF.2. *Information collected by the intersessional Correspondence Group on Intact Stability, Submitted by USA*. London.
20. International Maritime Organization (2012). SLF ISCG 54/19. *Proposal of revision of updated draft vulnerability criteria of levels 1 and 2 for the failure modes of pure loss of stability and parametric roll*. Submitted by Japan, 29 May 2012.
21. International Maritime Organization (2013). SDC 1/INF.8. *Information collected by the Correspondence Group on Intact Stability regarding the second generation intact stability criteria development*. Submitted by Japan, 13 November 2013.
22. International Maritime Organization (2015). SDC 2/WP.4. 2<sup>nd</sup> session. *Development of Second Generation Intact Stability Criteria, Development of Amendments to Part B of the 2008 IS Code on Towing and Anchor Handling Operations*.
23. International Maritime Organization (2016). SDC 3/WP.5. 3<sup>rd</sup> session. *Finalization of Second Generation Intact Stability Criteria, Amendments to Part B of the 2008 IS Code on Towing, Lifting and Anchor Handling Operations*.
24. International Maritime Organization (2016). *Observations regarding the feasibility of the current version of the level 2 criterion for parametric roll in the second generation intact stability criteria*. Submitted by Sweden to the Intact Stability Correspondence Group on 31<sup>st</sup> August 2016.

### **Second Generation Intact Stability Criteria**

25. Bassler C., Belenky V., Bulian G., Francescutto A., Spyrou K., Umeda N. (2009). *A Review of Available Methods for Application to Second Level Vulnerability Criteria*. Proceedings of the 10<sup>th</sup> International Conference on Stability of Ships and Ocean Vehicles, pp 111-128, St Petersburg, Russia.

26. Francescutto A., Umeda N. (2010). *Current Status of New Generation Intact Stability Criteria Development*. Proceedings of the 11<sup>th</sup> International Ship Stability Workshop, pp 1-5, Wageningen, NL.
27. Belenky V., Bassler C., Spyrou K. (2011). *Development of Second Generation Intact Stability Criteria*. US Navy, Naval Surface Warfare Center Carderock Division, NSWCCD-50-TR-2011/065.
28. Bulian G., Francescutto A. (2011). *Considerations on Parametric Roll and Dead Ship Conditions for the Development of Second Generation Intact Stability Criteria*. Proceedings of the 12<sup>th</sup> International Ship Stability Workshop, pp 7-18, Washington, USA.
29. Wandji C., Corrigan P. (2012). *Test Application of Second Generation IMO Intact Stability Criteria on a Large Sample of Ships*. Proceedings of the 11<sup>th</sup> International Conference on the Stability of Ships and Ocean Vehicles, pp 129-139, Athens, Greece.
30. Umeda N. (2013). *Current Status of Second Generation Intact Stability Criteria Development and Some Recent Efforts*. Proceedings of the 13<sup>th</sup> International Ship Stability Workshop, pp 138-157, Brest, France.
31. Krüger S., Hatecke H., Billerbeck H., Bruns A., Kluwe F. (2013). Investigation of the 2<sup>nd</sup> Generation of Intact Stability Criteria for Ships Vulnerable to Parametric Rolling in Following seas. 32<sup>nd</sup> International Conference on Ocean, Offshore and Arctic Engineering OMAE2013, Nantes, France.
32. Peters W., Belenky V., Chouliaras S., Spyrou K. (2015). *Requirements for Computational Methods to be Used for the IMO Second Generation Intact Stability Criteria*. Proceedings of the 12<sup>th</sup> International Conference on the Stability of Ships and Ocean Vehicles, Glasgow, UK.
33. Krüger S., Hatecke H., Gualeni P., Di Donato L. (2015). *On the application of the 2<sup>nd</sup> Generation Intact Stability Criteria to Ro-Pax and Container Vessels*. Proceedings of the 12<sup>th</sup> International Conference on the Stability of Ships and Ocean Vehicles, Glasgow, UK.
34. Francescutto A. (2015). *Intact Stability Criteria of Ships – Past, Present and Future*. Proceedings of the 12th International Conference on the Stability of Ships and Ocean Vehicles, Glasgow, UK.
35. Umeda N., Francescutto A. (2016). *Current state of the second generation intact stability criteria - achievements and remaining issues*. Proceedings of the 15<sup>th</sup> International Ship Stability Workshop, 13-15 June 2016, Stockholm, Sweden.

### ***Pure Loss of Stability***

36. Taylan M. (2005). *Anatomy of a Capsize: Then and Now*. Proceedings of the 8<sup>th</sup> International Ship Stability Workshop, Istanbul, Turkey.
37. Maron A., Carrillo E., Valle J., Prieto M.E., Gutierrez C., Taboada M. (2006). *Investigation on the capsizing of a small fishing vessel in following seas*. Proceedings of the 9<sup>th</sup> International Conference on Stability of Ships and Ocean Vehicles, Rio de Janeiro, Brazil.
38. Kluwe F., Krüger S. (2007). *Using Full-Scale Capsizing Accidents for the Validation of Numerical Seakeeping Simulations*. Proceedings of the 9<sup>th</sup> International Ship Stability Workshop, Hamburg, Germany.

39. Swedish Accident Investigation Board, SHK (2008). *Loss of M/S FINNBIRCH between Öland and Gotland, 1 November 2006, Case S-130/06*. Report RS 2008:03e. ISSN 1400-5735.
40. Krüger S., Kluwe F. (2010). *Development of Threshold Values for a Minimum Stability Criterion Based on Full Scale Accidents*. Final Report German BMWi Research Project LaSse, Project 03 SX 128 D.

### ***Parametric Roll***

41. France W. N., Levadou M., Treakle T. W., Paulling J. R., Michel R. K., Moore C. (2001). *An Investigation of Head-Sea Parametric Rolling and its Influence on Container Lashing Systems*. SNAME Annual Meeting.
42. Umeda N., Hashimoto H., Vassalos D., Urano S., Okou K. (2003). *Nonlinear Dynamics on Parametric Roll Resonance with Realistic Numerical Modelling*. Proceedings of the 8<sup>th</sup> International Conference on Stability of Ships and Ocean Vehicles, Madrid, pp 281-290.
43. American Bureau of Shipping (2004). *Guide for the Assessment of Parametric Roll Resonance in the Design of Container Carriers*. Sept. 2004, Updated June 2008, Houston, Texas.
44. Bulian G. (2006). *Development of analytical nonlinear models for parametric roll and hydrostatic restoring variations in regular and irregular waves*. PhD Thesis, University of Trieste, Italy.
45. Carmel S. M. (2006). *Study of parametric rolling event on a panamax container vessel*. Journal of the Transportation Research Board, vol. 1963, pp 56–63.
46. Sadat-Hosseini H., Stern F., Olivieri A., Campana E. F., Hashimoto H., Umeda N., Bulian G., Francescutto A. (2010). *Head-wave parametric rolling of a surface combatant*. Ocean Engineering, 37(10), pp 859-878.
47. Galeazzi R., Blanke M., Jensen J. J. (2010). *Autonomous Supervision and Control of Parametric Roll Resonance*. Kgs. Lyngby, Denmark: Technical University of Denmark.

### ***Roll Damping***

48. Ikeda Y., Himeno Y., Tanaka N. (1978). *Components of roll damping of ship at forward speed*. Department of Naval Architecture University of Osaka Prefecture, Report No 404.
49. Himeno Y. (1981). *Prediction of Ship Roll Damping - State of the Art*. University of Michigan, Department of Naval Architecture and Marine Engineering, Report No 239.
50. Kawahara Y., Maekawa K., Ikeda Y. (2009). *A simple prediction formula of roll damping of conventional cargo ships on the basis of Ikeda's method and its limitation*. Proceedings of the 10<sup>th</sup> International Conference on Stability of Ships and Ocean Vehicles, St Petersburg.

### ***Ship Resistance***

51. International Towing Tank Conference (1957). *Proceedings of the 8<sup>th</sup> ITTC*. Published by Canal de Experiencias Hidrodinamicas, El Pardo, Madrid, Spain.

52. Holtrop J., Mennen G. (1982). *An Approximate Power Prediction Method*. International Shipbuilding Progress vol. 329, pp 166-170.
53. Holtrop J. (1984). *A Statistical Re-Analysis of Resistance and propulsion Data*. International Shipbuilding Progress vol. 353, pp 272-276.
54. Fung S.C. (1991). *Resistance and Powering Prediction for Transom Stern Hull Forms During Early Stage Ship Design*. SNAME Transactions, vol. 99, pp 29-84.

### ***Ship Accidents other than that due to Pure Loss of Stability or Parametric Roll***

55. Det Norske Veritas (1998). *FSA of HLA on Passenger Vessels*. Report No. 97-2053, Oslo.
56. BEA mer (2000). *Rapport d'enquête sur le naufrage de l'ERIKA survenu au large de la Bretagne le 12 décembre 1999*.
57. BEA mer (2003). *Perte totale suite à avarie de coque du pétrolier bahaméen Prestige survenue dans l'ouest de la Galice - 13-19 novembre 2002 - Contribution provisoire au rapport d'enquête technique*.
58. Marine Accident Investigation Branch (2008). *Report on the investigation of the structural failure of MSC Napoli English Channel on 18 January 2007*. Report No 9/2008. Southampton, UK.
59. European Maritime Safety Agency (2008). *Maritime Accident Review 2008*.
60. Kaufmann J. (2009). *Fatal Accident on Board the CMV Chicago Express During Typhoon "Hugupit" on September 24 2008 off the Coast of Hong Kong*. Bundesstelle für Seeunfalluntersuchung. Investigation Report 510/08.
61. Bureau of Maritime Affairs (2009). *Report of Investigation in the Matter of Sinking of Passenger Vessel EXPLORER (O.N. 8495) 23 November 2007 in the Bransfield Strait near the South Shetland Islands*. Monrovia, Liberia.
62. Committee on Large Container Ship Safety (2013). *Interim Report of Committee on Large Container Ship Safety*. December 2013, Japan.
63. Bundesstelle für Seeunfalluntersuchung (2014). *Fire and explosion on board the MSC FLAMINIA on 14 July 2012 in the Atlantic and the ensuing events*. Investigation Report 255/12.

### ***Other Papers***

64. Service Historique de la Défense (1957) CAAPC, Jeanne d'Arc 1961. *Plan des formes*. Plan n° 6174.
65. Grim O. (1961). *Beitrag zu dem Problem der Sicherheit des Schiffes im Seegang*. Schiff und Hafen, Heft 6, S. 490-497.
66. Nayfeh A. H. (1981). *Introduction to Perturbation Techniques*. Wiley-Interscience, New York.
67. Garne K. (1997). *Model Seakeeping Experiments Presented in the Time-Domain to Facilitate Validation of Computational Tool*. Kungl Tekniska Högskolan, Stockholm.

68. Moelgaard A. (2000). *PMM-tests with a model of a frigate class DDG-51*. Danish Maritime Institute 2000071, Report No. 1.
69. International Association of Classification Societies (2001). Rec. No. 34. *Standard Wave Data, Rev.1*.
70. Maritime Research Institute Netherlands (2011). *Fredyn User's manual, Version 10.3*. May 2011.
71. International Towing Tank Conference (2011). *ITTC Symbols and Terminology List*. September 2011.
72. Billard J.-Y., Vonier P., Mogenicato E., Leguen J.-F., Ditta R. (2012). *Estimation of Capsizing Risk for French Frigates*. 13<sup>èmes</sup> journées de l'hydrodynamique, Chatou, France.
73. Billard J.-Y., Grinnaert F., Delumeau I., Vonier P., Creismeas P., Leguen J.-F., Ferreiro L. D. (2014). *Forensic Study of BOUVET Capsizing*. Proceedings of the 14<sup>th</sup> International Ship Stability Workshop, Kuala Lumpur, Malaysia.
74. Gnimavo G. P. (2016). *Etude analytique du roulis paramétrique*. Projet de voie d'approfondissement, Ecole navale.